

SPATIAL LOCALIZATION OF ATYPICAL MAPK P38 SIGNALING AND ITS  
IMPLICATION IN PULMONARY INFLAMMATION AND DISEASE PROGRESSION

by

JEREMY CALEB BURTON

(Under the Direction of Neil Grimsey)

ABSTRACT

Despite the central role of mitogen-activated protein kinase (MAPK) p38 in driving pathological inflammation - including during pulmonary injury - effective therapeutic targeting remains elusive. Atypical p38 signaling, mediated by interaction with the adaptor protein Tumor Growth Factor  $\beta$  Activated Kinase 1 (TAK1) Binding Protein 1 (TAB1) is activated only in pathological responses, representing a selective and alternative target during pulmonary inflammation. Our prior work established that G-protein coupled receptors (GPCRs) rapidly activate atypical p38 signaling in primary human endothelial cells, inducing vascular disruption and inflammatory cytokine production, potentially implicating atypical signaling in acute lung injury (ALI).

However, there are key gaps in our knowledge about how atypical signaling differentiates from canonical activation and how this pathway impacts human health. Emerging evidence suggests that kinase activity is spatiotemporally regulated, and downstream signaling is mediated by spatially restricted substrate access. We hypothesize that differences in kinase localization and activity may be the driving factor behind the physiological effects of atypical p38 signaling. This work encapsulates the current knowledge on kinase localization dynamics and atypical signaling

as emerging fields of study. Our studies branch into two projects, where we seek to elucidate the spatial dynamics of p38 activity and uncover the first known roles of atypical signaling in infectious pulmonary inflammatory disease progression. To accomplish this, we use a combination of *in vitro* studies utilizing Fluorescence Resonance Energy Transfer (FRET) microscopy paired with genetically encoded kinase activity reporters and *in vivo* studies of a mouse model of influenza infection. Our results indicate that canonical, MKK3/6-driven p38 activity via osmotic stress results in rapid, transient kinase signaling that is strongest in the nucleus. In contrast, atypical signaling by GPCR agonists initiates sustained signaling primarily in the cytosol and endosome. Additionally, we report that systemic knock-in mice deficient for TAB1-p38 interaction are protected from influenza-induced ALI as measured by weight loss curves, histopathological scoring, mRNA expression, and immune recruitment to the lung. The collective discoveries in this dissertation demonstrate the potential therapeutic benefit of targeting atypical p38 signaling and lay the groundwork for future studies exploring how spatially restricted kinase/substrate interaction contributes to pathological outcomes.

INDEX WORDS: Mitogen activated protein kinase (MAPK) p38, TAB1, atypical signaling, fluorescence resonance energy transfer (FRET), fluorescent biosensors, activity reporters, kinase localization, influenza, acute lung injury (ALI), pulmonary inflammation

SPATIAL LOCALIZATION OF ATYPICAL MAPK P38 SIGNALING AND ITS  
IMPLICATIONS IN PULMONARY INFLAMMATION AND DISEASE PROGRESSION

by

JEREMY CALEB BURTON

BS, Biology, Emmanuel College, 2018

A Dissertation Submitted to the Graduate Faculty of The University of Georgia in Partial  
Fulfillment of the Requirements for the Degree

DOCTOR OF PHILOSOPHY

ATHENS, GEORGIA

2024

© 2024

Jeremy Caleb Burton

All Rights Reserved

SPATIAL LOCALIZATION OF ATYPICAL MAPK P38 SIGNALING AND ITS  
IMPLICATIONS IN PULMONARY INFLAMMATION AND DISEASE PROGRESSION

by

Jeremy Caleb Burton

Major Professor:	Neil Grimsey
Committee:	Shelley Hooks
	Somanath Shenoy
	Karen Norris

Electronic Version Approved:

Ron Walcott  
Vice Provost for Graduate Education and Dean of the Graduate School  
The University of Georgia  
December 2024

DEDICATION

To my son,  
Marlo Robin Burton

Secrets

\*\*

You are made of secrets  
hidden in my life,  
slipped between my days,  
like a four-letter code  
written on the daily passages  
I search through while awake.  
I found one in springtime squalling rain,  
warmly drumming the windows,  
swelling puddles that ripple  
with each falling drop  
like tears  
reflecting the gray sky.  
I found one in the birdsong  
chiming in the branches  
high above our worries,  
lilts of laughter hidden in the leaves.  
I found one in the hope  
of March daffodils and April daisies  
dancing softly with the bees,  
transience shining in sunlit petals  
like the warm smile  
of a kept promise  
known only to us.

You are made of secrets  
you've kept to yourself,  
woven in a perfect double helix  
transcribed and translated  
in the language of the stars.  
I will never stop searching,  
for each and every one I find,  
the rain and birdsong and smiling daisies,  
and all the ones I cannot imagine,  
my whole world and everything in it  
is a part of you.  
And all of me, too,  
is just a part of you.  
They fit safely into my heart  
where there's always room to spare,  
for secrets are precious things,  
like birthday wishes  
whispered between you and little flames,  
that cast shadows a lifetime long  
and fill that cavernous emptiness  
with the light of dreams.  
There, in that place,  
I'll keep your secrets for you.

\*\*

## ACKNOWLEDGEMENTS

I would like to thank the educators, professors, and mentors that have helped me on my academic journey over the years. To my professors at my undergraduate institution that inspired me to pursue a career studying and seeking to understand the beauty of biology. To my major advisor, Dr. Neil Grimsey, for taking on the task of training me to think like a scientist and equipping me with the skills needed to build my own sense of self confidence, and for being patient, willing, and always available to help me find my success or just to listen to me. To my graduate committee, Dr. Somanath Shenoy, Dr. Karen Norris, and Dr. Shelley Hooks, for advice, guidance, and for serving over the years. I'd also like to thank the other students from my ILS cohort and in my department that have been my friends, have grown alongside me, and have graduated and found their success elsewhere. To my lab mates, current and former. To Julie Simmons, who has always truly cared for the success of all her graduate students. To Dr. Wided Najahi-Missaoui, and who has always been in my corner to support me. To Steven and Sheena Patrick, Andy Haygood, and Renee Smagur, who supported me through difficult times and who got me into college and on my way here.

To my friends and my family. To our best friend Grace, to Rachel, Lindsay, Jade, Tim, Stephen, Kaleb and Adam, and to my oldest friend, Patrick. To my parents, Yamna and Papas, for encouraging me no matter what I want to do in life. To my brothers, Matthew, who showed me the strength of finding my own way, and Shawn, who showed me confidence. To my extended family, especially my mother-in-law Mindy, who has accepted me fully.

And most of all, I have no words by which to adequately express my thanks to my wife, Kora. She has been my strength and my support, my partner, my love and my center. She is an

amazing mother, and the strongest person I will ever know. Thank you for your patience with me throughout my Ph.D. studies, and always. I love you.

## TABLE OF CONTENTS

	Page
ACKNOWLEDGEMENTS .....	iv
LIST OF TABLES .....	vii
LIST OF FIGURES .....	viii
CHAPTER	
1 INTRODUCTION AND LITERATURE REVIEWS .....	1
Part 1: Atypical p38 Signaling, Activation, and Implications for Disease .....	1
Part 2: Spatiotemporal Control of Kinases and the Biomolecular Tools to Trace Activity .....	29
Part 3: Atypical signaling, pulmonary disease, and rationale.....	57
2 FLUORESCENCE RESONANCE ENERGY TRANSFER (FRET) SPATIOTEMPORAL MAPPING OF ATYPICAL P38 REVEALS AN ENDOSOMAL AND CYTOSOLIC BIAS .....	70
Introduction.....	71
Results.....	73
Discussion.....	86
Materials and Methods.....	93
Chapter 2 Supplemental Figures.....	98
3 THE ROLE OF ATYPICAL MAPK P38 SIGNALING IN THE PROGRESSION OF INFLUENZA A-INDUCED PULMONARY INFLAMMATION .....	112

Introduction.....	113
Results.....	116
Discussion.....	127
Conclusion and Future Directions .....	133
Methods and Materials.....	134
Supplemental Figures for Chapter 3 .....	141
4. SUMMARY AND FUTURE DIRECTIONS.....	144
Summary of Research Aims and Findings.....	144
Potential Experiments and Future Perspectives.....	150
REFERENCES .....	156
APPENDIX	
Standard Laboratory Methodologies.....	208

## LIST OF TABLES

	Page
Table 1.1.1: Clinical Trials Targeting MAPK P38 .....	9
Table 1.1.2: Pathological roles of MAPK p38 Signal Transduction in a Variety of Diseases .....	19
Table 1.1.3: Physiological Roles of TAB1 Dependent Atypical p38 Signaling.....	28
Table 1.2.1: Kinases associated with LLPS condensates .....	52

## LIST OF FIGURES

	Page
Figure 1.1.1: Mechanisms of MAPK p38 activation .....	15
Figure 1.2.1: Post-translational modifications (PTMs) and their role in cellular physiology .....	31
Figure 1.2.2: Modes of Activation and Spatial Regulation of Kinases .....	34
Figure 1.2.3: Kinase Activity Imaging Tools with Subcellular Resolution.....	48
Figure 1.3.1: P38 is a known therapeutic target for acute lung injury.....	68
Figure 1.3.2: Atypical signaling is conserved in human lung endothelial cells .....	69
Figure 2.1: Model of P38 activation, localization, and translocation .....	74
Figure 2.2: P38 biosensor platform localized to subcellular compartments.....	77
Figure 2.3: Subcellular mapping of MKK3/6 dependent p38 activity.....	81
Figure 2.4. P38 activation is differentially regulated by thrombin.....	82
Figure 2.5. FRET response driven by p38 activity .....	83
Figure 2.6: Blockade of GPCR internalization changes spatial FRET bias .....	85
Figure 2.7: Atypical p38 signaling model.....	87
Supplemental Figure 2.1: p38 biosensors colocalize with compartment-specific probes and proteins.....	99
Supplemental Figure 2.2: Pseudo color images of biosensor responses to NaCl.....	100
Supplemental Figure 2.3: Pseudo color images of biosensor responses to Thrombin.....	101
Supplemental Figure 2.4: Thrombin-induced p38 activity is not altered by addition of DMSO vehicle control.....	102



## CHAPTER 1

### Part 1

#### ATYPIAL P38 SIGNALING, ACTIVATION, AND IMPLICATIONS FOR DISEASE<sup>1</sup>

---

<sup>1</sup> Burton, J.C., Antoniadou, W., Okalova, J., Roos, M. M., & Grimsey, N.J. *Int J Mol Sci*, 22(8), April 2021.  
Reprinted here with permission of the publisher

## Introduction

The p38 mitogen-activated protein kinase (MAPK) family are critical cellular signaling regulators that drive many physiological and pathophysiological pathways. Therefore, it is not surprising that since their discovery in 1994<sup>1</sup>, over 45,000 research articles and reviews have been published describing the mechanism of p38 activation and the role of p38 during development and disease progression. The broader MAPK family includes c-Jun activated Kinase (JNK), extracellular signal-related kinase 1 and 2 (ERK1/2), and protein kinase B, also known as AKT kinase (AKT), all of which are critical in regulating a multitude of cellular processes from cell division to cell death and everything in between. Cellular stimuli/stress induces the activation of MAPKs, including hormones, growth factors, and cytokines, as well as environmental stressors such as osmotic shock, UV radiation, and ischemic injury<sup>2</sup>. As such, p38 MAPKs have been the subject of intense study to generate clinically effective therapeutics. Despite ongoing clinical trials for many diseases, including ischemic cardiac damage, COPD, multiple cancers, various neuropathies, and ARDS/COVID-19, only one non-selective p38 inhibitor (pirfenidone) has been approved for clinical use to treat idiopathic pulmonary fibrosis<sup>3,4</sup>. An underlying contributor to the loss of efficacy and on-target toxicity of these drugs is thought to be due to the ubiquitous and critical role p38 plays in normal physiology. Additionally, almost all current approaches have centered around therapeutics that target the ATP binding site of p38 resulting in blockade of all p38 activity, both physiological and pathophysiological, regardless of the stimulus. Therefore, there is an increased focus on researching the downstream signaling targets of p38 induced only during disease progression, such as the critical inflammatory kinase MAPK activated protein kinase 2 (MK2), or the alternative p38 activation pathways selectively induced during inflammation and disease progression (see Fig. 1.1.1).

In light of the sheer volume of p38 research articles and the wealth of excellent reviews available, it would be impractical and redundant to cover all aspects of p38 MAPK signaling. Therefore, this review will initially provide a brief overview of the history of p38 and the many roles it plays in disease progression. This will be followed by a more focused examination of the novel atypical p38 activation pathways, specifically including atypical p38 activation by GPCRs, and their implications for disease progression and therapeutic intervention. In comparison to classical p38 activity, atypical p38 signaling has been understudied with only 44 publications, however this growing body of work represents a fresh perspective on p38 activity and function in disease.

### **Classical Activation of Mitogen-Activated Protein Kinases (MAPK)**

The classical pathway for MAPK activation is through a three-tiered kinase cascade, where MAP kinase kinase kinases activate a MAP kinase kinase which in turn activate MAPKs such as p38 (**Fig. 1.1.1**). The most direct regulators of MAPK activity are the serine/threonine MAP2ks that phosphorylate conserved threonine sites on the activation loop of MAPKs<sup>5</sup>. Phosphorylation of the activation loop induces a conformational change to open the substrate-binding site<sup>6</sup>. One distinct feature of the subfamilies of MAPKs is their activating phosphorylation motifs. C-Jun N-terminal kinases (JNK) feature a Thr-Pro-Tyr sequence, extracellular-signal-regulated kinase (ERK) have a Thr-Glu-Tyr sequence, and p38 MAPK uses Thr-Gly-Tyr<sup>7</sup>. P38 MAPK was initially discovered as a MAP kinase activated in response to endotoxin with a sequence distinct from MAPK1 (ERK1)<sup>1</sup>. Further studies revealed p38 to be activated by a pair of unique MAP2Ks (MAPKK3/MKK3 and MAPKK6/MKK6)<sup>6,8</sup>.

## Activation of p38 by MAPKK3 and MAPKK6

MKK6 and MKK3 share a high degree of sequence homology with an 86% amino acid identity and selectively activate p38 MAPK over other MAP2Ks<sup>7,9</sup>. MKK3/6 are ubiquitously expressed in all tissues, although MKK3 and MKK6 have differing expression levels<sup>10,11</sup>. While MKK3/6 preferentially activate p38 MAPK, they can also activate other MAPK family members, such as JNK<sup>12</sup>. However, MKK3/6 are essential for classical p38 activation through phosphorylation of Threonine [T180] and Tyrosine [Y182] residues on the active loop of p38<sup>13</sup>. Although under extreme conditions, p38 can also be activated by MKK4, typically selective to JNK<sup>14</sup>. The functional role of MKK3/6 is further emphasized through embryonic lethality seen in MKK3/6 double knockout mice (*mkk3*<sup>-/-</sup>, *mkk6*<sup>-/-</sup>), suggesting functional conservation<sup>14</sup>. While recent evidence demonstrates that MKK3 and MKK6 can differentially activate specific p38 isoforms (see below)<sup>15</sup>.

MAP2Ks are activated by MAP3Ks, which are less specific than MAPK2Ks and activate an array of regulatory proteins. MAP3Ks are categorized into three broad families: MEK kinases, mixed lineage kinases (MLKs), and thousand and one kinases (TAOs)<sup>2</sup>. Several factors regulate MAP3Ks, such as membrane recruitment, oligomerization, and phosphorylation<sup>16</sup>. Over 50 different MAP3Ks and adaptors can regulate MAP2K activation; many of the activation and recruitment mechanisms are still being actively investigated and substantial gaps remain in the pathways for activation. One example for adaptor mediated activation is the MAP3K transforming growth factor- $\beta$ -activated kinase (TAK1) dependent MKK3/6 activation. TAK1 has a direct role in p38 MAPK activation as a mediator of the transforming growth factor- $\beta$  signaling pathway<sup>9,12</sup>, and several other common inflammatory ligands including IL-1 $\beta$ , TNF $\alpha$ , and LPS<sup>17-19</sup>. Critically, TAK1 is activated through direct binding to the adaptor proteins, TAK1 binding protein 1 and 2

(TAB1 and TAB2)<sup>20</sup>. In contrast to the MKK3/6 dependent pathway recent studies have identified two atypical activation pathways, discussed below.

### **Distribution, Activation, and Function of the p38 Isoforms**

There are four isoforms of p38 ( $\alpha$ ,  $\beta$ ,  $\gamma$ , and  $\delta$ ). MAPK p38 $\alpha$  is the founding member of the family and is ubiquitously expressed throughout the body. The four isoforms share a high degree of homology, p38 $\beta$  with 74% homology to p38 $\alpha$ , p38 $\gamma$  with 63% homology to p38 $\alpha$ , and p38 $\delta$  with 60% homology to p38 $\alpha$ <sup>21-23</sup>. Contrary to p38 $\alpha$  the other isoforms display differential tissue expression patterns. P38 $\beta$  is expressed mostly in the brain, heart, and lungs, p38 $\gamma$  is only expressed in skeletal muscle, and p38 $\delta$  is expressed in the lungs and kidneys<sup>13, 21-23</sup>. It is therefore not surprising that there is predicted to be little to no functional redundancy in their activity. MKK3 and MKK6 can differentially activate the separate isoforms, but all isoforms can be activated by MKK6<sup>15</sup>. For example, MKK3/6 are both essential for activation of p38 $\beta$  and p38 $\gamma$  after environmental stress. While MKK6 regulates p38 $\gamma$  after TNF $\alpha$  stimulation, MKK3 activates p38 $\delta$  after UV radiation, hyperosmotic anisomycin and TNF $\alpha$  stimulation<sup>15</sup>. Furthermore, p38 $\delta$  is activated by MKK4 more so than the other isoforms<sup>24</sup>. Even though p38 $\alpha$  and p38 $\beta$  experience similar phosphorylation levels, activation of p38 $\beta$  is more often carried out by MKK6<sup>15, 21</sup>. Opposingly, MKK3 is demonstrated to be the primary activator of p38 $\delta$ <sup>15</sup>. The third isoform, p38 $\gamma$ , can be activated by MKK3 and MKK6<sup>15</sup>.

Notably, p38 $\alpha$  the only isoform that is essential for embryonic development, where it regulates placental vasculogenesis and morphogenesis<sup>25, 26</sup>. Additionally, while some studies argue for it, p38 $\beta$  cannot compensate for p38 $\alpha$ -controlled embryonic development, and it has instead been suggested that p38 $\beta$  is redundant when in the presence of a functional p38 $\alpha$ <sup>27, 28</sup>.

The differential activation and signal transduction by MAPKs appear to be in part regulated by binding to specific scaffold proteins<sup>29-32</sup>. Scaffolding proteins residing in different subcellular locations may assist in the spatiotemporal activation of MAPKs. An example of which is osmotic stress that induces the formation of a complex, including Rac GTPase osmosensing scaffold for MEKK3 (OSM), MEKK3, and MKK3 for specific activation of p38<sup>33</sup>. In comparison, the PB1 domain of MAPK kinase of ERK kinase (MEK2) drives endosomal ERK1/2 activation<sup>34</sup>. Furthermore, recent studies have shown that GPCR ubiquitination causes p38 $\alpha$  activation through an atypical mechanism, utilizing TAB1 and TAB2 to form a signaling complex at endosomal structures to enhance vascular inflammation and endothelial barrier disruption<sup>31</sup>.

### **P38 Substrate Activation**

As the downstream signal transduction pathways for p38 are highly complex, we refer the reader to several outstanding and exhaustive reviews<sup>35-37</sup>. Briefly, the first downstream targets identified for p38 MAPK were the mitogen activated protein kinase-activated protein kinase 2 and 3 (MAPKAPK2, MAPKAPK2/3 or MK2, MK3 respectively)<sup>38,39</sup>. Phosphorylated MK2 and MK3 can then further activate other substrates such as cyclic AMP-responsive element binding protein (CREB)<sup>40</sup> and heat shock protein 27 (HSP27) to regulate actin filament remodeling<sup>41</sup>. MK2 is also an important regulator of post-transcriptional regulation of gene expression through modulation of adenylate-uridylate-rich elements (ARE)-binding proteins tristetraprolin (TTP) and HuR (reviewed here<sup>42</sup>). Whereas mitogen- and stress-activated kinase 1 and 2 (MSK1 and MSK2) translocate to the nucleus to mediate activation of nucleosome components and transcription factors<sup>43</sup>.

There are over 100 substrates identified for the p38 family with selective activation of specific substrates determined by the stimulation mechanism, including inflammation, DNA repair, cell

differentiation, stem cell physiology, stress responses, and neuronal function<sup>35, 36, 44</sup>. An interesting problem in the field is determining how p38 can selectively modulate subsets of target proteins in different disease settings. One clue is that activation of p38 never occurs in isolation, with multiple signaling pathways working in synergy to regulate physiological outcomes. P38 substrate expression levels are often dynamically regulated and cross-talk between different signaling pathways are likely to contribute to the availability of specific substrates. Likewise, the magnitude of p38 activation, which is often robustly activated during disease is likely to influence which substrates can be phosphorylated and for how long. This raises the question of how p38 MAPK signaling can be turned off.

### **Signal Termination**

With p38 MAPK playing a critical role in many cellular functions, dephosphorylation of both threonine and tyrosine residues in the active loop is required for inactivation of the kinase and signal termination. The most widely studied family responsible for dephosphorylating p38 are the dual specificity phosphatases (DUSPs) also referred to as MAPK phosphatases (MKPs). The DUSP family can dephosphorylate all members of the MAPK family. However, DUSP1/MKP1, DUSP10/MKP5, DUSP26/MKP8, and DUSP12 display a higher degree of specificity to p38 $\alpha$  than the other DUSP family members<sup>45-47</sup>, whereas no DUSPs have been reported for p38 $\delta$  and p38 $\gamma$ . Recent studies have shown that temporal oscillations of MPK1 are key to robust proinflammatory gene expression<sup>48</sup>. Additional studies are required to determine whether the same phenomenon is displayed by all DUSP family members and whether MKP1 oscillations are required for all p38 $\alpha$  activity. In addition to the DUSP family members, protein phosphatase 2 (PP2)<sup>49</sup>, Wip1<sup>50</sup>, and Calcyclin binding protein/Siah-1 interacting protein (SIP1)<sup>51</sup> have all been shown to dephosphorylate p38. However, the broader roles of these phosphatases has yet to be established.

## Molecular Inhibition

Since its discovery, p38 has been recognized as a potentially critical therapeutic target<sup>52, 53</sup>. Multiple small molecule p38 kinase inhibitors have since been developed with tremendous specificity, largely owing to the rich structural information generated by X-ray crystallography studies available for the p38 family of kinases<sup>54-56</sup>. Many of these compounds have entered clinical trials, as shown in [Table 1.1.1]. These include inhibitors for the p38 kinase family (doramapimod, ralimetinib, losmapimod) as well as more specific p38 $\alpha$  inhibitors (PH-797804 and related pyridinone scaffold inhibitors). Pyridinone inhibitors exploit a unique binding model of a dual H-bond motif involving Met109 and Gly110 residues with a flipped backbone conformation of Gly110 in its apo state<sup>57, 58</sup>. The unique methionine and glycine configuration in the gatekeeper region is only conserved in the human kinome in p38 $\alpha/\beta$  and Myt-1, the latter of which bears little kinase resemblance to the former and has not shown to be cross-reactive with pyridinone scaffold inhibitors<sup>59</sup>. Specific p38 inhibitors almost invariably have been designed to target p38 kinase activity, primarily through binding to or near the ATP-binding pocket, and display effectiveness at selectively inhibiting p38 in preclinical studies<sup>57, 60</sup>. In early-stage investigations, many of these inhibitors show anti-inflammatory efficacy and favorable toxicity profiles<sup>61-65</sup>, but so far none have achieved prolonged efficacy against chronic inflammatory disease, and only the p38 $\gamma$  inhibitor pirfenidone has reached the market for treatment of idiopathic pulmonary fibrosis. Many promising compounds have been reassigned for further investigation as combinatorial therapies such as purposing ralimetinib for combination therapy in breast cancer (ClinicalTrials.gov ID: NCT01663857). Such an approach has proven effective for improving existing therapies, as seen in a study of doramipimod administration alongside antibiotics improving mycobacterium clearance in mice<sup>66</sup>, and the well-studied losmapimod is currently

Compound	Isoform specificity	Diseases Targeted	Identifier
AZD7624	P38 $\alpha$ , P38 $\beta$	Endotoxin-induced inflammation, COPD	NCT01937338 NCT02238483
LY2228820 (Ralimetinib)	P38 pan-inhibition	Ovarian cancer, Glioblastoma (both concomitant), Metastatic breast cancer	NCT02322853 NCT02364206 NCT01663857 NCT01393990
LY3007113	P38 pan-inhibition	Metastatic cancer	NCT01463631
VX-745 (Neflamapimod)	P38 $\alpha$	Alzheimer's disease, Huntington disease, Lewy body dementia	NCT03980938 NCT04001517 NCT03402659 NCT03435861
VX-702	P38 $\alpha$	Rheumatoid arthritis	NCT00395577 NCT00205478
PH-797804	P38 $\alpha$	Rheumatoid arthritis, COPD	NCT01321463 NCT00559910 NCT01589614
SB681323 (Dilmapimod)	P38 $\alpha$	Neuropathic pain, COPD, ALI/ARDS, Coronary heart disease	NCT00134693 NCT00564746 NCT00390845 NCT00144859 NCT00320450 NCT00996840 NCT00291902
Losmapimod GW856553X or GSK- AHAB (Losmapimod)	P38 pan-inhibition	Acute coronary syndrome, COPD, Neuropathic pain, SARS-CoV-2, Atherosclerosis, Acute coronary syndrome, Focal segmental glomerulosclerosis, Facioscapulohumeral muscular dystrophy	NCT04264442 NCT04511819 NCT02000440 NCT02299375 NCT04003974 NCT01541852 NCT01756495 NCT02145468 NCT01218126 NCT00633022
BMS-582949	P38 pan-inhibition	Arterial inflammation, Atherosclerosis	NCT00162292 NCT00399906
ARRY-371797	P38 $\alpha$	LMNA-related dilated cardiomyopathy, Rheumatoid arthritis, Osteoarthritis of the knee, Ankylosing spondylitis	NCT02351856 NCT03439514 NCT00729209 NCT01366014 NCT00811499
PF-03715455	P38 $\alpha$	Asthma, COPD	NCT02219048 NCT02366637
BIRB 796 (Doramapimod)	P38 pan-inhibition	Crohn's disease, Plaque-type psoriasis, Rheumatoid arthritis, Endotoxin-induced inflammation	NCT02214888 NCT02209753 NCT02209792 NCT02209779 NCT02211170
SCIO-469 (Talapimod)	P38 $\alpha$	Rheumatoid arthritis, Multiple myeloma	NCT00095680 NCT00087867 NCT00043732 NCT00508768

Pirfenidone	P38 $\gamma$	Idiopathic pulmonary fibrosis	NCT03208933
BCT-197 (Acumapimod)	P38 $\alpha$	COPD	NCT01332097 NCT02700919

**Table 1.1.1** Clinical Trials Targeting MAPK p38

being evaluated in a clinical trial for safety and efficacy to treat SARS-CoV-2 (ClinicalTrials.gov ID: NCT04511819).

The consistent short-lived efficacy of current inhibitors suggests that compensatory inflammatory pathways are upregulated over time in response to total p38 activity inhibition. While p38 has been many well-designed investigations studying p38 as a therapeutic target, there remains much unknown about p38 subcellular localization and access to downstream substrates after stimulation, especially pertaining to MKK3/6 versus atypical activation. Current investigations into inhibitor design are shifting away from targeting the catalytic site of p38 and instead focus on substrates and downstream signaling pathways<sup>67-72</sup>. Future therapeutics could avoid long-term efficacy issues from targeting the catalytic site by focusing on alternate drugable sites on p38. Several promising leads have recently been discovered. One example is a lead compound UM101, that binds to the glutamate-aspartate (ED) substrate-docking site rather than the catalytic domain. UM101 is selective for p38 $\alpha$  and able to suppress LPS induced acute lung injury in mice, inflammation, and endothelial barrier disruption in mice, while leaving anti-inflammatory MSK1 activation intact<sup>68</sup>. Another example targets a unique binding pocket in p38 $\alpha$ , that is only bound by the adaptor protein TAB1 during atypical p38 activation. A virtual screen has revealed several promising lead compounds and is described in the following section<sup>73</sup>. However, these compounds have yet to be assessed in cell based or animal models.

As such, these new generation of selective atypical targets provide a promising new direction for clinically viable approaches for anti-p38 therapeutics. Furthermore, it is predicted that the combinatory therapies described above will provide a template moving forward to enable clinically viable strategies to target p38 activity.

## Mechanisms of Atypical p38 Activation

MKK3/6 kinase activity is widely considered to be the primary mechanism for p38 phosphorylation. Nevertheless, there is a growing body of evidence to support alternative mechanisms for p38 activation (**Fig. 1.1.1, A-C**). Two "atypical" or MKK3/6 independent mechanisms exist that facilitate activation of the p38 $\alpha$  through autophosphorylation in cis, true autophosphorylation rather than phosphorylation of a neighboring p38<sup>74</sup>. The first example of atypical p38 signaling was discovered in 2002, when p38 $\alpha$  was shown to directly associate with transforming growth factor  $\beta$  activated kinase 1 (TAK1) binding protein 1 (TAB1), an adaptor protein critical for both TGF $\beta$  and TAK1 signaling<sup>75</sup>. During osmotic stress responses<sup>76</sup>, TAB1 is responsible for oligomerization and autophosphorylation of TAK1 after O-glycosylation, leading to TAK1 activation<sup>77, 78</sup>. Conversely, in atypical p38 signaling, TAB1 binds directly and selectively to two discrete binding domains on p38 $\alpha$ . Specifically, TAB1 residues 404-412 interact at a canonical site used by other p38 substrates, including MKK3 and MEF2a, and residues 389-394 bind to a non-canonical binding site on the c-terminal lobe of p38 $\alpha$ . This site does not exist on any of the other p38 isoforms, and at the time of writing, no other proteins have been shown to bind to the same site on p38 $\alpha$ <sup>67, 71</sup>. The direct interaction of TAB1 with p38 $\alpha$  induces a conformational change moving the active loop into the catalytic domain and enhancing ATP-binding, thus enabling cis-autophosphorylation of the active loop at Thr180 and Tyr182<sup>74</sup>. Consequently, this leads to p38-induced phosphorylation of TAB1 at Ser423, downregulating TAB1 binding to TAK1 and inhibiting TAK1 mediated MKK3/6 activation<sup>79</sup>. Additional studies have also shown that TAB1 phosphorylation can alter its intracellular localization, where increased phosphorylation at S452/453/456/457 blocks its nuclear translocation causing TAB1 retention in

the cytosol<sup>80</sup>. Intriguingly, TAB1 remains bound to p38 $\alpha$  potentially suppressing the capacity of nuclear translocation<sup>71</sup>.

Reactive oxygen species are thought to be the initial driving force behind atypical p38 signaling in cardiac ischemia-reperfusion damage<sup>71,81</sup>. Similarly, cigarette smoke extract (CSE) induced oxidative stress in fetal tissue upregulating TGF $\beta$  production and resulting in TAB1-mediated p38 phosphorylation in a manner independent of TAK1 signaling or the ASK1-signalosome<sup>82</sup>. In a separate cardiac ischemia model, the p38-TAB1 interaction is upregulated in an AMPK-dependent manner<sup>83</sup> (**Fig. 1.1.1, B ii**). The interaction is negatively regulated by the HSP90/CDC37 chaperone complex in myocytes<sup>84</sup>. TAB1 expression is also negatively regulated by the E3 ligase itch through ubiquitin-mediated degradation. There are dramatically increased dermal inflammation levels in an MKK3/6 independent manner in the itch-deficient mice<sup>85</sup>. The WW-domain in itch binds directly to a conserved PPXY motif in TAB1 (aa145-148). This interaction drives TAB1 K<sup>48</sup>-linked ubiquitination to regulate TAB1 turnover/degradation. TAB1 expression is significantly elevated in the absence of itch, leading to enhanced atypical p38 activation and increased cytokine production, including interleukin-6 (IL-6), interleukin-1beta (IL-1 $\beta$ ), interleukin-11 (IL-11), and interleukin-19 (IL-19). Critically, Wang et al. in 2013 developed a peptide inhibitor fused to the HIV-TAT peptide, generating a cell-penetrating peptide inhibitor that selectively disrupts the TAB1 interaction with p38, substantially attenuating atypical p38 activation<sup>86,87</sup>. When used in the itch<sup>-/-</sup> mice, the peptide blocked atypical p38 $\alpha$  signaling and dermal inflammation was significantly suppressed<sup>85</sup>. Further studies have shown that mutation of a critical proline proximal to the p38 binding peptide of TAB1 [P419] blocks TAB1 binding to p38 $\alpha$  and prevents atypical p38 $\alpha$  signaling<sup>31,74,88</sup>, as does mutation of four key residues within the p38 $\alpha$  binding peptide of TAB1 [V390A, Y392A, V408G, and M409A]<sup>71,74</sup>. Critically, unlike

the systemic knockout of TAB1 or p38a, which are embryonically lethal<sup>25, 89</sup>, the TAB1 knock-in (TAB1-KI) mouse displays no physiological abnormalities but is protected from myocardial ischemic damage<sup>71</sup>.

This critical interaction provides a novel opportunity to further develop the peptide inhibitors or screen for small molecule inhibitors to target atypical p38 signaling selectively. Indeed, using a virtual small fragment screen, a group of functionalized adamantanes, specifically 3-amino-1-adamantanol, was found to bind to a critical hydrophobic pocket, forming hydrogen bonds with two key residues, leucine 222 and 234, in the non-canonical TAB1 binding site on p38 $\alpha$ . Further screening found there to be three distinct fragment binding sites within the non-canonical binding site. Linking sulphonamide scaffolds to the adamantanol generated a small molecule with a high affinity to the three regions in the non-canonical binding site<sup>67</sup>. Additional development of these compounds will hopefully yield a viable therapeutic. However, it remains to be shown whether these lead hits can block atypical p38 signaling in cells or *in vivo*.

Despite these detailed studies describing the exact molecular mechanism of TAB1-p38 $\alpha$  interaction and degradation, there are significant gaps in our understanding, specifically for how osmotic stress, oxidative stress, LPS, or inflammatory cytokines such as TNF- $\alpha$  and IL-1 $\beta$  initiate the TAB1-p38 $\alpha$  interaction and atypical p38 signal transduction. Conversely, recent studies have shown that a family of G protein-coupled receptors (GPCRs) can initiate the TAB1-p38 interaction through a novel ubiquitin-driven pathway (described below and **Fig. 1.1.1, B**). This is the first example of a clearly defined mechanism for the induction of atypical p38 signaling and

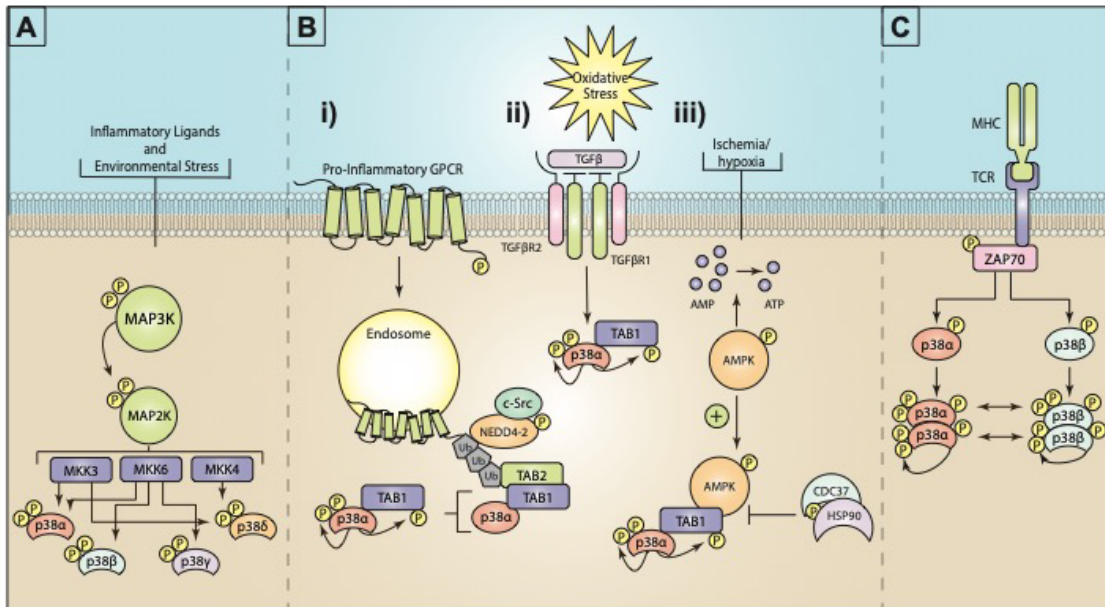


**Figure 1.1.1: Mechanisms of MAPK p38 activation:** **A)** Inflammatory ligands and environmental stress triggers the activation of a three-tiered kinase cascade. Environmental or inflammatory ligands induced the activation of MAP3Ks through a complex array of different mechanisms. MAP3Ks then activate the critical MAP2Ks, MKK3, MKK6, or (less commonly) MKK4. These MAP2Ks can then differentially activate the four isoforms of p38 ( $\alpha$ ,  $\beta$ ,  $\gamma$ , and  $\delta$ ). **B)** The known mechanisms for atypical p38 signaling are **i)** GPCR stimulation triggers G-protein dependent c-Src phosphoactivation of the E3 ubiquitin ligase NEDD4-2. GPCRs recruit and are ubiquitinated by NEDD4-2. K63 ubiquitin chains recruit the Ubiquitin binding adaptor protein TAB2. In turn, TAB2 then recruits TAB1 binds and induces p38 $\alpha$  autophosphorylation. **ii)** Oxidative stress triggers TGF $\beta$  activation with drive TAB1 and p38 activation, although the exact mechanism is unclear. **iii)** Ischemia or hypoxia events drive activation of AMP-activated protein kinase (AMPK), which in turn promotes the formation of the TAB1- p38 $\alpha$  complex and p38 $\alpha$  autophosphorylation. This process is negatively regulated by the heat shock protein 90 (HSP90)-Cdc37 complex. **C)** T-cell receptor (TCR) ligation to major histocompatibility complex (MHC) drives intracellular activation of the src-family zeta chain associated protein kinase 70 (Zap70). Zap70 phosphorylates p38 at Tyrosine 323, enabling autophosphorylation of p38 $\alpha$ , or  $\beta$ .

demonstrates conservation of the mechanism for at least 4 GPCRs critical for vascular inflammatory signaling and vascular homeostasis <sup>31, 32, 90</sup>.

In addition to TAB1, a second discrete mechanism for p38 autophosphorylation has also been demonstrated through src-family zeta chain associated protein kinase 70 (Zap70). This pathway is critical for T-cell activation through a T-cell receptor (TCR) specific mechanism <sup>91</sup>. In contrast to TAB1-mediated autophosphorylation, p38 $\alpha$  and p38 $\beta$  isoforms are phosphorylated at Tyr323 by ZAP70, leading to dimerization and mutual trans-autophosphorylation of the kinases at Thr180 alone. Tyr323 is located on the L16 loop of p38, facilitating this autophosphorylation by inducing a shift in the flexible phosphorylation lip of p38 (residues 171-183) <sup>92</sup>. Together, both TAB1 and ZAP70 mediated autophosphorylation of p38 reveal the kinase's atypical activation in an MKK3/6 independent manner. The functional significance of these distinct activation mechanisms is still unclear. Additional studies are required to elucidate how atypical activation alters p38 $\alpha$  substrate activation and induction of distinct signal transduction events. Notably, p38 $\alpha$  is phosphorylated at the same sites in both canonical and TAB1-mediated signaling, indicating that differential downstream signaling may instead be regulated in a spatiotemporal context rather than kinase functionality.

### **Activation of Atypical p38 by GPCRs**

As the most extensive and versatile family of membrane proteins, G protein-coupled receptors (GPCRs) regulate many cellular pathways by activating MAPKs via G protein-dependent and independent mechanisms <sup>93-97</sup>. Many of the GPCR family can activate p38 $\alpha$ , but until recently, the mechanism for GPCR mediated p38 $\alpha$  activation remained unclear or was predicted to be controlled through the classical MKK3/6 pathway. However, several recent studies have linked vascular inflammatory GPCRs to the activation of the TAB1-dependent atypical p38 signaling

pathway<sup>31, 32, 75, 90, 98, 99</sup>. The initial studies examined thrombin-mediated activation of the protease-activated receptor 1 (PAR1) in vascular endothelial cells. The authors noted that after activation, PAR1 was ubiquitinated, despite being trafficked and degraded in a ubiquitin-independent manner<sup>98, 100-102</sup>.  $\alpha$ -Thrombin, activation of PAR1 induces the receptor to couple to the G protein subunits  $G\alpha_q$  or  $G\alpha_{12/13}$  to induce activation of the proto-oncogene tyrosine-protein kinase c-Src (Src short for sarcoma) and subsequent activation of the E3 ubiquitin ligase, neural precursor cell expressed developmentally downregulated 4-2 (NEDD4-2)<sup>32</sup>. NEDD4-2 is one of a family of nine Homologous to E6-AP Carboxy Terminus (HECT) domain-containing E3 ligases and mediates the covalent coupling of ubiquitin to the intracellular c-tail or intracellular loops of GPCRs<sup>31, 90</sup>. C-Src activates NEDD4-2 through tyrosine phosphorylation of a critical tyrosine residue, Y485, on a linker peptide between WW domain 2 and 3 (2,3-peptide). This 2, 3-linker peptide acts as a molecular switch that holds NEDD4-2 in an inactive conformation. Phosphorylation of Y485 by c-Src induces a conformational change that releases NEDD4-2 from an autoinhibited state. After activation, most likely at the plasma membrane, NEDD4-2 is recruited to PAR1, leading to PAR1 ubiquitination<sup>32</sup>, although the exact mechanism as to how NEDD4-2 is recruited to PAR1 is unknown. Traditionally, GPCR ubiquitination serves as a sorting signal to cause endolysosomal trafficking and protein degradation<sup>31, 98</sup>. However, in this case, NEDD4-2 mediated ubiquitination drives the recruitment of the TAB2-TAB1-p38 signaling complex<sup>31, 32, 90, 98</sup>. TAB2 has an NP14 zinc finger (NZF) domain that binds to the lysine 63-linked NEDD4-2 ubiquitin chains and functions as an adaptor protein. It is predicted but has not been conclusively shown that TAB2 subsequently binds to and recruits TAB1 and p38 $\alpha$ , inducing p38 $\alpha$  autophosphorylation and TAB1 phosphorylation<sup>31, 103</sup>. Interestingly, a structural homolog to TAB2, TAB3, is also able to bind to TAB1 to produce p38 pro-inflammatory signaling by GPCRs.

However, it is not known what the contribution of each homolog is when expressed in the same cell or whether they are functionally redundant<sup>90</sup>. As stated above, the ubiquitinated endosomal receptors nucleate the formation and activation of the TAB1-p38 $\alpha$  complex and increase TAB1 phosphorylation and stability<sup>31</sup>. It is still unclear whether GPCR activated TAB1 sequesters p38 in the cytosol. Likewise, it is not known how TAB1-p38 signaling is terminated.

Importantly, this pathway is not unique just to PAR1 and  $\alpha$ -thrombin. NEDD4-2 dependent regulation of atypical p38 signaling is also conserved for the purinergic receptor P2Y1. Furthermore, a recent study also demonstrated that the pathway is conserved for prostaglandin E2 (PGE2), histamine, ADP, and  $\alpha$ -thrombin mediated p38 activation and inflammatory cytokine production in primary human microvascular and macrovascular endothelial cells. Additional studies are required to determine how many GPCRs utilize this pathway, whether atypical p38 signaling is critical for all cells, and how it selectively contributes to pathophysiological responses.

### **Pathophysiological Implications of MKK3/6-Dependent p38 MAPKs**

As p38 MAPKs play a critical role in the modulation of many physiological processes, the dysregulation of their signaling pathways can result in the pathogenesis of a range of inflammatory diseases, neurological diseases, retinopathies, and cancers. There have been multiple recent outstanding studies and reviews that extensively cover the many pathological pathways controlled by classical p38 signaling, and a small example are highlighted in [Table 1.1.2].

Early studies revealed that p38 MAPKs have a central role in developing various chronic inflammatory diseases due to pro-inflammatory cytokine (PIC) production<sup>35, 104</sup>. Specifically, p38 $\alpha$  MAPK signaling regulates the biosynthesis of many inflammatory mediators in cells of the

	Disease	Pathological outcome	References
<b>Cardiovascular</b>	Myocardial Infarction/ Ischemia-Reperfusion	Induces overexpression of pro-inflammatory cytokines like IL-6, TNF- $\alpha$ , and IL-1 $\beta$ elevates intracellular calcium (Ca <sup>2+</sup> ) levels, inflammation, and apoptosis	71, 105-114
	Diabetic Cardiomyopathy	Overexpression of pro-inflammatory cytokines induces cardiomyocyte apoptosis	115, 116
	Atherosclerosis	Promotes ANG-II dependent MerTK shedding in macrophages resulting in defective efferocytosis and, in turn, induces plaque progression	117-121
<b>Pulmonary</b>	Chronic Obstructive Pulmonary Disease (COPD)	Activates transcription factors and induces overexpression of pro-inflammatory cytokines and chemokines, amplifying lung inflammation	122-127
	Acute Respiratory Distress Syndrome (ARDS)	Induces decreased corticosteroid responsiveness, alveolar macrophage induced impairment of respiratory function, overexpression of pro-inflammatory cytokines like IL-6, IL-8, TNF- $\alpha$ and IL-1 $\beta$	105, 128-130
	Acute Lung Injury (ALI)	Induces overexpression of pro-inflammatory cytokines like IL-6, TNF- $\alpha$ , and IL-1 $\beta$ cell apoptosis	61, 131-134
	Viral Infections and SARS-CoV-2	Induction of type 1 interferons, expression of IL-12, promotion of viral replication expression of pro-inflammatory cytokines resulting in inflammation, thrombosis, vasoconstriction in SARS-CoV-2	61, 135-137
<b>Oncology</b>	Non-Small Cell Lung Cancer (NSCLC)	Enhances proliferation, migration, chemoresistance, Inflammatory cytokine expression	138-144
	Head and Neck Small Cell Carcinoma (HNSCC)	Inhibition of p38 increases HNSCC sensitivity to cisplatin, cannabinoids promote progressive HNSCC via p38 <sup>42</sup> , increases mRNA stability via MK2, p38 isoforms as a diagnostic of HNSCC, regulates angiogenesis and lymphangiogenesis	145-148
	Breast Cancer	Elevated p38 $\delta$ levels promote cell detachment, migration, invasion, and increased metastatic lesions, inhibition of p38 triggers DNA damage and tumor cell death	141, 149, 150
	Bladder Cancer	Induces cell invasion and metastasis by increasing MMP-2 and MMP-9 Activity	143, 151
<b>Neurodegenerative</b>	Alzheimer's Disease	Elevated p-p38 levels progress neuroinflammation tau phosphorylation, neurotoxicity, and synaptic dysfunction	152-155
	Parkinson's Disease	p-p38 overload induces a COX-2 mediated inflammation and subsequent dopaminergic neuron degeneration	156-158
	Amyotrophic Lateral Sclerosis (ALS)	Induces defects in axonal retrograde transport of signaling endosomes	159-161
	Spinal Muscular Atrophy	Induces p38 MAPK-dependent p53 phosphorylation leading to selective degeneration of motor neurons	162
<b>Ocular</b>	Age-Related Macular Degeneration (AMD)	Induces VEGF expression and angiogenesis, regulates Ang-II mediated MMP-2 and MMP-14, basigin expression, and extracellular matrix accumulation in AMD	163, 164
	Diabetic Retinopathy	ASK/p38 NLRP3 inflammasome signaling, retinal angiogenesis, retinal endothelial cell dysfunction, inner-blood-retinal-barrier leakage	116, 165-169
	Glaucoma	Induces anterograde transport degradation and axon degeneration in the optic nerve	170, 171

**Table 1.1.2:** Pathological Role of p38 MAPK Signal Transduction in a Variety of Diseases

immune system, epithelial cells, fibroblasts, and endothelial cells <sup>172</sup>. These mediators' excessive production is associated with the pathological progression of acute and chronic inflammatory diseases including chronic obstructive pulmonary disease (COPD), rheumatoid arthritis (RA), gastritis, and psoriasis <sup>35, 173, 174</sup>. However, the story is complicated by a dichotomy of responses where p38 can exert both pro- and anti-inflammatory effect during disease progression. P38 can directly phosphorylate pro-inflammatory transcription factors such as MEF2C <sup>175</sup>, and indirectly regulate inflammatory cytokine production through the MK2/3-TTP axis, where p38 phosphorylation of TTP prevents TTP dependent degradation of AU-rich cytokine mRNA, leading to an accelerated inflammatory responses <sup>39, 42, 140</sup>. As such p38 is an essential driver of inflammatory mediators such as COX2, MMP9, iNOS, TNF $\alpha$ , and IL6 <sup>36, 176-179</sup>. Conversely, p38 also plays a central role in anti-inflammatory signaling. An example of this is p38 dependent regulation of IL10, a powerful anti-inflammatory cytokine which is important in resolving inflammatory insults <sup>180, 181</sup>. IL10 expression is regulated through p38 activation of MSK1/2. Additionally, MSK1/2 also enhances DUSP1 expression which is required to restrain damaging hyperinflammation through dephosphorylation of p38 as described above <sup>182</sup>.

Likewise, there is strong evidence for p38 in both tumor suppressive cellular homeostasis, balancing proliferation, differentiation, and apoptosis, and tumor promoting roles through promoting cell survival, proliferation and angiogenesis <sup>144</sup>. Furthermore, p38 can both sensitize some tumor types to chemotherapy and facilitates resistance in others, where p38 inhibition may be beneficial in therapeutic approaches <sup>144, 183-185</sup>. Of note, p38 MAPK activity and increased expression have been linked to the progression of breast cancer, prostate cancer, bladder cancer, liver cancer, lung cancer, and thyroid cancers, leukemia, and many more <sup>35, 143, 186, 187</sup>. In solid tumor biology, the p38 MAPK pathway has been shown to promote tumor cell survival and

angiogenesis during periods of hypoxia, reoxygenation, and nutrient deficiency by inducing expression of metalloproteinases and vascular endothelial growth factor A (VEGFA) <sup>143</sup>. The context-dependent functions of p38 are therefore critical to determine the therapeutic potential of p38 inhibitors in cancer treatment, although p38 therapeutics have so far been unsuccessful in clinical trials.

In a similar manner, MAPK p38-induced cytokine expression during neuroinflammation accelerates the development of chronic neurodegenerative diseases such as multiple sclerosis (MS) <sup>188</sup>, Alzheimer's disease (AD) <sup>152</sup>, and Parkinson's disease (PD) <sup>156</sup>, potentially through dysregulation of the neurovascular unit. Additionally, during the pathophysiological progression of AD, elevated p38 $\alpha$  MAPK signal transduction in both microglia and astrocytes results in subsequent neuroinflammation driving detrimental tau phosphorylation <sup>153, 154, 156</sup>. Conversely, p38 $\gamma$  signaling has recently been shown to mediate site-specific increase post-synaptic tau phosphorylation and reduce Tau-mediated memory deficits <sup>155</sup>. Furthermore, p38 MAPK mediated, microglial signaling is vital in dopamine neuron degeneration in PD patients <sup>189</sup>. Again, these data suggest that p38 therapeutics targeting the ATP pocket or catalytic domain are likely to be unsuccessful due to the dual roles of p38 in both physiological, protective, and pathological signaling.

### **Pathophysiological Implications of Atypical p38 Signaling**

Contrary to the highly studied MKK3/6 dependent pathway, the impact of TAB1-p38-dependent signaling in physiology and disease remains largely understudied with just 44 research articles on the subject (**Table 3**). As mentioned above, the recent development of the viable p38 $\alpha$ -KI mouse <sup>190</sup> or the TAB1-KI mouse <sup>71</sup> suggests that perturbation of the atypical pathway is less critical for developmental and physiological signaling compared to the embryonically lethal

systemic knockout of p38 $\alpha$  or TAB1<sup>25, 89</sup>. It is perhaps then not surprising that atypical p38 activation has so far only been identified as a contributor to disease progression, which will be discussed below.

There is a growing awareness that atypical p38 $\alpha$  activation plays a key role in multiple p38 driven pathologies. The initial studies describing atypical p38 $\alpha$  activation demonstrate its role in ischemic cardiac damage, ischemia-reperfusion injury, and amyloidosis. In an MKK3<sup>-/-</sup> ischemic mouse, the TAB1-p38 interaction was a leading contributor to necrosis in cardiomyocytes<sup>110</sup>. The role of atypical p38 was further confirmed in the progression of ischemic damage when a cell-penetrating inhibitor peptide was developed that reduced infarct size in ischemic rats<sup>86</sup>. Supporting this, the recent TAB1-KI mice where TAB1-induced autophosphorylation of p38 was genetically perturbed had significantly reduced infarction volume after induction of myocardial ischemia. Furthermore, the transphosphorylation of TAB1 was disabled<sup>71</sup>, and cyclic GMP kinase 1 was found to inhibit TAB1-p38 $\alpha$  to prevent apoptosis in cardiomyocytes during IR<sup>191</sup>. Additionally, basal activation of p38 autophosphorylation is suppressed by the HSP90/CDC37 complex where CDC37 directly interacts with p38 $\alpha$ <sup>84</sup>. Inhibition of HSP90 during cardiac stress is thought to dissociate HSP90 from p38 $\alpha$ , enabling TAB1 interaction and p38 $\alpha$  autophosphorylation to drive IL-6 and TNF $\alpha$  expression and cardiomyocyte apoptosis<sup>84</sup>. Additional studies have also shown that in a zebrafish model of amyloid light-chain (AL-LC) amyloidosis, AL-LC drives TAB1-p38 $\alpha$  signaling causing cardiotoxic signaling, impaired cardiac function, pericardial edema, cell death, and subsequent heart failure<sup>192, 193</sup>.

Aside from the heart, p38 autophosphorylation has also been indicated in pathological inflammation in both dermal disorders, preterm birth, and more broadly in vascular inflammation. In the *itch*<sup>-/-</sup> mice, TAB1 expression is significantly enhanced, leading to robust p38

autophosphorylation and subsequent increases in inflammatory cytokine expression, immune cell recruitment, and spontaneous skin lesions<sup>85</sup>. The use of the cell-penetrating peptide inhibitor significantly reduced these phenotypes, suggesting that itch-mediated p38 signaling could be exploited therapeutically<sup>85</sup>. The use of the cell-penetrating inhibitor peptide significantly reduced these phenotypes, suggesting that itch-mediated p38 signaling could be exploited therapeutically. In the field of reproductive biology, term and preterm parturition are tied to oxidative-stress and inflammatory TGF- $\beta$  induced TAB1-p38 activity resulting in amniochorion senescence<sup>82</sup>. Atypical p38 is also considered an essential component of the careful balance of endothelial mesenchymal transition (EndoMT) and mesenchymal endothelial transition (MEndoT) in human and murine amnion cells that contributes to the timing of parturition<sup>194</sup>. Vascular inflammation also directly activates GPCR-dependent p38 signaling in endothelial cells. In these studies, GPCR ligand  $\alpha$ -thrombin induces endothelial barrier disruption driving vascular leakage and permeability.

Additionally, recent studies of GPCR-mediated TAB1-p38 activity have demonstrated that it is conserved in multiple endothelial vascular beds and activated by a family of GPCR ligands associated with inflammation such as histamine, PGE<sub>2</sub>, ADP, and potentially many others<sup>31, 32, 90</sup>. While it has not yet been definitively shown, it stands to reason that any cell that expresses these GPCR receptors has the potential to induce atypical p38 signaling. This being the case, it will be essential to understand the role of GPCR signaling in fibroblasts, epithelial cells, mural/pericyte cells, and neuronal cells. Therefore, the impact of GPCR induced atypical signaling is likely to play an, as of yet, undiscovered or overlooked role in many other vascular inflammatory diseases.

Beyond the vasculature, the role of atypical p38 is also explored in the modulation of the immune system by inflammatory ligands, attenuation of the TCR, and response to pathogens.

Basophils and eosinophils isolated from healthy patients undergo p38 autophosphorylation in response to cytokine exposure from TNF $\alpha$  and GM-CSF, contributing to prolonged inflammation like that seen in pulmonary inflammatory disorders <sup>195</sup>. Conversely, TAB1-p38 interaction is also associated with maintaining anergic CD4<sup>+</sup> T-cells through increased expression of TAB1 following antigen exposure and abrogating TCR <sup>196</sup>. Similarly, TAB1-p38 drives T-cell senescence via an AMPK-dependent regulatory pathway, resulting in downregulation of TCR signalosome <sup>197</sup>. AMPK also plays an essential role in the TAB1-p38 activation of HSP27 in simulated sepsis, maintaining vascular integrity <sup>198</sup>. Intracellular infection leading to TAB1-p38 activity was first shown in macrophages in mice infected with *Toxoplasma gondii*, resulting in pro-inflammatory IL-12 production specific to atypical signaling <sup>199</sup>. *Leishmania* infection results in parasite GP63 induced degradation of TAB1 to reduce p38 activation <sup>200</sup>, the reversal of which sharply attenuates infection <sup>201</sup>. These studies suggest a vital role for the p38-TAB1 interaction in the host defense during intracellular pathogen infection.

Another example of atypical p38 activation comes from a recent study that demonstrated that viral infections utilize atypical p38 signaling to drive viral infections. Inhibition of TAB1-dependent p38 activation impaired hepatitis C virus (HCV) assembly and viral replication. This was also confirmed for severe fever with thrombocytopenia syndrome virus (SFTSV), herpes simplex virus type 1 (HSV-1), and severe acute respiratory syndrome coronavirus 2 (SARS-CoV-2) <sup>135</sup>. Indeed, the p38 inhibitor Losmapimod is currently in a clinical trial to treat SARS-CoV-2 (ClinicalTrials.gov ID: NCT04511819). It will be important for future studies to understand how atypical p38 signaling contributes to viral and bacterial infections and whether selective atypical p38 inhibitors could support current therapeutic regimens.

In the realm of type 1 diabetes, a link was found for TAB1-p38 interaction in the apoptosis of beta cells via oxidative stress by NO<sup>202</sup> and cytokine-induced beta-cell death<sup>203</sup>. These investigators noted that the effect of TAB1 signaling was specific to the TAB1 $\alpha$  splicing product of the TAB1 gene located on chromosome 22, which has also been linked to systemic sclerosis and type 2 diabetes, hinting at a potential genetic component involving TAB1 mutation in the initiation of these diseases.

Contrary to TAB1-dependent signaling, Zap70-dependent activation of p38 is exclusive to T-cell activation via the TCR response, which is negatively regulated by p38 phosphorylation of upstream Zap70<sup>91, 92</sup>. However, a recent study also showed that TCR-mediated p38 activation occurs simultaneously through a classical kinase cascade and inflammatory augmentation by the alternative, atypical p38 activation. Intriguingly, it is suggested that uncoupling of the classical p38 activation mediated by the adaptor protein LAT and the guanine nuclear exchange factor, Son of Sevenless 1/2 (SOS1/2), reduced T-cell development and exacerbated autoimmune disease in mice<sup>204</sup>. At the same time, the genetic blockade of the TAB1-Zap70 suppressed T helper cell activation (T<sub>H1</sub> and T<sub>H17</sub>) and expression of IFN $\gamma$  and IL17. Suggesting that both the classical and atypical p38 activation pathways work synergistically to induce a balance between pro- and anti-inflammatory responses<sup>204</sup>. It is currently unclear whether there are some cases when TAB1-p38 activation may work in consort with MKK3/6, albeit in a TAK1 independent manner as TAB1 phosphorylation by p38 during atypical p38 signaling blocks TAB1's interaction with TAK1 preventing TAB1-TAK1 dependent MKK3/6 activation<sup>79</sup>.

## **Conclusion**

The 25-year history of p38 MAPK has clearly demonstrated that this family of inflammatory kinases are essential for normal physiological processes and, if dysregulated, can be significant

contributors to many diseases. Yet, despite many outstanding studies and carefully controlled clinical studies, therapeutic interventions targeting the conserved ATP pocket or structural scaffolds have so far been unsuccessful in the clinic. However, there are some promising avenues, like targeting downstream signaling transducers such as MK2. Furthermore, the selective inhibition of pathological atypical p38 signaling represents a significantly under-investigated avenue and potentially critical target for therapeutic intervention.

Although there has been important progress in understanding the structural basis of the TAB1-p38 interaction, and a clear mechanism has been defined for GPCR induced activation of atypical p38 signaling, there remain many gaps in our understanding of where, when, and why this pathway exists. There is still little understanding of how atypical p38 signaling alters the functional outcome of p38 activation to drive disease progression.

As outlined above, there is a growing body of clear evidence describing TAB1-dependent atypical p38 signaling [Table 1.3]. Atypical p38 signaling has yet to be implemented in physiological pathways but is instead initiated only during disease progression, including cancer, viral infections, cardiac diseases, dermal inflammation, and vascular inflammation. This does raise a question of what evolutionary pressure resulted in the establishment of this pathway separate to MKK3/6 driven p38 activity. As more selective therapeutics are developed it will be critical to determine whether blockade of TAB1-mediated p38 activation alters physiological or protective pathways. An important area of research should be in defining how TAB1 biases p38 signaling and identifying what substrates lay downstream of TAB1-p38. These studies would provide critical insight into how TAB1-p38 activity drives functional outcomes that, at present, appear to be only activated to drive disease progression.

Based on the significant role of GPCR ligands and p38 in the progression of so many diseases, it is clear that the current research has only just scratched the surface of the potential import of atypical p38 signaling. Future studies will yield critical detail to the broader mechanism of activation, and the development of TAB1-p38 selective inhibitors could pave the way forward to developing a clinically viable therapeutic.

Disease	Mechanism of p38 Autophosphorylation	Model	Specific Cell or Animal Line
Cardiovascular Ischemia and Reperfusion	TAB1-mediated	Murine <i>in-vivo</i> <sup>71, 83, 108, 110, 111</sup>	MKK3 <sup>-/-</sup> <sup>83, 110</sup> ; C57BL/6 <sup>83, 108</sup> ; Sprague Dawley <sup>83</sup> ; Wistar <sup>111</sup> ; TAB1 KI <sup>71</sup>
		Murine <i>in-vitro</i> <sup>71, 81, 108, 110, 111, 205</sup>	H9c2 <sup>110</sup> ; Sprague Dawley <sup>108, 111, 205</sup> ; Wistar <sup>111</sup> ; C57BL/6 <sup>71, 81</sup>
		Human <i>in-vitro</i> <sup>71, 87, 108, 111, 114</sup>	HEK293 <sup>71, 108, 111, 114</sup>
		Structural modeling <sup>73</sup>	
Myocardial Infarction, Amyloidosis, and Cardiomyopathy	TAB1-mediated	Murine <i>in-vivo</i> <sup>113</sup>	Sprague Dawley
		Murine <i>in-vitro</i> <sup>84, 113, 206</sup>	H9c2 <sup>113</sup> ; Wistar <sup>206</sup>
		Human <i>in-vitro</i> <sup>206</sup>	Patient heart
		Zebrafish <i>in-vivo</i> <sup>192</sup>	
General Inflammation and Cancer	TAB1-mediated	Murine <i>in-vivo</i> <sup>31, 85, 207</sup>	BALB/c <sup>207</sup> ; CD1/CD1 <sup>31</sup> ; C57BL/6, Itch <sup>-/-</sup> <sup>85</sup>
		Murine <i>in-vitro</i> <sup>31, 85, 207</sup>	Vβ8.1, OT-II <sup>207</sup> ; TAB1 <sup>-/-</sup> <sup>31</sup> ; C57BL/6, Itch <sup>-/-</sup> <sup>85</sup>
		Human <i>in-vitro</i> <sup>31, 32, 90</sup>	HUVEC <sup>31, 32, 90</sup> ; HEK293 <sup>31</sup> ; HDMEC <sup>90</sup>
		Structural modeling <sup>92, 208</sup>	
Parasitic Infection	TAB1-mediated	Murine <i>in-vivo</i> <sup>209</sup>	BALB/c
		Murine <i>in-vitro</i> <sup>199, 200, 209</sup>	RAW264.9 <sup>209</sup> ; MKK3 <sup>-/-</sup> <sup>199</sup> ; BALB/c <sup>200</sup>
Viral Infection	TAB1-mediated	Murine <i>in-vitro</i> <sup>136</sup>	C57BL/6, BC-1
		Human <i>in-vitro</i> <sup>135</sup>	Huh7.5.1, HEK293, Patient liver
Bacterial Infection	TAB1-mediated	Human <i>in-vitro</i> <sup>198</sup>	HPMEC
		Shrimp <sup>210</sup>	
Diabetes	TAB1-mediated	Murine <i>in-vitro</i> <sup>211, 212</sup>	β-TC6 <sup>211, 212</sup> ; Sprague Dawley, NMRI <sup>212</sup>
		Human <i>in-vitro</i> <sup>212</sup>	Islet
Leukocyte Dysfunction	TAB1-mediated	Murine <i>in-vivo</i> <sup>213</sup>	Vβ8.1
		Murine <i>in-vitro</i> <sup>213</sup>	2B4
		Human <i>in-vitro</i> <sup>195, 197, 214</sup>	Patient blood
Pregnancy Complications	TAB1-mediated	Murine <i>in-vitro</i> <sup>215</sup>	CD-1
		Human <i>in-vitro</i> <sup>82, 215</sup>	Patient placenta
Other	TAB1-mediated	Murine <i>in-vitro</i> <sup>216, 217</sup>	MKK3 <sup>-/-</sup> /6 <sup>-/-</sup> <sup>216</sup> ; MKK3 <sup>-/-</sup> <sup>217</sup>
		Human <i>in-vitro</i> <sup>75, 80, 88, 218</sup>	HEK293 <sup>75, 80, 88, 218</sup> ; MDA231 <sup>218</sup>
		Structural modeling <sup>219</sup>	
Immune System (T-Cell) Modulation	Zap70-mediated	Murine <i>in-vivo</i> <sup>91</sup>	P116
		Murine <i>in-vitro</i> <sup>220-223</sup>	Gadd45a <sup>-/-</sup> <sup>220</sup> ; CD4SP <sup>221</sup> ; C57BL/6 <sup>222, 223</sup>
		Human <i>in-vitro</i> <sup>91, 224-227</sup>	Jurkat, P116
		Chicken <i>in-vitro</i> <sup>226</sup>	DT40

**Table 1.1.3:** Physiological Roles of TAB1 Dependent Atypical p38 Signaling

## CHAPTER 1

### Part 2

# SPATIOTEMPORAL CONTROL OF KINASES AND THE BIOMOLECULAR TOOLS TO TRACE ACTIVITY<sup>2</sup>

---

<sup>2</sup> Burton, J.C., Royer, D., Grimsey N.J. *Journal of Biological Chemistry*, 300(11), October 2024.

## Introduction

The packing and regulation of proteins in cells requires orchestrating their location and interaction with adaptors, cofactors, and substrates. The spatial organization of core biochemical processes, including signal transduction, is essential for cellular homeostasis and health. Central to this is the compartmentalization of signaling machinery by association with or encapsulation by membranes, organelles, and membraneless condensates. This concept of signaling compartmentalization is also utilized by receptor-mediated signaling cascades such as receptor tyrosine kinase (RTKs) and G-protein receptor kinases (GPCRs). Compartmentalization of the downstream host factors, which are associated with receptor activation, plays a role in a variety of cellular functions.<sup>228-230</sup> The discrete environmental conditions and substrate concentrations encoded within each location mediate signaling specificity for rapid and selective responses during development and stress, both homeostatic and pathological.

In addition to location, post-translational modifications (PTMs) of proteins govern their specific protein-protein interactions (PPIs), activity (activation and inhibition), secretion, and lifespan before degradation and recycling. These modifications include ubiquitylation, palmitoylation, acetylation, and phosphorylation. For functional roles and recent reviews, see (**Fig. 1.2.1**). For the rest of this manuscript, we will focus on arguably one of the most critical PTMs: protein phosphorylation.

Protein phosphorylation is a central regulatory mechanism controlling almost every cellular process, including cell growth, motility, differentiation, and division. The human kinome accounts for nearly 2% of the human genome; as such, it is one of the largest homologous protein superfamilies, consisting of >500 kinases.<sup>231</sup> Kinase activity catalyzes the transfer of  $\gamma$ -phosphate

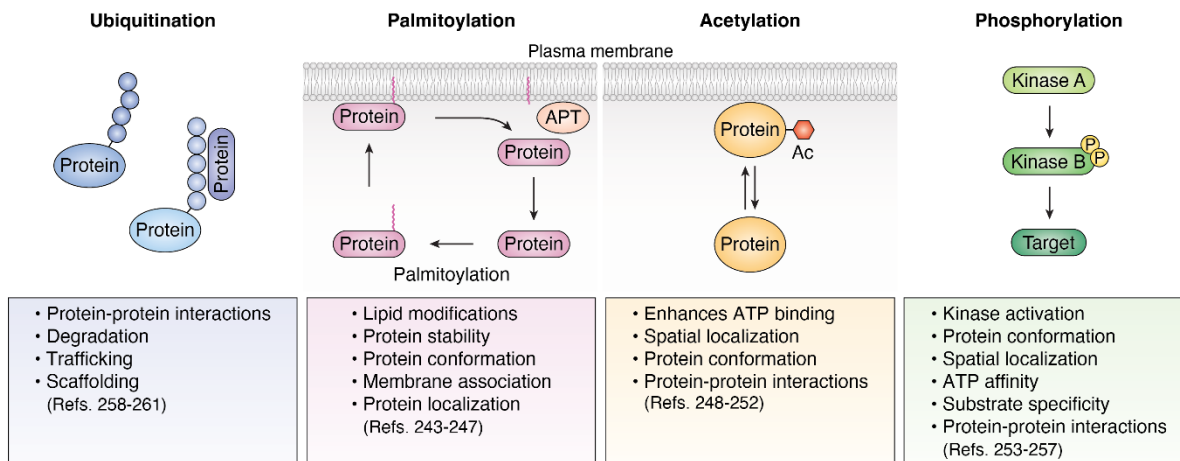


**Figure 1.2.1: Post-translational modifications (PTMs) and their role in cellular physiology.**

Proteins can be dynamically regulated by modifications, including ubiquitination, palmitoylation, acetylation, and phosphorylation. Each PTM changes the protein, altering its functional responses. Palmitoylation,<sup>232-236</sup> Acetylation,<sup>237-241</sup> Phosphorylation,<sup>242-246</sup> and Ubiquitination<sup>247-251</sup>

of ATP to serine, threonine, tyrosine, or histidine residues on substrate proteins.<sup>252-254</sup> Protein phosphorylation acts as a molecular switch rapidly triggering a shift in protein folding, activity, location, or interaction with other biochemical structures, including proteins, RNA, and DNA. The tight regulation of phosphorylation is essential for "normal" homeostatic control, and mutation or dysregulation of protein kinases or adaptors drives the progression of a wide spectrum of human diseases, including chronic inflammation, cancer, and ischemia.<sup>60, 255</sup> Because of their critical roles, kinases are one of the most important targets of precision medicine.<sup>256, 257</sup> Consequently, advances in therapeutic approaches are explicitly tied to our understanding of when, where, and how kinases are activated.

**Kinase Activation.** The general conserved structure of most kinases consists of a bilobal catalytic domain with an N-terminal lobe made of a  $\beta$ -sheet, one  $\alpha$ -helix (C-helix), and an  $\alpha$ -helical C-terminal lobe (**Fig. 1.2.2A and B**).<sup>258</sup> The active site of  $\gamma$ -phosphate transfer is buried in the interface between the two lobes. The ATP-binding pocket is primarily conserved between kinases and surrounded by additional pockets that are less conserved and are often the sites targeted by small-molecule inhibitors.<sup>259</sup> The activation of kinases is tightly regulated by interaction with adaptor proteins, as seen for mitotic kinase activation first established for the cyclin-dependent kinase (CDK) family or sequential phosphorylation by kinase signaling pathways. The mitogen-activated protein kinase (MAPK) p38 sub-family is a classic example of the complexity of kinase regulation. All eukaryotes express p38 MAPKs, and their structural and regulatory characteristics are predominantly conserved from yeast to humans. The current models of molecular activation of kinases are still being refined. However, it is widely accepted that the N-terminal lobe facilitates ATP binding. In contrast, the C-lobe mediates effector and substrate binding at the kinase interaction motif (KIM or D-motif), requiring active loop phosphorylation and a conformational

change that fully activates the kinase.<sup>260, 261</sup> Recent studies challenging this model show that dual phosphorylation of the active loop is required in conjunction with the allosteric modulation induced by substrate binding. Combined, these two forces drive the critical conformational changes in the C- and N-lobes to fully activate the kinase.<sup>262-264</sup>

Using MAPK p38 as an illustration of the complexity of kinase activation, p38 is classically activated by dual phosphorylation of the active loop (Thr180, Tyr 182) by a MAP2K, which is, in turn, phospho-activated by a MAP3K. Alternatively, autoactivation of p38 can be induced through either Zap70 phosphorylation of p38 (Tyr323) or TGF $\beta$ -activated kinase 1 binding protein 1 (TAB1) binding to p38.<sup>71, 81, 91, 226</sup> In both cases, these events bypass the requirement of MAP2K and cause a conformation change that drives the active loop into the catalytic domain, enabling autophosphorylation (cis-phosphorylation). Zap70-mediated autoactivation occurs only in T-cells and almost exclusively on Thr180, further enabling auto- and trans-phosphorylation between p38 $\alpha$  and p38 $\beta$ . Meanwhile, TAB1-mediated activation appears to be broadly applicable to most, if not all, cell types and is associated with autoactivation of p38 $\alpha$  (**Fig. 1.2.2C**). Autoactivation itself is not exclusively found for p38. Indeed, cis-and trans-autoactivation has been reported for a wide range of kinases. These include pyruvate dehydrogenase kinase1 (PDK1),<sup>265</sup> Aurora Kinase 1 and 2,<sup>266, 267</sup> interleukin receptor-associated kinase 4 (IRAK4),<sup>268, 269</sup> and protein kinase D (PKD).<sup>270,</sup>

271

However, the mechanism for activation varies and, in many cases, is still controversial. The diverse mechanisms of activation contribute to the differential signal transduction pathways. One way is through allosteric modulation, where cofactor interactions can inhibit or enhance kinase activity and substrate binding. Another is the dynamic sequestration or retention of kinases at specific subcellular locations, as seen by nuclear or cytosolic translocation of activated kinases,

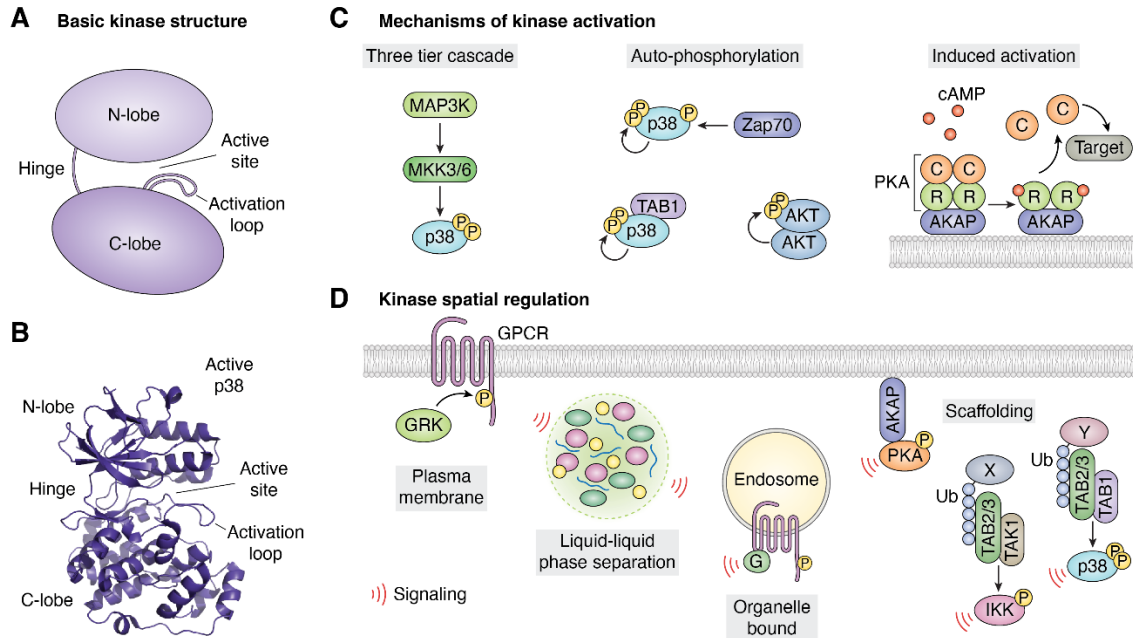


**Figure 1.2.2: Modes of Activation and Spatial Regulation of Kinases.** **A.** Schematic representation of basic kinase structure, including, N-lobe, C-lobe, hinge region, catalytic- loop, and active site. **B.** Structural model of TAB1 activated MAPK p38, PDB:4L00, showing the p38 structure. **C.** The basic mechanisms of kinase activation. Divided into three broad categories: i) Three-tier kinase cascades, where MAP3K activates MAP2K, and finally, the MAPK. ii) Autoactivation, where either an adaptor can bind, causing a conformational change and kinase autophosphorylation, or phosphorylation outside of the active loop that causes a conformational change and autophosphorylation, or dimer formation enabling cis- or transphosphorylation. iii) signaling molecular induced activation; in this example, cAMP binds to the regulatory subunit of PKA, triggering activation and release of the catalytic subunit. **D.** Spatial regulation of kinases. **Plasma membrane:** Localization to the plasma membrane initiates GPCR-mediated signaling. G-protein receptor Kinases (GRKs) are recruited to the membrane to phosphorylate GPCRs and induce receptor internalization. **LLPS:** Compartmentalization of concentrated host factors such as DNA & RNA leads to the formation of LLPS. These membraneless compartments allow for dynamic multivalent interactions within the condensate. The dynamic formation enables fine-tuning of cellular signaling within and downstream signaling out of the LLPS condensate. **Organelle:** Multiple organelles are spatial hotspots for cellular signaling responses. These include the nucleus, endoplasmic reticulum (ER), mitochondria, and Golgi apparatus (GA). PTM's of proteins can enhance their membrane binding or translocation to specific organelles and influence their interactions. **Scaffolding:** Proteins that act as scaffolds help to sequester cytosolic, soluble protein families. This method of compartmentalization initiates local cellular signaling cascades by supporting interactions of adapter proteins, leading to phosphorylation events and downstream signaling. Scaffolding proteins can be localized cytosolically or anchored to organelles such as endosomes, Golgi, ER, and mitochondria. Scaffolding proteins such as ubiquitin and AKAP are the drivers of signaling cascades. AKAP's act as an anchor for PKA. Similarly, ubiquitin chains drive the recruitment of the adapter protein complex, such as TAB2, leading to the autophosphorylation of p38.

which effectively biases their access to specific substrate pools. Spatially defined signaling hotspots enhance the activation of some substrates while blocking or reducing access to others.<sup>258,</sup>

263, 272

In turn, hyperactivation of kinases often disrupts the carefully controlled homeostatic balance inside the cell, leading to pathologic responses. Therefore, signal termination is critical to maintain balance. For p38, desensitization requires dephosphorylation of the activation loop, principally through the action of the MAPK phosphatase (MPK)/dual-specificity phosphatases (DUSP) families. Humans have ~ 250 phosphatases, with many pseudo-phosphatases represented (including TAB1).<sup>273</sup> Each kinase will be regulated by a subset of phosphatases, which tend to be less selective than the kinase activation pathways. Interestingly, activation of most kinases triggers the regulation of negative feedback loops to limit hyperactivation. In our example, p38 can induce DUSP1 and MKP1 to terminate signaling and is important for pro-inflammatory signaling and stress-induced cell death.<sup>48, 274, 275</sup> Alternatively, p38 can directly trigger negative feedback by limiting MKK6 expression,<sup>276</sup> or phosphorylating TAB1 after auto-activation, which then blocks TAB1 regulation of the classical MKK3/6 pathway.<sup>79</sup>

Taken together, selective activation and desensitization pathways provide a significant array of routes to fine-tune kinase signaling in each context. Therefore, the opportunities for additional regulation are enhanced when you factor in where the kinases are and the locally available adaptor and substrate interactomes.

## **Mechanisms of sequestration, protein-protein interactions, and functional compartmentalization.**

**Adaptors and Scaffolding Proteins Sequester Kinases Near Substrates.** Scaffolding proteins help bring order to the soluble pool of proteins in the cytosolic space by regulating specific protein interactions, shaping the local space, and focusing or facilitating specific intracellular signaling responses, including propagation, termination, and localization.<sup>277, 278</sup> One well-studied family of scaffolding proteins driving kinase activity are the A-kinase anchoring proteins (AKAP), which direct 3', 5'-cyclic adenosine monophosphate (cAMP)-dependent protein kinase, or protein kinase A (PKA), a member of the AGC kinase family<sup>279</sup>. PKA is a tetrameric holoenzyme composed of dimerized regulatory subunits (RI or RII) bound to two catalytic subunits (**Fig. 1.2.2C**). The activation of PKA is facilitated by the release of cAMP-bound regulatory subunits, which allow for diverse downstream signaling responses.<sup>280</sup> While cAMP and PKA are cell-diffusible, cAMP has long been suspected of existing in functional gradients<sup>281-283</sup> and microdomains.<sup>284-291</sup> PKA activity is directed by binding to AKAP proteins to regulate signaling and mediate cross-talk between signaling pathways.<sup>292</sup> This is regulated by sequestering PKA within compartments or signalosomes and coupling PKA to substrates and other components of the signaling axis, such as phosphodiesterases.<sup>293</sup> AKAPs can positively or negatively regulate signaling by limiting kinase access to substrates. There are over 50 known AKAPs, many of which have alternative splice variants that alter localization,<sup>294, 295</sup> such as dAKAP1, which traffics to the endoplasmic reticulum or the mitochondria depending on the presence of an Asp(31) at the N-terminus sequence.<sup>296</sup> Other locations AKAPs are trafficked to include the cell membrane, lysosomes, Golgi, nucleus, mitochondria, cytoplasm, and non-membranous signalosomes such as the centrosome and radial spokes.<sup>297</sup> Although AKAPs were named for their recruitment of PKA, these proteins act as

scaffolds for the assembly of many other signaling pathways in specific compartments such as extracellular signal-related kinase 1 and 2 (ERK1/2), hypoxia-inducible factor 1 $\alpha$  (HIF-1 $\alpha$ ), p68 RNA helicase, cyclins, c-Src and Calmodulin, among others.<sup>298, 299</sup> AKAPs define the specific access of active C units to selective substrates. Almost all AKAPs have a PKA RII subunits binding domain (RIIBD), a highly conserved amphipathic alpha-helix of 14/18 amino acids that bind to the four-helix D/D domain R-subunit dimers.<sup>300-303</sup> AKAPs localize with bound PKA at subcellular locations via protein-lipid or protein-protein interaction.<sup>295</sup> AKAPs undergo PTMs, including myristoylation/palmitoylation, to draw PKA toward its substrates and enhance membrane-localization. For example, palmitoylation of AKAP150 promotes localization to recycling endosomes and post-synaptic density in neurons, promoting PKA-regulated AMPAR trafficking,<sup>304, 305</sup> while Gravin is myristoylated and AKAP18 is myristoylated and palmitoylated to facilitate docking to the plasma membrane.<sup>306, 307</sup> Some AKAPs, such as AKAP450, have a pericentrin-AKAP450 centrosomal targeting (PACT) domain, known to interact with CIP4, a cdc42 effector regulating actin dynamics that drives localization to the Golgi and centrosomes.<sup>308,</sup>

309

Alternatively, the RTK family can directly act as scaffolding proteins. These single-pass transmembrane receptors have cytoplasmic-facing tyrosine kinase domains that autophosphorylate in trans. The phospho-group facilitates the recruitment of downstream signaling proteins, usually using a Src homology 2 (SH2) or phosphotyrosine-binding (PTB) domain.<sup>310</sup> In addition, signaling is further defined depending on protein polarization to the apical or basolateral membranes in the epithelium, which can drive signaling responses and cancer progression.<sup>311, 312</sup> RTK activation also modulates the localization of Phosphatidylinositol 3-kinase (PI3K)-AKT signaling at intracellular membranes. After stimulation, PI3K $\alpha$  is trafficked along microtubules via direct binding of

microtubule-associated protein 4 (MAP4), leading to PI3K interaction with receptors at endosomal compartments and contributing to the generation of phosphatidylinositol-3,4,5-trisphosphate (PIP3) and AKT activation.<sup>313</sup> PI3K also plays a central role in regulating plasma membrane signaling dynamics. Controlling cellular responses to membrane-bound receptor activation increases PIP3 concentrations and the subsequent activation of protein kinase D and AKT.<sup>314-316</sup> As such, the relative concentrations of lipids in cellular organelles play critical roles in regulating protein association and activation. They also directly impact membrane topology, trafficking, and signaling transduction.<sup>317-321</sup> Although beyond the scope of this review, lipid membrane microdomains or nanodomains of lipids can, in turn, play essential roles in regulating kinase recruitment and activation, including caveolae lipid raft recruitment of PKC<sup>322</sup> and diacylglycerol activation of PKC.<sup>323</sup> However, the broader implications of lipid microdomains/nanodomains have been investigated and reviewed extensively.<sup>324-326</sup>

AKT signaling also drives changes to the subcellular localization of other proteins, including SR Protein Kinases (SRPKs), where direct<sup>327</sup> or indirect phosphorylation<sup>328</sup> by AKT drives nuclear translocation. Subcellular localization can also be regulated by scaffold or adaptor proteins. In this example, SRPK's association with heat shock protein (HSP) can act as a cytosolic anchor<sup>329, 330</sup> or facilitator of translocation to the nucleus.<sup>328</sup> Alternatively, selective scaffold proteins, JNK interacting proteins 1 and 2 (JIP1 and JIP2), bind to form oligomeric complexes that facilitate JNK activation and signal transduction in the cytoplasm near the plasma membrane by aggregating activators of the JNK kinase module.<sup>331</sup>

Localization can be more complex, as seen for AMP-activated protein kinase (AMPK), where activity can be localized to the Golgi, endoplasmic reticulum, mitochondria, and lysosome in response to metabolic inhibition or genetic knockdown.<sup>332-334</sup> Lysosomal localization requires

AMPK and Liver Kinase B1 (LKB1) to form a complex with AXIN and Late Endosomal/Lysosomal Adaptor, MAPK And MTOR Activator 1 (LAMTOR1).<sup>335, 336</sup> AMPK $\alpha$  subunits are necessary for cytosolic and nuclear localization and contain sequences recognized by nuclear transport receptors (NTR).<sup>337, 338</sup> However, although a nuclear localization sequence (NLS) in AMPK $\alpha$ 2 has been proposed to be necessary for nuclear transport<sup>339</sup> and the NLS is typically recognized by the nuclear translocation importin family of proteins,<sup>340</sup> direct evidence for importin interaction with NLS-containing AMPK $\alpha$ 2 has not yet been shown.<sup>341, 342</sup> There is also evidence that specific AMPK isoforms ( $\alpha$ 1/ $\alpha$ 2/ $\beta$ 2/ $\gamma$ 1) are localized to the outer mitochondrial membrane, and activity only upregulated during more severe metabolic stress, indicating that there may be a hierarchical activation of AMPK at different subcellular locations depending on the severity of stress.<sup>343</sup> Scaffolding proteins can also assemble core components critical for tiered kinase activation, as seen for ERK1/2. Kinase suppressor of Ras 1 (KSR1) and IQ motif-containing guanosine triphosphatase activating protein 1 (IQGAP1) form a complex, where mitogen-activated protein kinase kinase (MEK) bound to IQGAP activates ERK1/2 bound to KSR1 at defined signaling puncta in the cytosol.<sup>344</sup>

Lastly, MAPK p38 signaling can be directly modulated by binding to adaptors and scaffolding proteins. The spatial localization can be controlled by binding nuclear importins that induce nuclear translocation.<sup>345, 346</sup> Meanwhile, p38 binding to TAB1 spatially restricts the kinase to the cytosol, limiting nuclear translocation and directly biasing or reducing access to nuclear substrates.<sup>80, 347</sup> Conversely, the interaction with scaffolding proteins such as DLGH1, OSM, or JIP4 can localize p38 to specific cell areas while also orchestrating intersection with other signaling pathways by tethering p38 to alternate complexes.<sup>33, 222, 348</sup>

**Spatially Biased G-Protein Coupled Receptor (GPCR)-Dependent Signaling.** GPCRs are typically associated with activating heterotrimeric G proteins following agonist stimulation at the plasma membrane, resulting in subsequent activation of effectors and secondary messengers. Recent studies have established that intracellular GPCRs can orchestrate spatially restricted G-protein signaling at sub-cellular compartments. These include the nucleus, endoplasmic reticulum, mitochondrion, Golgi, and the early endosome, and have been reviewed.<sup>349</sup> Additionally, G protein signaling drives the activation of secondary messengers that initiate the regulation and activation of kinases.  $\beta$ -arrestins are multivalent adaptors that bind GPCRs and scaffold essential signaling complexes such as the c-RAF-MEK1-ERK1/2 signaling cascade.<sup>350</sup> Prior models postulated that GPCR-induced plasma membrane recruitment and activation of ERK1/2.<sup>351, 352</sup> However, recent work challenges this hypothesis by showing that GPCR-stimulated MAPK signaling can also occur independently from  $\beta$ -arrestins<sup>353, 354</sup> and that ligand-induced GPCR endocytosis displays distinct subcellular ERK1/2 signaling dynamics.<sup>355, 356</sup> Paired with the known subcellular ERK activity,<sup>357</sup> these studies led investigators to explore subcellular pockets of ERK activity after endocytosis of  $\beta$ 2-adrenergic receptor ( $\beta$ 2-AR), discovering that GPCR activity does not result in ERK1/2 activation at the plasma membrane but is localized to the endosome.<sup>358</sup> This mechanism was further explored and found to be mediated by a signaling axis involving endosomal-localized active  $G_{\alpha S}$ -Raf-MEK, resulting in endosomal activation of ERK.<sup>358</sup> The investigators noted that active ERK then trafficked to the nucleus, affecting the activation of downstream transcription factors, suggesting that this was facilitated by the proximity of the nucleus to the endosome.<sup>358</sup>

In addition to AKAP-directed PKA localization, it has been shown that the location of GPCR activation within the cell can also drive compartmentalized PKA activity.  $\beta$ 2-AR signaling at the endosome drives active PKA localization to the nucleus in a PDE-dependent manner;

however, disrupted endosomal GPCR activation or endosome location perturbs PKA function in the nucleus.<sup>359</sup> These findings illustrate that compartmentalized signaling can protect kinase activity by shortening the distance the kinase travels in a cellular environment that's "hostile" to active kinases.

**Ubiquitin As a Signaling Scaffold and Spatially Restricted Kinase Activation.** *Fig. 1.2.1* summarizes how PTMs can impact cellular functions. Polyubiquitination classically regulates protein trafficking and degradation but can also scaffold the formation of spatially restricted kinase signaling complexes.<sup>98</sup> Tumor-necrosis factor (TNF)-mediated pro-survival signaling involves the IKK (I $\kappa$ B kinase) and TAK1/TAB2/3 (transforming growth factor beta-activated kinase 1, TAK1-binding proteins 2/3), which are recruited in a ubiquitination-dependent manner. Specifically, K63 polyubiquitin chains recruit TAB2/3 via their carboxy-terminal zinc-finger (ZnF) domains that then recruit TAK1. These resulting signaling complexes are important for activating NF- $\kappa$ B and MAPK c-Jun N-terminal kinase (JNK) pathways.<sup>20, 360</sup>

Correspondingly, K63 polyubiquitin of the C-terminal tail of activated GPCRs facilitates the scaffolding or recruitment of TAB2/3 to endosomes. This initiates the formation of a TAB2-TAB1-p38 complex, resulting in autophosphorylation of p38 at the endosome.<sup>31, 361</sup> Notably, GPCR-mediated p38 activation is focused away from the nucleus,<sup>362</sup> contrary to osmotic-stress-induced p38 activation, which is driven to the nucleus.<sup>347</sup> This finding provides some of the first evidence of a mechanism of p38 sequestration away from the nucleus, biasing p38 toward cytosolic substrate pools rather than nuclear transcription factors.<sup>363</sup> This ubiquitin-dependent sequestration mechanism differs from the recently uncovered MAPK ERK1/2 endosomal activation, but suggests a conserved strategy to spatially bias GPCR-induced MAPK activity (*Fig. 1.2.2D*).

**Liquid-Liquid Phase Separation-Dependent Sequestration of Kinases Activity.** The eukaryotic cellular organization also extends to membrane-less compartments that transiently occur or form in stress responses known as molecular condensates or liquid-liquid phase separation (LLPS). Broadly speaking, biomolecular condensates comprise biomolecules with structural features that allow multivalent interactions between proteins, RNA, and DNA, inducing LLPS formation. The physical properties of these condensates exhibit liquid-like behavior and form as the result of phase transitions when the molecular components of the condensates coalesce to form LLPS. Phospholipid metabolism can also contribute to the formation of phase-separated condensates.<sup>364</sup> LLPS enable a dynamic localized layer of regulation that can be turned on and off by their formation and dissolution. Proteins capable of forming these condensates also typically have intrinsically disordered regions (IDR) with low amino acid complexity but can also be highly structured proteins that oligomerize into higher structures.<sup>365</sup> It is becoming increasingly clear that LLPS condensates play important roles in kinase signal transduction<sup>366</sup> and are increasingly a focus when exploring spatial signaling dynamics; see **(Fig. 1.2.2D) [Table 1.2.1]**.

In addition to its roles as a membrane scaffolding protein, described above, polyubiquitin chains also show properties of liquid-liquid phase separation. Specifically, after interleukin-1 (IL1) or TNF $\alpha$  stimulation, the NF- $\kappa$ B essential modulator (NEMO) regulatory subunit of I $\kappa$ B kinase (IKK) is known to phosphorylate the inhibitory I $\kappa$ Bs to facilitate activation of IKK, which it accomplishes via binding to polyubiquitin chains (polyUb).<sup>367</sup> Additionally, linear ubiquitin chain assembly complex (LUBAC)-catalyzed M1- and Lys63- linked linear polyUb binding to NEMO, resulting in the formation of liquid-like droplets. Phase-separation formed modules of IKK activation, and mutations associated with the loss of this phase-separation are associated with immunodeficiency.<sup>368, 369</sup>

As discussed above, AKAP directs PKA function to selective organelles. Recent studies have revealed that a non-canonical higher-level organization also occurs, where the type I regulatory subunit of cAMP-dependent PKA, RI $\alpha$ , undergoes phase separation in response to GPCR-induced cAMP signaling. RI $\alpha$  LLPS biomolecular condensates enable compartmentalization of cAMP but also restrict the movement of catalytic subunit (PKA-C), concentrating activity in LLPS. The D/D and CNB-A domains are both required for LLPS formation, which act as cAMP "sponges" that increase localized microdomains of cAMP that provide protection from cAMP-hydrolyzing phosphodiesterases (PDEs) activity.<sup>370, 371</sup>

**Viral-associated LLPS.** Viruses coerce host cellular machinery to enhance their replication and manipulate immune responses. A growing body of evidence suggests that DNA and RNA viruses can compartmentalize viral and host factors to enhance their replication<sup>372</sup> and manipulate immune responses.<sup>373</sup> A wide variety of terminologies are used for these viral events, including LLPS,<sup>374</sup> biomolecular condensates,<sup>372, 375</sup> processing bodies,<sup>373, 376-379</sup> cytoplasmic membrane-less organelles,<sup>380-382</sup> stress granules (SG),<sup>383-385</sup> cytoplasmic Virion Assembly Compartments (cVACs),<sup>386-388</sup> or nucleocapsid assembly sites/inclusion bodies (IB).<sup>372, 389, 390</sup> Condensates are induced through multiple factors, including cellular pH, rapid increase in host cell nucleic acid concentrations, binding of heat shock proteins (HSP70), and activation of host kinases, including double-stranded RNA-dependent protein kinase (PRK).<sup>391, 392</sup>

DNA viruses (such as herpesvirus<sup>388</sup>) utilize nuclear inclusion bodies to transcribe the viral genome and cVACs for virion assembly and maturation.<sup>374</sup> Herpes Simplex Virus 1 (HSV-1) progeny are assembled in membraneless viral replication compartments within the nucleus,<sup>393</sup> demonstrating the properties of LLPS.<sup>374, 394</sup> RNA viruses such as Respiratory Syncytial Virus (RSV),<sup>395</sup> Human Metapneumovirus (HMPV),<sup>396</sup> and Human Immunodeficiency Virus (HIV-1)<sup>397</sup>

also utilize bimolecular condensates. During RSV infection, the NF $\kappa$ B protein, p65, translocates to inclusion bodies containing viral components,<sup>395</sup> enhancing proinflammatory signaling and the host immune response<sup>398</sup>. Conversely, RSV sequesters host proteins *O*-GlcNAc transferase (OGT) and phosphorylated p38.<sup>399</sup> Retaining p38 to the condensate impairs p38-induced MAPK2 activity, limiting NF $\kappa$ B signaling.<sup>391</sup> Most viruses intersect with the NF $\kappa$ B pathway. Therefore, it is tempting to postulate that they all likely directly impact host kinase localizations and activities through PRK activation and Ub-mediated LLPS formation.

### **3. Tools Developed to Study Spatial Signaling.**

To study the critical transient biochemical events that regulate subcellular signal transduction, a variety of tools have been developed that allow real-time reporting of compartmentalized events or augmentation of trafficking machinery. Many of these tools are genetically encoded optical biosensors designed to use fluorescence as a readout for a biochemical event, such as kinase phosphorylation. These biosensors have a kinase-responsive component that induces changes in conformation, altering fluorescence that can be detected by high-resolution microscopy. Fluorescence Resonance Energy Transfer (FRET) is a proximity-dependent energy transfer from a donor molecule to an acceptor molecule via dipole-dipole interactions. This electrodynamic phenomenon is frequently utilized in biosensor designs because for FRET to occur, the donor molecule must be within close physical proximity to the acceptor molecule, directly enabling the development of sensitive, specific biosensor reporters (*Fig. 1.2.3*). The field of genetically encoded biosensors is extensive and has been excellently reviewed elsewhere.<sup>400</sup> Here we will focus on some of the ways that fluorescence and FRET-based biochemical tools allow us to study subcellular kinase signaling.

**Single and Tethered Fluorophore Activity Reporters.** Single fluorophore biosensors are straightforward methods of detecting biochemical activity through the integration of a molecular switch on the beta-barrel of a fluorophore that alters fluorescence emission based on biosensor conformation (*Fig. 1.2.3A*). A strength of these reporters is that they can be multiplexed in a single cell to measure multiple cellular processes simultaneously, for example, the detection of PKA, PKC, and ERK signaling.<sup>401</sup> Single-fluorophore kinase activity reporters can also elucidate compartmentalized kinase signaling through fluorescence changes rather than translocation. An example is the excitation-ratiometric AMPK activity reporter (ExRai AMPKAR), which detects endogenous AMPK in this manner. The biosensor was directed to measure cytoplasmic, lysosomal, mitochondrial, and nuclear AMPK.<sup>333</sup>

Kinase translocation reporters (KTRs) are used to study kinase activity via their design of a fluorophore fused to a kinase substrate and a bipartite nuclear localization signal (bNLS) and nuclear export signal (NES). The sensor's phosphorylation imparts a negative charge that modulates nuclear import/export. KTRs facilitate rapid kinase activity measurement as a cytoplasmic to nuclear ratio of fluorescence and can be multiplexed to track multiple kinases in a single cell when using spectrally separated fluorophores but are nonspecific to kinase distribution within the cell.<sup>402</sup>

Tethered fluorophore biosensors utilize FRET to report kinase activity. This reporter class was first used to detect Ca<sup>2+</sup> signaling using a calcium-sensing calmodulin linked to a peptide derived from the myosin light chain, between a blue fluorescent protein and YFP.<sup>403</sup> Sensitivity was enhanced by exchanging the fluorophores for enhanced YFP (EYFP) and enhanced cyan fluorescent protein (ECFP),<sup>404</sup> the general design of which became the basis for subsequent biosensors, including kinase activity reporters. Alternatively, “bait” substrate amino acid sequence

specific for a kinase of interest can be linked to a flexible peptide containing a phosphoamino acid binding domain linking together a pair of FRET fluorophores. Phosphorylation of the bait substrate by the target kinase causes the phospho-recognition domain to bind to it, facilitating a conformational change in the peptide and drawing the fluorophores into close proximity where FRET can occur (*Fig. 1.2.3B*). Tethered-fluorophore kinase activity reporters have been designed and utilized for many kinases, from PKA, PKC, PKB/Akt, MTORC1, aurora kinases, ERK1/2, and p38.<sup>48, 334, 347, 405-412</sup> These activity reporters have been further refined as improved fluorophores are designed and implemented. Critically, the growing library of kinase reporters can be further modified with subcellular localization motifs that direct the activity reporters to other subcellular locations such as lipid rafts, the plasma membrane, endosome, mitochondria, or nucleus.<sup>358, 362, 413, 414</sup> An online database listing many of these biosensors can be found at <https://biosensordb.ucsd.edu/>. Spatial targeting of these biosensors enables detailed studies of how biomolecular factors control kinase associated with organelles within each cell, revealing key insights into spatiotemporal dynamics of kinase activity and how they drive disease-inducing signaling transduction.<sup>347, 358, 371, 412</sup>

**Tools to Study Subcellular Kinase Activity.** Aside from kinase activity reporters, investigators have developed novel tools to delineate and better understand kinase substrate availability and the subcellular context of signaling. Using a genetically encoded system of rapamycin-induced endosomal redistribution, fusion proteins anchored in the endosome and plasma membrane can be manipulated to direct the endosome to the cell periphery (*Fig. 1.2.3C*). Using this model, the investigators uncovered the functional roles of PDE-mediated cAMP hydrolysis and location-specific PKA activity.<sup>359</sup> To better understand compartmentalized PKA signaling and cAMP-

degrading phosphodiesterase (PDE) activity, investigators developed FRET nanorulers to measure nanometer-size cAMP gradients in intact cells. These nanorulers consist of a FRET-based cAMP reporter (Epac1-camps)<sup>415</sup> and a PDE, separated by single alpha-helices (SAH) of set nanometer length (**Fig. 1.2.3D**). These rigid ER/K helices allow for precise measurement of the distance between active PDEs and cAMP biosensors, representing molecular rulers to measure the size of low cAMP pockets generated by PDE activity. These were subsequently used to determine that cAMP buffering<sup>416</sup> and local PDE activity can “protect” cAMP effectors from activation until cAMP concentrations are sufficiently high to overcome buffering and initiate signaling responses.<sup>417</sup>

#### **4. Roles of Kinase in Cellular Compartments and Their Impact on Physiology**

As our understanding of the mechanism driving the spatial compartmentalization of kinases and the tools to detect the spatial bias are refined, so is our understanding of the physiological and pathophysiological impact. Below, we discuss some of the latest studies describing compartmentalized signaling utilized in physiology and how mutations that disrupt or alter kinase localization can result in disease.

Since their discovery as modulators of PKA and other kinase activity, AKAPs have long been considered attractive avenues for therapeutic intervention, as AKAPs play key roles in cancer, ischemic stroke, and cardiovascular pathologies such as cardiac hypertrophy, heart failure, and hypertension,<sup>297, 418, 419</sup> among others. These diseases generally arise from mutations or changes in the expression of the AKAP proteins, causing them to lose or alter function, leading to mislocalized or loss of effective PKA signaling, substrate sequestration, or dysregulated increases in signaling responses. For example, AKAP-Lbc is needed for both cardiac development as it localizes to the cytoskeleton and scaffolds with many kinase binding partners, but is also responsible for the

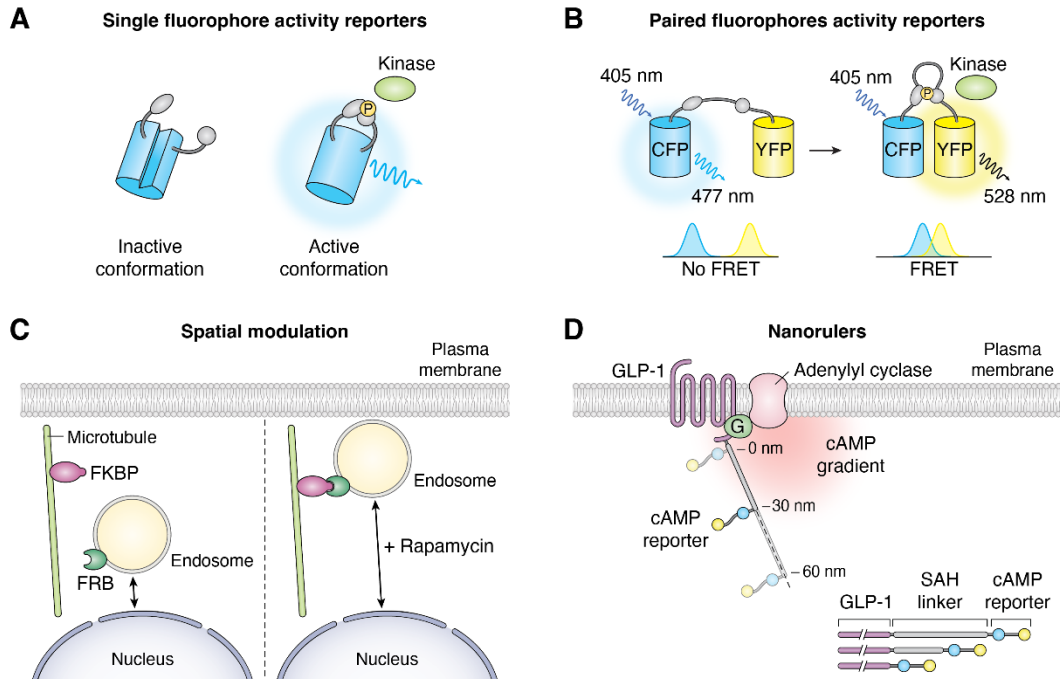


**Figure 1.2.3: Kinase Activity Imaging Tools with Subcellular Resolution**

**A.** Single fluorophore activity reporters. This type of reporter utilizes a circularly permuted fluorophore tethered to a sensing unit composed of a kinase-specific substrate and phosphoamino acid binding domain (PAABD). Phosphorylation of the substrate results in conformational change in the fluorescent protein, altering fluorescence readout. **B.** Paired fluorophore activity reporters. This type of reporter utilizes tethered fluorophores joined by a linker peptide containing a kinase-specific substrate and PAABD. Phosphorylation of the substrate results in a conformation change of the peptide, bringing the fluorophores into close physical proximity, allowing for transfer of fluorescence energy from the donor (CFP) fluorophore to the acceptor (YFP) and detection of kinase-mediated FRET activity via acceptor emission. **C.** Spatial modulation. This rapamycin inducible system modulates endosomal localization using early-endosomal antigen 1 (EEA1)-tethered FK506-binding protein-rapamycin-binding (FRB) fused to GFP alongside a plus-end-directed kinesin motor Kif1a fused to a FK506-binding protein (FKBP) and tandem dTomato, mediating microtubule and kinesin motor directed migration of endosomes away from the nucleus. **D.** Nanorulers. This system utilizes fluorescence biosensors such as Epac1-camps separated by rigid single-alpha-helical (SAH) domain linkers of set size to measure cAMP gradients at different locations within the cell.

development of pathological myocyte hypertrophy when upregulated, due to an increase in MEF2-mediated transcriptional reprogramming.<sup>420-422</sup> Conversely, loss of AKAP-Lbc via miR-629-5p results in malignant prostate cancer.<sup>423</sup> Mutations in PKAc itself, however, can also alter localization, leading to disease. An example of these is the PKAc<sup>W196G</sup> mutation that increases kinase affinity for RI-type regulatory subunits and their associated AKAPs, resulting in Cushing's syndrome.<sup>424</sup>

AMPK is an essential energy sensor and master regulator of cellular metabolism that is subcellularly localized to monitor and react to cellular energy states and response to stress.<sup>425</sup> Zong *et al.* investigated how signaling cues regulate differential subcellular AMPK activation.<sup>343</sup> They discovered that early-stage glucose starvation leads to lysosomal AMPK activation via the aldolase-v-ATPase-Regulator-AXIN-LKB1 complex, leading to phosphorylation of downstream substrates. However, moderate starvation increased AMP levels corresponding with lysosomal and cytosolic AMPK activation, whereas severe energy stress resulted in high levels of AMPK activity in the cytosol, lysosome, and mitochondria. In addition to this work, it was also shown that phosphorylation of AMPK $\alpha$  also drives the kinase to the nucleus in response to stimulation by leptin, a hormone involved in energy regulation.<sup>339</sup> These results indicate a novel mechanism for functional spatial kinase distribution as a sensor of metabolic stress response.<sup>343</sup>

**Differential Signaling and Pathological Outcomes by GPCR-Activated Kinases.** Active GPCRs facilitate the recruitment of G-protein-coupled receptor kinases (GRK)s to the plasma membrane, where they bind to and phosphorylate the GPCR. Phospho-patches then recruit arrestins, which can initiate desensitization, receptor internalization, and internalized signaling.<sup>426</sup><sup>427</sup> GRKs have additional roles; for example, GRK5 possesses an NLS motif enabling nuclear translocation in myocytes to facilitate maladaptive growth and fibrosis in a calcium/calmodulin

(CaM) dependent manner.<sup>428</sup> Alternatively, GRK2 in cardiac tissue is shown to translocate to the mitochondria during myocardial ischemia and oxidative stress in an ERK and HSP90-dependent manner, driving alteration of mitochondrial substrate utilization.<sup>429-432</sup> GRK2 mitochondrial translocation also occurs in response to LPS, leading to increased mt-DNA transcription, reduced ROS, and cytokine expression<sup>299</sup> during inflammatory disease. Much remains unknown about kinase substrate pools in the mitochondrial compartment in a disease context, and further research is needed.

The original models for GPCR desensitization required GRK phosphorylation and GPCR internalization to the endosome principally to terminate signal transduction. However, it's clear that the signaling landscape of internalized GPCRs is diverse and facilitates subcellular compartmentalized kinase signaling. Ligand-stimulated, internalized  $\beta$ 2-AR facilitates Gas-mediated ERK activation at the endosome, regulating cell proliferation through nuclear-transported ERK and upregulation of substrates like nuclear c-Myc. These findings identify a functional role for internalized signaling and could be linked to cancer progression.<sup>358</sup>

Conversely, stimulation triggers spatially distinct pools of MAPK p38 activation. P38 has over 100 substrates and is responsible for physiological cell development, growth, injury responses and dysregulated pathological inflammation.<sup>35</sup> Much research has gone into deciphering the context of p38 signaling in health and disease to identify novel therapeutic strategies. Recent studies argue that adaptor binding and spatial distribution is central to the physiological and pathological outcomes. The clear nuclear-cytosolic distribution of p38 differentially controls access to subsets of substrates.<sup>363</sup> It remains a matter of intense research to define how the conserved dually phosphorylated p38 can be switched to pathological outcome in both the classical and atypical p38 pathways and what differentiates them. One possibility is that spatially selective

substrates/adaptors can allosterically modulate the binding potential for secondary targets of p38.<sup>263, 264, 433</sup> One example is the spatiotemporal signaling bias exerted by TAB1-dependent p38 autophosphorylation.<sup>347</sup> FRET biosensors revealed that atypical p38 is differentially localized, displaying enhanced cytosolic activity and restricted nuclear access,<sup>347</sup> disrupting access to key nuclear targets and increasing access to cytosolic targets. The direct TAB1-p38 $\alpha$  interaction drives atypical p38 signaling-dependent vascular inflammation and edema,<sup>31, 32, 434</sup> cardiac ischemic damage,<sup>71, 81, 86</sup> amyloidosis,<sup>206</sup> dermal inflammation,<sup>85</sup> and viral replication.<sup>135</sup> Further studies are required to determine the molecular mechanisms of signal transduction in each case and whether a conserved spatial bias is critical to driving these pathologies.

**Kinases Involved with Liquid-Liquid Phase Separation Drive Physiological Processes and Disease.** Ribonucleoproteins (RNPs) and other LLPS-driven cellular mechanisms are increasingly studied for their roles in physiology and disease.<sup>435</sup> We've discussed how LLPS mechanisms sequester kinases, but kinases also play key roles in the formation, function, and maintenance of LLPS [Table. 1.2.1]. The centromere, essential for cell division, contains disordered histone tails that cause it to exhibit macromolecule phase separation and interact with nucleosomes. Kinase activity within the inner centromere is driven by LLPS activity,<sup>436</sup> and in turn, both LLPS and phosphorylation via Aurora kinases drive effective centromere function during mitosis.<sup>437</sup> Similarly, viral infections rapidly increase the amount of cytosolic nucleotides, whose negative charge and multivalency promote RNA-protein and protein-protein interactions, inducing phase separation into LLPS. The condensed nucleotides drive local nucleotide concentrations higher, activating double-stranded RNA-dependent protein kinase (PKR) and PKR-like endoplasmic reticulum kinase (PERK) at the ER to initiate the integrated stress response (ISR) and formation of stress granules and the antiviral responses.<sup>438</sup> However, multiple viruses also manipulate the

<b>Kinase</b>	<b>Type of Condensate</b>	<b>Mechanism of Kinase-condensate localization</b>	<b>Reference</b>
<b>Plk4</b>	Centriole assembly	Phosphorylation-dependent intrinsic phase separation	439
<b>PKA</b>	Condensates with cAMP	R $\alpha$ -mediated intrinsic tendency	370
<b>MARK2</b>	Condensates with Tau protein	Possibly recruited by substrate TAU	440
<b>FAK</b>	Integrin-mediated adhesion complex	Intrinsic scaffolding with p130Cas	441
<b>TBK1</b>	Polyubiquitin condensates	Recruited by adaptor proteins	442
<b>ULK1</b>	Polyubiquitin condensates	Recruited by adaptor proteins	443-445
<b>TNK1</b>	Polyubiquitin condensates	Kinase-intrinsic ubiquitin-binding domains	446
<b>RTKs</b>	RTK-mediated LLPS	Intrinsic phase separation tendency	447
<b>S6K1/2</b>	Stress granules	Mechanism unclear, possible interaction with adaptor proteins	448
<b>PKC</b>	Stress granules	P-body associated scaffold proteins G3BP2	449, 450
<b>PKR</b>	Stress granules	P-body associated scaffold proteins G3BP1	451
<b>DYRK3</b>	Stress granules	N-terminus dependent localization to stress granules and intrinsic kinase activity	452
<b>CK2</b>	Stress granules	P-body associated scaffold proteins G3BP1	453
<b>Sky1</b>	Stress granules	Intrinsic phase separation tendency	454
<b>Syk</b>	Stress granules	Phosphorylation-dependent recruitment by Grb7	455
<b>eIF4</b>	Stress granules	Modifies RNA recruitment to stress granules	456
<b>MAPK p38</b>	Stress granules/viral inclusion bodies/anti mycobacterial immune LLPS	Recruitment by substrate, viral-mediated sequestration	399, 457
<b>Lck/ZAP70</b>	T-cell signaling phase-separated droplets	Recruited by TCR	458

**Table 1.2.1:** Kinases associated with LLPS condensates

PKR responses, to enhance viral production, as seen in the case of the Hepatitis C Virus (HCV).<sup>459</sup> Alternatively, other viruses co-opt stress granule (SG) protein G3BP1 to inhibit PKR and prevent ISR.<sup>460</sup> Thus, host kinases can be instrumental in forming and controlling pro- and antiviral SGs.<sup>461</sup>

Processing bodies (P-bodies) are formed transiently in the cell from untranslated mRNA associated with decay machinery and other protein interactors in response to stimuli. Protein kinase recruitment to these particles initiates signaling responses, sequestering kinases away from other substrates during cellular responses and stabilizing key proteins co-localized to the granules. PKA is a key regulator of P-body assembly and is hypothesized to regulate the formation of larger P-body aggregates by phosphorylation of Pat1, a key constituent of p-bodies.<sup>462</sup> NF $\kappa$ B is also involved in the formation of p-bodies. I $\kappa$ B complex IKK controls p-body formation through binding and phosphorylation of enhancer of decapping 4 (EDC4), leading to recruitment of mRNA-decapping enzyme complex subunit 1a and 2 (DCP1a and DCP2). In the absence of stimulus, the IKK-EDC4 complex promotes the degradation of pro-inflammatory mRNAs, indicating diverse roles of kinases within p-bodies.<sup>463</sup>

Subcellular kinase activity can dynamically control LLPS condensates,<sup>464</sup> where phase separation is both positively and negatively affected by phosphorylation, controlling both aromatic-cationic and aromatic-aromatic interactions.<sup>465</sup> For example, DNA-dependent protein kinase (DNA-PK) phosphorylates the neurodegeneration-linked RBP Fused in Sarcoma/Translocated in LipoSarcoma (FUS) protein,<sup>466-468</sup> interrupting phase separation and reducing binding affinity to low complexity domain hydrogels.<sup>469-472</sup> Conversely, Tau protein binds RNA and induces fibrilization, which forms insoluble neurofibrillary tangles during Alzheimer's disease.<sup>473-475</sup> Serine phosphorylation of the microtubule-binding region of Tau protein by microtubule-affinity regulating kinase 2 (MARK2) kinase promotes LLPS of Tau

protein<sup>476</sup> and possibly contributes to the pathology. Further studies are needed to determine if targeting kinase activity for LLPS modulation could perturb disease progression or offer novel therapeutic avenues.

## **5. Conclusions and Ongoing Challenges**

It is becoming increasingly clear that current therapeutic strategies fall short for certain valuable kinase targets. Defining the mechanisms that control the spatial and temporal control of kinases and their impact on subcellular compartments represent a relatively untapped focus of therapeutic development. As described above, there is a growing acceptance that spatially distinct signaling defines the pathological bias in kinase signal transduction.

However, there are many ongoing challenges in studying spatial kinase activity. For one, it is difficult to identify substrate pools specific to subcellular localization and directly correlate endogenous, localized kinase activity with their substrates. Additionally, the spatial regulation of phosphatase, proteases, and specific localized substrate access requires the development of additional tools. One of the benefits of utilizing biosensors to detect kinase activity is it allows the study of endogenous protein kinase without their overexpression and the associated potential for off-target effects. However, exogenous expression of the biosensor itself could also trigger secondary effects by introducing foreign proteins to a balanced system or taking up essential “space” on membranes. This sterically blocks access for endogenous proteins, nudging signaling out of its endogenous temporal or spatial state. The “bait” kinase reporters are typically derived from native proteins and therefore could outcompete endogenous kinase substrates.

Additionally, subcellular biosensor targeting can lead to overexpression or saturation at the location of interest, possibly leading to false reports of FRET activity as tethered fluorophores from different individual molecules emit FRET from interactions in *trans*. As brighter

fluorophores are developed, expression can be minimized to avoid saturation. Additionally, these studies are typically performed *in vitro* and imaging *in vivo* remains challenging due to low penetrance of fluorescence through complex tissues. This is being addressed through alternative imaging strategies such as multi-photon excitation systems<sup>477-479</sup> and fluorophore pairs that excite and emit near the infrared spectrum.<sup>480</sup>

Spatial signaling offers an opportunity to personalize kinase inhibitors to a specific subset of pathological kinase responses. For example, MAPK p38 $\alpha$  is an extensively studied kinase, and several recent reviews have covered the kinase's roles and therapeutic potential for cancer,<sup>150, 481</sup> arthritis,<sup>482</sup>, viral regulation,<sup>61, 483</sup> and other inflammatory disorders.<sup>484</sup> However, clinical trials for small molecule drug inhibitors of p38 $\alpha$  have largely failed in the clinic. For p38 $\alpha$ , this research is increasingly focused on MK2.<sup>140, 482, 485</sup> With greater knowledge of the mechanisms of kinase sequestration and access to substrate pools, we suggest there is the potential to develop strategies that block subsets of kinase activity associated with pathological outcomes. A molecular mechanism driven by GPCR polyubiquitination and recruitment of the active kinase to the endosome via TAB1 binding and autophosphorylation has recently been discovered.<sup>31, 32</sup> However, therapeutic targeting of spatially restricted MAPK has remained underexplored.

Conversely, spatially targeted Plk1 or Aurora A kinase (AurA) inhibitors (Local kinase inhibitors, LoKI) can selectively block kinase activity, disrupting microtubule-kinetochore functions.<sup>486</sup> Establishing a valuable tool to study spatial signaling and setting a precedent for the future development of other LoKI. However, clinically viable spatially targeted LoKI have yet to be developed.

An alternative emerging therapeutic strategy in perturbing kinase activation is the modulation of LLPS condensates. This field is rapidly growing as we learn how kinases are

recruited to condensates, which are similarly essential for kinase function.<sup>366</sup> The protein-protein biophysical interactions between IDRs that induce LLPS play key roles in diseases such as Alzheimer's, ALS, Huntington's disease, and other neurological conditions. Many groups are now investigating the interruption of LLPS as a therapeutic strategy.<sup>487</sup> LLPS could be controlled by targeting kinase activity responsible for nucleation of LLPS condensates or through selective targeting of subsets of kinases trafficked to condensates via co-localization of small molecule inhibitors to condensates.

The development of selective and efficacious therapeutics that target the adaptors or scaffolds for subcellular location may be challenging as, in many cases, the molecular drivers of kinase activity are conserved. However, spatially targeted inhibition represents an exciting, relatively untapped approach to selectively block pathological signaling and potentially reduce some of the current strategies' toxicity or off-target impacts.

In summary, a wide range of finely tuned processes regulate the cell's kinase activity. A greater understanding of the mechanisms that drive spatial and temporal kinase activity and the development of advanced tools to visualize and dissect their dynamic activation will likely provide essential insight into how dysregulated kinase signaling drives disease. Critically, these studies are essential to inform the future development of spatially targeted therapeutics.

## CHAPTER 1

### Part 3

#### INFECTION-INDUCED ACUTE LUNG INJURY, THE ROLES OF KINASE SIGNALING IN ACUTE LUNG INJURY, AND GOALS OF THIS WORK

Here, we will review the pathology and progression of acute lung injury, the specific etiology of infection-induced acute lung injury with emphasis on influenza, and the roles of kinase signaling both in response to infection and the roles in its progression. Lastly, we will state the goals of this dissertation research.

#### **The Pathology and Progression of ALI**

Acute lung injury (ALI) and acute respiratory distress syndrome (ARDS) are life-threatening inflammatory disease manifestations in the lung that are caused either by a direct insult from local viral or bacterial infection, physical injuries such as aspiration, burns, and trauma, or indirectly via systemic infection such as sepsis. This syndrome of pathological conditions is driven by dysregulated inflammation, primarily transmitted through the expression of pro-inflammatory cytokines. Subsequently, the breakdown of the epithelial barrier leads to edema in the lungs, resulting in loss of gas exchange function, with low oxygen levels in the blood (hypoxemia), and high levels of carbon dioxide (hypercapnia) and overall reduced pulmonary compliance leading to shortness of breath and increased impact for breathing.<sup>488, 489</sup> This loss of homeostasis and breaching of the epithelial barrier is perpetuated further by the release of proinflammatory cytokines and chemokines from responding innate immune cells and the vasculature itself, leading to the recruitment of immune

mediators such as monocytes to the lungs, which directly contributes to epithelial cell apoptosis<sup>490</sup>. The process of inflammatory signaling and recruitment becomes a self-perpetuating cytokine storm. This, and the physical stress resulting from mechanical ventilation needed to sustain breathing, leads to hyaline membrane formation and lung tissue fibrosis, a dysregulation of the wound-healing process<sup>491</sup>. Wound healing is carried out by myofibroblasts, which are fibroblasts that have differentiated by the secretion of TGF- $\beta$ 1 and mechanical stress response<sup>492</sup>. These cells synthesize components of the extracellular matrix (ECM) during the restoration of lung tissue and, under normal circumstances, are eliminated via apoptosis following resolution of inflammation. However, during the prolonged inflammation of ALI, myofibroblasts do not undergo apoptosis and become hyperproducers of ECM, resulting in pulmonary fibrosis and, ultimately, permanent loss of lung function<sup>493, 494</sup>.

Therefore, ALI/ARDS is a disease state that arises in response to a primary injury or illness, and the discreet players of ALI may differ depending on the origin of the disease. For example, physical or mechanical injury, such as ventilator-induced lung injury (VILI) occurs when the patient experiences stress due to high transpulmonary pressure, leading to excessive strain from overdistension of the lungs. This triggers epithelial stretch responses that result in expression of early growth response gene (Egr)1, heat-shock protein (HSP)70, IL-1 $\beta$  and macrophage inflammatory protein (MIP)-2, inducing an innate immune response<sup>495, 496</sup> where recruited neutrophils and monocytes drive the induction of VILI through IL-8 and MCP-1-signaling<sup>497, 498</sup>. Infection-induced ALI, on the other hand, contends with the presence of pathogens that have evolved mechanisms for hijacking and subverting host immune responses, often leading to further inflammatory dysregulation. In the next section, we will focus on how virus infection, particularly influenza, propagates ALI, beginning with an overview of influenza viral infection and replication.

## **Brief Introduction to Influenza A Virus**

Influenza A virus (IAV) is a segmented, single-stranded RNA virus encapsulated in a lipid envelope with surface glycoproteins hemagglutinin (HA) and neuraminidase (NA) that are essential for viral infection of host cells. The sloppy but rapid viral polymerase of IAV results in a high mutation rate and replication rate that allows the virus to quickly adapt to environmental changes and escape immune detection. For this reason, influenza is endemic in human populations and is one of the most common viral infections of the lung<sup>499, 500</sup>. Influenza viral infection is initiated when viral HA protein binds to 2-6 linkage sialic acid residues on the host cell surface. Virions, after binding to their “receptors” are internalized and trafficked to the endosome, where endosomal acidification facilitates conformational change in HA proteins, facilitating viral particle release of vRNPs and proteins into the cell. These vRNPs possess nuclear localization motifs and utilize cellular importin alpha and beta proteins to translocate to the nucleus where viral mRNA is produced. Viral proteins are translated from either the cytosolic ribosomes (PB1, PB2, PA, NP, NS1, NS2, and M1) or from the endoplasmic reticulum-associated ribosomes (HA, NA, and M2), where lipid membrane-bound protein is translocated to the plasma membrane for viral packaging and budding. The PB2 subunit of the viral mRNA transcription complex binds to the 5' caps of host cell mRNA, cleaving off these caps to act as primers for viral mRNA transcription, a process termed “cap-snatching” in order to stabilize production of its own mRNA<sup>501</sup>. Viral replication and viability is an important aspect of viral fitness in the host, as a virus whose growth is retarded or cannot form complete infectious virions is more easily cleared by the body. Following translation of viral polymerase components PA, PB1, PB2, and NP, these are translocated back to the nucleus. vRNPs are translocated out of the nucleus and to the plasma membrane via association with cellular Rab11.

Although the exact mechanisms of vNRP enrichment at the plasma membrane are unknown, the virions are assembled at sphingosine and cholesterol-rich rafts<sup>502</sup>. The IAV cycle of infection, replication, and egress is dependent on proper trafficking of viral vNRP and proteins, which is dependent on the virus' fitness for hijacking host cellular processes, such as host kinase activity.

### **The Etiological Signature of Viral Infection-Induced ALI.**

Severe infections in vulnerable populations or with pathogenic viral strains can result in rapid onset of ALI<sup>503</sup>. This occurs when alveolar type 1 and 2 epithelial cells become infected and lead to loss of sodium pump activity and thus osmotic homeostasis, and development of pneumonia and damage to tight junctions. Additionally, infected cells contribute to production of inflammatory cytokines<sup>504</sup>, which rapidly increases as infection progresses. Alveolar macrophages are the first-responders to influenza infection, and rapidly secrete Type I interferons (IFNs) for the recruitment of inflammatory monocytes and generation of the early-infection antiviral state<sup>505, 506</sup>. The endothelium surrounding the lungs is sensitive to infection or tissue injury, triggered by stimuli such as inflammatory cytokines like TNF $\alpha$ , interleukins and interferon- $\gamma$ , or pattern recognition receptor (PRR) activation. The morphological and functional changes that occur in the endothelium upon stimulation by pathogen-associated molecular patterns (PAMPs) or damage-associated molecular patterns (DAMPs), which are present during infection is termed as endothelial activation<sup>507</sup>. In this manner, the endothelium acts as a sentinel for the immune system. During severe influenza infection and pneumonia, the endothelium becomes a key mediator of cytokine and chemokine production and expression of E-Selectin and P-selectin, which contribute to the recruitment of leukocytes and damage to the alveoli<sup>503, 508</sup>. Endothelial activation also shifts the endothelium to a prothrombotic

state, inducing intravascular coagulation and the generation of the protease thrombin which subsequently triggers inflammatory signaling and endothelial barrier disruption<sup>509, 510</sup>. The onset of ALI in some cases of severe influenza infection have been shown to occur due to a dysregulation in the type of immune cells recruited, such as in patients who had reduced monocyte recruitment after infection, leading to worse influenza outcomes<sup>511</sup>.

The stepwise manner in which infection accelerates deterioration of lung homeostasis, beginning when the epithelial layer is breached and resulting in innate immune activation and strong endothelial response which escalates the inflammatory and immune response, can be modeled in mice using strains of influenza adapted to mouse infection<sup>512, 513</sup>, and is also evidenced in intratracheal models of bacteria infection<sup>514</sup>.

In the next sections, we will introduce how kinase signaling mediates and drives both pulmonary virus infection and host-mediated ALI.

### **Kinase Activity, Downstream Signaling, and ALI**

At the core of the disease, ALI is perpetuated by cell signaling pathways, which are mediated by kinase activity. Following infection, the activation of the endothelium occurs when innate immune cells secrete initiation factors TNF $\alpha$  and IL-1 $\beta$ , and the resulting release of thrombin initiates downstream signaling of Nuclear factor kappa-light-chain enhancer of activated B cells (NF- $\kappa$ B) and mitogen activated protein kinase (MAPK) pathways<sup>515</sup>.

These pathways, in turn, drive the endothelial dysfunction through increased leukocyte-endothelial cell interactions, loss of vascular integrity, and coagulation processes through transcription<sup>516</sup>. However, these signaling events are not homogeneous or redundant, but rather, downstream kinases are simultaneously activated and trafficked differentially depending on the

stimulus of origin. For example, the release of thrombin induces cleavage of the extracellular GPCR domain of PAR1 to stimulate G protein signaling, resulting in a spread of kinase activity. G $\beta\gamma$  leads to phosphatidylinositol 3 kinase (PI3K)/Akt activation, leading to subsequent IKK complex phosphorylation and the release of RelA/p65 for transport to the nucleus and activation of transcription factors, while G $\alpha_q$  leads to downstream activation of PKC, c-Src, and the activation of MAPK p38. Yet, the signaling outcomes and initiated pathways are cell- and receptor-specific. NF- $\kappa$ B and MAPK pathways are also activated through different downstream pathways when stimulated by TNF $\alpha$ , signaling through its receptor via PI3K $\gamma$  to activate PKC $\zeta$ , leading to NADPH-mediated reactive oxygen species formation, triggering degradation of I $\kappa$ B $\alpha$  and RelA/p65 nuclear translocation, while p38 is separately activated downstream of PKC $\delta$ .<sup>515</sup> These branching kinase signaling pathways are complex, and represent a major question in the field of kinase signaling and the progression of ALI: which signaling events drive which specific downstream events, and can targeted inhibition of subsets of inflammatory kinase signaling result in improved therapeutic outcomes? To explore this question, we will now focus on a major driver of influenza-induced ALI, MAPK signaling, with a focus on p38.

### **MAPK Signaling Drives ALI**

The focus on MAPK signaling for this work is rooted in the multi-faceted roles this pathway plays in disease propagation, both from the side of the host and from the virus itself. P38 in particular plays a key role in the progression ALI (**Fig. 1.3.1 A**).

MAPK signaling is an essential modulator of innate immune cells during ALI. MAPKs ERK, JNK and p38 increase macrophage expression of heme oxygenase-1 (HO-1) via nuclear factor erythroid 2-related factor 2 (Nrf2), promoting the production of Type 1 IFNs<sup>517,518</sup>. MAPK p38 activity shifts

macrophages toward an M-1 like, or proinflammatory polarization, and has not shown to be involved in M-2, or anti-inflammatory macrophage polarization <sup>519, 520</sup>.

P38 drives vascular destabilization during ALI. Microtubule-associated protein 4 (MAP4), a tubulin assembly-promoting protein, is necessary for preserving cell-cell junctional structures in the endothelium. In *in vitro* studies in human pulmonary microvascular endothelial cells (HPMECs) exposed to TNF $\alpha$  or LPS (triggering TLR-4 activation) p38 phosphorylates MAP4 directly <sup>521</sup>.

P38 plays roles in lymphocyte activation and chemotaxis to sites of infection. The kinase, through MK2-mediated cytosolic accumulation of Human antigen R (HuR), a posttranscriptional regulatory factor, modulates the expression of intracellular cell adhesion molecule-1 (ICAM1) expression, leading to increased neutrophil adhesion to the endothelium <sup>522</sup>. Additionally, p53 is a direct target of p38, leading to its accumulation and positively regulating ICAM-1 expression in part alongside NF- $\kappa$ B signaling <sup>523, 524</sup>. HuR binds to AU-rich element (ARE) found in the 3' untranslated regions of mRNA, and influences the half-life and translation of mRNAs such as TNF $\alpha$ , COX-2 and TLR4 <sup>525, 526</sup>. Indeed, p38's function in post-translational regulation via MK2 and HuR may function as a key factor in the positive feedback loops associated with ALI progression. HuR also binds to and protects the mRNA for High mobility group box 1 (HMGB1) <sup>527</sup>. HMGB1 is a DNA binding protein that triggers cytokine expression, potently activates TLR4 signaling and can activate p38, which, in turn, positively regulates HMGB1 expression via IL-1 $\beta$  and TNF $\alpha$  <sup>528</sup>. HMGB1 has also been shown to bind to influenza nucleoprotein (NP), promoting viral growth and enhancing activity of viral polymerase <sup>529</sup>.

P38 drives viral replication. In addition to host-mediated responses during ALI, p38 is also involved in respiratory viral infection and replication. P38 is involved with Sars-CoV and Sars-Cov-2 infection via viral-mediated downregulation of ACE2 expression, leading to inflammation <sup>61</sup>. Sars-

CoV also expresses a viral protein that upregulates p38 *in vitro*, possibly inducing endocytosis of viral receptors that facilitates entry<sup>530</sup>. In the same study, inhibition of the kinase in an *in vitro* lung epithelial cell model reduced viral replication in *Adenoviridae*, *paramyxoviridae*, *Picornaviridae*, and *Orthomyxoviridae* (the family of viruses including influenza A) and was activated ten-fold higher in infection by influenza vs RSV<sup>530</sup>. P38 activity has been shown to be essential for highly pathogenic influenza protein expression, with nearly 90% of viral proteins inhibited by kinase inhibition, concomitant to a reduction in viral-induced cytokine expression<sup>531</sup>.

Kinase signaling is also self-regulating in normal function. In addition to all its roles in propagating pathology, the p38 kinase is also important for the anti-inflammatory response. P38 $\alpha$ , alongside the other MAPK kinases ERK1 and ERK2, activate mitogen- and stress-activated kinases (MSKs) to result in increased transcription of anti-inflammatory cytokines such as IL-10 and IL-1 receptor agonist (IL-1RA) following TLR signaling in macrophages. MAPK-induced MSKs also negatively regulate through induction of expression of dual specificity phosphatases (DUSPs)<sup>532, 533</sup>. For these important reasons, pan-inhibition of kinase function may have unintentionally deleterious effects, such as the loss of anti-inflammatory mediators.

In the next section, we will cover current therapeutic options for treatment of ALI.

### **Current Treatment and Investigations into Therapeutics for ALI**

The most critical component of acute lung injury is the loss of gas exchange, and effective treatment begins at the restoration of the epithelial/endothelial barriers. Current standard of care treatments for lung injury center around careful open lung ventilation strategies, which utilize positive expiratory-end pressure (PEEP) alongside low tidal volume ventilation to prevent alveolar

collapse. However, the heterogeneity of respiratory distress during ALI makes the tuning of PEEP difficult<sup>534</sup>.

Pharmacological interventions for pulmonary injury, including acute phase glucocorticoid therapies<sup>535, 536</sup>, inhaled nitric oxides<sup>537</sup>, the free radical scavenger procysteine<sup>538</sup>, N-acetylcysteine<sup>539</sup> and others<sup>489</sup> have not been successful. Over a decade ago, investigators began to shift away from modulating inflammation to pursuing cell-based therapies, such as bone marrow-derived mesenchymal stem cells, which are able to help repair damaged tissue, alter the secretion of cytokines, and increase rate of alveolar fluid clearance<sup>540</sup>. Other ongoing studies are investigating nanopeptides that target sodium channels to clear alveolar fluid, which show promising results in animal models<sup>541</sup>, but were ineffective in a Phase IIa clinical trial<sup>542</sup>. Conversely, interferon  $\beta$ -1a has been shown to help prevent endothelial leakage and improve patient outcomes in a phase I/II open-label study in the UK, through induction of CD73, an ectonucleotidase which dephosphorylates extracellular AMP to adenosine.<sup>543</sup> However, since this study's completion in 2011 there have been no follow-up studies in ARDS models according to clinicaltrials.gov. Lastly, microRNAs, or small non-coding RNA that control gene expression, could be used or targeted to modulate the main pathophysiological drivers of lung injury<sup>544, 545</sup>.

New therapeutic avenues for exploration are needed. In the previous sections, we introduced atypical p38 signaling as a potent driver of inflammation and ischemic reperfusion injury. However, atypical p38 signaling by interaction with TAB1 remains almost entirely uncharacterized in the lung environment, including inflammatory disease states. We uncovered that the atypical p38 signaling pathway is conserved in human pulmonary microvascular endothelial cells (HPMEC) of the lung when stimulated by GPCR agonists histamine and prostaglandin E2 (PGE2) (**Fig. 1.3.2 A**), which have previously been associated with atypical

signaling in other endothelial cell lines <sup>90</sup>. The conservation of atypical signaling in these cells after GPCR agonist stimulation is indicated by blockade of p38 autophosphorylation (lanes 2,3) by SB203580 (lanes 5,6). As a precursor model to our studies, we investigated if another inflammatory agent, lipopolysaccharide (LPS), induces the secretion of secondary signaling cytokines and GPCR agonists that initiate atypical p38 signaling, **(Fig. 1.3.2 B)**. When stimulated by media from cells that had been previously exposed to LPS, p38 phosphorylation was increased (LPS, 10-25 min), but in cells pre-treated with SB203580 prior to exposure, this phosphorylation was inhibited, and TAB1 migration was shifted down correspondingly (LPS + SB Preinc, 10-25 min). While preliminary, these results indicate that atypical signaling is involved in the complex cellular response following an inflammatory insult, and may thus be a targetable subset of p38 activation in the context of ALI.

### **The Goals of This Dissertation Research**

As we covered in part 1, the study of atypical p38 signaling is a rapidly growing field, with roles for and therapeutic potential for targeting the interaction between TAB1 and p38 becoming better defined. This, paired with the development of novel imaging tools to study endogenous protein-protein interaction with subcellular resolution as was covered in part 2, allows investigators to pursue some of the questions surrounding the molecular regulation of atypical signaling within the cell, and its role in the progression of inflammatory disease. Given the known roles of atypical signaling in endothelial vascular stability <sup>31</sup>, cytokine expression <sup>85</sup>, and inflammatory cell recruitment <sup>199</sup>, a glaring unknown in the field is the role the atypical pathway plays in the lung environment during acute lung injury (ALI) **(Fig. 1.3.1 B)**.

In chapter 3, we utilized a low pathogenicity H3N2 X31 influenza model to explore potential roles of the atypical signaling pathway in the progression of inflammatory lung injury. In the next chapter, we explored another unknown; how atypical signaling is regulated in a subcellular manner.

In summary, the objectives of this work were:

Objective 1: To better understand the spatiotemporal regulation of MAPK p38 (Chapter 2).

Objective 2: To elucidate the impact of TAB1-p38 interaction in the progression of inflammatory lung disease (Chapter 3).

Overall, we hypothesized that atypical MAPK signaling has differential localization relative to canonical signaling, and that spatially driven atypical MAPK drives influenza-induced acute lung injury.

In chapter 4, we will reflect on these findings and interpret how they might fit into the larger questions of atypical p38 signaling as an understudied phenomenon. Lastly, we will suggest future directions for this research.

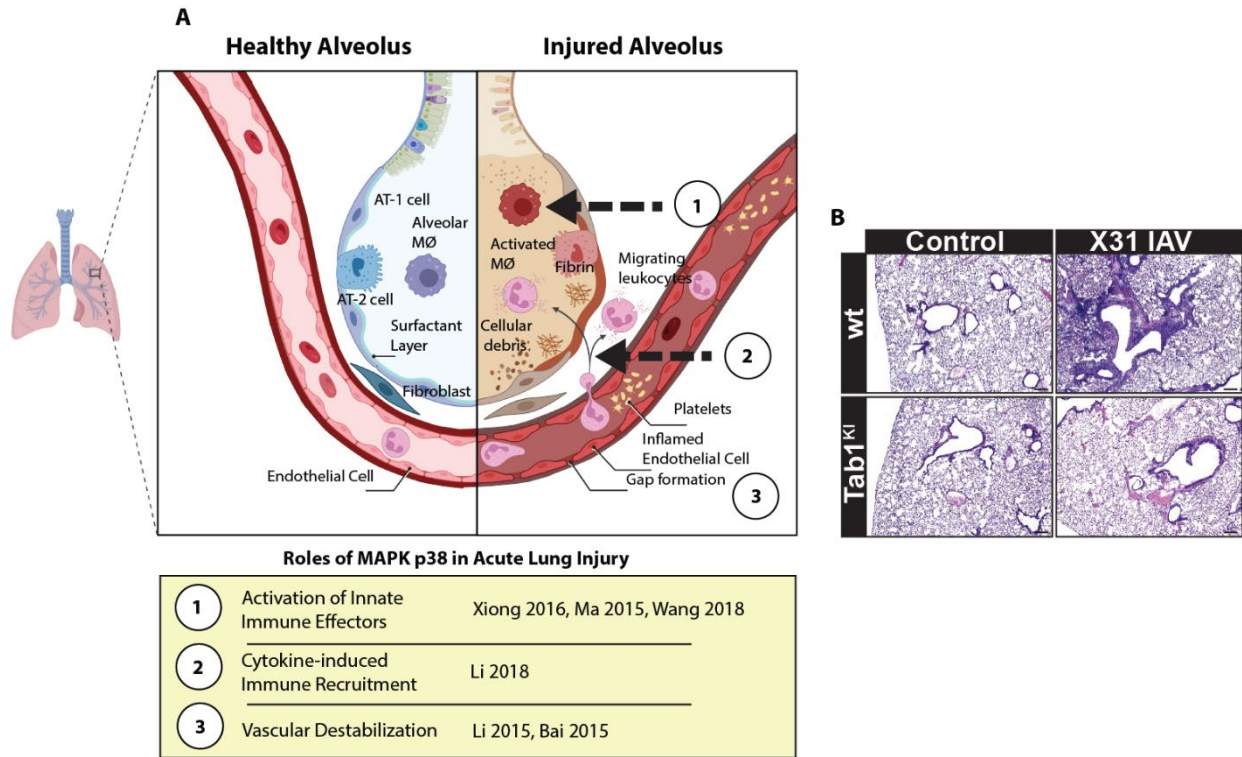
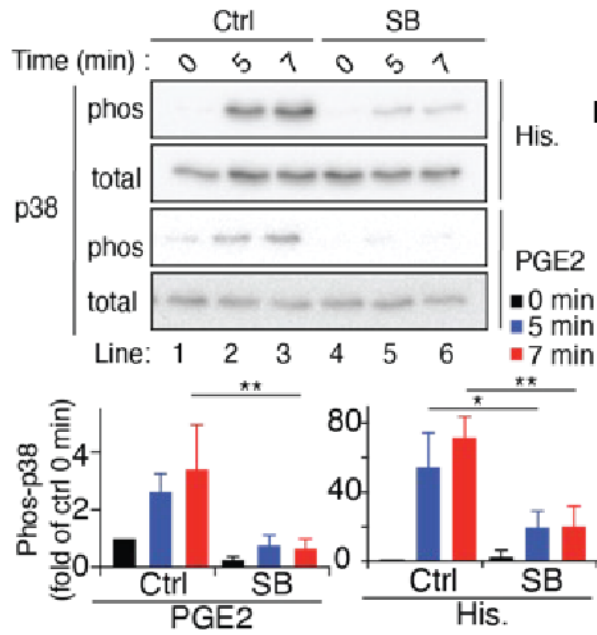


**Figure 1.3.1: P38 is a known therapeutic target for acute lung injury.** A) Model of a healthy lung alveolus and an alveolus during ALI. During healthy lung function, alveolar macrophages (MØ) patrol the alveolus for pathogens, alveolar type-2 cells secrete a layer of surfactant to protect alveolar structure, and a thin barrier between the alveolar epithelium and endothelium is maintained. During ALI, macrophages are activated and secrete cytokines and chemokines that drive immune recruitment and vascular destabilization, leading to barrier disruption, fluid buildup in the alveolus, and loss of gas exchange function. Recruited fibroblasts synthesize components of the ECM, leading to scarring. MAPK p38 is a known driver these processes. B) Hematoxylin and Eosin (H&E) lung tissue slides from wild-type (WT) and TAB1-KI (TAB1<sup>KI</sup>) mice at baseline (control) or following infection with X31 influenza (IAV). Scale bars, 200  $\mu$ M.

A.



B.

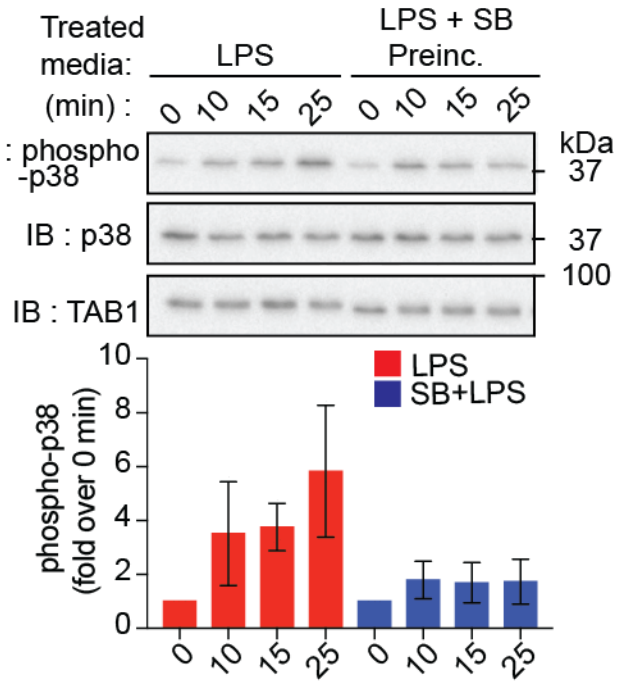


**Figure 1.3.2: Atypical signaling is conserved in human lung endothelial cells.**

A.) HPMEC pretreated with 5 $\mu$ M SB203580. Histamine and PGE2 mediated p38 phosphorylation (lanes 1-3) is blocked by SB203580 (lanes 4-6, quantified in graphs, N = 3, mean +/- SD, \*\* = P < 0.01.) Comparisons made by one-way ANOVA. B.) HPAEC stimulated with media from cells exposed to LPS or pre-treated with SB203580 and exposed to LPS.

## CHAPTER 2

# FLUORESCENCE RESONANCE ENERGY TRANSFER (FRET) SPATIOTEMPORAL MAPPING OF ATYPICAL P38 REVEALS AN ENDOSOMAL AND CYTOSOLIC SPATIAL BIAS<sup>3</sup>

Published in *Scientific Reports*, DOI /10.1038/s41598-023-33953-y

Jeremy Burton<sup>1</sup>, Jennifer Okalova, Neil Grimsey<sup>1</sup>

---

<sup>3</sup> Burton, J.C., Okalova, J & Grimsey, N.J. *Scientific Reports*, 13:7477, April 2023.

## Introduction

The highly conserved subfamily of MAPK p38 (consisting of four members  $\alpha$ ,  $\beta$ ,  $\gamma$ ,  $\delta$ ) are essential regulators of intracellular stress responses. Dual phosphorylation of p38 at the conserved Threonine-Glycine-Tyrosine (TGY) motif (T180 and Y182) by the upstream MAP kinase kinase (MKK3/6) is essential for classical p38 activation. MKK3/6 can activate all four family members, regulating many physiological and pathological processes, including cell growth, proliferation, wound healing, and inflammation <sup>60</sup>. The diverse physiological functions and the conserved mechanism of activation by MKK3/6 dictates that intracellular signaling is regulated through substrate availability and intracellular localization of p38.

Cellular stress induces p38 activation and intracellular redistribution, targeting p38 to selective pools of substrates. In a resting state, p38 is typically distributed between the cytosol and nucleus. However, after activation, all p38 isoforms are rapidly translocated to the nucleus, a step that is critical for nuclear resident transcription factor activation <sup>363</sup>. Conversely, p38 also has critical roles in the cytosol, activating cytosolic transcription factors to induce their nuclear translocation and activating other cytosolic kinases <sup>35,363</sup>.

In addition to the classical MKK3/6 activation pathway (**Fig. 2.1Ai**), p38 can also be activated by two selective atypical mechanisms that direct p38 autophosphorylation and activation <sup>255</sup>. The first selectively occurs in T-cells, utilizing the tyrosine kinase Zap70 to phosphorylate p38 at Tyr323. Phospho-Tyr323 triggers a conformational change driving p38 autophosphorylation at Thr180 in *trans* between homo or heterodimers of p38 $\alpha$  and p38 $\beta$  <sup>91,226</sup>. The second atypical p38 pathway is mediated by the direct binding of p38 to the adaptor protein Transforming growth factor beta-activated-kinase-1-binding protein-1 (TAB1) <sup>75</sup>. The c-terminal peptide of TAB1 selectively binds only the p38 $\alpha$  isoform at two distinct binding sites, inducing a conformational change and

enabling p38 $\alpha$  autophosphorylation<sup>71, 74, 81</sup>. Critically, TAB1-dependent atypical p38 activity has been shown to regulate key pathological processes in a widening array of diseases, including cardiac damage, vascular inflammation, viral and parasite infections, recently reviewed<sup>255</sup>.

Atypical p38 is initiated through several mechanisms, including hypoxia, oxidative stress, and G protein-coupled receptors (GPCRs). Stimulation of multiple inflammatory GPCRs can trigger activation of an E3 ubiquitin ligase, NEDD4.2, through a conserved tyrosine phosphorylation switch mechanism, inducing GPCR ubiquitination and scaffolding of the atypical p38 signaling complex through TAB2 binding to ubiquitinated GPCRs and recruitment of TAB1<sup>31, 32, 90</sup> (**Fig. 2.1Aii**). Nevertheless, the explicit mechanisms that control TAB1-p38-dependent atypical activity through GPCR-independent pathways have not been described in detail<sup>71, 74, 75, 255</sup>. Regardless, there are several common factors during atypical signaling: the TAB1-p38 interaction is relatively stable<sup>71</sup>, atypical p38 activation induces TAB1 phosphorylation, TAB1 phosphorylation blocks TAB1 interaction with TAK1 further amplifying the atypical pathway<sup>79</sup>, and the dual phosphorylation of p38 is identical to MKK3/6 dependent phosphorylation (T180 and Y182)<sup>75</sup>. Atypical p38 signaling must therefore exhort differential cellular responses through an alternative regulatory process.

Recent studies have highlighted the spatiotemporal control of G-proteins and MAPKs at the endosome, Golgi, and ER, driving selective and physiologically critical signaling responses where the subcellular location of the kinases or receptors induces selective cellular responses<sup>356, 546-548</sup>.

Advances in genetically encoded Fluorescence Resonance Energy Transfer (FRET)-biosensors have enabled detailed spatial studies of ERK1/2 activity using the EKAR4 ERK activity biosensors<sup>358</sup>. Despite the development of a comparable p38 activity FRET biosensor<sup>48</sup> there have been no studies into the spatial control of atypical p38 MAPK.

This study aimed to develop a platform of subcellular targeted genetically encoded FRET biosensors to spatially map p38 activity. Using live-cell imaging of cells transfected with p38 FRET sensors targeted to the plasma membrane, cytosol, nucleus, and endosome, (**Fig. 2.1B**), we compared the kinase activity between osmotic stress and thrombin-mediated activation of protease-activated receptor 1, PAR1. We are the first to map the spatial dynamics of p38 activity in live cells and demonstrate a differential spatiotemporal profile for atypical p38 signaling, biasing p38 to the endosome and cytosol. These studies provide critical insight into how atypical p38 drives differential pathological inflammatory signaling during vascular inflammation and establish a broader paradigm for understanding atypical p38 responses.

## **Results**

### **Spatial targeting of P38 FRET sensors.**

Recent studies described using a p38 FRET sensor to examine MKK3/6-dependent p38 oscillations in HeLa cells <sup>48</sup>. The FRET biosensor is a single molecule, with an n-terminal YFP and c-terminal SECFP, linked by a flexible peptide containing a p38 binding and phosphorylation motif and a WW domain (**Fig. 2.1B**) <sup>48</sup> We proposed that the addition of subcellular targeting motifs to this previously characterized activity biosensor would enable spatiotemporal mapping of MKK3/6 and TAB1-dependent p38 activation pathways (**Fig. 2.1A**). To determine the activity of p38 at distinct intracellular sites of the cell, we generated c-terminal tagged p38 FRET with a KRAS (Kirsten Rat Sarcoma viral oncogene homolog)-motif to target the plasma membrane (PM) <sup>549</sup>, the 2x FYVE (Fab1, YOTB/ZK632.12, Vac1, and EEA1, zinc finger) domains from hepatocyte

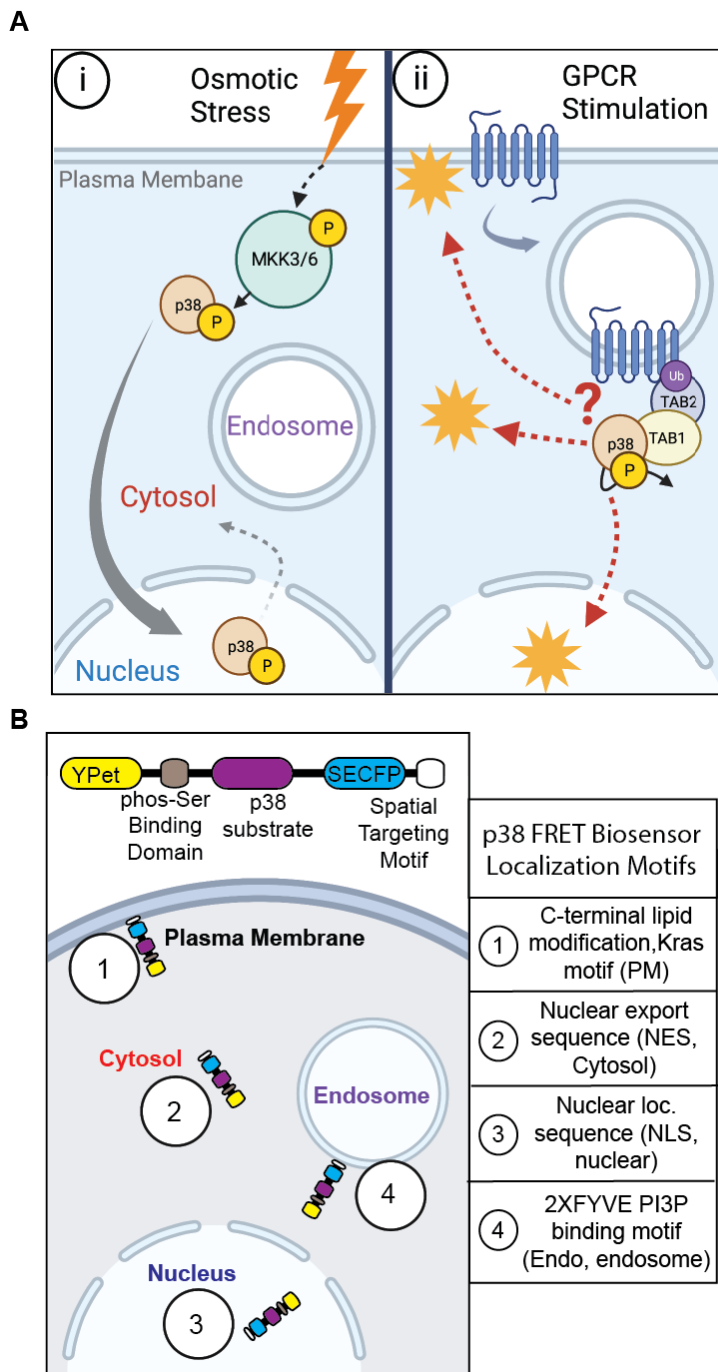


**Figure 2.1: Model of P38 activation, localization, and translocation. A)** (i) Schematic representation of cellular stress-induced Mkk3/6 activation and translocation of p38 cohorts. Rapid translocation to the nucleus and recycling back into the cytosol (ii) Atypical p38 activation after GPCR stimulation, unclear spatiotemporal dynamics **B)** Schematic representation of spatially targeted p38 FRET biosensors, C- terminal fused subcellular localization motifs 1) Plasma membrane, 2) cytosol, 3) Nucleus, 4) Endosome.

growth factor-regulated tyrosine kinase substrate (HRS) to target the endosome via binding to the membrane lipid phosphatidylinositol 3-phosphate, PtdIns3P which are enriched in early endosomes<sup>550, 551</sup>, a nuclear export sequence (NES, cytosol) to target the cytosol<sup>552</sup>, and nuclear localization sequence (NLS, nuclear) to target the nucleus,<sup>553</sup> (**Fig. 2.1B**). The spatial p38 FRET sensors were transiently expressed in HeLa cells, and confocal imaging revealed the predicted localizations of each biosensor (**Fig. 2.2A**), confirmed via costaining with specific spatial markers and calculating Pearson correlation coefficients ( $r$ ); Biotracker<sup>TM</sup> orange = plasma membrane,  $r= 0.466 \pm 0.131$ ; GAPDH-647 = cytosol,  $r= 0.351 \pm 0.107$ ; RedDot<sup>TM</sup>2-far-red nuclear stain = nucleus,  $r= 0.436 \pm 0.132$ ; (**Suppl. Fig 2.1A-C**). The subcellular localization of the 2xFYVE endosomal sensor was additionally validated by coexpression with the endosomal associated wild type GTPase Rab5 (Rab5-mRFP), or constitutively active Rab5 Q79L-mRFP, which displays an endosomal trafficking and fusion defect leading to enlarged endosomes<sup>554, 555</sup>. Pearson correlation coefficients ( $r$ ) (wt Rab5  $r= 0.448 \pm 0.13$ , or Q79L Rab5  $r= 0.0446 \pm 0.15$ ) confirmed that 2xFYVE targeting is the biosensor colocalized with Rab5 positive early endosomes (**Suppl. Fig 2.1D and E**), as previously shown<sup>554-556</sup>.

### **Osmotic stress by NaCl induces rapid p38 activation with the peak in the nucleus.**

To validate the platform of spatial biosensors, we first utilized NaCl-induced osmotic shock. Osmotic shock is a classic example of MKK3/6 p38 activation, where RAC GTPase interacts with and activates an osmosensing complex driving MEKK3-dependent MKK3 activation. MKK3-dependent p38 phosphorylation induces a rapid translocation of p38 to the nucleus<sup>33</sup>. Osmotic stress was induced using 300 mM NaCl in cells expressing the p38 sensor panel. Baseline FRET responses were allowed to stabilize before stress induction. Osmotic stress induced rapid p38 activity in all four spatial constructs, with p38 activity measured as normalized

FRET/SECFP ratio over time, the grey lines representing individual cells, and the color line representing the experimental average (**Fig. 2.3A-E**), representative examples for ratiometric FRET responses displayed as pseudo color look up table (LUT) images (**Suppl. Fig.2**). Maximal FRET response ( $FRET_{MAX}$ ) was rapidly achieved with a  $FRET_{T\frac{1}{2}}$  (half the time to reach  $FRET_{MAX}$ ) within 30 seconds in all but the cytosol, in which individual cells had a greater distribution of  $FRET_{T\frac{1}{2}}$  values over 2-4 minutes with an average of 2 minutes (**Fig. 2.3F, G**). The PM and cytosolic biosensor  $FRET_{MAX}$  peaked at 1.08 (**black**) and 1.14 (**red**) over baseline, respectively (**Fig. 2.3A, B, E, & F**). The endosomal population peaked at 1.17, which was not significantly different from the cytosolic signal. Conversely, the nuclear  $FRET_{MAX}$  peaked at 1.24 over baseline, significantly higher than the other populations (**Fig. 2.3C, E, & F, blue**). Note that NaCl induced p38 activity returned close to basal levels at 30 minutes and SB203580 addition displayed no further reduction in FRET responses, **Fig. 2.3A-E** as indicated).

### **Spatial mapping of thrombin activation of PAR1 reveals a differential atypical p38 profile.**

We have previously established that the thrombin activated GPCR, PAR1, induces a robust atypical p38 activation pathway<sup>31,32</sup>. To determine whether thrombin activation of PAR1 induced spatially selective atypical p38 dynamics we co-transfected HeLa cells with PAR1 and each of the four biosensors. Thrombin-induced robust p38 activity in the cytosol, peaking with a  $FRET_{MAX}$  of 1.2 (**Fig. 4B, E, F, red**, and pseudo color LUT images **Suppl. Fig.3A**). A reduction of p38 FRET consistently preceded the increase in p38 activity immediately after thrombin stimulation. This transient drop of p38 cytosolic activity lasted ~5 minutes before increasing. Notably, thrombin displayed slower p38 activation dynamics with a  $FRET_{T\frac{1}{2}}$  of ~8 minutes compared to osmotic stress (**Fig. 4G** and **Fig. 3G**). Contrary to the cytosolic signal, thrombin induced a rapid initial increase in p38 activity at the endosome. Within 1 minute, the FRET ratio reached ~ 1.05, before

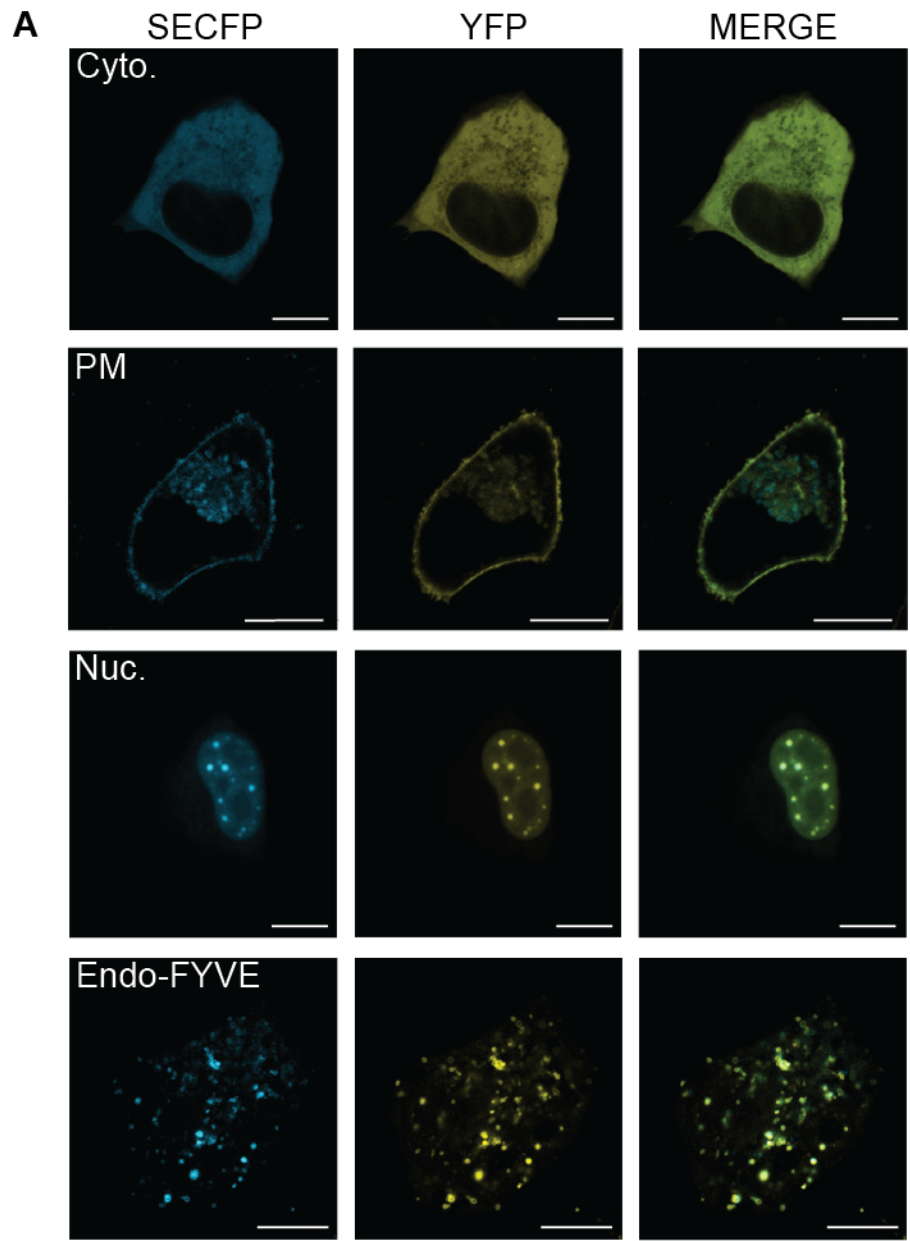


**Figure 2.2: P38 biosensor platform localized to subcellular compartments**

**A)** Representative fluorescent (SECFP, YFP, merged) confocal images of HeLa cells transiently expressing biosensors with spatial targeting motifs for the plasma membrane (PM), cytosol (Cyto.), nucleus (Nuc.), or endosome (Endo-FYVE). Scale bars, 10  $\mu$ m.

a slower gradual rise to a FRET<sub>MAX</sub> of 1.19. The FRET<sub>MAX</sub> was comparable for the endosomal and the cytosolic sensors (**Fig. 4B, D, and E**, pseudo color LUT images **Suppl. Fig. 3B**, compared to NaCl treatment **Fig. 3B, D, and E, red and purple**). Contrary to the transient activation of the p38 FRET responses after osmotic shock, thrombin activity was sustained. To confirm that the FRET sensor was not locked in active confirmation, endosomal and cytosolic FRET activity were blocked at 30 minutes using the p38 selective chemical inhibitor, SB203580<sup>557</sup> (**Fig. 4A-E** as indicated), but not after DMSO addition (**Suppl. Fig. 4A-D** as indicated) demonstrating that the detected increase in FRET ratios and SB203580 dependent loss are due to p38 activity. The endosome is hypothesized to be a central nexus of PAR1 p38 signaling<sup>31, 32, 98</sup>. To confirm the rapid endosomal signaling by thrombin, we targeted the FRET biosensor to the endosome by replacing the small 2xFYVE PtdIns3P binding domain with the larger full-length early endosomal GTPase, Rab5<sup>550</sup>, on the c-terminus of the FRET biosensor. The Rab5-directed sensor colocalized with the early endosomal associated protein 1, EEA1 (**Suppl. Fig. 1**) and also displayed a rapid thrombin-mediated activation reaching a FRET<sub>MAX</sub> of 1.09 at 3 minutes before dipping and rising again (pseudo color LUT images **Suppl. Fig. 3E, Suppl. Fig. 5A purple**). However, contrary to the 2xFYVE sensor, NaCl failed to solicit a robust Rab5-FRET response (pseudo color LUT images **Suppl. Fig. 2E, Suppl. Fig. 5B**). Unlike the rapid nuclear FRET response seen for NaCl, thrombin induced a minimal but consistent nuclear signal, with a FRET<sub>MAX</sub> peaking at ~1.06 (**Fig. 2.3C, E, 4C, E blue**, pseudo color LUT image **Suppl. Fig.3C**).

While NaCl induced a rapid increase in p38 activity at the plasma membrane (**Fig. 2.3A, E black**), thrombin-induced plasma membrane responses were distinctly different, as FRET ratios rapidly dropped below baseline to ~0.95 before slowly recovering, but never rising above baseline FRET signal (**Fig. 2.4A, E black**, pseudo color LUT image **Suppl. Fig. 3C**). Of note, all

acquisition parameters were identical to those during NaCl treatment. SB203580 addition post-stimulation had no detectable influence on the thrombin induced PM-FRET activity (**Fig. 2.4 A, E black**).

While GPCR-induced p38 activity was detected in the endosome and cytosol, thrombin-mediated activation of p38 displayed a distinctly differential profile to that seen for osmotic stress in **Fig. 3**, biasing p38 activity away from the nucleus into the cytosol and endosome (**Fig. 4**). We have previously shown that atypical p38 signaling is conserved for a family of inflammatory GPCRs. To confirm the GPCR-specific spatiotemporal bias for p38 activity, we examined prostaglandin activation of the prostaglandin E receptors 2 and 4, EP2 (PTGER2) and EP4 (PTGER4). Both receptors displayed comparable spatial profiles to that seen for thrombin-activated PAR1, with peak activations for cytosolic and endosomal sensors and minimal activation at the PM or in the nucleus (**Suppl. Fig. 6A-F (EP2) and 7A-F (EP4)**), although cytosolic activation was slower for both receptors than seen for  $\alpha$ -thrombin (**Suppl. Fig. 6G (EP2) and 7G (EP4)**).

#### **FRET response is driven by p38 activity.**

The p38 biosensor was previously shown to be selective for p38 $\alpha$  in response to interleukin 1 $\beta$ <sup>48</sup>. We show in **Fig. 2.4A-D** that the addition of SB203580 suppresses FRET responses in the cytosolic, endosomal, and nuclear compartments, but as thrombin did not induce activity at the plasma membrane, the inhibitor did not reduce this FRET value further. To confirm that the detected FRET response for GPCR signaling is specific to p38 activity, cells were preincubated with SB203580 before stimulation with thrombin or NaCl. All FRET sensors displayed reduced FRET<sub>MAX</sub> compared to values shown in Fig. 2.3 and 2.4 (**combined in Fig. 2.5**). SB203580 blocked thrombin responses in cytosolic, endosomal, and nuclear FRET ratios. Notably, the drop

in PM FRET ratio in response to thrombin (**Fig. 2.4A**) was blocked by SB203580 pretreatment, with the FRET ratio remaining close to the baseline and comparable to cytosolic, endosome and nuclear biosensors pretreated with SB203580 (**Fig. 2.5B, compare black dotted line with black full line**). SB203580 preincubation also suppressed Rab5 FRET responses (**Suppl. Fig. 2.5C,D**). To further confirm the specificity of the p38 FRET sensor we also generated a null-FRET-cytosolic sensor, mutating the critical p38 target serine residues to alanine (**Suppl. Fig. 2.8A**). The cytosolic null-FRET blocked both  $\alpha$ -thrombin (**Suppl. Fig. 2.8B**) and NaCl (**Suppl. Fig. 2.8C**).

### **Inhibition of receptor internalization spatially flips GPCR signaling dynamics.**

After thrombin activation, PAR1 is rapidly removed from the plasma membrane via clathrin-mediated endocytosis (CME)<sup>558-560</sup>. Prior studies demonstrated that PAR1 ubiquitination and activation of p38 signaling is retained when CME is blocked via the dynamin inhibitor Dyngo4A (**Fig. 2.6A**)<sup>32</sup>. This suggests that atypical p38 activity is initiated and sustained at the plasma membrane when CME is inhibited. To examine whether endosomal trafficking is required to drive the spatial bias GPCR-induced signaling to the cytosol/endosome, we treated cells with Dyngo4A before activation.

Initially, we assessed the effect of Dyngo4A pretreatment on osmotic stress-induced p38 activation. Pretreatment of cells with Dyngo4A had a minimal impact on NaCl-induced p38 activation profiles of all four biosensors (**Fig. 2.6B-F, and Suppl. Fig. 2.9A-F**) FRET<sub>MAX</sub> values from **Fig. 2.3F**, solid bars plotted next to Dyngo4A FRET<sub>MAX</sub> checkered bars). NaCl activity analysis of the FRET<sub>MAX</sub> for all sensors revealed no significant change (**Fig. 2.6B-F**). Dyngo4A also did not change the FRET<sub>T1/2</sub> (**Suppl. Fig. 2.9G**), demonstrating that Dyngo4A does not alter osmotic stress (MKK3/6) dependent p38 activation, confirmed by immunoblotting (**Suppl. Fig. 2.11 A,B, lanes 1-6**).

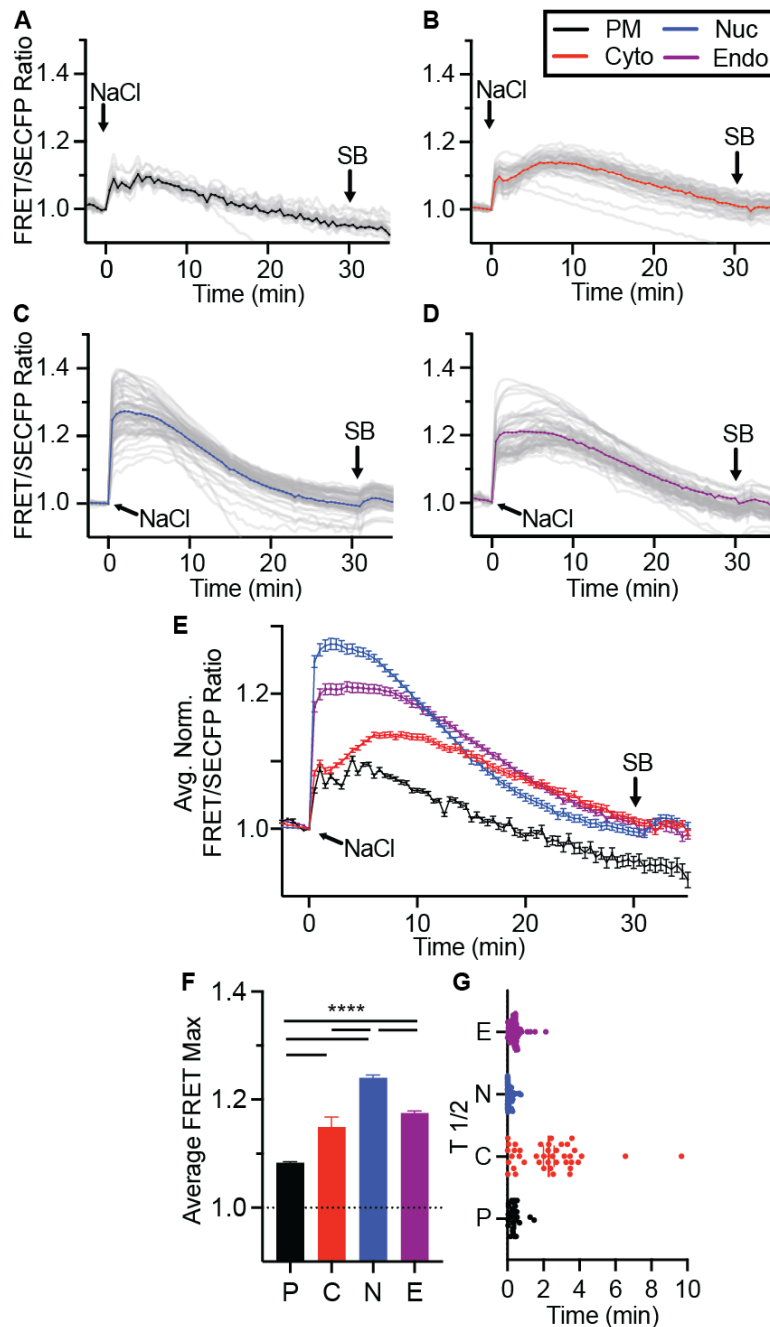


**Figure 2.3: Subcellular mapping of MKK3/6 dependent p38 activity.** A-D) Activation of p38 using FRET biosensors localized to the plasma membrane A), cytosolic B), nuclear C), or endosomal D) expressed in HeLa cells incubated with 300 mM NaCl and SB203580 (SB). FRET ratios were normalized prior to NaCl addition. Individual cell FRET ratios are depicted in gray ( $n > 30-60$  cells per biosensor). Average FRET ratio is indicated by colored lines. E) Overlay of representative normalized averages of FRET ratio in biosensor platform from A-D). F) Maximum change in FRET ratio (FRET<sub>MAX</sub>) of individual cells pooled from 3 independent repeats, ( $n > 80-150$  ROIs per biosensor. mean  $\pm$  SEM) were analyzed by One-Way ANOVA (\*\*\*\*,  $p < 0.0001$ ). G) FRET response kinetics, T<sub>1/2</sub> values of cells in A-D (mean  $\pm$  SEM).

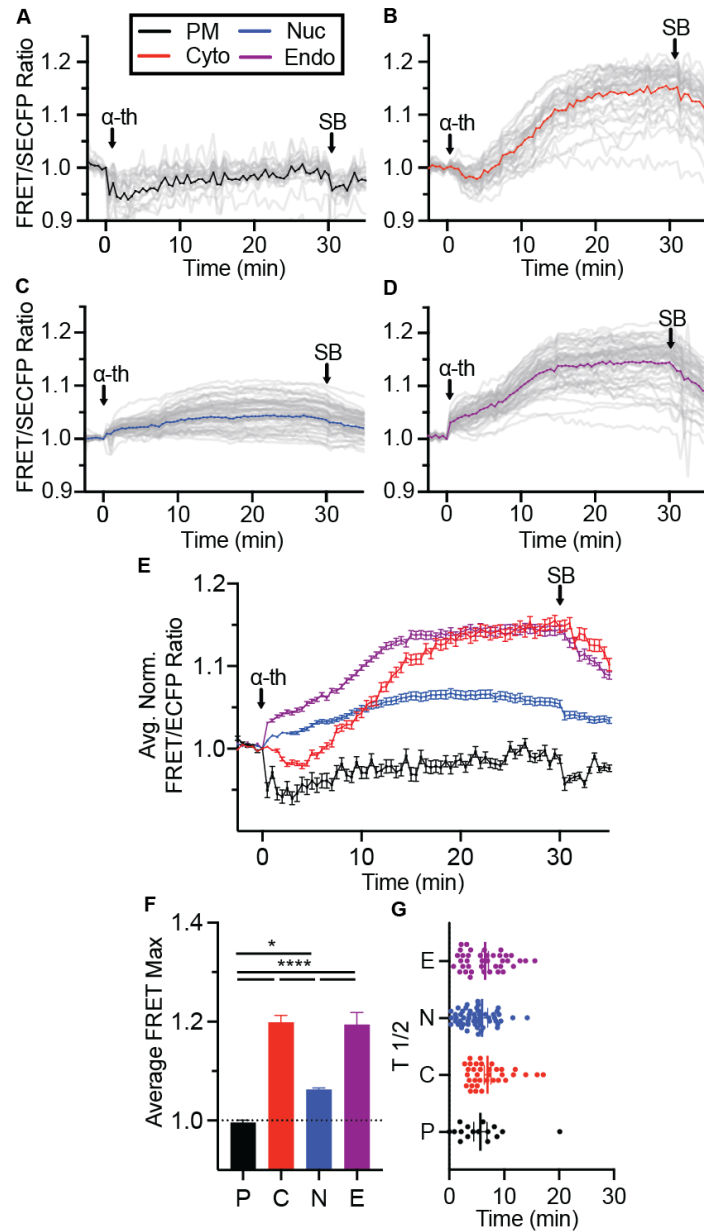


**Figure 2.4. P38 activation is differentially regulated by thrombin.** **A-D)** Activation of p38 using FRET biosensors localized to the plasma membrane **A)**, cytosolic **B)**, nuclear **C)**, or endosomal **D)** expressed in HeLa cells incubated with 10nM  $\alpha$ -thrombin and SB203580 (SB). FRET ratios were normalized prior to  $\alpha$ -thrombin addition. Individual cell FRET ratios are depicted in gray ( $n > 30$ -60 cells per biosensor). Average FRET ratio is indicated by colored lines. **E)** Overlay of representative normalized averages of FRET ratio in biosensor platform from **A-D)**. **F)** Maximum change in FRET ratio (FRET<sub>MAX</sub>) of individual cells pooled from 3 independent repeats, ( $n > 80$ -150 ROIs per biosensor, mean  $\pm$  SEM) were analyzed by One-Way ANOVA (\*,  $p < 0.05$ , \*\*\*\*,  $p < 0.0001$ ). **G)** FRET response kinetics, T<sub>1/2</sub> values of cells in A-D (mean  $\pm$  SEM).

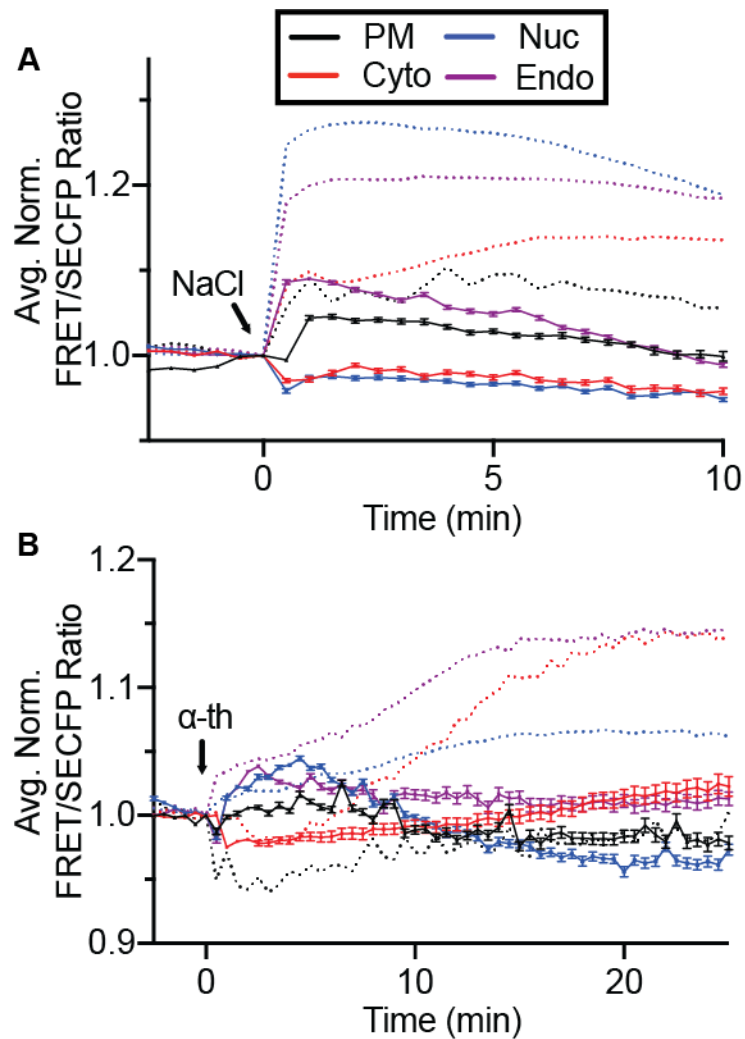


**Figure 2.5. FRET response driven by p38 activity.** Activation of p38 using FRET biosensors localized to the plasma membrane, cytosolic, nuclear, or endosomal expressed in HeLa cells preincubated with SB203580 (SB) prior to 300 mM NaCl **A**) or 10nM  $\alpha$ -thrombin **B**). FRET ratios were normalized prior to the addition of NaCl or  $\alpha$ -thrombin. The average FRET ratio is indicated by solid-colored lines, dashed lines indicate representative plots from Fig. 3 in A and Fig. 4 and B, and representative plots from >2 independent repeats (n > 30-60 cells ROIs per biosensor. mean +/- SEM).

Contrary to NaCl treatment, Dyngo4A treatment was predicted to enhance thrombin-induced PM p38 signaling as CME traps active PAR1 at the PM, recruiting NEDD4-2 to the PM<sup>32</sup>. Dyngo4A pretreatment blocked thrombin-induced loss of FRET signaling at the PM and displayed a small but significant thrombin dependent increase relative to controls (**Fig. 6B**, FRET<sub>MAX</sub> values from **Fig. 4F**, solid bars plotted next to Dyngo4A FRET<sub>MAX</sub> checkered bars, **Suppl. Fig. 10 A,F black**). However, FRET<sub>MAX</sub> for both endosomal and cytosolic biosensors were significantly reduced after inhibition of CME (**Fig. 6 C, E**, FRET<sub>MAX</sub> values from **Fig. 4F**, solid bars plotted next to Dyngo4A FRET<sub>MAX</sub> checkered bars from **Suppl. Fig 10B, D, E, F, red and purple**). Rab5 endosomal signaling was also blocked by pretreatment with Dyngo4A (**Fig. 6F and Suppl. Fig. 12A,B**). Contrary to the cytosol and endosome, the nuclear p38 displayed a significant increase in FRET<sub>MAX</sub> of 1.13 (**Fig. 6D blue, Suppl. Fig 10C, E, F blue**). Despite these changes in spatial FRET signaling, p38 phosphorylation was unaffected by Dyngo4A (**Suppl. Fig. 11A,B, lanes 7-12**).

When correlating the contribution of each compartment to the collective maximal FRET signal for all locations, the relative ratios of NaCl FRET responses were unchanged after the addition of Dyngo4A. Nuclear p38 represented 37%, endosome 27% cytosol 23% and plasma membrane 13% (**Fig 2.7A**). Whereas thrombin displayed 45% endosome, 42% cytosol, and 13% nuclear signaling. After Dyngo4A treatment, the ratios switched for thrombin activation, with 12% at the plasma membrane, 20% endosome, 31% cytosolic, and 37% nuclear. Intriguingly the Dyngo4A flipped the distribution of p38 activation (**Fig. 2.7 A,B**) so that it mirrored the distribution seen after NaCl treatment (**Fig. 2.7A and Biii**). Together these data suggest that atypical p38 signaling is spatially biased to the cytosol/endosome and that blockade of receptor

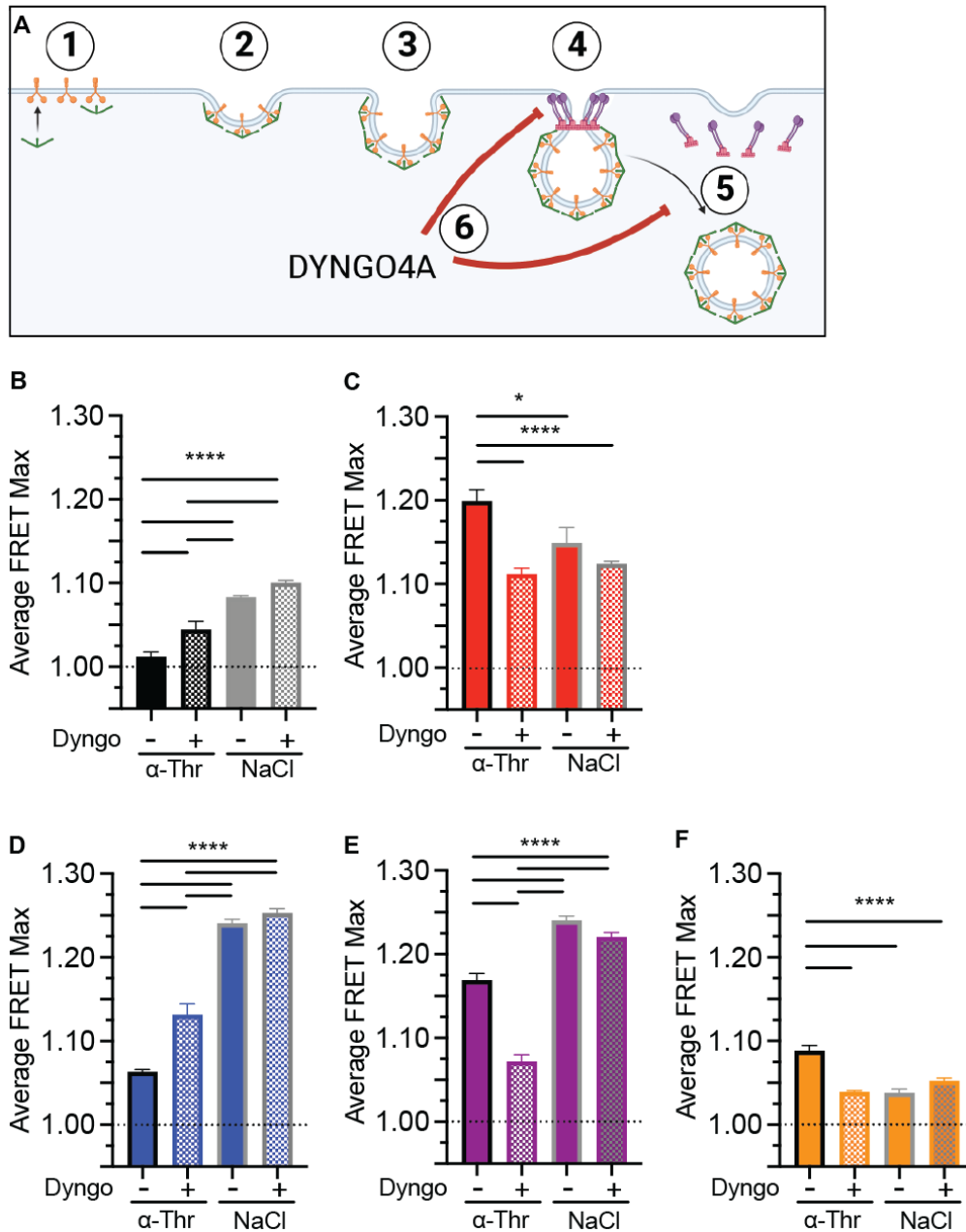


**Figure 2.6: Blockade of GPCR internalization changes spatial FRET bias.**

HeLa cells transiently expressing biosensors and PAR1 were preincubated with 15  $\mu$ M Dyngo4A for 45 min prior to stim with 10 nM  $\alpha$ -thrombin ( $\alpha$ -Thr) or 300 mM NaCl. **A**) Schematic representation of clathrin mediated endocytosis and the site of action of Dyngo4A inhibition, 1-3) cargo and adaptor proteins drive the formation and stabilization of clathrin coated pits on the plasma membrane, 4) dynamin is recruited to the clathrin coated pit 5) with assistants from actin dynamin drives scission and coated vesicle release, 6) Dyngo4A block dynamin dependent scission events. **B-F**) Average F-max values from figures 2.3 and 2.4 were compared to respective Dyngo4A F-max grouped by expression of **B**) plasma membrane, **C**) cytosol, **D**) nucleus, **E**) endosome (FYVE) or **F**) endosome (Rab5). Data (mean +/- SEM) analyzed by One-Way ANOVA (\*\*\*\*,  $p < 0.0001$ )

internalization can flip the spatial bias to mimic that seen for MKK3/6-dependent signaling driving p38 activity into the nucleus (**Fig. 2.7 Biii**).

## **Discussion**

Spatial regulation of kinases is critical for determining downstream functional outcomes. While there have been extensive studies into the spatial control of MKK3/6-dependent p38 activation, there is a limited understanding of the spatial kinetics of atypical p38 activation, specifically after GPCR activation. In this study, we utilized a platform of spatially targeted p38 FRET biosensors to conduct live-cell imaging experiments to investigate the spatiotemporal landscape of p38 activation in response to osmotic stress or thrombin-dependent GPCR activation. We demonstrate that GPCR-induced TAB1-p38 signaling displays a differential temporal profile of activity. Contrary to MKK3/6 dependent signaling, TAB1 mediated atypical p38 perturbs nuclear translocation of p38, sequestering and biasing kinase action to the cytosol and endosome (**Fig. 7B**). We have previously hypothesized that GPCR endocytic trafficking plays a critical role in this spatial bias. However, we now show that the endosomal spatial bias can be switched through inhibition of clathrin-mediated endocytosis, flipping p38 activity to a nuclear bias.

Initially discovered in 2002, atypical p38 activation is mediated by the direct interaction between TAB1 and p38. TAB1 binding drives a critical conformational change in p38, enabling p38 autophosphorylation independent from the classical MKK3/6 mediated activation<sup>75, 81</sup>. GPCRs drive atypical p38 activation via a ubiquitin-dependent scaffold, initiating the formation of a critical TAB2-TAB1-p38 signaling complex<sup>31, 98, 255</sup>. Ubiquitin-dependent initiation of atypical p38 signaling is a conserved mechanism for a family of GPCRs in both macrovascular and microvascular beds<sup>90</sup>.

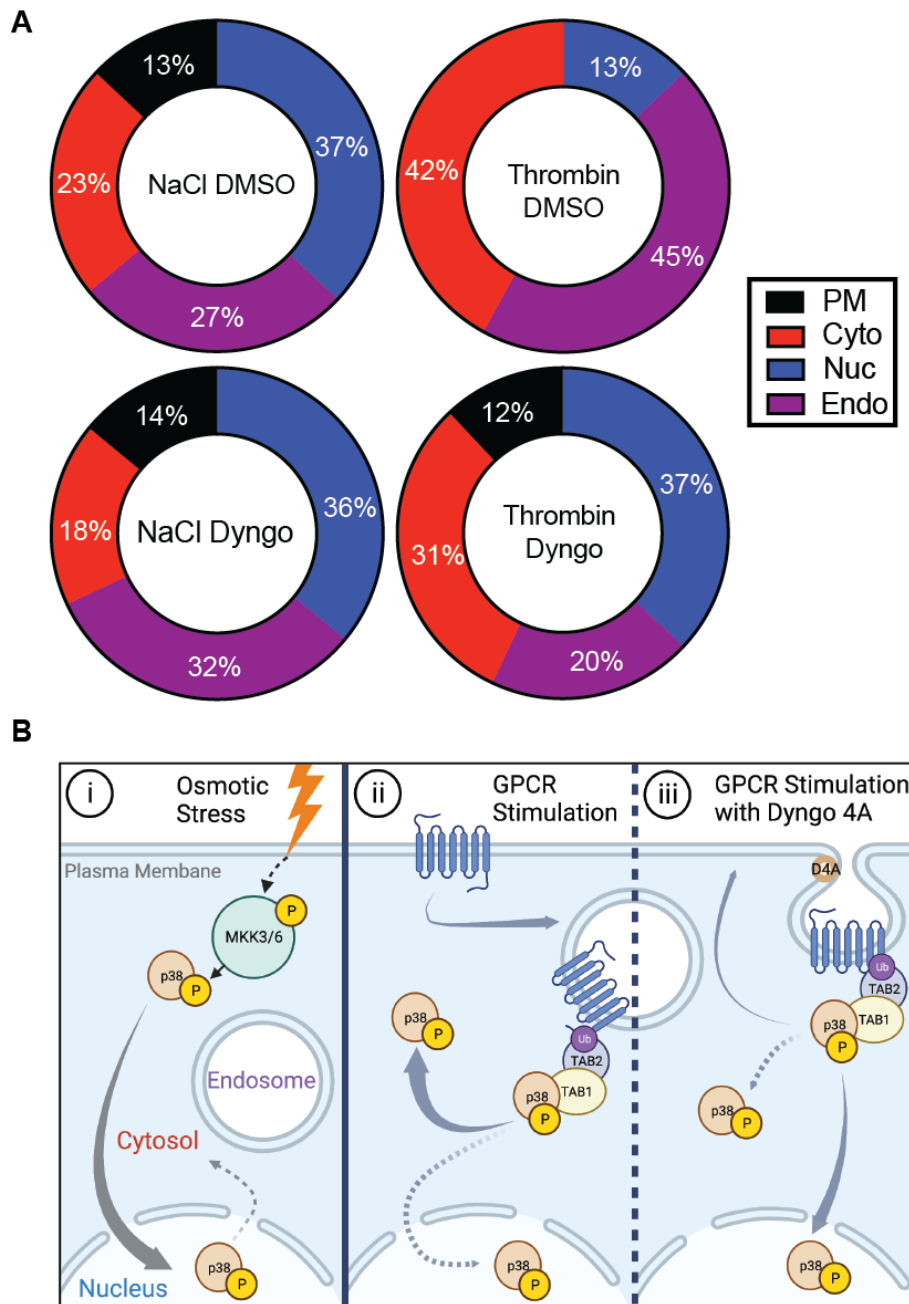


**Figure 2.7: Atypical p38 signaling model**

A) FRET max values from each biosensor previously calculated in figures 2.3,4, suppl. 2.6,7, compiled as a percentage of the total FRET<sub>MAX</sub> responses. **B)** Proposed schematic of p38 spatial localization. I) osmotic stress as described in figure 1. ii) GPCR-mediated TAB1-p38 activation is rapidly trafficked off the plasma membrane to the endosome and the cytosol, with a small portion of nuclear p38. iii) GPCR-mediated stimulation with Dyngo4A preincubation arrests internalization and reduces p38 activity in the cytosol and endosome, increasing p38 trafficking to the nucleus.

Despite the predictions regarding the sequestration of TAB1-p38 in the cytosol, prior studies have relied upon fixed time points and overexpression studies to explore nuclear translocation and stabilization of the TAB1-p38 complex<sup>71, 75, 79, 80, 88, 111, 114, 218</sup>. While these studies are highly suggestive, there are advantages to live-cell imaging, which allows for a comprehensive assessment of the spatially guided signaling dynamics in individual cells. Recent studies have highlighted this potential by exploring intracellular G-protein dynamics, and spatially resolved ERK1/2 signaling<sup>356, 546-548</sup>, PKA<sup>561</sup>, and AMPK nuclear signaling<sup>562</sup>, defining the critical spatial control of kinases, where adaptor and substrate accessibility drives their functional roles. While it is well known that p38 has a central role in the regulation of both cytosolic and nuclear proteins<sup>35, 363</sup>, direct analysis of the spatiotemporal p38 dynamics has not been carried out. To overcome the lack of tools to explore p38 spatiotemporal signaling dynamics our current study compared the spatial kinetics of p38 activation at the plasma membrane, cytosol, endosome, and nucleus. As expected, osmotic stress-induced rapid activation at the PM and almost simultaneous translocation to the nucleus, where p38 activity peaked within seconds of activation. This is consistent with prior biochemical studies, as recently reviewed<sup>363</sup>.

On the contrary, GPCR activation displayed a distinctly different activation profile, with limited activity in the nucleus and a loss of activation at the PM. This is consistent with prior studies indicating PAR1 is rapidly trafficked away from the plasma membrane through clathrin-mediated endocytosis, CME<sup>32, 559, 560, 563</sup>. Although the E3 ubiquitin ligase NEDD4.2 is critical for atypical p38 activation by GPCRs, blockade of CME using Dyngo4A did not suppress receptor ubiquitination or p38 activation, which suggested that the atypical p38 signaling can occur at the PM. We had predicted that Dyngo4A treatment would lock atypical p38 at the PM, mirroring NaCl signaling dynamics. However, Dyngo4A failed to induce a rapid increase of p38 signaling at the

PM, suggesting that either the association with ubiquitinated PAR1 is so rapid that it is undetectable or CME inhibition changes p38 activity by restricting access to the endosome.

Indeed, the temporal dynamics of GPCR CME and endosomal trafficking of the ubiquitinated receptors suggested that atypical p38 signaling would be initiated at the endosome. Prior studies showed ubiquitinated PAR1 rapidly recruits TAB2 to endosomes via a Zinc finger ubiquitin-binding motif (ZnF)<sup>31</sup>. The endosome-targeted FRET sensor showed the fastest p38 activity after thrombin treatment, rapidly responding within 1 minute of activation, followed by a later second phase of activation increasing further. Cytosolic p38 activation by thrombin displayed an unexpected initial signal loss, which then steadily increased to match endosomal FRET<sub>MAX</sub> after 25 minutes of stimulation. It is tempting to hypothesize that the initial loss of GPCR-induced cytosolic p38 stems from the rapid recruitment of p38 to endosomes.

The cytosolic redistribution was conserved with the prostaglandin receptors EP2 and EP4 but not seen for NaCl treatment which displayed a two-phase increase in p38 activity, an initial rapid activation, followed by a slower rise to FRET<sub>MAX</sub> at ~7 minutes. We have previously shown that PGE2 activation induces atypical p38 activity, and our data demonstrates that atypical p38 signaling drives a comparable spatial bias for PGE2-induced p38 signaling by the human EP2 and EP4 receptors (PTGER2 and 4, respectively). Further studies will be required to explore how conserved this bias is across GPCRs and non-GPCR-induced atypical p38 signaling.

Of note, NaCl stimulation induced rapid endosomal signaling, suggesting that the endosome may also play a role in the initial phases of osmotic stress-mediated activation of p38.

In addition to the PI(3)P binding 2xFYVE<sup>550</sup> early endosomal targeted FRET sensor, we also included an alternative endosomal targeting strategy using the full-length wt-Rab5-FRET sensor. Rab5 is an early endosome GTPase that plays critical role in endosomal trafficking and is

classically used as a marker for the endosome<sup>564, 565</sup>, Rab5 binds to and colocalizes with EEA1 at PI3P lipid membranes<sup>550</sup>. Differing from the FYVE targeting, Rab5-FRET displayed a rapid peak in p38 activation after thrombin signaling before dipping and rising again. However, NaCl failed to activate Rab5-FRET biosensor responses. As Rab5 is being used as a targeting motif and the GTPase activity is not explicitly being measured, it is possible that the full-length Rab5 could be acting as a steric hindrance displacing the FRET sensors too far from the endosome to detect NaCl-dependent signaling. Conversely, atypical p38 is scaffolded by GPCR-ubiquitin chains that drive the formation of the TAB2-TAB1 signaling complex, and this additional structure may position p38 activity to ideally activate the Rab5-FRET complex. Additional studies will be required to explore this in more detail.

The endosome is essential in the regulation of signaling dynamics for multiple pathways, including for opioid receptors<sup>566</sup>, follicle-stimulating hormone (FSH)<sup>567</sup>, and endosomal signaling<sup>356</sup>. Each case alters the specific interactions with molecular adaptors that drive kinase activity. While Dyngo4A treatment didn't induce the predicted rapid increase in PM p38 signaling, inhibition of CME significantly reduced thrombin-dependent FRET<sub>MAX</sub> of both endosomal and cytosolic p38 activity (**Fig. 2.7A**). Interestingly, in this context thrombin-dependent p38 displayed a temporal map similar to NaCl signaling with a rapid transient peak, albeit activated at a lower intensity than NaCl. Furthermore, Dyngo4A had the most pronounced effect on nuclear FRET activity after thrombin stimulation, inducing a rapid transient nuclear FRET response, with an average FRET<sub>MAX</sub> double that of the control cells. But, again, Dyngo4A did not affect NaCl-treated nuclear FRET responses. This suggests that the spatial bias of GPCR-induced atypical p38 signaling at the endosome and cytosol (**Fig. 2.7Bii**) specifically requires clathrin-mediated \

endocytosis or at least passage through the endosome. Disruption of this critical step flips the spatial signaling so that the atypical p38 dynamics mimic NaCl-dependent MKK3/6 profile (**Fig. 2.7A and Biii**).

The substrate and adaptor accessibility of p38 dynamically controls cellular functions, including the regulation of transcription factors<sup>363, 568</sup>, or cell cycle regulators (usually inhibitors). Furthermore, differential signaling by p38 has been demonstrated by the duration/strength of p38 activity, where transient activity leads to the proliferation of fibroblasts, but sustained signaling drives cell cycle arrest<sup>569</sup>. Our data clearly demonstrates that atypical p38 drives a spatiotemporal bias and so perturbing access to essential adaptors and transcription factors in the nucleus. Importantly, the p38 biosensor used in this platform detects spatial kinase activity and substrate availability. However, FRET responses are also a measure of phosphatase activity to control p38 activation and dephosphorylation of the sensor to terminate FRET signaling. While NaCl activity led to transient biosensor activation, demonstrating that FRET activation is reversible, thrombin activity was sustained for 30 minutes post-stimulation. Critically, SB203580 addition at 30 minutes demonstrated that the FRET sensor was not locked into an active conformation, triggering a decaying FRET response that confirms the presence of active phosphatases, and suggesting that p38 kinase activity is sustained to maintain a FRET response to 30 minutes. A specific phosphatase has not yet been identified for atypical p38 activity, and studies are ongoing to determine how atypical p38 signaling is terminated physiologically. Additional studies are also required to characterize the kinetics of dephosphorylation of activity reporters in models of endogenous GPCR expression. Defining temporal changes in phosphorylation and transcriptional control in the nucleus and cytosol will be essential for understanding the pathological triggers regulated by atypical p38 in vascular inflammation and cardiac damage.

In summary, we have successfully demonstrated a distinctive profile for spatiotemporal atypical p38 signaling by GPCRs. After the formation of the TAB1-p38 complex, TAB1 remains bound to p38, which is thought to spatially bias p38 from entering the nucleus or slow its translocation<sup>71,74</sup>. Indeed, p38-dependent phosphorylation of TAB1 has also been suggested to spatially bias TAB1 away from the nucleus into the cytosol<sup>79,80</sup>, and that over-expression of TAB1 can antagonize MKK3/6 activation, altering p38 subcellular localization<sup>205</sup>. Spatial restriction is an essential regulatory mechanism for many kinases. Our current data shed new light on these dynamics, demonstrating that although p38 activation by both MKK3/6 or TAB1 leads to the identical dual phosphorylation of p38, differential functional outcomes of atypical p38 are likely driven by limiting access to specific adaptors and transcription factors in the nucleus. Indeed TAB1-p38 activation is known to play essential roles in inflammation, including endothelial barrier homeostasis and activation of cytokine expression<sup>32, 90, 570, 571</sup>. Spatial sequestration in the cytosol likely enhances access to these critical elements driving pathological signaling. However, further studies are required to define the specific downstream targets of atypical p38 and the specific mechanism that TAB1-p38 harness to regulate pathological signaling. Furthermore, Dyngo4A-dependent blockade of CME flipped the temporal dynamics of atypical p38 signaling, shifting the focus from endosomal and cytosolic to nuclear signaling responses. The current studies provide a framework by which to explore the spatiotemporal dynamics of atypical p38 signaling in GPCR-dependent and -independent mechanisms and screen for molecular regulators that could be therapeutically targeted. Future studies should focus on determining how the endosome selectively controls the spatial bias in atypical p38 activity and identifying the spatially restricted targets that drive pathological atypical p38 responses.

## **Methods and Materials**

*Cell culture* - HeLa cells (Cat. No. Hela CCl2, ATCC Manassa, VA, USA) were used for all experiments. Dulbecco's modification of Eagle's medium (DMEM, Cat. No. 10-013-CV, Corning, Mediatech Inc., Manassas, VA, USA) supplemented with 10% (v/v) fetal bovine serum (FBS; Cat. No. 35-010-CV, Corning, Mediatech, CA, USA) was used for cell maintenance. Cells were incubated at 37 °C in humidified conditions with 95% air and 5% CO<sub>2</sub>.

*Plasmids and Cloning of Spatial FRET biosensors*- pcDNA3.1 FLAG-PAR1 was as previously described<sup>31</sup>. PTGER 2 and 4 (Prostaglandin E receptor 2 and 4) were a gift from Bryan Roth (Addgene plasmid #66484 and #66486, respectively. Each receptor subcloned from FLAG-PTGER2-TANGO and FLAG-PGTER4-TANGO, with a 3' stop codon added to remove the TANGO tag<sup>572</sup>. The p38 FRET-NES (PerKy) biosensor was a kind gift from Dr. Saito (University of Tokyo, Japan) and has been previously characterized<sup>48</sup>. The FRET sensor was subcloned into pcDNA3.1 with spatial targeting motifs PCR-cloned onto the C-terminus of SECFP. The targeting motifs were 1) the plasma membrane, using a C-terminal lipid modification, Kras motif<sup>549</sup>, 2) the early endosome using 2xFVYE PI3P binding motif from mouse Hrs<sup>550</sup>, or the full-length wild-type Rab5<sup>555</sup>, 3) the nucleus using a nuclear localization signal motif<sup>553</sup> and 4) diffuse cytosolic with nuclear export sequence<sup>48</sup>. mRFP-Rab5 was generated for this study using PCR-directed cloning. Briefly, mRFP (pcDNA3-mRFP was a gift from Doug Golenbock (Addgene plasmid #13032 ; <http://n2t.net/addgene:13032> ; RRID:Addgene\_13032) was cloned onto the n-terminus of pcDNA3.1 Rab5 wt and Q79L<sup>573,574</sup> using 5' BamHI and 3' EcoRI, sequences were verified using Sanger sequencing.

*Cell transfections* - Cells were transfected in suspension with polyethyleneimine (PEI, Cat. No. 23966 polysciences) incubated with plasmid DNA in Gibco OptiMem Reduced Serum media (Cat. No. 31985-070, Life Technologies Corporation, NY, USA) before plating in 35mm microscopy

dishes (Cat. No. 81156, Ibidi, Gräfelfing, Germany) coated with human fibronectin, 1.5  $\mu\text{g}/\text{cm}^2$  (Cat No. 356008 Corning, Mediatech Inc., Manassas, VA, USA) with DMEM (10% FBS) in a humidified incubator for 24 or 48h.

*Chemicals and reagents* - Starvation medium composed of 0.1% bovine serum albumin (BSA, Cat. No. BP1600-100, Fisher bioreagents, NJ, USA) 20mM HEPES (Cat. No. H3537, Sigma-Aldrich, MA, USA) 1mM CaCl (Cat. No. BDH9224, BDH Chemicals, OH, USA) in phenol-red free DMEM (Cat. No. SH30284.01, HyClone, UT, USA) and filtered through a nylon 0.45 $\mu\text{m}$  filter, was applied to transfected cells for 24h before live-cell imaging and exchanged to FRET imaging buffer (20 mM HEPES, 1mM CaCl<sub>2</sub>, 2g/L D-glucose (158968-500G, Sigma-Aldrich, MO, USA) 0.23mM Sodium Pyruvate (SH30239.01, HyClone, UT, USA) in Gibco Hanks Modified Balanced Salt Solution (Cat. No. 14065-056, Life Technologies Corporation, NY, USA), pH 7.4. SB203580, (Cat. No. S-3400, LC Laboratories, MA, USA, used at 25 $\mu\text{M}$  for 1h), Dynamin Dyngo 4A (Cat. No. ab120689, Abcam, Cambridge, UK, used at 15 $\mu\text{M}$ , 1h.). Rabbit anti-EEA1 (Cat No. C45B10 Cell signal Technologies), rabbit-anti-GAPDH-Alexa647 (Cat No. 3907, Cell signaling technologies), rabbit Alexa fluor-594 (Cat No. A11012. Fisher Scientific). Rabbit anti-total p38 (Cat No. 9212, Cell signal Technologies), Rabbit anti-phospho-p38 (Cat No. 4511, Cell signal Technologies), HRP-conjugated goat-anti-rabbit (Cat No. Bio-Rad Laboratories. Biotracker 555 Orange cytoplasmic membrane dye (Cat No. SCT107, EMD Millipore Corp). RedDot™2-far-red nuclear stain (Cat No. 40060, Biotium).

*Fluorescence resonance energy transfer (FRET)-based live cell imaging* - Images for live-cell fluorescence assays were acquired using a Zeiss LSM-800 microscope (Zeiss, Jena, Germany), Colibri LED, Axiocam 506 mono, and Plan-Apochromat 20x/0.8 M27 objective. With a heated environment stage 37 °C in humidified conditions with 95% air and 5% CO<sub>2</sub>. An excitation

wavelength of 433 nm, emission 475 nm filter, was used for “SECFP”, while an excitation wavelength of 433 nm, emission 524 nm filter was used for “FRET”. Channel images were acquired sequentially with 60 ms exposure for each channel. Image collection used Zeiss Zen Blue 3.0 software. Each channel was background corrected, and the pixel-by-pixel brightness ratio of the “FRET” channel to the “SECFP” channel within each Region of interest (ROI) was calculated. FRET/SECFP channel light intensity was adjusted prior to data collection to achieve a baseline ratio average of 1.0. Typically, between thirty and fifty individual whole-cell ROIs were taken per experiment. In addition, ROIs were mapped across the experiment to follow cell movement. Cell exclusion criteria were limited to cells with a saturated SECFP or FRET intensity, cells morphologically indicative of death/division (rounded up or blebbing), or if cells were not wholly in the imaging frame. Images were collected using epifluorescence microscopy and presented as a ratiometric analysis of the emission from cyan (SECFP) and yellow (YFP/FRET). Fluorescence intensities were background-corrected by subtracting the background fluorescence intensity of a cell-free region from the emission intensities of biosensor-expressing cells. As such the FRET ratio from a small area versus the whole cell is comparable as the FRET response is normalized to the total CFP in the ROI rather than a fraction of the total area. As such an endosome/PM versus the whole cell ROI yields comparable dynamic responses (**Supp. Fig13**). Cells were acclimated in the heated environment for 10 minutes prior to imaging. Cells were incubated for 5 minutes or until fluorescent signals stabilized before stimulation. Dyngo4A-treated trials were performed in parallel to non-treated trials to ensure experimental comparability between conditions.

For high-resolution 63x confocal imaging, live-cell images were collected with a 0.4 $\mu$ m z-section. FRET sensor expressing cells were co-labeled with RedDot2 (1:200) at 37 °C for 20 minutes, media was exchanged with phenol red free DMEM before live-cell imaging. For PM biotracker

orange, cells were placed at 4 °C and stained with 5µl per ml for 15 minutes. Cells were then rinsed with phenol red free DMEM before being fixed with 4% paraformaldehyde, washed with PBS and immediately imaged, as slide mounting disrupted PM labelling. For co-labeling with EEA1 or GAPDH-647, transfected cells were fixed with 4% paraformaldehyde, permeabilized with 0.1% in triton X100, then incubated overnight at 4 °C with a primary rabbit anti-EEA1 (1:250) antibody and secondary anti-rabbit Alexa-596 (1:500), or GAPDH-647 (1:250) mounted and imaged with a plan-apochromat 63x/1.4 oil DIC M27 objective. Pearson Correlation Coefficient ( $r$ ) was calculated within Zen Blue 3.0 software from whole cell ROIs.

*Immunoblotting* – HeLa cells were seeded into 24-well plates, transfected, and grown as described above. Cells were serum starved O/N at 37°C before agonist stimulation with 10nM thrombin or 10µM PGE2 as previously described<sup>31,90</sup>. Cells lysed in 1X Laemmli sample buffer plus 100mM DTT, sonicated at 10% amplitude and cell lysates resolved by SDS-PAGE, and processed for immunoblotting as previously described<sup>90</sup>, with antibody dilutions of 1:4,000 for total p38 and 1:3,500 for phospho-p38. Immunoblots were quantified by densitometry using NIH ImageJ software.

*Data analysis and Availability* – All data were analyzed using Prism 9.0 software (GraphPad Software, La Jolla, CA) to unbiasedly calculate FRET max and T1/2 values. Prism was also used to calculate statistical significance using Student's *t-test* and two-way analysis of variance (ANOVA), as indicated. All datasets used and/or analyzed during the current study are available from the corresponding author upon reasonable request.

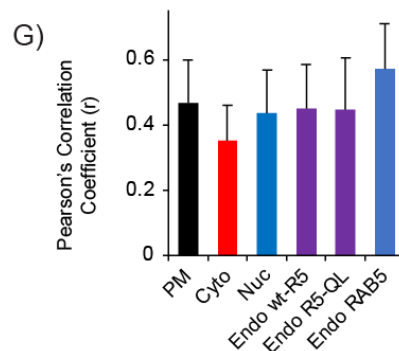
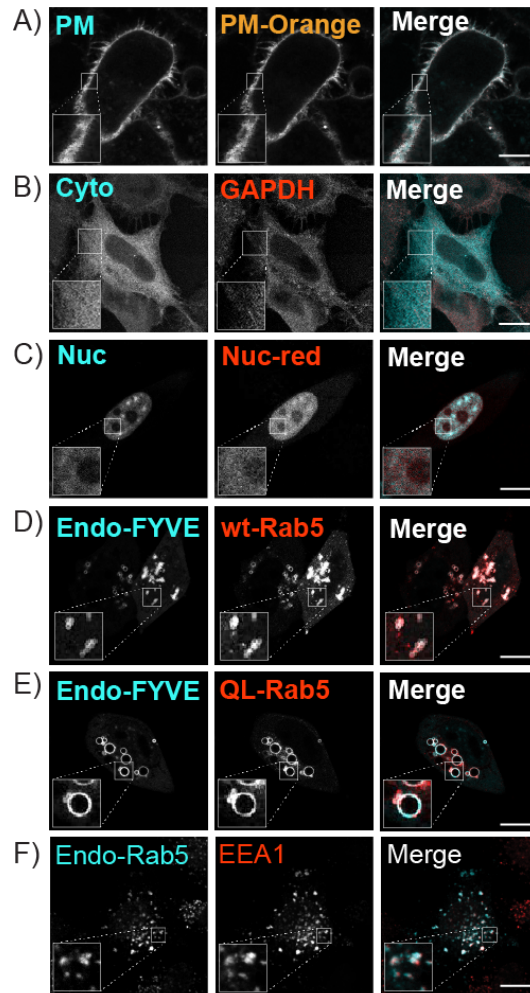
**Acknowledgments:** We thank all members of the Grimseylab@UGA for comments and advice.

**Conflict of interest:** The authors declare they have no conflict of interest with the contents of this article.

## **FOOTNOTES**

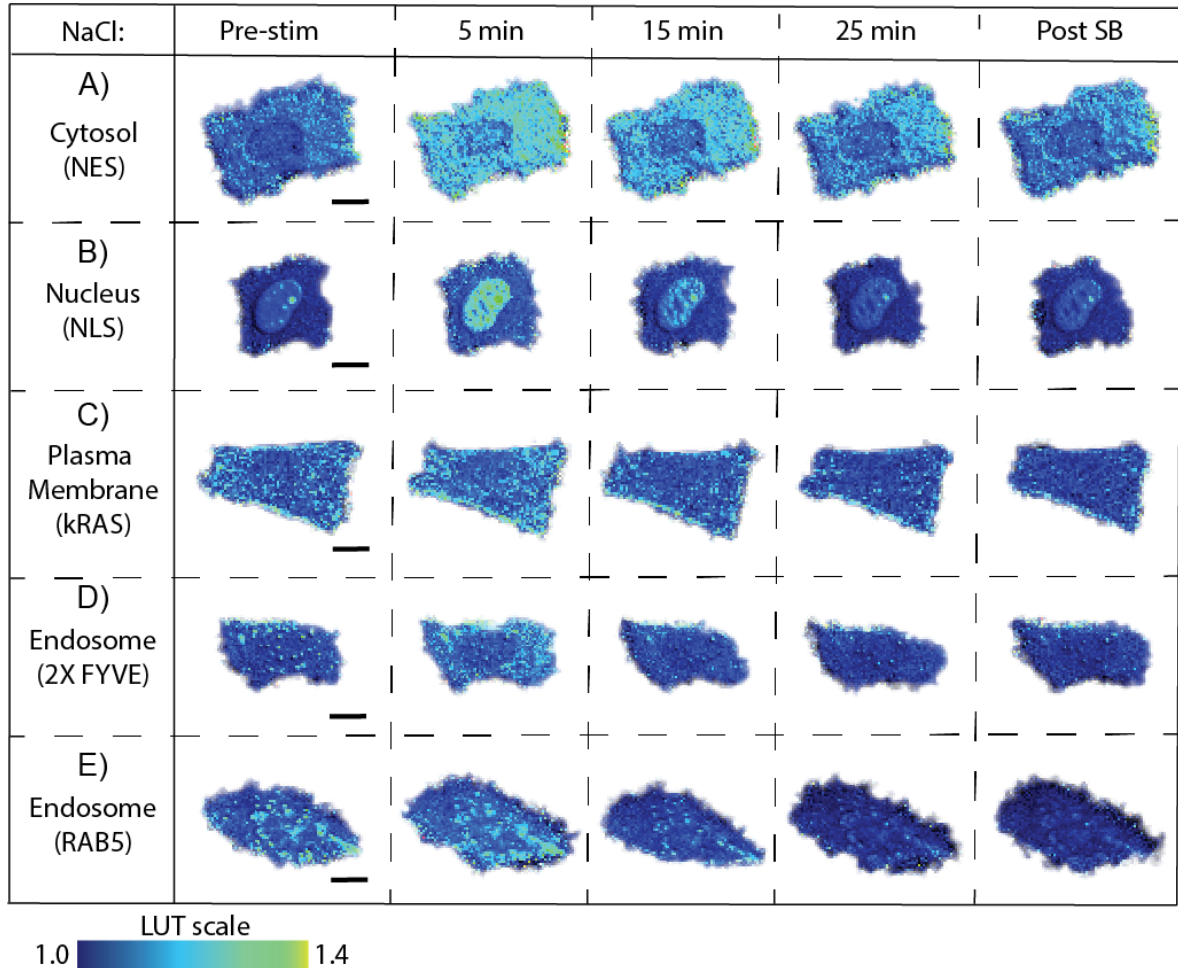
The abbreviations used are; ANOVA, analysis of variance; FRET, Fluorescence Resonance Energy Transfer; GPCR, G protein-coupled receptor; MAPK, mitogen-activated protein kinase; MKK, mitogen-activated protein kinase kinase; PAR1, protease-activated receptor-1; PGE2, prostaglandin E2; TAB, transforming growth factor- $\beta$  activated kinase-1 binding protein1;  $\alpha$ -Th, thrombin.

## Supplemental Figures for Chapter 2



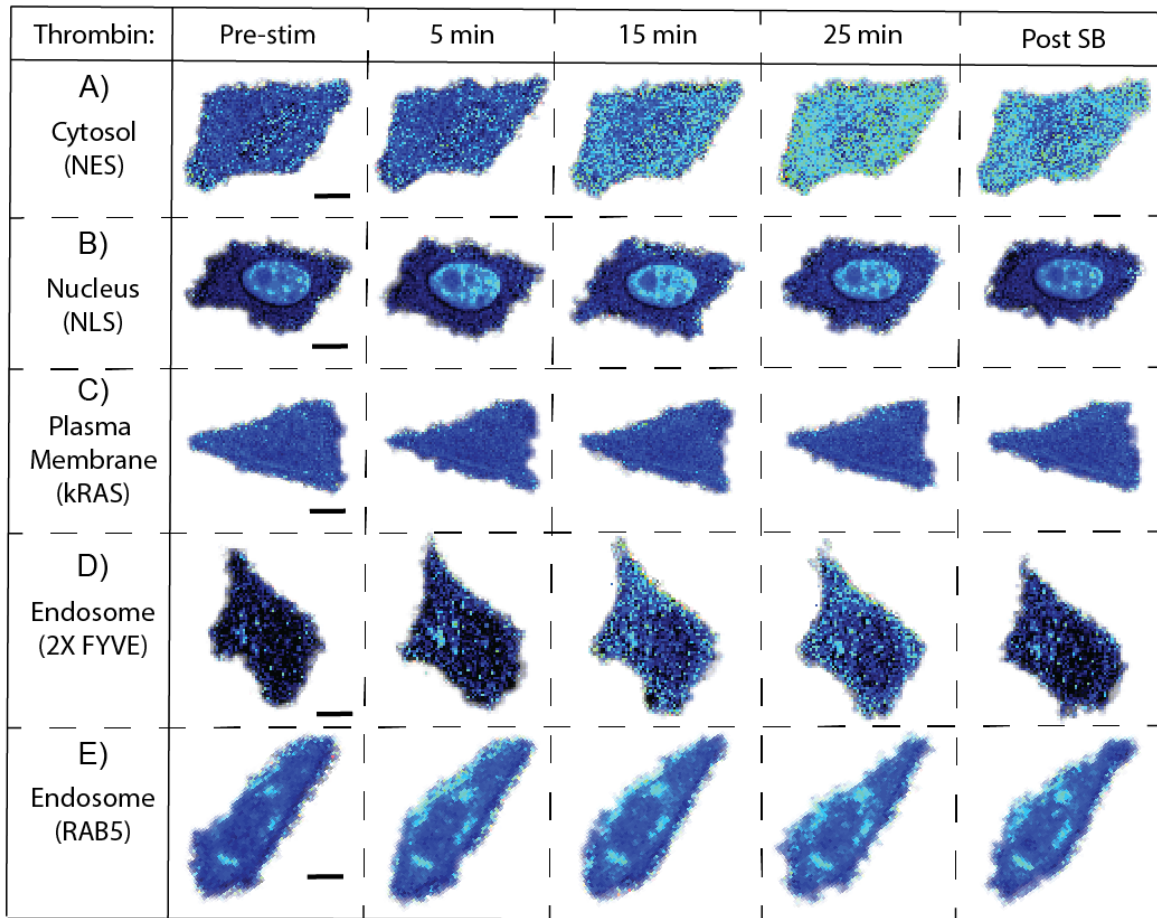
### Supplemental Figure 2.1: p38 Biosensors Colocalize With Compartment-Specific Probes And Proteins

Immunofluorescence confocal microscopy of fixed HeLa cells transiently expressing localized biosensors (displaying-SECFP) and probed for subcellular-specific markers (as indicated) as follows: **A)** plasma membrane with PM-Orange **B)** cytosolic with GAPDH-Alexa647 **C)** nucleus with Nuc-red **D)** 2XFYVE endosomal with wt-RAB5-mRFP **E)** 2XFYVE endosomal co-transfected with Q79L-RAB5-mRFP **F)** RAB5 endosomal with EEA1(Alexa 594) **G)** Pearson's Correlation Coefficient ( $r$ ) quantifying biosensor-protein colocalization as described in **A-F**.  $n$  = number of individual cells, representative of >2 independent biological repeats. Scale bars, 10  $\mu$ m.



### Supplemental Figure 2.2: Pseudo Color Images Of Biosensor Responses To NaCl

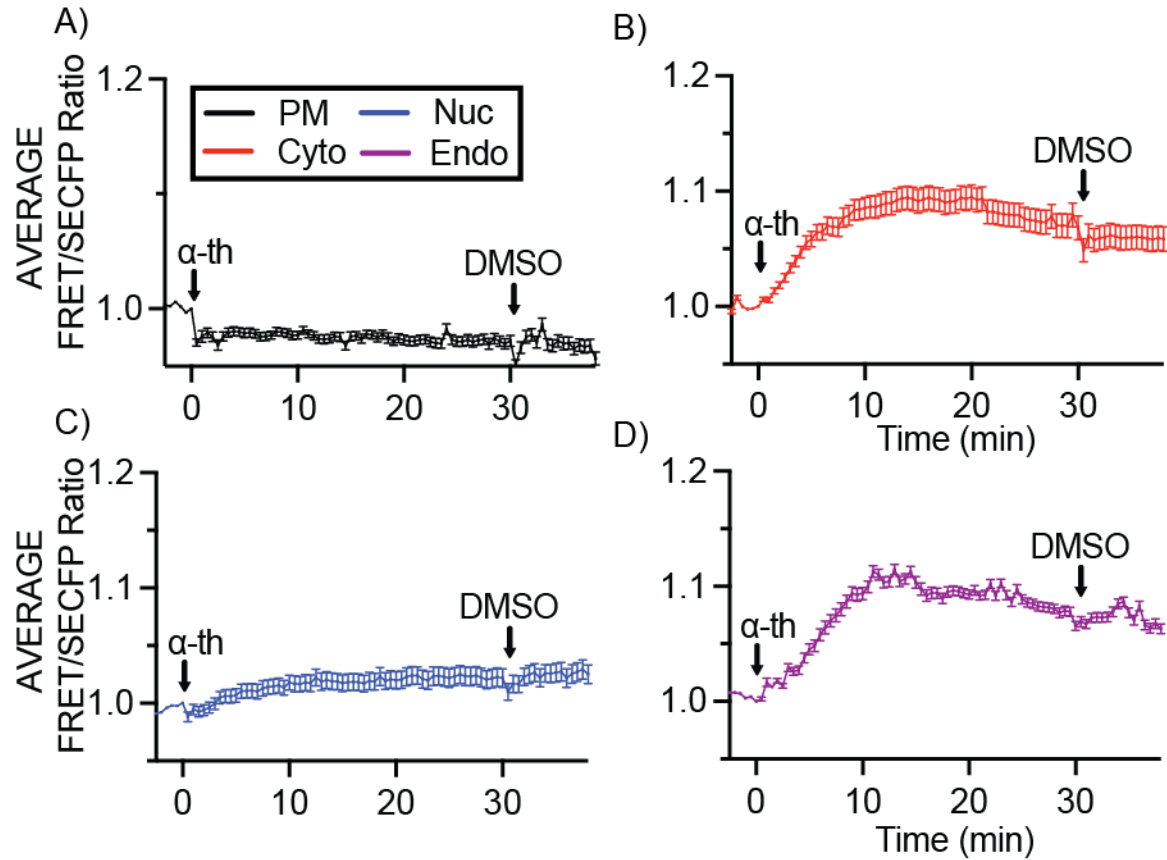
Representative FRET/SECFP ratiometric images (pseudo colored) before and after treatment with NaCl, cells expressing **A)** NES - cytosolic **B)** NLS - nuclear **C)** KRAS - plasma membrane **D)** 2XFYVE - endosome or **E)** RAB5 - endosome. Look Up Table (LUT) pseudo coloring where warmer colors represent higher FRET emission ratios and indicate spatially localized activity. Scale bars, 10  $\mu$ m.



LUT scale  
1.0  1.4

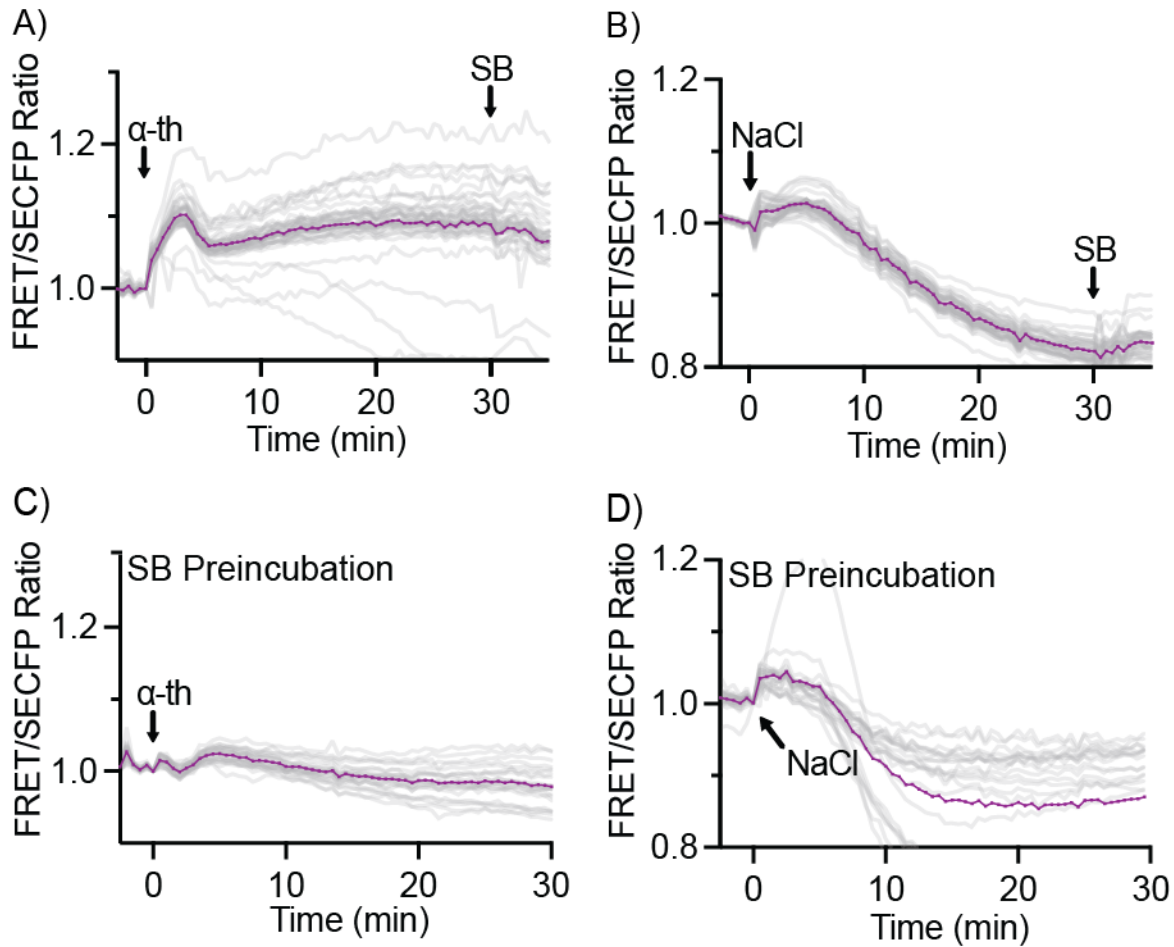
### Supplemental Figure 2.3: Pseudo Color Images Of Biosensor Responses To Thrombin

Representative FRET/SECFP ratiometric images (pseudo colored) before and after treatment with thrombin, cells expressing **A)** NES - cytosolic **B)** NLS - nuclear **C)** KRAS - plasma membrane **D)** 2XFYVE - endosome or **E)** RAB5 - endosome. Look Up Table (LUT) pseudo coloring where warmer colors represent higher FRET emission ratios and indicate spatially localized activity. Scale bars, 10  $\mu$ m.

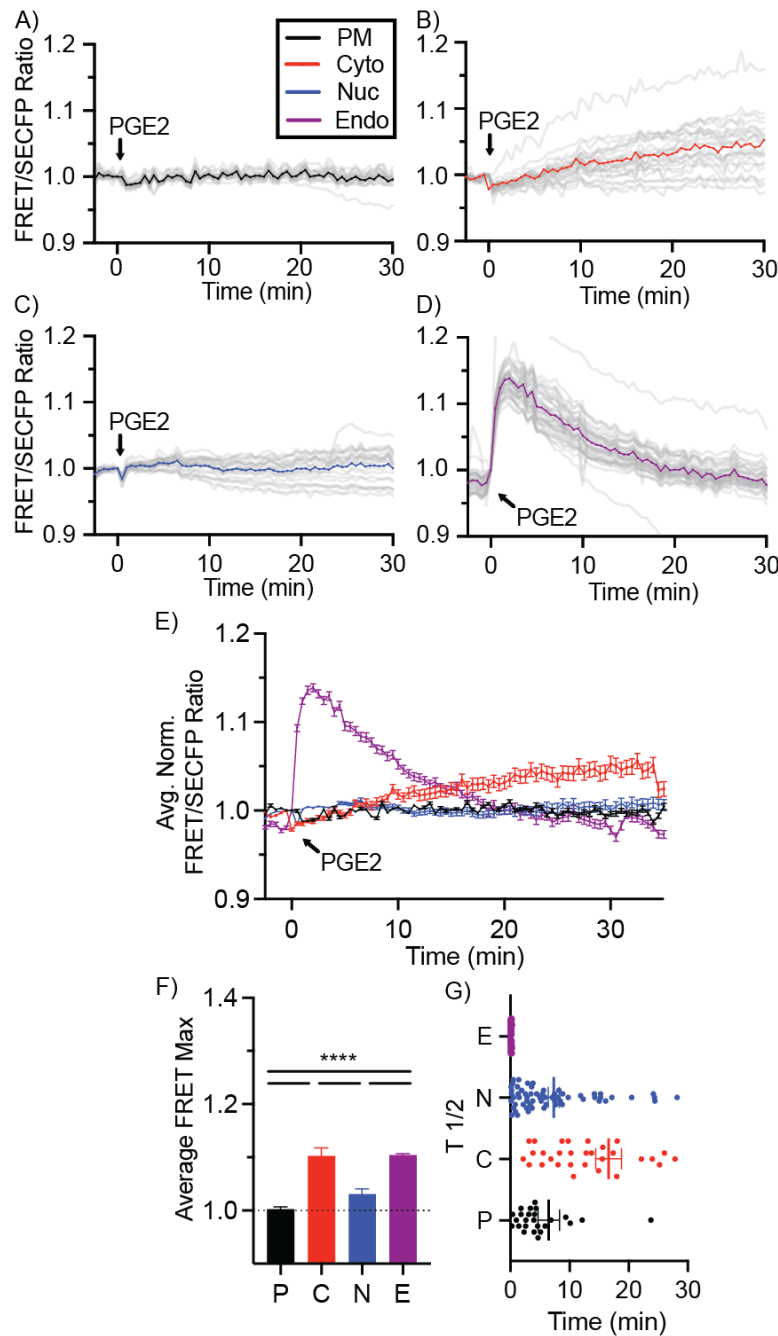


**Supplemental Figure 2.4: Thrombin-induced p38 Activity Is Not Altered By Addition Of DMSO Vehicle Control**

Activation of p38 using FRET biosensors localized to the **A)** plasma membrane **B)** cytosol **C)** nucleus or **D)** endosome, expressed in HeLa cells incubated with 10nM thrombin and vehicle DMSO. FRET ratios were normalized prior to thrombin addition. Representative normalized average FRET ratio,  $n > 20$  cells  $\pm$  SEM, two independent biological repeats per biosensor.

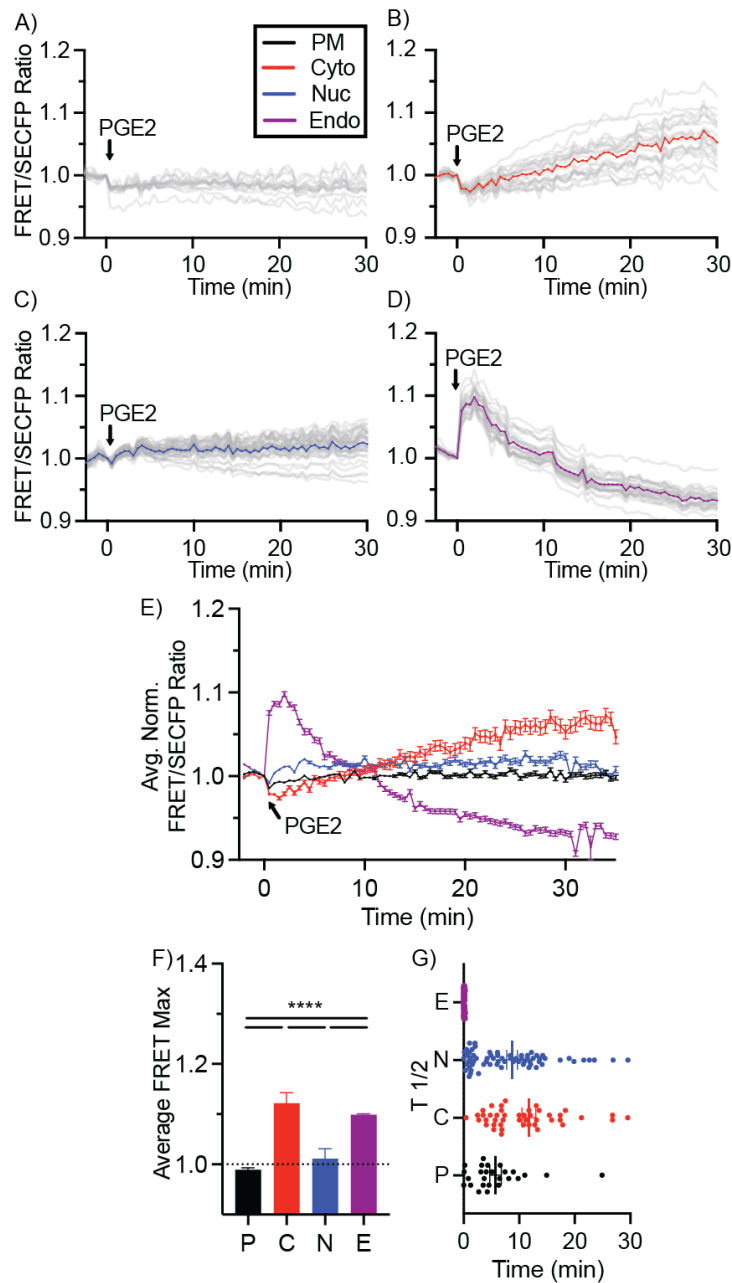


**Supplemental Figure 2.5: RAB5 Biosensor Endosomal Signaling By NaCl And Thrombin**  
 Activation of p38 using wt-RAB5 endosomal biosensor expressed in HeLa cells incubated with **A)** thrombin 10 nM **B)** NaCl 300 mM. **C)** SB203580 25  $\mu$ M preincubation and thrombin, or **D)** SB203580 25  $\mu$ M preincubation and NaCl. Representative FRET ratios were normalized prior to agonist addition. Individual cell FRET ratios are depicted in gray ( $n > 30$ -60 cells per biosensor). Average FRET ratio is indicated by colored lines.



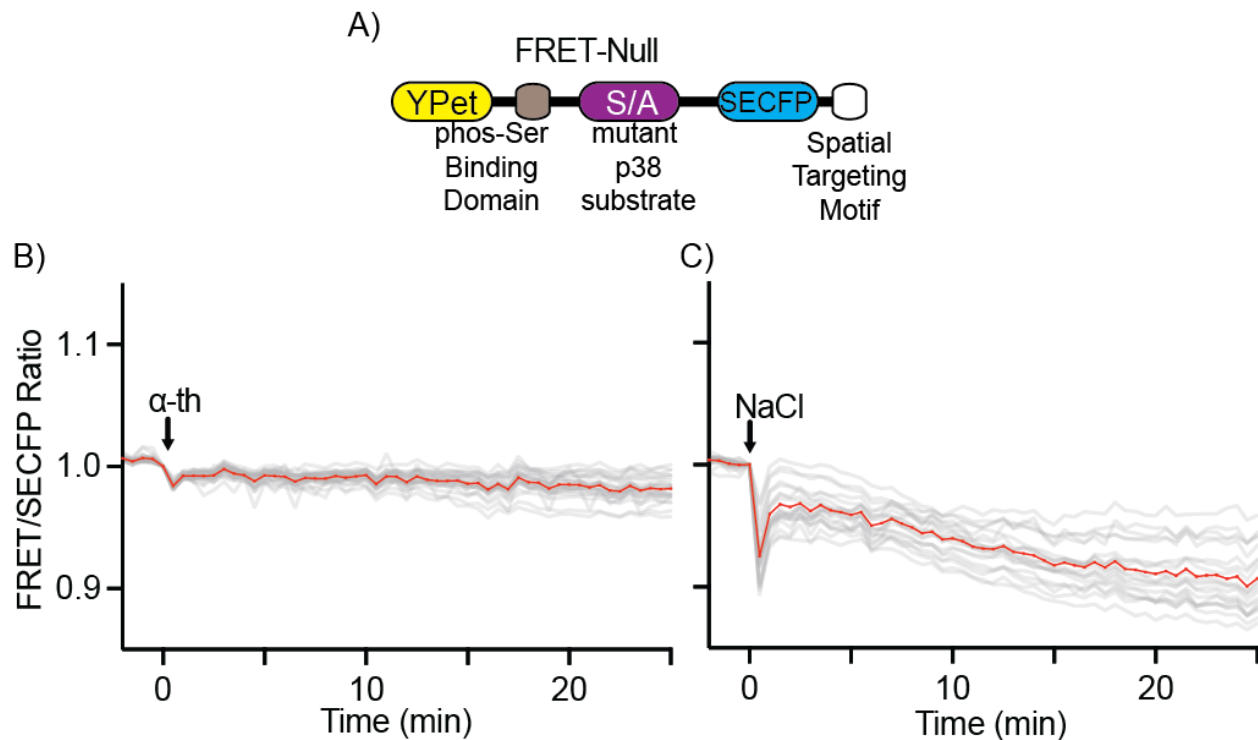
### Supplemental Figure 2.6: EP2 Induced p38 Activation

Activation of p38 using FRET biosensors localized to the plasma membrane **A**) cytosolic **B**) nuclear **C**) or endosomal **D**) expressed in HeLa cells co-expressing EP2, incubated with 10  $\mu$ M PGE2. FRET ratios were normalized prior to PGE2 addition. Individual cell FRET ratios are depicted in gray ( $n > 30-60$  cells per biosensor). The average FRET ratio is indicated by colored lines. **E**) Overlay of representative normalized averages of FRET ratio in biosensor platform from **A-D**). **F**) Maximum change in FRET ratio (FRET<sub>MAX</sub>) of individual cells pooled from 3 independent repeats, ( $n > 80-150$  ROIs per biosensor. mean  $\pm$  SEM) were analyzed by One-Way ANOVA (\*\*\*\*,  $p < 0.0001$ ). **G**) FRET response kinetics, T<sub>1/2</sub> values of cells in A-D (mean  $\pm$  SEM).



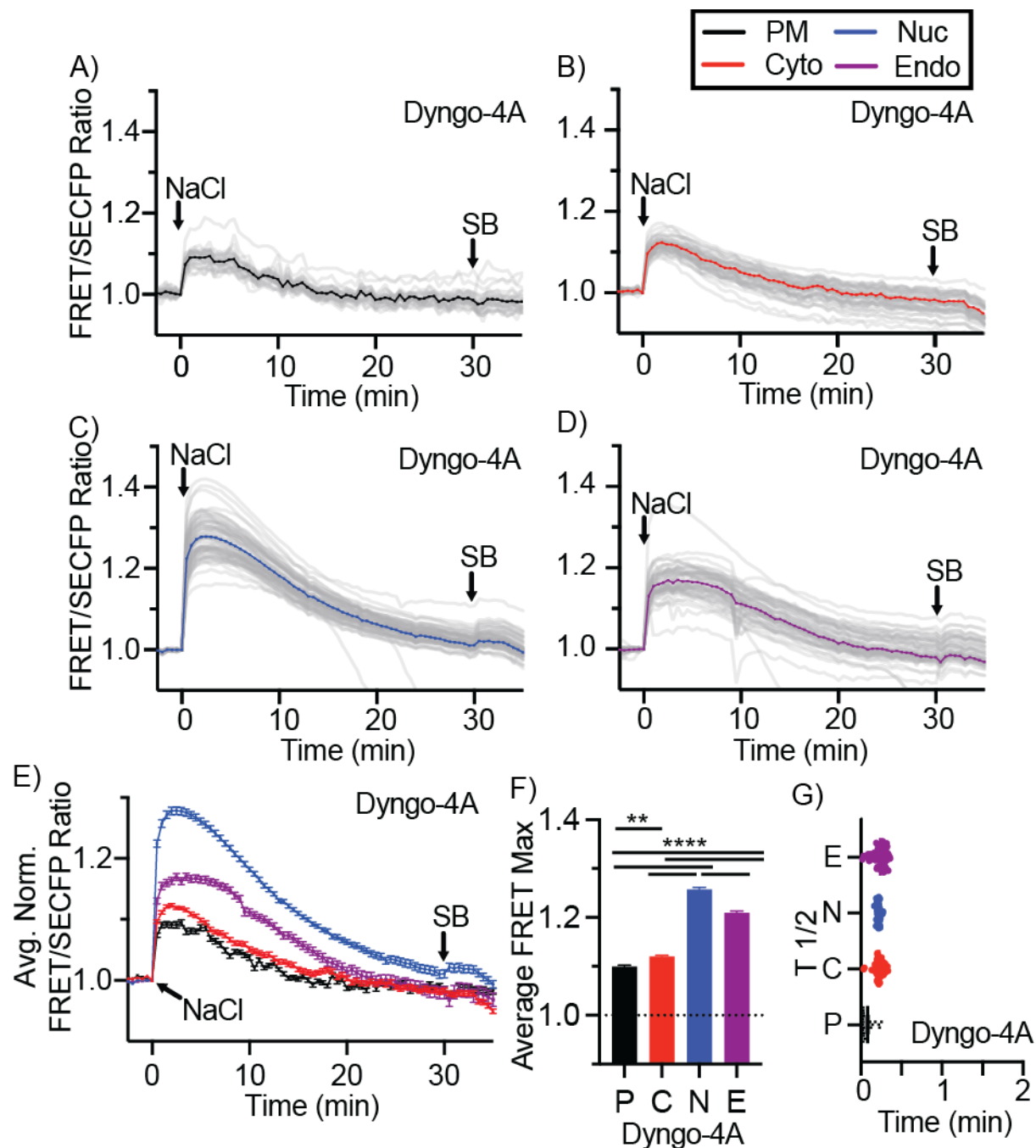
### Supplemental Figure 2.7: EP4 Induced p38 Activation

Activation of p38 using FRET biosensors localized to the plasma membrane **A**) cytosolic **B**) nuclear **C**) or endosomal **D**) expressed in HeLa cells co-expressing EP4, incubated with 10  $\mu$ M PGE2. FRET ratios were normalized prior to PGE2 addition. Individual cell FRET ratios are depicted in gray ( $n > 30$ -60 cells per biosensor). The average FRET ratio is indicated by colored lines. **E**) Overlay of representative normalized averages of FRET ratio in biosensor platform from **A-D**). **F**) Maximum change in FRET ratio (FRET<sub>MAX</sub>) of individual cells pooled from 3 independent repeats, ( $n > 80$ -150 ROIs per biosensor. mean  $\pm$  SEM) were analyzed by One-Way ANOVA (\*\*\*\*,  $p < 0.0001$ ). **G**) FRET response kinetics, T<sub>1/2</sub> values of cells in A-D (mean  $\pm$  SEM).



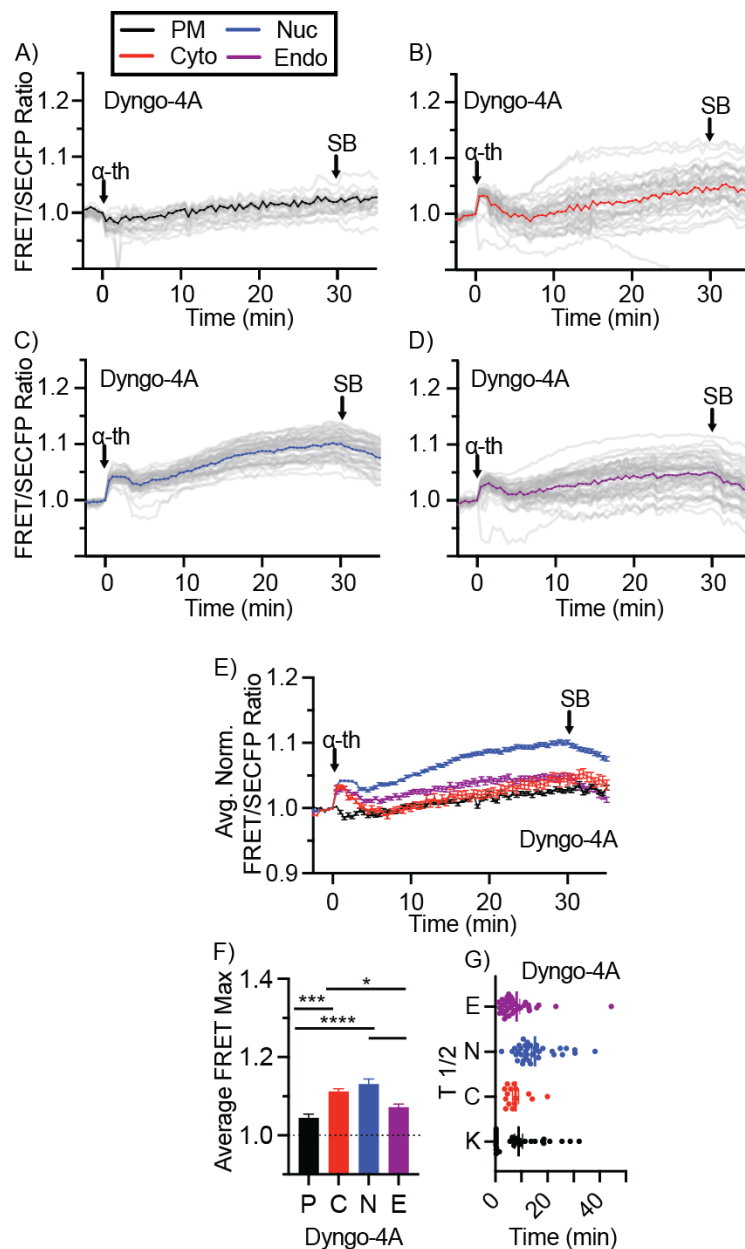
**Supplemental Figure 2.8: p38 Biosensor is Specific to Kinase Activity**

A) Schematic of biosensor design for FRET-Null, with key serine residues in p38 bait substrate mutated to alanine. Null-biosensor expressed in HeLa cells incubated with, **A)** thrombin 10nM **B)** NaCl 300 mM. Representative FRET ratios were normalized prior to agonist addition. Individual cell FRET ratios are depicted in gray ( $n > 30-60$  cells per biosensor). The average FRET ratio is indicated by colored lines.



### Supplemental Figure 2.9: Dyngo Treatment Does Not Alter Signaling Dynamics of Osmotic Stress

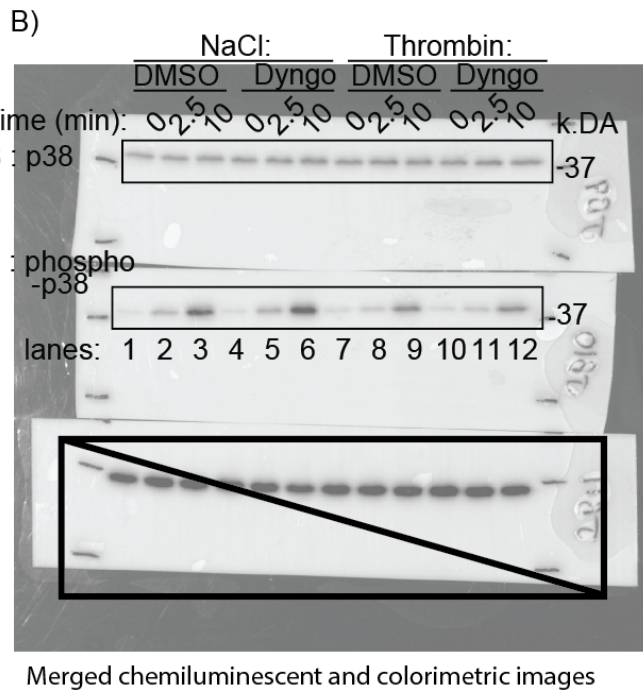
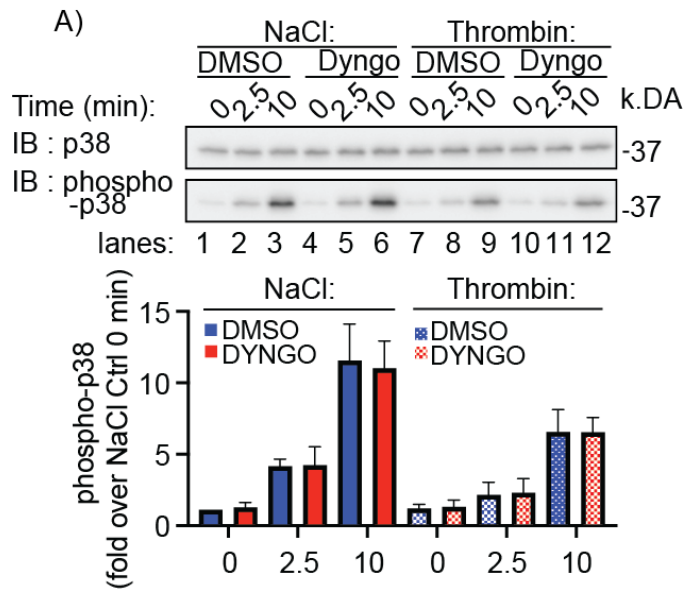
Activation of p38 using FRET biosensors localized to the plasma membrane **A)** cytosolic **B)** nuclear **C)** or endosomal **D)** expressed in HeLa cells incubated with 300 mM NaCl. FRET ratios were normalized prior to NaCl addition. Individual cell FRET ratios are depicted in gray ( $n > 30-60$  cells per biosensor). The average FRET ratio is indicated by colored lines. **F)** Overlay of representative normalized averages of FRET ratio in biosensor platform from **B-E)**. **G)** Maximum change in FRET ratio ( $FRET_{MAX}$ ) of individual cells pooled from 3 independent repeats, ( $n > 80-150$  ROIs per biosensor, mean  $\pm$  SEM) were analyzed by One-Way ANOVA (\*\*\*\*,  $p < 0.0001$ ). **H)** FRET response kinetics,  $T_{1/2}$  values of cells in A-D (mean  $\pm$  SEM).



### Supplemental Figure 2.10: Dyngo Treatment Shifts p38 Activity Away From The Cytosol And Endosome

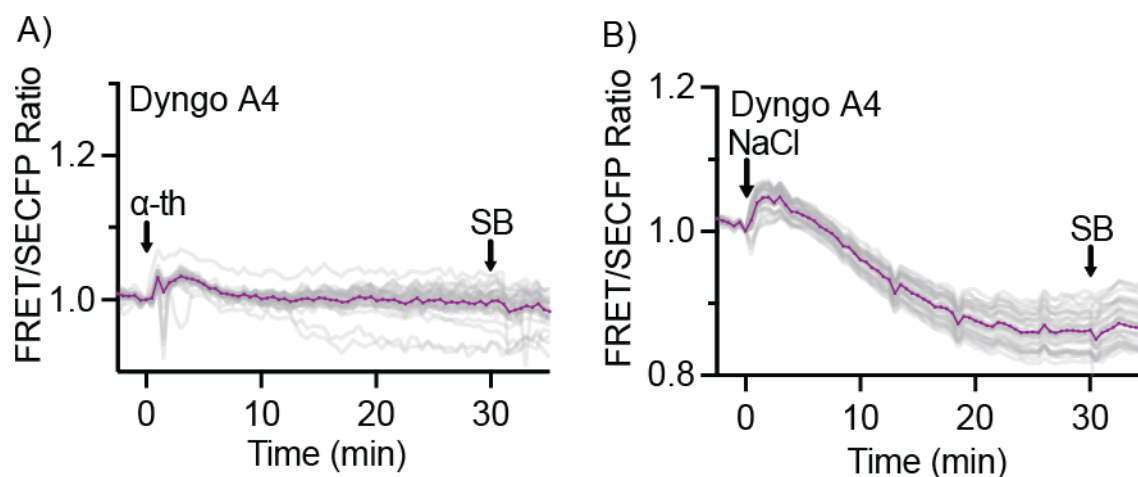
Activation of p38 using FRET biosensors localized to the plasma membrane **A)** cytosolic **B)** nuclear **C)** or endosomal **D)** expressed in HeLa cells co-expressing PAR1, incubated with 10 nM thrombin. FRET ratios were normalized prior to thrombin addition. Individual cell FRET ratios are depicted in gray ( $n > 30-60$  cells per biosensor). The average FRET ratio is indicated by colored lines. **E)** Overlay of representative normalized averages of FRET ratio in biosensor platform from **A-D)**. **F)** Maximum change in FRET ratio (FRET<sub>MAX</sub>) of individual cells pooled from 3 independent repeats, ( $n > 80-150$  ROIs per biosensor, mean  $\pm$  SEM) were analyzed by One-Way ANOVA (\*\*\*\*,  $p < 0.0001$ ). **G)** FRET response kinetics, T  $\frac{1}{2}$  values of cells in A-D (mean  $\pm$  SEM).

Supplemental Figure 11



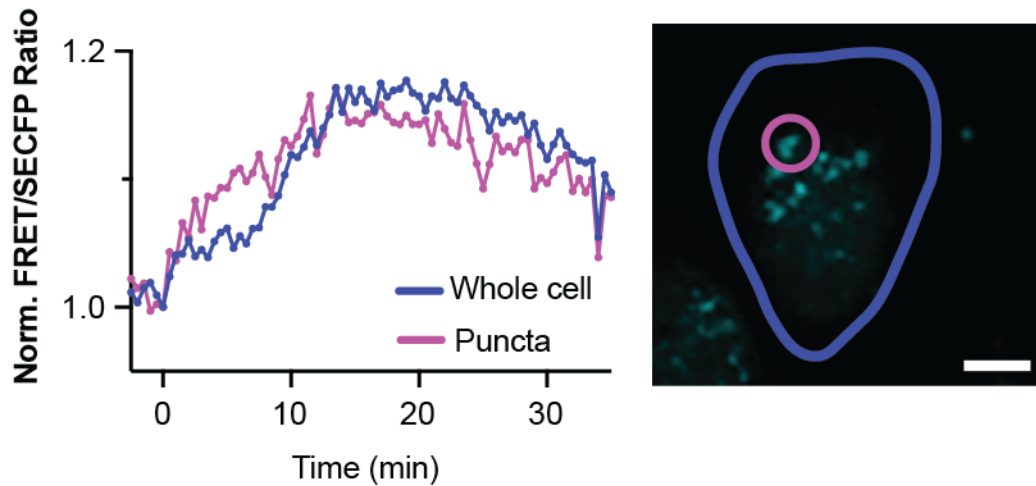
**Supplemental Figure 2.11: Dyngo Treatment Does Not Inhibit P38 Activation**

**A)** Representative immunoblot of HeLa cells transiently expressing PAR1 and stimulated with NaCl 300 mM or 10 nM thrombin for the indicated times in the presence of 15 $\mu$ M Dyngo-4A or DMSO control. Fold change of phospho-p38 over total p38 quantified from three independent repeats. (mean +/- StDev). **B)** Unprocessed chemiluminescent image of blot from A), merged with colorimetric image to show molecular weight marker.



**Supplemental Figure 2.12: Dyngo Treatment RAB5 Signaling**

Activation of p38 using wt-RAB5 endosomal biosensor expressed in HeLa cells incubated with **A)** cells preincubated with Dyngo 4A (15  $\mu$ M) for 1h prior to stimulation with thrombin 10nM **B)** NaCl 300 mM. SB203580 added at 30 minutes of stimulation as indicated. Representative FRET ratios were normalized prior to agonist addition. Individual cell FRET ratios are depicted in gray ( $n > 30$ -60 cells per biosensor). Average FRET ratio is indicated by colored lines.



**Supplemental Figure 2.13: Comparable FRET Responses From Whole Cell or Endosomal Puncta**

Representative FRET/SECFP channel emission ratio time course comparing responses from an ROI drawn around a whole cell (in blue) and an ROI drawn around a single endosome (in purple) in HeLa cells transfected with pcDNA3.1 FLAG-PAR1 and 2XFYVE endosome localized biosensor, that endosomal p38 activity responses specifically come from endosomes. Representative fluorescent (merged YFP/SECFP) Colibri image. Scale bar 10  $\mu$ M.

CHAPTER 3  
THE ROLE OF ATYPICAL MAPK P38 SIGNALING IN THE PROGRESSION OF  
INFLUENZA-A INDUCED PULMONARY INFLAMMATION<sup>4</sup>

---

<sup>4</sup> Burton, J.C., Fahey, D., Royer, F., Zhu, Y., Sakamoto, K., Zhang, D., Watford, W., Grimsey, N.G. To be submitted to Lung Cellular and Molecular Physiology

## INTRODUCTION

Acute lung injury (ALI) is a serious inflammatory complication of the lungs that can be caused by physical trauma, toxic inhalants, or infection<sup>489, 575</sup>. Viral infection of the lungs by pathogenic coronavirus or influenza induces severe ALI in patients<sup>576</sup>. ALI is characterized by a rapid onset of dysregulated immune and inflammatory responses that lead to respiratory failure. Severe lower respiratory diseases such as ALI are typically treated by symptom management and mechanical ventilation, itself a cause of lung injury exacerbation. Previous pharmacological interventions to target inflammation have been unsuccessful<sup>489</sup> and novel therapeutic strategies are needed to address the underlying causes of ALI.

Host-mediated antiviral signaling involves immune cell recruitment to the site of infection, expression of pro-inflammatory cytokines including, interleukin (IL)-1, IL-6, IL-8, interferon- $\beta$ , interferon-stimulated genes (ISG)-15 and tumor necrosis factor (TNF)- $\alpha$ <sup>489, 577</sup>. Cytokine expression is controlled by kinase-mediated signaling pathways downstream of viral sensing, such as the Nuclear factor kappa-light-chain-enhancer of activated B cells (NF- $\kappa$ B) family, and mitogen-activated protein kinase (MAPK) signaling pathways<sup>578, 579</sup>. These kinases normally drive a tightly regulated inflammatory response that is negatively self-regulated during the resolution phase, but during ALI, overwhelming signaling occurs, leading to cytokine storm and prolonged vascular disruption<sup>580</sup>. Despite selective targeting of the NF- $\kappa$ B signaling pathway with small molecule inhibitors, preclinical results have been inconclusive<sup>581</sup>. It has been proposed that the moderate impact of kinase-activity targeting strategies is a result of simultaneously inhibiting the protective functions of kinase activity<sup>515</sup>. Therefore, it would be advantageous to target only a subset of kinase signaling involved with disease propagation, leaving physiological or beneficial signaling intact.

MAPK p38 is a central regulator of cytokine expression, vascular stability, and immune activation. Expression and activation of p38 correlate with increased severity of lower respiratory lung diseases, including asthma, chronic obstructive pulmonary disease, and ALI<sup>61, 105, 122-130, 133-136, 531, 582</sup>. Indeed, p38 is directly associated with the propagation of pro-inflammatory responses in multiple cell types, including endothelial cells and alveolar epithelium, alongside macrophages and monocytes recruited to the inflammatory sites through the secretion of inflammatory cytokines<sup>90, 122, 128, 129, 133, 582-585</sup>. P38 is also a key mediator of endothelial activation during acute lung injury<sup>112, 129, 133, 134</sup>. P38 phosphorylation is associated with ALI, and kinase signaling contributes to endothelial barrier dysfunction via microtubule-associated protein 4 (MAP4) phosphorylation-dependent microtubule disassembly in inflammation-induced acute lung injury<sup>521</sup>. However, like NF- $\kappa$ B signaling, p38 inhibition has underperformed as a therapeutic candidate in inflammation-based disease due to toxicity effects related to inhibition of all p38, including kinase functions not related to inflammation<sup>35</sup>. However, p38 is dynamically activated through multiple mechanisms; canonical kinase cascades mediated by upstream MAPKK3/6 activity, and two methods of atypical activation. The first, critical for T cell activation via T-cell receptor, is mediated by zeta-chain-associated protein kinase 70 (Zap70) phosphorylation of p38 $\alpha/\beta$ , leading to kinase dimerization, trans-autophosphorylation, and ultimately partial kinase activation<sup>92</sup>. The second atypical method of p38 activation, and the focus of this study, is mediated by direct kinase interaction with the adaptor protein TGF-Beta Activated Kinase 1 Binding Protein 1 (TAB1)<sup>255</sup>. TAB1 binds to p38 at two sites; a canonical p38 substrate binding site and a non-canonical binding site at the c-terminal lobe of p38 $\alpha$ , leading to *cis*-autophosphorylation of p38 at Thr180 and Tyr182 and activation of the kinase<sup>67, 71, 81</sup>. Atypical p38 activation subsequently leads to phosphorylation of TAB1 in *trans*<sup>74</sup>. This protein interaction has been shown to play a key role in disease, where

blockade of TAB1-p38 interaction reduces infarct volume following myocardial ischemia in mice<sup>71, 110</sup>. As well, the TAB1-p38 interaction is implicated in viral infection, where it has been shown that blockade of TAB1-interaction with p38 inhibits viral assembly and replication in hepatitis C virus (HCV), thrombocytopenia syndrome virus (SFTSV), herpes simplex virus type 1 (HSV-1), and severe acute respiratory syndrome coronavirus 2 (SARS-CoV-2)<sup>135, 255</sup> and also plays a role in RIG-1 mediated interferon production<sup>136</sup>. However, the role of atypical p38 signaling has not been investigated in influenza-induced acute lung disease.

In this study, we hypothesized that the TAB1-p38 interaction is necessary for the immune and inflammatory response during influenza infection. To test this hypothesis, we explored the role of TAB1-p38 in the propagation of pulmonary inflammatory disease progression using a *Tab1*-knock-in mouse (TAB1<sup>KI</sup>) previously developed to explore the role of atypical p38 in ischemia-reperfusion injury<sup>71, 81</sup>. Genetic knock-in mutations to four key residues of TAB1 required for p38 binding (V390A, Y392A, V408G, M409A) blocks the formation of the p38-TAB1 complex<sup>71, 81</sup>. Critically, while ablating TAB1 or p38 is embryonically lethal<sup>25, 89</sup>, the TAB1<sup>KI</sup> mice are not only viable but protected from myocardial ischemic damage following coronary artery occlusion<sup>71</sup>. In our study, we use the C57BL/6 TAB1<sup>KI</sup> mice inducing ALI via an intranasal model of influenza infection, with analysis of mRNA and protein expression, histological characterization, and immune profiling. We report the first evidence that blockade of atypical p38 signaling by TAB1 reduces influenza-induced weight loss, improves histopathological outcomes, and leads to increased monocyte recruitment to the lungs in male mice. These studies provide crucial first evidence for further study of atypical p38 signaling as a therapeutic target in conjunction with existing therapies to combat influenza-induced ALI.

## RESULTS

### **TAB1<sup>KI</sup> mice display differential weight loss compared to WT**

To first determine differences in influenza-induced disease progression and recovery in mice, a standard weight curve was performed. 6–8-week-old wildtype C57BL6 (WT) control mice and C57BL6-TAB1<sup>KI</sup> mice were intranasally infected with 50  $\mu$ L of  $1 \times 10^4$  PFU X31 influenza (see methods) and weighed daily. To control for sex as a variable, each cohort was separated by sex. Both male and female mice experienced weight loss following infection with influenza, while control mice maintained stable weight. In both sexes, weight loss continued for 7-8 days before beginning to recover. Male TAB1<sup>KI</sup> mice display significantly reduced weight loss, reaching a maximum weight loss of around 10% D0 weight, compared to an average loss of 15% in WT mice. TAB1<sup>KI</sup> male mice also had decreased recovery time compared to male WT mice starting on day 6 post-infection, recovering to pre-infection weight by day 11, whereas WT male mice did not fully recover by day 14 (**Fig. 3.1A**). Female TAB1<sup>KI</sup> mice displayed a less distinct change in weight loss compared to WT, although there was significantly less weight loss in TAB1<sup>KI</sup> female mice during the peak of influenza infection around day 7 (**Fig. 3.1B**), with KI females experiencing an average loss of around 14%, compared to WT experiencing on average a 20% weight loss. Both TAB1<sup>KI</sup> and WT female mice recovered to pre-infection weights by day 12.

### **Histopathological features of WT vs KI mouse lungs before and after influenza infection.**

Following identification of a phenotype based on weight loss, we selected days 3 and 5 post-infection to further assess the histopathological features of acute IAV infection in TAB1<sup>KI</sup> vs WT mice. H&E-stained mouse lung samples were sectioned, stained, and scored by pathologist, with increasing scores corresponding to increased histopathology (see Methods). TAB1<sup>KI</sup> Mice did not display baseline differences in lung physiology in male or female mice compared to WT

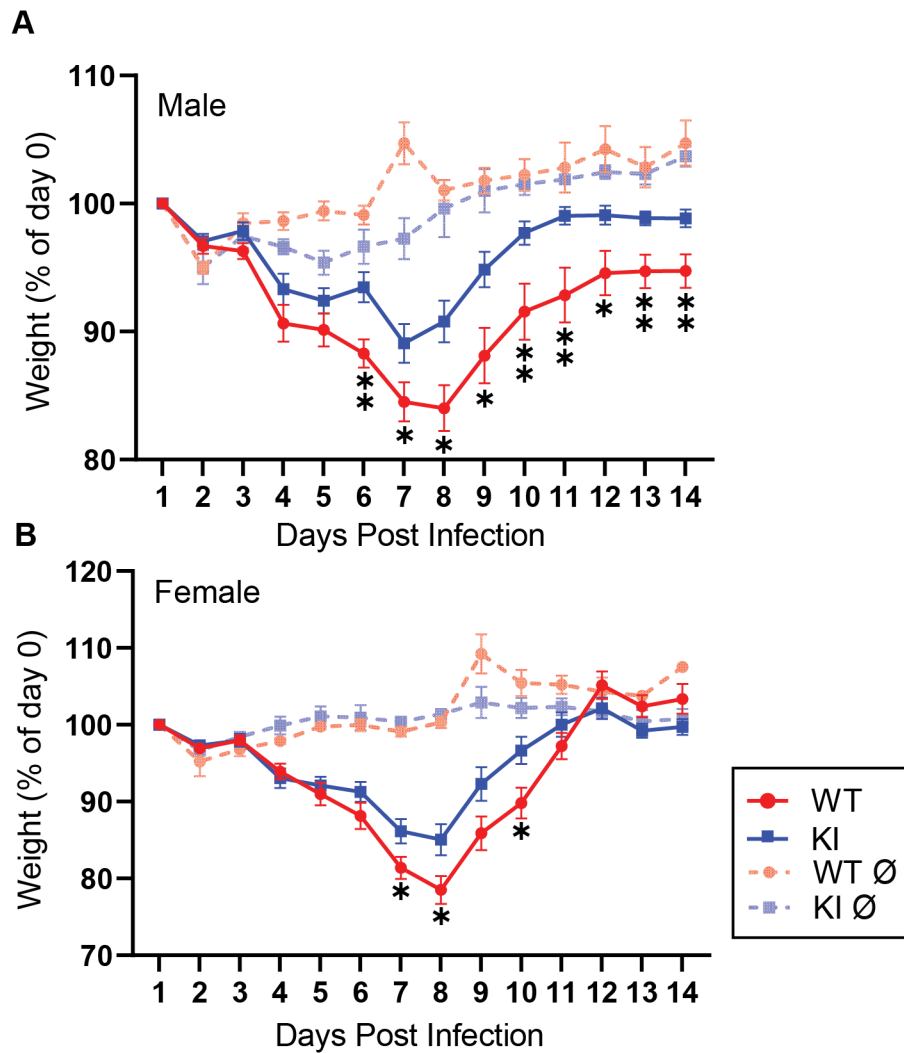


**Figure 3.1:  $TAB1^{KI}$  mice display differential weight loss compared to WT.** Influenza-infected or non-infected control mice were weighed daily for 14 days and divided by their day 0 weights to determine percentage weight loss of (A) male or (B) female mice. WT male N = 11, KI male N = 15, WT female N = 12, KI female N = 15. Male control (uninfected mice) N = 3 for WT/KI. Female control mice N = 4/3 for WT and KI respectively. Comparisons made using unpaired two-tailed Student's T tests. Data shown as average weight for each condition, error bars in SEM.

(Fig. 3.2 A,-D), compare mock panels. However, following infection, male TAB1<sup>KI</sup> mice displayed significantly less immune recruitment to the alveoli compared to WT at day 3. By Day 5 however, TAB1<sup>KI</sup> male mice were comparable to WT mice. Mice were also assessed for influenza score, which consisted of combined histopathological features of interstitial pneumonia (IP), bronchiolitis (Br) and alveolar edema. WT male mice displayed significantly more inflammation by day 3 compared to control, while KI mice did display inflammation it was not significantly increased at day 3 above day 0 (Fig. 3.2 B,F). Interestingly, KI male mice did display significantly higher influenza scores by day 5 compared to baseline and day 3 KI mice, while WT mice did not display a significantly more severe phenotype compared to day 3 (Fig. 3.2 B,F). Male TAB1<sup>KI</sup> mice also did not show significant increase in perivascular cuffing at day 3, while WT mice did (Supp. Fig. 3.1 A,C). These findings indicate that male TAB1<sup>KI</sup> mice have a delayed histopathological response to influenza infection compared to WT. Female mice were assessed separately, with no significant difference in alveoli score in TAB1<sup>KI</sup> compared to WT at day 3 or day 5, and both genotypes had significant increases in score compared to respective control mice (Fig. 3.2 C,G). Female mice also displayed comparable influenza and perivascular cuffing scores (Fig. 3.2 D,H, Supp. Fig. 3.1 B,D), indicating that the protective effect in the TAB1<sup>KI</sup> mice is insignificant in females.

#### **Influenza replication is not altered in the TAB1<sup>KI</sup> mice.**

Next, to assess whether viral replication plays a role in TAB1<sup>KI</sup> phenotype, viral plaque assays were performed using whole lung homogenate derived from infected mice at day 3 and day 5 post-infection. No significant difference was determined in viral plaque forming units between WT and TAB1<sup>KI</sup> mice (Fig. 3.3 A,C). Parallel to plaque assays, we also performed qPCR on lung homogenates to detect M protein mRNA transcripts, a key capsid protein needed for viral



replication. No significant differences were detected in levels of M protein transcripts between WT and TAB1<sup>KI</sup> mice (**Fig. 3.3 B,D**). Together, these results indicate that TAB1-p38 interaction does not play a role in the viral replication of X31 influenza M protein or viral infectivity.

### **TAB1<sup>KI</sup> mice display a loss of interaction between TAB1 and p38**

Atypical p38 activity is driven by the selective interaction between the c-terminal regions of p38 $\alpha$  kinase lobe and TAB1 (371-416)<sup>71, 81</sup>. The binding of TAB1 to p38 is critical to induce p38 autophosphorylation, subsequently followed by TAB1 phosphorylation at Ser423 by p38<sup>81, 114</sup>. To confirm TAB1-p38 interaction we first isolated protein from mouse lung homogenates (D0 and D3 after X31 infection). Immunoblotting of mouse lung homogenates was probed for TAB1, revealing a shift in the migration speed of TAB1<sup>KI</sup> mice consistent with a lack of phosphorylation; as we and others have previously shown<sup>31, 71, 81</sup>, both saline control and influenza infection samples displayed the same mobility shifts (**Fig. 3.4A, lanes 1,2 vs 3,4**). In addition, the phosphorylation of TAB1 was assessed via phospho-tag SDS gel (**Fig. 3.4B**), which slows the electrophoretic mobility of phosphorylated proteins versus non-phosphorylated counterparts<sup>586</sup>. The loss of phosphorylation of TAB1 in the TAB1<sup>KI</sup> mouse (**Fig. 3.4B, lanes 2,4**) is evident through increased protein migration relative to WT (**Fig. 3.4B, lanes 1,3**). Lastly, to determine that TAB1<sup>KI</sup> mice have disrupted the interaction between TAB1 and p38 during influenza infection, p38 was immunoprecipitated and probed for TAB1 (**Fig. 3.4C**), where the loss of a band above the 50 kDa marker seen in lanes 5 and 6 are absent in lanes 7 and 8, indicating that the loss of TAB1 interaction with p38 is conserved after influenza infection. WT mice do not display a robust increase in the TAB1-p38 interaction after influenza infection compared to baseline (**Fig. 3.4C, compare lanes 5 and 6**). Together, these results indicate that the TAB1<sup>KI</sup> mice have disrupted

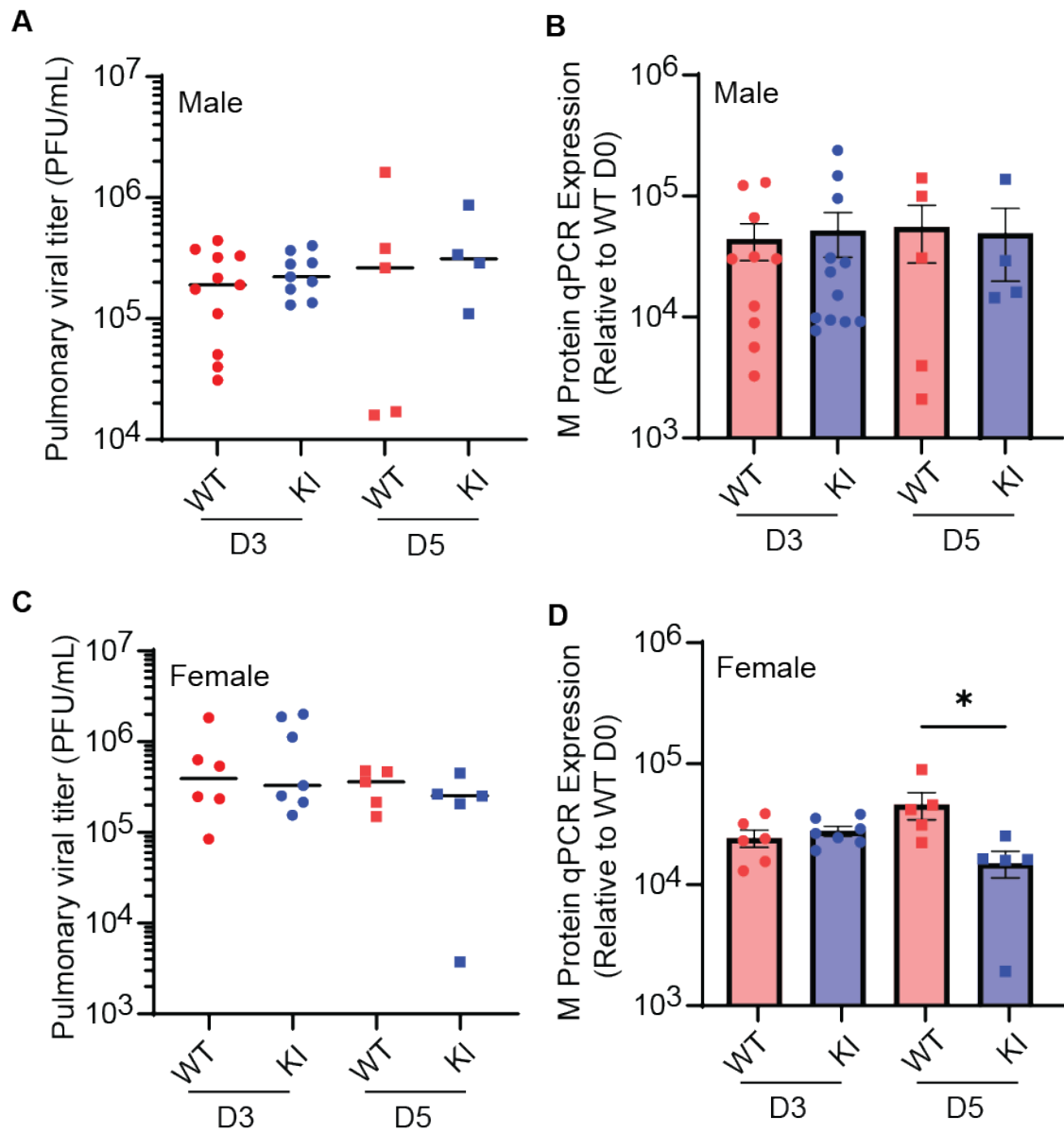


**Figure 3.3: Influenza replication is not altered in the TAB1<sup>KI</sup> mice.** (A) Pulmonary viral titer determined from plaque assay of MCDK cells infected via mouse lung homogenate after 3 or 5 days post-intranasal infection in male or (C) female mice. (B) Viral M protein mRNA expression relative to uninfected WT in male or (D) female mice. Day 3 post-infection mice; WT male N = 11, female N = 5, KI male N = 11, female N = 5. Day 5 post-infection; WT male N = 5, female N = 5, KI male N = 4, female N = 5. Comparisons made using 2-way ANOVA with post hoc Tukey testing for multiple comparisons. Error bars in SEM.

interaction of TAB1-p38 at baseline and following influenza infection, as well as altered phosphorylation of TAB1 protein.

### **TAB1<sup>KI</sup> mice display altered pro-inflammatory mRNA expression.**

To assess changes in mRNA transcription of pro-inflammatory and anti-viral cytokines associated with influenza infection, we performed qPCR on whole lung homogenate, separated by sex. Comparisons were made between genotypes matched by day and across days per genotype. Male KI mice trended toward less mRNA expression at day 3 relative to wild-type (**Fig. 3.5 A-F**). KI males did not have significantly more expression of IFN- $\beta$ , TNF $\alpha$ , IFN- $\lambda$ , or ISG-15 relative to baseline at day 3, while WT mice did (**Fig. 3.5A,C,D,F respectively**). However, KI males did have significantly increased expression of IFN- $\beta$  by day 5 relative to day 3, and generally, the levels of cytokine mRNA were comparable by day 5 between the genotypes. Female mice showed comparable responses between genotypes; both KI and WT mice had increased expression of IL-1 $\beta$ , TNF $\alpha$ , IFN- $\lambda$ , IL-6, and ISG-15 by day 3 (**Fig. 3.5G,I,J,K,L respectively**). Interestingly, female KI trended toward higher mRNA expression at day 5 relative to WT for IFN- $\beta$ , IL-1 $\beta$ , TNF $\alpha$  and ISG15 (**Fig. 3.5 G,H,I,L respectively**), although data was not significant. Female mice also had reduced IL-6 production by day 5, (**Fig. 3.5K**). These results indicate that male and female and male TAB1<sup>KI</sup> mice have different expression profiles of cytokines at day 3 and day 5, whereas day 5 mRNA levels were comparable between sexes, save for IL-6.

### **TAB1<sup>KI</sup> cytokine expression is comparable to WT.**

Altered trends in mRNA expression may reflect changes of greater magnitude at the post-translational level. Therefore, protein expression of inflammatory, anti-inflammatory, and antiviral cytokines were assessed from mouse lung homogenate using a cytokine bead array panel, separated by sex. Comparisons were made between genotypes matched by day and across days per

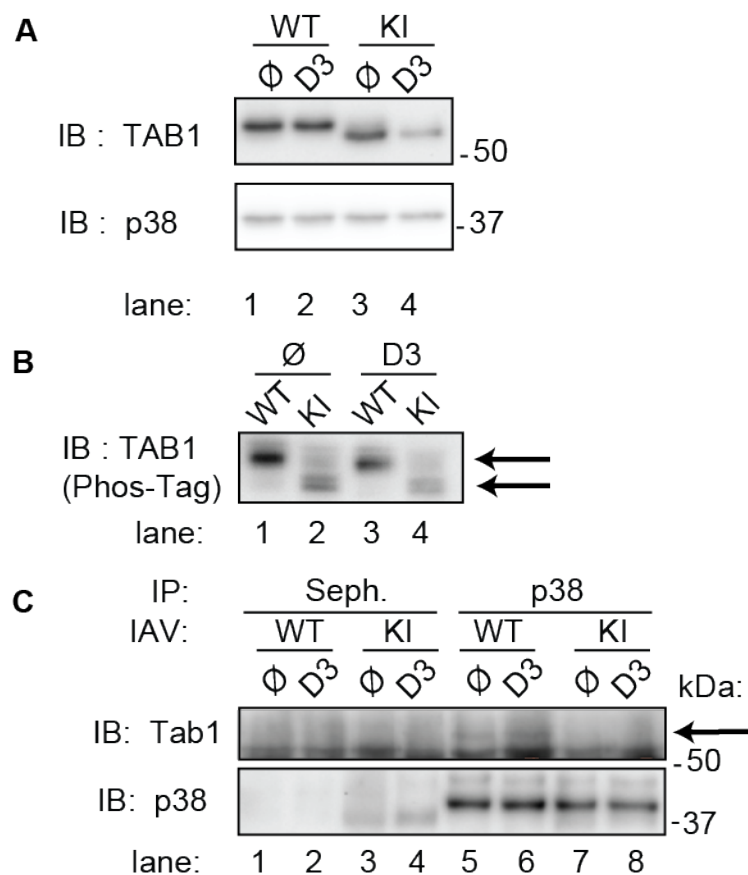


**Figure 3.4: TAB1<sup>KI</sup> mice display a loss of interaction between TAB1 and p38 .** Mouse lung homogenates from male WT and TAB1<sup>KI</sup> mice, uninfected and D3 post-infection, were immunoblotted and resolved on SDS page gels to detect (A) TAB1 and p38, or on (B) Phos-tag gel to detect TAB1<sup>KI</sup> mobility (indicated by arrows). (C) MAPK p38 was immunoprecipitated from male mouse lung homogenate from either non-infected or D3-post infection with influenza mice and probed for TAB1<sup>KI</sup> (indicated by arrow). Seph = Sepharose bead control.

genotype. In general, male KI and WT mice had increased protein expression at day 3 and day 5 relative to D0 control mice. Male KI and WT mice did not have an increase in IL-17A at day 3, but KI males had significant increase of IL-17A expression at D5 relative to D3, while WT mice had greater variance in expression (**Fig. 3.6A**). Variation in male WT mice expression was also notably higher compared to KI mice at D5 for all other cytokines analyzed (**Fig. 3.6 A-F, Supp. Fig. 3.2 B,E**), potentially leading to the loss of statistical significance compared to KI males relative to baseline. Female mice trended similarly between genotypes at day 3 (**Fig. 3.6G-L**) however female KI mice did not have significant increase in IL-6 production at D3 or D5 relative to KI D0, although not significant when compared between genotypes (**Fig. 3.6K**). Overall, female TAB1<sup>KI</sup> mice trended toward less cytokine expression at D5 compared to WT (**Fig. 3.6H-L, Supp. Fig. 3.2G,J**), although results were not statistically significant. IL-19, VEGF-A, and IL-10 were also assessed for both sexes, but did not show increase in expression relative to D0 (**Supp. Fig. 3.2, A,C,D,F,H,I**).

#### **Male TAB1<sup>KI</sup> mice have increased monocyte recruitment after influenza infection.**

To assess if TAB1<sup>KI</sup> mice have differential recruitment of immune cells involved in influenza infection, bronchoalveolar lavage (BAL) was extracted from mice at baseline and D3-post infection, and cells from BAL were sorted using flow cytometry. The total number of cells extracted from BAL were counted and percentages were calculated for alveolar macrophages, monocytes, and neutrophils. Males and females were assessed separately. As expected, TAB1<sup>KI</sup> and WT mice lacked neutrophils and monocytes at baseline, while KI males had lower alveolar macrophages at baseline compared to WT, with average 6.5% compared to average 15.8% for males, respectively (**Fig. 3.7A**). At D3-post infection, male TAB1<sup>KI</sup> mice had lower levels of alveolar macrophages compared to WT, average 6% compared to average 9% (**Fig. 3.7A**), slightly

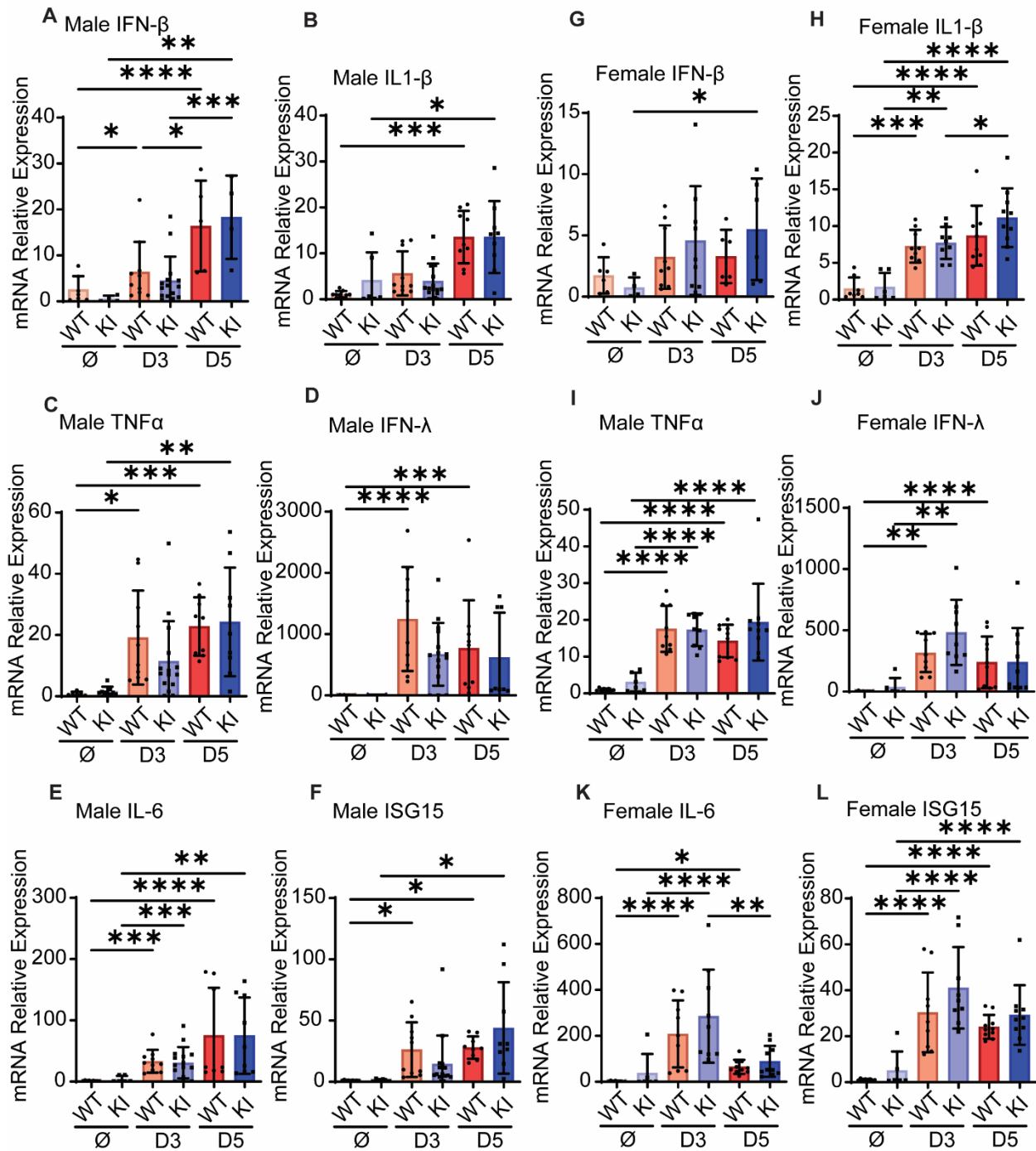


**Figure 3.5: TAB1<sup>KI</sup> mice display altered pro-inflammatory mRNA expression.** Relative mRNA expression via qPCR for (A-F) male or (G-L) female mice. Uninfected controls; WT male N = 9, female N = 8, KI male N = 6, female N = 6. Day 3 post-infection; WT male N = 11, female N = 9, KI male N = 15, female N = 9. Day 5 post-infection; WT male N = 9, female N = 10, KI male N = 9, female N = 10. Comparisons made using 2-way ANOVA with post hoc Tukey testing for multiple comparisons.

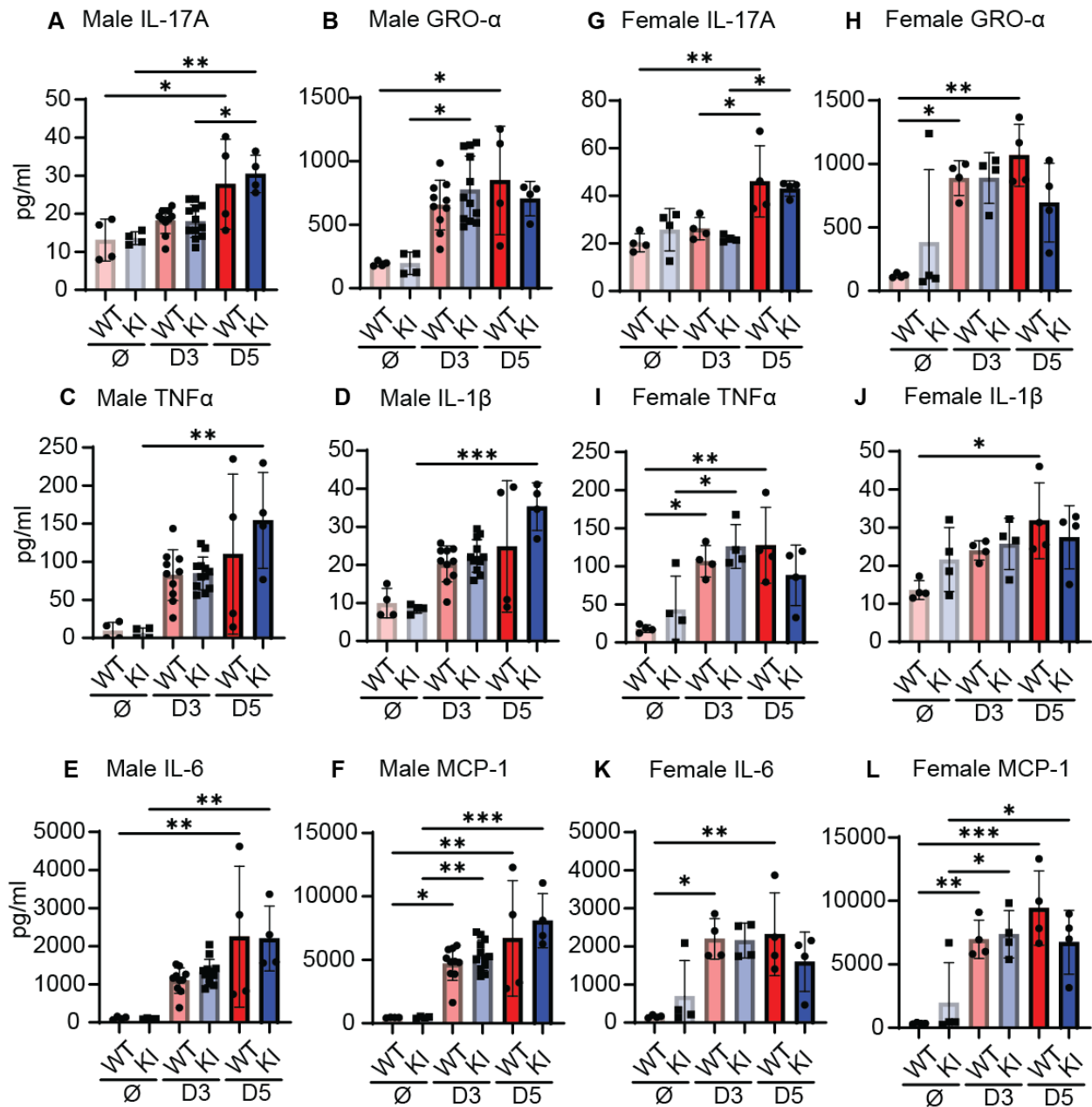


**Figure 3.6. TAB1<sup>KI</sup> cytokine expression is comparable to WT.** (A-K) Protein concentration as indicated from mouse lung homogenate before and after influenza infection. Uninfected controls; WT male N = 4, female N = 4, KI male N = 4, female N = 4. Day 3 post-infection; WT male N = 10, female N = 4, KI male N = 12, female N = 4. Day 5 post-infection; WT male N = 4, female N = 4, KI male N = 4, female N = 4. Comparisons made using 2-way ANOVA with post hoc Tukey testing for multiple comparisons.

higher levels of neutrophils (Fig. 7G), but notably had significantly more monocytes at D3 than in WT mice, with an average of 10.5% monocytes in KI mice, compared to an average of 6.5% in WT mice (**Fig. 3.7D**). Female KI mice did not have significant differences in cell percentage compared to female WT mice, although females had slightly higher monocytes (**Fig. 3.7F**). These results indicate that male TAB1<sup>KI</sup> mice have differential recruitment of immune cells following influenza infection relative to WT males.

## **Discussion**

Here, we report that the TAB1<sup>KI</sup> male mice are protected from influenza-induced lung injury as demonstrated by significant attenuation of weight loss and decreased time to recovery compared to WT mice, and reduced histopathological scoring for alveolar immune recruitment, bronchitis and interstitial pneumonia. We also report a significantly increased investment of Lys6<sup>+</sup> monocytes in TAB1<sup>KI</sup> males into the lungs, almost double by percentage what we report in WT mice. There are also notable differences in the KI females as well, including significant weight loss attenuation at the peak of infection, although KI females did not replicate the histology-scored protections or alterations in immune investment as seen in males. We also observed trends in reduced inflammatory mRNA expression and inflammatory cytokine expression in KI males at day 3 post-infection, but this trend does not carry into day 5 samples. It is interesting to consider these findings in context of the weight curve, as they may indicate that the critical junction for the trajectory of influenza infection occurs in the acute onset, and this junction is influenced by the interaction between TAB1 and p38.

P38 kinase activity plays a multi-faceted and complex role in the pathogenesis of viral-induced ALI. P38 is hyperactivated during influenza infection via pattern recognition receptor

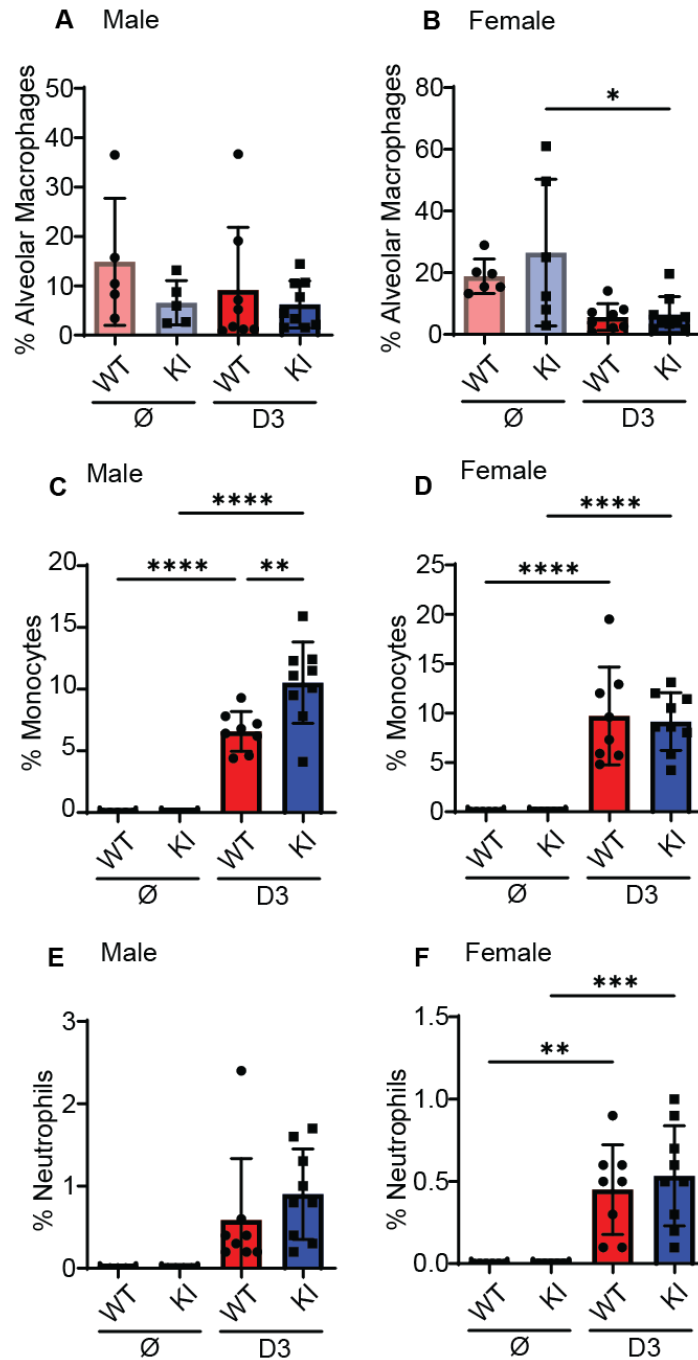


**Figure 3.7: Male  $TAB1^{KI}$  mice have increased monocyte recruitment after influenza infection.** Cells from BAL counted by flow cytometry, with percentages calculated by type of cell as indicated over total cell number. Uninfected controls; WT male N = 5, female N = 6, KI male N = 5, female N = 6. Day 3 post-infection; WT male N = 8, female N = 8, KI male N = 9, female N = 9. Comparisons made using one-way ANOVA with post hoc Tukey testing for multiple comparisons.

(PRR)-induced myeloid differentiation primary response 88 (MYD88) signaling. The influenza virus paradoxically uses this antiviral pathway to gain entry into the cell and is associated with increased viral uptake and cytokine expression in a p38-dependent fashion,<sup>530</sup>. Hyperactivated p38, alongside dysregulated NF- $\kappa$ B signaling leads to an induction of cytokine storms, resulting in dysregulated signaling cascades and ALI<sup>515, 587</sup>. Considering that the p38 kinase plays roles in multiple branches of the virus-mediated and host-mediated response to infection, it is essential for investigators to sort out which subsets of kinase activity can be attributed to which functions. The TAB1<sup>KI</sup> mouse model allows us to determine which functions are attributed to atypical signaling when compared to wild-type mice.

Prior studies have investigated the role of p38 in viral replication. The kinase plays an essential role in Sars-CoV replication, and atypical signaling by TAB1-p38 has been shown to be essential for replication of HCV and others<sup>135, 531, 588</sup>. Additionally, inhibition of p38 by p38 $\alpha/\beta$ -specific inhibitor SB202190 has previously been shown to reduce expression of over 90% of influenza viral protein expression in human umbilical vein endothelial cells (HUVEC)<sup>531</sup>, indicating that p38 is important for viral replication during ALI and other diseases. Our studies indicate that blockade of TAB1-p38 interaction in the TAB1<sup>KI</sup> mice is independent of influenza viral replication or infectivity, as noted by our qPCR data and plaque assays, respectively. Viral titers between male and female mice were comparable, suggesting that the noted differences between the influenza-infected male and female mice in our data are independent of viral burden.

P38 has been implicated in ALI as an essential driver of the pro-inflammatory response. P38 is both activated by TNF $\alpha$  signaling, leading to IL-6 production<sup>589</sup>, but also leads to the further production of TNF $\alpha$  and other factors via its downstream signaling through MK2<sup>590</sup>. P38 also

positively regulates HMGB1, which is a strong promoter of TLR-4 signaling, ARDS, and is recruited by influenza viruses to aid in viral replication. Despite these well-entrenched roles involving canonical-p38 driven activity, inhibition of atypical p38 signaling altered cytokine expression in male mice in early-stage influenza injury. These initial results may hint at greater differences that may be more apparent at earlier timepoints in the influenza infection cycle that have yet to be uncovered. Our prior studies uncovered that atypical signaling is spatiotemporally localized and sustained in the cytosolic compartment of the cell, in contrast to MKK3/6 mediated signaling, which was primarily nuclear-localized <sup>362</sup>. These results indicate that the kinase may have access to different substrate pools depending on the method of kinase activation and trafficking and, therefore, play different roles <sup>591</sup>. For example, p38 has many transcription-factor downstream substrates, which the kinase targets in the cytosol for translocation to the nucleus <sup>363</sup>. While differences in mRNA expression are modest in the TAB1<sup>KI</sup> mice compared to wild-type, our earlier timepoint of interest in this initial study (day 3 post-infection) is observed when the virus is still well-established in the host, and host mRNA expression may be affected by non-specific viral ribonucleoprotein complex cap-snatching of 5'-capped transcripts <sup>501</sup>.

We have already discussed how p38 therapeutics have struggled in the clinic, but one facet in which they have excelled is in co-treatment therapies. For example, p38 inhibitors PH-797804 and VX-702 were shown to reduce pro-inflammatory cytokines IL6, CXCL10 and TNF $\alpha$  during SARS-CoV-2 infection, but combined with nucleoside analogs Remdesivir and Molnupiravir, viral replication was also reduced <sup>592</sup>. In considering the close roles of p38 and NF- $\kappa$ B pathway signaling during ALI, a novel strategy would be the co-targeting of NF- $\kappa$ B and p38 signaling pathways. Some evidence suggests that targeting these two pathways together could be beneficial against influenza-induced ALI. 5-methoxyflavone (5-MF) treatment downregulates p38, I $\kappa$ B $\alpha$  and

p65 phosphorylation in an AMPK $\alpha$ -dependent manner, abrogating cytokine expression and vRNP nuclear import in influenza-infected cells<sup>593</sup>. However, there have been no *in vivo* ALI studies of co-inhibition of NF- $\kappa$ B and MAPK p38 pathways to date, and therefore represents a promising avenue for future studies.

There is emerging evidence that dysregulated recruitment of immune cells is a driver of ALI. In the lung environment, alveolar macrophages initiate the inflammatory cytokine response, which includes monocyte chemoattractant protein-1 (MCP-1). MCP-1 expression is dependent on p38 activity downstream of transcription factor ATF-2 phosphorylation and NF- $\kappa$ B activation following viral infection induced degradation of inhibitory I $\kappa$ B $\alpha$  in response to viral infection<sup>594</sup>. Alveolar macrophages quickly become depleted as they attack the viral infection, which we observe in our present study in both the WT and TAB1<sup>KI</sup> mice by D3 post infection, and are replaced by migrating immune cells, such as Ly6c<sup>+</sup> monocytes. Swift monocyte recruitment is indicative of a protective response following influenza infection, as recruited monocytes confer both an anti-viral response, but also a heightened anti-bacterial response that helps prevent opportunistic secondary infection following viral clearance<sup>595</sup>. The context of monocyte recruitment is essential, as increased monocyte recruitment was associated with pro-inflammatory disease outcomes in a mouse model of ventilator induced lung injury (VILI), driven by epithelial-cell secreted MCP-1 following high tidal volume ventilation. These investigators uncovered that monocyte chemotaxis by the GPCR CCR2 in response to MCP-1 expression is dependent on p38 activity<sup>498</sup>. Notably, when these investigators inhibited p38 activity utilizing SB203580, they reported a loss of p38 phosphorylation, which has been associated with atypical p38 autophosphorylation in GPCR-mediated signaling<sup>32,90</sup>, although CCR2 has not yet been directly investigated for conservation of this mechanism. Considering this for our results, the increased

monocyte recruitment seen in male TAB1<sup>KI</sup> mice is likely independent of MCP-1 expression as indicated by our protein expression panel, but further study is needed to indicate if atypical p38 activity could play a role in MCP-1 mediated chemotaxis and downstream signaling within monocytes. Additionally, it should be noted that VILI is considered a sterile manifestation of ALI and therefore, enhanced pro-inflammatory recruitment exacerbates stress in the lungs and does not reflect a virus-induced ALI model. On the contrary, it has been shown that human influenza patients with lower monocyte counts suffer much more severe influenza infection outcomes, resulting in mechanical ventilation, compared to patients who had rapidly elevated levels of monocytes in response to influenza infection <sup>511</sup>. That study, when paired with our data, could, therefore, indicate that blockade of atypical p38 signaling may be associated with a beneficial increase in monocyte recruitment at early-stage influenza infection that corresponds with improved infection outcomes. Further studies are necessary to define the role of atypical signaling in monocyte recruitment.

Biological sex is an important factor in the outcomes of respiratory viral infection and ALI in humans, although this association is complex and is the subject of many ongoing studies. In general, young male children and older men experience heightened pathogenesis during respiratory virus infection than females, while during reproductive years, females are generally more susceptible <sup>596</sup>. Some studies have corroborated these findings in mouse models <sup>597, 598</sup>. In the present study, we report some differences in male vs female TAB1<sup>KI</sup> mouse response to influenza infection. In our data, female mice, on average, lost slightly more weight than their male counterparts, with the TAB1<sup>KI</sup> losing less weight at peak of infection compared to WT. Interestingly, female TAB1<sup>K</sup> mice did not display the same trends of histopathological feature scores and mRNAion compared to WT counterparts as were seen in male mice. Others have

reported that sex-dependent variances in inflammatory signaling during ALI are due to sex hormone-dependent differences in toll-like receptor signaling or expression. Intriguingly, although no histological differences have so far been reported in the development of male vs female TAB1<sup>KI</sup> mice at baseline in previously published reports <sup>71</sup> or in this current study, potential differences in receptor expression have not yet been characterized in the TAB1<sup>KI</sup> mouse model, and our data presented here represents the first evidence for a potential sex-based role of atypical signaling during inflammation.

### **Conclusion and Future Directions**

In conclusion, our work here provides the first evidence for the role of atypical signaling an *in vivo* model of viral infection and acute lung injury. This initial study revealed the potential role for atypical p38 in mRNA and protein expression following initial insult. Future studies will be essential to explore the roles of atypical signaling at the earliest stages of viral infection response, as well as post-infection recovery. Additionally, the TAB1<sup>KI</sup> mouse is a systemic mutation; further studies targeting cell type-specific effects on the propagation of atypical p38-mediated signaling will be important to delineate the functional contributions of myeloid, endothelial, or epithelial cells to atypical p38-induced ALI. Additionally, while beyond the scope of this current study, p38 is strongly activated in highly pathogenic H5N1 influenza, and further studies are needed to compare the impact of atypical p38 on the progression of ALI by other strains of influenza.

In summary, atypical p38 is an underexplored regulation of pulmonary inflammation and further studies will be essential to define the molecular drivers of atypical p38 in acute lung injury and assess the potential to use selective atypical p38 inhibitors to protect against ALI, either independently or in combination with current anti-viral or anti-inflammatory regimens.

## Methods and Materials

**Mouse Strains:** WT C57BL/6J female mice were purchased from Charles River Laboratory and used to reconstitute the TAB1<sup>KI</sup> (V390A, Y392A, V408G and M409A) mice originally provided by the lab of Dr. Michael S. Marber (KCL, UK). Heterozygous KI mice were back-crossed with WT mice for 4 generations and genotyped using the primers:

Neo\_Del\_F: 5'-GCTGGCCTTGCTCAACTCCAG-3',

Neo\_Del\_R: 5'-GACCATCTGTCTCATAACCTGACCTCAC-3'

in order to confirm TAB1-mutations. Homozygous KI or KI mice were used for all experiments, and mice were used at 6-8 weeks old for influenza infections. All animal experiments were performed according to the National Institutes of Health Guide for Care and Use of Laboratory Animals and were approved by the University of Georgia Institutional Animal Care and Use Committee (IACUC).

**Viruses and Influenza Infection:** The influenza A/HKX31 (H3N2, referred to as X31) stock virus was propagated in specific pathogen-free eggs (Poultry Diagnostics and Research Center, UGA) as previously described<sup>599</sup>. 6-to-8 week old age-matched WT and KI were anesthetized with approximately 250 mg/kg of 2% weight/volume avertin by intraperitoneal injection (2,2,2-Tribromoethanol, T4802-25G Sigma-Aldrich, St. Louis MO, USA). Mice were intranasally inoculated with 50  $\mu$ L of  $1 \times 10^4$  PFU of X31 in PBS. Control/uninfected mice were intranasally inoculated with allantoic fluid in PBS and were observed until recovered from anesthesia. Mice were monitored daily for weight loss and clinical symptoms. For weight curves, mice were monitored for weight loss for 10 days post-infection and weighed daily. For tissue analysis, mice were euthanized as described below at days post-infection as indicated.

**Tissue Collection and Pathohistological Assessment:** For histological assessment and downstream tissue collection, mice were euthanized with an overdose of 2% avertin, with toe pinch to ensure complete sedation, followed by cervical dislocation and cutting of the diaphragm. Following euthanasia, the chest cavity was opened. The tissue surrounding the trachea was removed with scissors and a 20-gauge catheter was inserted down the trachea and tied off with a suture.  $300 \pm 20 \mu\text{L}$  of 4% paraformaldehyde was slowly injected through the catheter to inflate the lungs, the catheter was removed and the trachea was tied off with a suture. The lungs were dissected and immediately placed into room-temperature fresh 4% paraformaldehyde solution and placed on a rocker at room temperature. After fixation, lungs were paraffin-embedded and sectioned onto slides for IF or H&E stain. Histopathology was performed by a board-certified veterinary pathologist, blinded to mouse genotype and experimental conditions. Scoring for alveolar infiltrates, alveolar edema and bronchitis (Br) was on a scale of 0 to 4 based on distribution (0 = no lesions, 1 = focal, 2 = multifocal, 3 = coalescing, 4 = diffuse). The perivascular cuffing (PVC) score was based on thickness of leukocytes around blood vessels (0 = no cuffing, 1 = 1 layer of cells, 2 = 2-5 layers, 3 = 6-10 layers, 4 = greater than 10 layers). The interstitial pneumonia score was based on thickness of alveolar septa (0 = no infiltration, 1 = 1 leukocyte thickness, 2 = 2 leukocytes thick, 3 = 3 leukocytes thick, 4 = 4 leukocytes thick). Influenza score was calculated as the sum of the individual scores from alveolar edema, bronchitis and interstitial pneumonia. For mRNA, virus titers, and protein assessment, mice were euthanized as described above followed by cardiac puncture. Blood was removed with a 20-gauge needle and syringe. The chest cavity was opened and 10-12 mL of cold PBS + 1mM EDTA was injected through the right ventricle of the heart to flush the lung vasculature of blood. The lungs were then plucked with tweezers and placed in cold PBS on ice in 2 mL tubes pre-loaded with metal beads for

homogenization. Lungs were homogenized with a bead homogenizer and spun down at 500rcf. 100  $\mu$ L of supernatant was spun down at 5,000 rcf for cytokine assessment and immediately frozen at -80°C. Aliquots were taken of supernatant and placed into lysis buffer according to kit specifications. Aliquots of supernatant were taken for assessment of viral titer. Protein samples taken for further analysis for immunoblotting were lysed 1:1 in 2x triton lysis buffer containing 50 mM Tris-HCl pH 7.4, 100 mM NaCl, 1% Triton X-100, 10 mM NaF, 10 mM  $\beta$ -glycerophosphate, 10 mM NaPP, 2mM NaVO<sub>4</sub>, 10  $\mu$ g/ml leupeptin, aprotinin, trypsin protease inhibitor, pepstatin, and 100  $\mu$ g/ml benzamide.

**Cell lines for viral plaque assays:** Madin-Darby canine kidney (MDCK) cells were cultured in Dulbecco's modified Eagles' medium (DMEM) (Invitrogen), supplemented with 10% fetal bovine serum (FBS). MDCK cells were cultured at 37°C in a 5% CO<sub>2</sub>.

**Pulmonary viral titers:** On days 3 and 5 post infection WT and KI BL/6 mice were euthanized and lungs were extracted for viral titer examination via plaque assay. Clarified supernatant from lung homogenates were serially diluted in MEM containing TPCK trypsin (1:1000 dilution of 1 mg/mL stock). Next the virus dilution was added onto a confluent monolayer of MDCK cells. The cells were incubated with the inoculum for 1 h at 37 °C. The inoculum was then removed and replaced with a 1% Avicel overlay medium containing 1M HEPES, L-glutamine, NaHCO<sub>3</sub> , Penicillin/Streptomycin/Amphotericin B solution, and TPCK trypsin. The cells were then incubated at 37 °C for 48 hours, stained with crystal violet, and plaques were counted to determine viral PFU/mL.

**qPCR:** Aliquot of homogenized lung were collected as described above in TRK lysis buffer (Omega Bio-Tek Inc.). RNA was extracted from the lung homogenate using E.N.Z.A. Total RNA Kit I (Omega Bio-Tek Inc.) per kit instructions. For assessment of proinflammatory cytokines,

extracted RNA was converted into cDNA with the High Capacity cDNA Reverse Transcription Kit (Applied Biosystems). For viral titer samples, cDNA was generated using iScript (Cat No. 1708891, Bio-Rad Laboratories, Hercules CA). The relative gene expression was measured using Sensifast Probe High-ROX kit (Meridian Biosciences) and probes from Applied Biosciences. Real time quantitative PCR was performed using QuantStudio 3 (Applied Biosystems). Samples were normalized to the actin internal control and the WT sample for the experiment using the  $\Delta\Delta\text{CT}$  method. The following mRNA probes were measured: *I1b* (Mm00434228\_m1), *I16* (Mm00446190\_m1), *Tnf* (Mm00443258\_m1), *Ifnb1* (Mm00439552\_s1), *Ifnl3* (Mm00663660\_g1), *Isg15* (Mm01705338\_s1), and *Cox2* (Mm03294838-g1).

Primers used for assessment of viral titer:

M Protein:

F 5' GTGACAACAACCAATCCACTAATC 3'

R 5' CTCCAGCTCTATGCTGACAAA 3'

eEF1a1:

eEF1a1\_f 5' TCC CTG TGG AAA TTC GAG AC 3'

eEF1a1\_r 5' CCA GGG TGT AAG CCA GAA GA 3'

**Protein Assessment:** Cytokine protein concentrations in mouse lung homogenate were determined using the ProcartaPlex Mouse and Rat Mix & Match Panels (Thermo Fisher Scientific, MA). The probes selected were; CXCL1, IFN- $\beta$ , IL-1 $\beta$ , IL-10, IL-19, IL-17A, IL-28, IL-6, MCP-1 (CCL2), TNF- $\alpha$ , and VEGF-A. Samples were read on a Magpix Multiplex Reader (Bio-Rad, Hercules, CA) and analyzed with curve fitting software Milliplex Analyst 5.1 (Merck).

**Immunoprecipitation and Immunoblotting:** Lung homogenate protein samples were prepared in 2x triton lysis buffer containing 50 mM Tris-HCl pH 7.4, 100 mM NaCl, 1% Triton X-100, 10

mM NaF, 10 mM  $\beta$ -glycerophosphate, 10 mM NaPP, 2mM NaVO<sub>4</sub>, 10  $\mu$ g/ml leupeptin, aprotinin, trypsin protease inhibitor, pepstatin, and 100  $\mu$ g/ml benzamide.

. Homogenate lysates were cleared by centrifugation and protein concentrations determined by bicinchoninic acid assay (BCA). Equivalent amounts of lysates were used for immunoprecipitations using the anti-MAPK p38 antibody (Santa Cruz Biotechnology) and samples were eluted with 2X Laemmli sample buffer consisting of 125mM Tris-HCl pH 6.5, 5% SDS w/v, 20% w/v glycerol, bromophenol blue (>10 mg), and containing 200 mM dithiothreitol, resolved by SDS-PAGE and developed by chemiluminescence. Aliquots of cell lysates were also immunoblotted with antibodies as indicated.

**Antibodies used:** P38 (sc-271120, Santa Cruz Biotechnology, Santa Cruz CA). IP. p38 (9212S, Cell Signaling Technologies, Denvers MA), p-p38 (T180/Y182) (4511S, Cell Signaling Technologies, Denvers MA), TAB1 (GTX107571, GeneTex, San Antonio TX) Goat anti-rabbit IgG (H+L)-HRP Conjugate (Cat. No. 1706515, Bio-Rad Laboratories, Hercules CA), Peroxidase-Conjugated IgG Fraction Monoclonal Mouse Anti-Rabbit IgG, Light Chain Specific (211-032-171, Jackson ImmunoResearch Laboratories, West Grove PA).

**Phos-tag gels:** Phosphorylation of TAB1 was detected using Phos-tag gels (Wako Pure Chemical Industries) containing 100 $\mu$ M Phos-Tag acrylamide and 100uM MnCl<sub>2</sub> according to the manufacturer's instructions.

**Bronchoalveolar Lavage (BAL) Fluid Fluorescence-Activated Cell Sorting (FACS):** Bronchoalveolar lavage (BAL) fluid was isolated in 0.1% BSA in PBS. Cells were centrifuged for 10 minutes at 1250 RPM at 4 °Celsius. The supernatant was removed and the cells were resuspended in 0.1% BSA in PBS. Cells were stained for 20 minutes at 4 °Celsius with fluorescent labeled antibodies for the following cell surface markers: Fc blocker (eBioScience), CD11b (FITC,

Invitrogen/eBioScience), CD11c (Efluor 450, Invitrogen/eBioScience), Ly6G (APC, Invitrogen/eBioScience), Ly6C (PE-Cy7, Invitrogen/eBioScience), and Siglec F (PE, Invitrogen/eBioScience). Live, single cells were sorted into their respective populations on the Cytex Aurora CS (Cytex Biosciences) using the following gating strategy: inflammatory monocytes (CD11b<sup>high</sup> CD11c<sup>low</sup> Ly6C<sup>high</sup> Ly6G<sup>low</sup>), neutrophils (CD11b<sup>high</sup> CD11c<sup>low</sup> Ly6C<sup>high</sup> Ly6G<sup>high</sup>), and alveolar macrophages (Siglec F<sup>high</sup> CD11b<sup>int</sup>).

**Materials and Reagents:** Avertin (T4802-25G Sigma-Aldrich, St. Louis MO, USA) ketamine hydrochloride (Ketaset 40027676, Zoetis Manufacturing and Research, Girona, Spain) Xylazine (AnaSed Injection NDC 59399-110-20, Akom Inc, Lake forest, IL). Formalyde (Cat. No. 15714, Electron Microscopy Sciences, Hatfield, PA). E.Z.N.A. Total RNA Kit 1 (R6834-02, Omega Bio-Tek, Norcross GA) SensiFAST Hi-ROX Mix (Cat. No.: BIO-82020, Meridian Bioscience, Cincinnati OH) ProcartaPlex Mouse and Rat Mix & Match Panels (Thermo Fisher Scientific, Waltham MA). Phos-Tag gels (AAL-107, Wako Pure Chemical Industries, Richmond VA). PBS (21-040-CV, Corning, Manassas VA). EDTA (15575-038, Invitrogen, Grand Island NY). iScript cDNA Synthesis Kit (Cat No. 1708891, Bio-Rad Laboratories, Hercules CA). PerfecCTA SYBR Green FastMix (P/N 84069, Quantabio, Beverly MA). Dulbecco's modified Eagles' medium (DMEM) ( ) Fetal Bovine Serum (FBS) (Ref 35-010-CV, Corning, Woodland CA) MEM (Ref 11095-080, gibco, Grand Island NY). Antibiotic-Antimycotic Liquid (CA002-010, GenDEPOT, Katy TX). L-Glutamine (Ref 25030-081, gibco, Grand Island NY). Crystal Violet (Cat No. B21932.14, Thermo Scientific, Waltham MA) TPCK-treated trypsin (LS003740, Worthington Biochemical Corporation, Lakewood NJ).

**Statistical Analysis:** Data were analyzed using Prism software (version 10; GraphPad software). Comparisons of statistical significance was determined through either one-way or 2-way analysis

of variance (ANOVA) as indicated. Weight loss curves were analyzed for significance using mixed-effects analysis where ANOVA was conducted for each timepoint. Asterisks designate P values as following; <0.05 (\*), <0.01 (\*\*), 0.001(\*\*\*), <0.0001(\*\*\*\*).

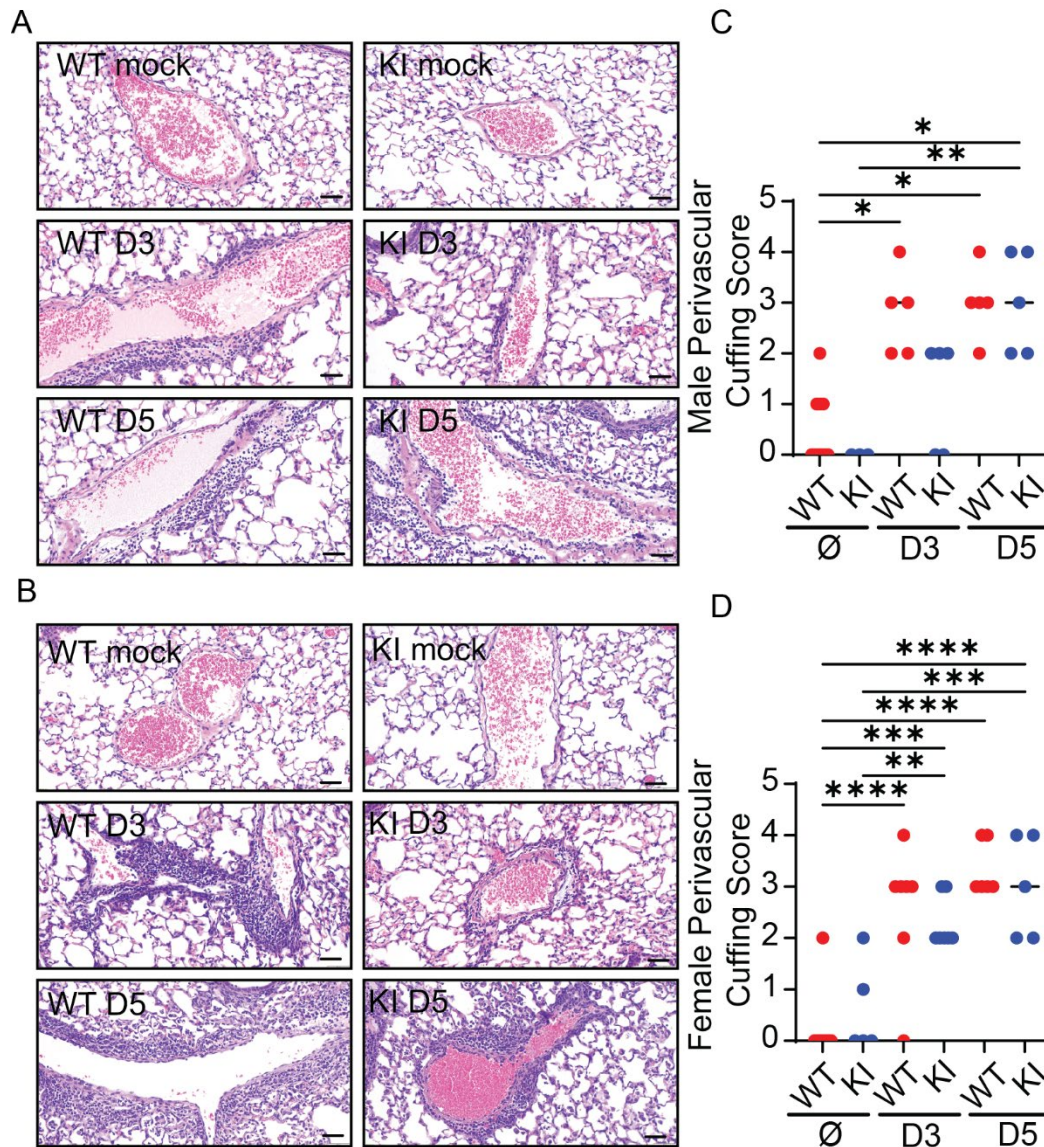
**Acknowledgments:** We thank all members of the Grimseylab@UGA for comments and advice.

**Conflict of interest:** The authors declare they have no conflict of interest with the contents of this article.

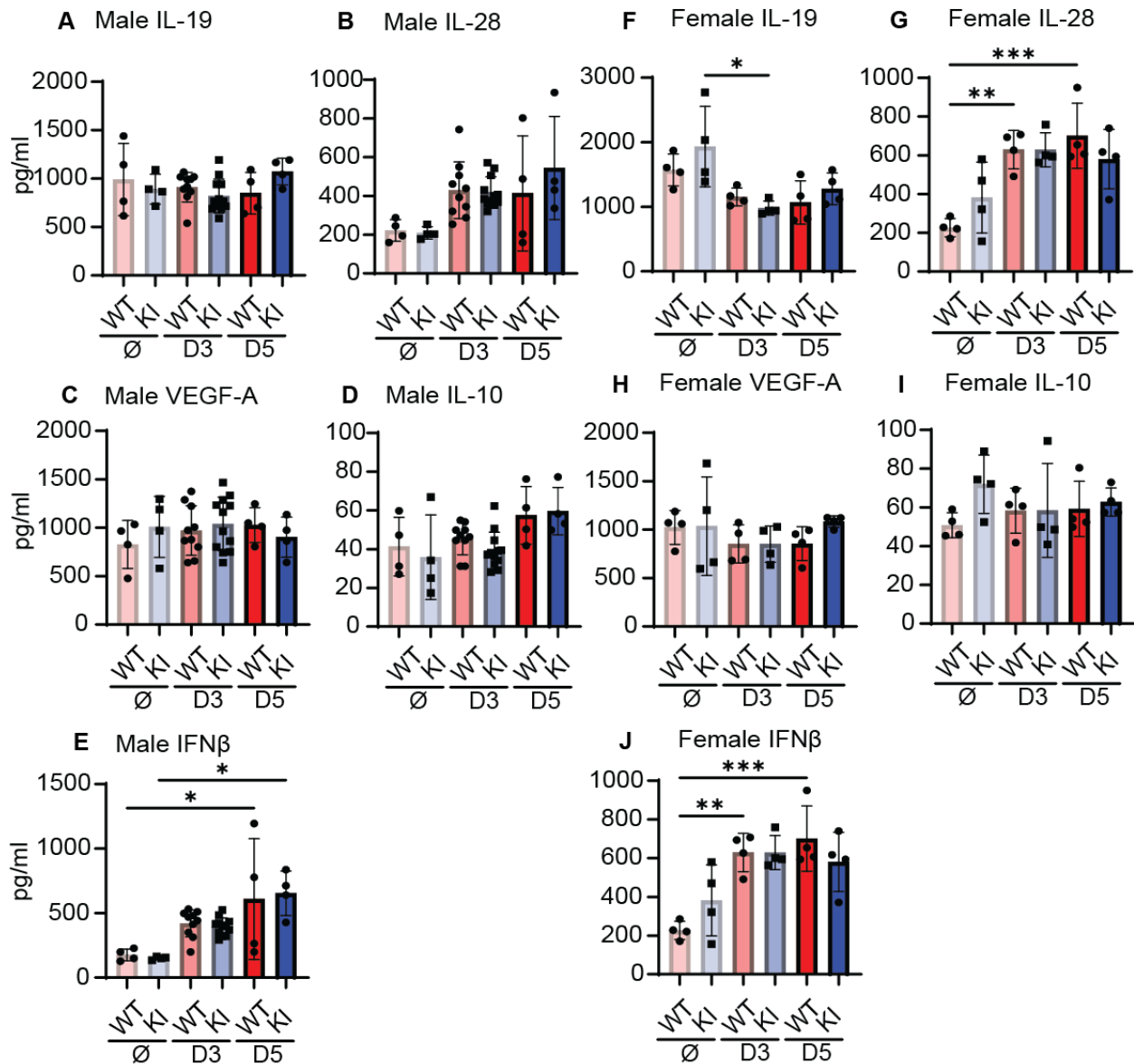
#### **FOOTNOTES:**

The following abbreviations used were; ANOVA, analysis of variance; GPCR, G protein-coupled receptor; MAPK, mitogen-activated protein kinase; TAB1, transforming growth factor- $\beta$  activated kinase-1 binding protein1; Human Pulmonary Microvascular Endothelial Cells (HPMEC)

## Supplemental Figures for Chapter 3



**Supplemental Figure 3.1: Perivascular cuffing in the KI and WT mouse lung.** (A,C) representative photographs of PFA-fixed, H&E stained mouse lungs displaying perivascular cuffing. Mice grouped and compared by sex; (A,C) males, (C,D) females. Uninfected controls; WT male N = 10, female N = 9, KI male N = 3, female N = 6. Day 3 post-infection; WT male N = 5, female N = 7, KI male N = 5, female N = 7. Day 5 post-infection; WT male N = 5, female N = 6, KI male N = 5, female N = 5. Bars in scatter-plots indicate median values. Comparisons made using 2-way ANOVA with post hoc Tukey testing for multiple comparisons. Scale bars, 200  $\mu$ M.



**Supplemental Figure 3.2: Cytokine expression in mouse lung following influenza infection.**

(A-J) Protein concentration from mouse lung homogenate before and after influenza infection as indicated. Uninfected controls; WT male N = 4, female N = 4, KI male N = 4, female N = 4. Day 3 post-infection; WT male N = 10, female N = 4, KI male N = 12, female N = 4. Day 5 post-infection; WT male N = 4, female N = 4, KI male N = 4, female N = 4. Comparisons made using 2-way ANOVA with post hoc Tukey testing for multiple comparisons.

## CHAPTER 4

### SUMMARY OF FINDINGS AND FUTURE DIRECTIONS

#### **Summary of Research Aims and Findings**

The overall goal of this work has been to explore our current understanding of atypical p38 signaling, to underline previous and ongoing work studying the subcellular localization of kinase activity, and to contextualize atypical p38 signaling in a previously unstudied *in vivo* disease model.

Recent advances in FRET-based activity reporters are beginning to allow for closer study of endogenous, subcellularly localized kinase activity, providing new evidence for the importance of understanding kinase distribution<sup>358, 600</sup>. Our study utilizing FRET-based activity reporters offers the first evidence for spatially regulated MAPK p38 kinase activity. We show that atypical signaling by protease-activated receptor 1 (PAR1) is initiated at the plasma membrane but is rapidly trafficked into the cytosol where signaling is maintained, alongside at the endosome, while osmotic stress-induced canonical p38 signaling is rapid, transient, and primarily nuclear. We also showed that this mechanism is conserved among other GPCRs known to undergo atypical signaling through the prostaglandin E receptors 2 and 4. Further work is needed to better understand if other GPCRs have similar trafficking and kinase activity profiles, or if there is greater variation within the umbrella of TAB1-p38 signaling at different subcellular locations. Additionally, new technologies are in development that utilize multiple simultaneous FRET biosensor activity reporters to study different signaling compartments within the same cell<sup>601</sup>. While the experimental design used in our study for this work allows us to generate reproducible data for individual activity reporters with high numbers of individually expressing cells, our comparisons made between the dynamics of kinase trafficking could be improved further if we

could take readings from two discretely localized activity reporters in the same cell. Additionally, future work will involve development of other subcellular signaling locations, such as at the endoplasmic reticulum (ER), where p38 phosphorylates ER-bound the E3 ubiquitin ligase Gp78, facilitating ER association with the mitochondria<sup>602</sup>, but direct study of kinase localization has not been performed. While this work has investigated canonical-mediated p38 activity through osmotic stress and activation via GPCRs, there have currently been no studies on the subcellular signaling dynamics of other known activation pathways for atypical signaling, i.e., by oxidative stress<sup>82</sup> or ischemia/hypoxic stress<sup>71, 81</sup>.

Liquid-liquid phase separation (LLPS) may also play an important role in kinase localization, as discussed in chapter 1, section 2. An ongoing question following our work in chapter 2 is how p38-TAB1 is regulated after GPCR-mediated activation. A recent study investigated how GPCR-mediated p38 signaling is terminated, utilizing an siRNA library screen targeting deubiquitinating enzymes (DUBs) and it was shown that depletion of cylindromatosis (CYLD) and ubiquitin-specific protease (USP)34 differentially affect p38 signaling outcomes. The investigators concluded that CYLD controls thrombin-induced endothelial barrier permeability, while both CYLD and USP34 regulate thrombin-stimulated IL-6 mRNA expression<sup>603</sup>. However, this study does not directly correlate siRNA knock-down of DUBs to receptor ubiquitination and it remains unknown if or how the p38-TAB1-TAB2 signaling complex at the ubiquitinated GPCR is regulated by DUBs, raising the question of whether the TAB1-p38 complex remains bound to internalized GPCR, or if not, then whether the complex de-couples from the GPCR, does it form LLPS-like signaling compartments proximal to the endosome?<sup>603</sup> In support of this latter idea, another study reports that the NF- $\kappa$ B essential modulator (NEMO) forms liquid-like droplets after binding to Lys63-linked polyubiquitin, leading to multivalent interactions between NEMO and

polyUb<sup>368</sup>. It is therefore possible that the Lys63-linked polyubiquitination of the p38-TABs complex could form similar condensates. To investigate this, there is a need for new technologies that will allow the study of “unbiased” cytosolic signaling that is not trafficked to membranes or subcellular structures, to better allow for study of transient signaling foci and where they form in the cell. We have begun to explore this idea ourselves, theorizing that, with sufficient magnification (63x) and cytosolic p38 FRET reporter, we could identify sub-cellular “hot-spots” of p38 activity within the cytosol during signaling near the endosome (**Fig. 4.1 A**). We show that in (**Fig. 4.1 B**) p38 activity is not equally distributed in the cytosol, but is increased next to RFP-RAB5, an early endosomal marker protein. Future studies will expand on this preliminary data, incorporating other subcellular markers to better define p38 near other compartments, as well as refining imaging conditions for increased resolution.

Naturally, the question that arises following our work studying the spatial localization of kinase activity is: what are the targets of kinase activity in these locations, or what are the functional molecular roles of kinase restriction for atypical p38? Evidence is limited in this regard, but the potential p38 substrate pool is distributed throughout the cell, with subpopulations that are principally nuclear or cytosolic. This suggests that spatial restriction of the kinase as seen from our data alters the pools of substrates available to the kinase in order to dynamically control physiological outcomes. Previous studies into downstream phosphorylation targets of PAR1-mediated p38 activity in endothelial cells identified several key proteins involved in endothelial barrier stabilization through adherens junctions, including  $\alpha$ -catenin, ANKRD50, and casein kinase-1 (CSNK1), as well as identification of other kinases such as PKA, PKD, and MK2, all of which are associated with endothelial barrier stability<sup>571, 604-607</sup>. This study also uncovered a role

for p38-mediated negative regulation of ERK1/2 activity that is increased when p38 is inhibited by SB203580, although it remains unknown where exactly in the ERK-pathway p38 is involved<sup>607</sup>. It was noted by the authors that siRNA depletion of p38 $\alpha$  reversed the changes in phosphorylation seen from p38 $\alpha$  inhibition in  $\alpha$ -catenin and ERK1/2, indicating potential redundancy mechanisms in the former, possibly by p38 $\beta$ , and a steric block of MEK access to the latter, which the investigators suggest means that the p38 $\alpha$  isoform is in direct contact with these proteins<sup>607</sup>. In the context of our spatial data, these results could indicate that p38 $\alpha$  may be spatially restricting these targets in the cytosol and near the endosome. In endothelial cells,  $\alpha$ -catenin functionally acts as a key protein in the Cadherin-Catenin complex, linking  $\beta$ -catenin with F-actin and promoting a strong endothelial barrier<sup>608</sup>. The p38-TAB1 interaction may be facilitating the physical restriction of  $\alpha$ -catenin, preventing this essential function. Future studies could utilize immunofluorescence to analyze direct p38- $\alpha$ -catenin interaction following thrombin stimulation, as this interaction has not yet been characterized, but would support other known roles of the p38-TAB1 interaction as a modulator of actin stability via HSP27 phosphorylation<sup>571</sup>.

We also conducted the first study of atypical signaling in an *in vivo* model of pulmonary viral infection and inflammation. Previous *in vitro* data supports that atypical signaling is a driver of inflammation, vascular destabilization, and cytokine production. We report that blockade of the TAB1-p38 interaction in male TAB1<sup>KI</sup> mice reduces influenza-induced weight loss, increases rate of recovery, and improves acute-phase histopathological outcomes and increased Ly6c+ monocyte recruitment to the lungs compared to wild-type. There are consistent trends in the reduction of pro-inflammatory mRNA and inflammatory cytokines in the acute, day-3 post-infection phase in male mice. While female TAB1<sup>KI</sup> mice do not carry the same trends, they do display some weight loss

protection at the peak of infection, compared to WT female mice. Regardless, we conclude a possible sex-based link between the TAB1-p38 interaction in TAB1<sup>KI</sup> mice.

Prior evidence for sex-linked susceptibility to influenza infection is associated with circulating sex steroid hormone levels<sup>609</sup> that influence immune development<sup>610, 611</sup>. For this reason, age also plays a role in susceptibility due to sex-hormone expression variation between males and females<sup>596, 612</sup>. In mice, males are generally more susceptible to infection. Mechanistically, this could potentially be attributed to sex-linked expression of TLR receptors<sup>612</sup>. *TLR7* in humans is an X-linked chromosome gene, expressed in plasmacytoid dendritic cells (pDCs), patrolling immune presentation cells that detect viral antigens and respond with rapid, massive expression of type 1 interferons<sup>613</sup>, and females display greater expression of TLR7 and Type 1 interferons than males due to *TLR7* escape from x chromosome inactivation<sup>614</sup>. TLRs and other infection-detecting receptors have not been characterized in the TAB1<sup>KI</sup> mice and further study is necessary.

While viral susceptibility has been well studied, influence of sex on infection severity is much less clear. A prior study investigating H3N1 influenza infection in mice determined that there were differential histopathological features, specifically greater tissue hyperresponsiveness, alongside greater methacholine responsiveness (indicators of impairment to lung function) in female mice. These features were noted an absence of sex-based differences in BAL protein levels and inflammatory cytokine expression, and viral titers were equivalent between sexes<sup>598</sup>. This could indicate that phenotypic differences may be decoupled with our more traditional reported measures of infection severity, and further study may be needed to characterize mouse lung function in the TAB1<sup>KI</sup> mice.

Ultimately, the practical goal of this work and future studies in the field of kinase signaling is to elucidate the functional implications of atypical p38 and its impact in human health and disease. MAPK p38 therapeutics have had limited success in the clinic despite the potential benefits of inhibiting a master regulator of dysregulated inflammation. Similarly, many kinase inhibitors for other targets, such as NF- $\kappa$ B, have failed. However, as we have summarized in this work, pan-inhibition of kinase activity is a flawed strategy. Kinases have diverse functions, sometimes simultaneously, within the cell. A good example is PAR1 activation by thrombin, which results in signaling cascades of NF- $\kappa$ B, MAPK, and protein kinase C, triggering discreet downstream responses<sup>515</sup>. Next-generation therapeutics will target subsets of kinase activity attributed to disease, while leaving essential kinase activity in-tact. Additionally, while the inflammatory response is often targeted in therapeutic design due to inflammatory-mediated disease such as ALI, the pro-inflammatory response is still a necessary aspect of combating infection, and the goal shouldn't be to eliminate inflammatory signaling or reduce it as much as possible, as this could be deleterious toward effective clearance of the pathogen. Rather, the goal should be to restore balance in the pro-inflammatory and resolution responses to disease. The interaction between TAB1 and p38 is an appealing and viable target for this approach. Our studies in the TAB1<sup>KI</sup> mice illustrate that perturbing the interaction of these proteins does not necessarily attenuate the mouse inflammatory response, but instead alters the timing of immune response in the lung tissue, allowing for quicker recovery from infection. We would suggest, therefore, that the therapeutic benefit for TAB1-p38 inhibitors lies in its potential to “re-calibrate” or normalize dysregulated inflammatory responses. For the past several years, discussion in the field of MAPK and NF- $\kappa$ B inhibitors have shifted toward the idea of targeted suppression of kinase activity, leaving beneficial signaling in-tact<sup>515, 615, 616</sup>. Recent work using bioinformatics combining x-ray

crystallography with fragment screens identified targetable interaction sites in the TAB1-p38 complex using adamantane scaffolds that are independent of the kinase binding pocket, but interfere with p38's ability to phosphorylate TAB1<sup>71, 73</sup>. Separately, a recent study on small molecule inhibitor design targeting p38 autophosphorylation further shows the potential of this approach toward reducing cardiomyocyte death in *in vitro* models of ischemic reperfusion injury<sup>617</sup>. These small molecule inhibitors will enable further validation of our results, but critically, will also allow us to explore other disease models and corroborate our results from these studies in alternate disease models.

Investigators studying next-generation therapeutics are also beginning to look at how drugs subcellularly localize within the cell and how this affects drug efficacy, both in membrane-bound organelles and membrane-less structures<sup>618</sup>.

### **Potential Experiments and Future Perspectives**

Our focus was on understanding the progression of influenza infection in mice, but we did not investigate early onset time points such as day 1 following infection and at post-infection resolution/immune recovery. Follow-on future studies should include these wider time points to allow us to provide a more complete snapshot of the role of atypical p38 in onset and resolution. The focus of this work was on induction of acute inflammation diseases such as ALI, but the adaptive immune response to viral infection in TAB1<sup>KI</sup> mice has not been investigated. A previous study investigating a sex-based link between influenza infection and protective immunity in secondary infection uncovered that females mount higher neutralizing and total anti-IAV antibodies, with differential viral titers in the lungs compared to males<sup>597</sup>. Given these results in context of our own, investigation of sex-linked antibody production in our model could be warranted.

While our results uncover differences in immune investment, trends in mRNA and protein expression at Day 3 post infection, we did not look at the role of our pathway immediately following viral infection. We hypothesized that atypical signaling mediated by GPCRs would be more apparent after the initial infection/inflammatory insult that would ultimately induce the production and release of agonists related to our pathway, such as prostaglandin E-2 (PGE2), synthesized from secreted COX-2, and release of histamine. Atypical signaling is also mediated by hypoxia-induced oxidative stress, as shown in myocardial ischemic reperfusion injury <sup>71</sup>, and therefore may also play a role in the hypoxic state of the lungs during acute inflammation state <sup>619</sup>, although we do not yet know how the pathway is activated or regulated by oxidative stress <sup>71, 82</sup>. However, we uncovered in our studies that there is a baseline TAB1 interaction with p38 in WT mice that is blocked in the TAB1<sup>KI</sup> mice, and that the interaction between these proteins carries into IAV infection but is not increased. This could imply that the TAB1-p38 interaction may already be primed even at the earliest stages of infection, and therefore further investigation into early-onset influenza infection is necessary.

The immune response to viral infections like influenza is robust and highly conserved, with mechanisms of redundancy in both the host response and viral escape mechanisms that have proven to be stubborn to affect from a pharmacological, interventional perspective in the past <sup>489, 620-622</sup>. Despite this, preventing interaction of TAB1 with p38 in the TAB1<sup>KI</sup> mouse is enough to substantially alter monocyte recruitment and induce a replicable phenotype in our TAB1<sup>KI</sup> mice, and is encouraging that future development of pharmacological inhibitors against this protein interaction might prove more effective than previous attempts at targeting all p38 kinase activity.

Follow-up studies to this work will include early/late timepoints post-infection, adjusted dosages of influenza based on mouse weight, and examining additional strains of influenza. H3N2

influenza used in the present study is a great starting point for characterizing the p38-virus-ALI connection, and we believe the results shown here form a strong basis for further study into highly pathogenic influenza. In particular, the pathogenic H5N1 strain of influenza has been shown to highly activate MAPK p38<sup>531, 623</sup>, and hijacked/dysregulated kinase activity may be especially apparent in investigations of this model, as p38 has been shown to play a role in viral-induced epithelial barrier disruption via E3 ubiquitin ligase, Itch<sup>624</sup>. While H1N1 and H3N2 also infect the upper respiratory tract, this may actually deter virus entry into the lower respiratory tract as the virus becomes bogged down through attachment to submucosal gland cells and their mucus, in contrast to H5N1, which doesn't infect upper airway<sup>625</sup>. H5N1 poses a severe risk for pneumonia in patients, as this virus also infects type II pneumocytes which drives loss of surfactant protein expression, as well as alveolar macrophages<sup>626, 627</sup>. Infection of alveolar macrophages By H5N1 subsequently leads to p38- and IRF-3 dependent upregulation of proinflammatory cytokines leading to ALI<sup>628</sup>.

The immediate next steps for this project would be to expand our investigation of the TAB1<sup>KI</sup> transcriptomic landscape within the lung compared to WT mice, in order to get a full idea of other potential targets for further investigation and to determine if, transcriptionally, the TAB1<sup>KI</sup> mice are differential to WT at baseline. As the TAB1<sup>KI</sup> mouse is a systemic knock-in, the isolation and characterization of individual cell types, such as innate immune cells, lung epithelial/endothelial cells, and others is possible through established experimental procedures using antibody and bead-based selection<sup>629, 630</sup>.

At the conclusion of these studies, we have shown that p38 activity is spatially and temporally biased depending on method of activation, which could affect kinase access to substrate pools, and that atypical signaling mediated by interaction with TAB1 drives inflammatory disease

progression and delayed recovery in an *in vivo* model of influenza infection (**Fig. 4.2**). These results support further research into understanding subcellular kinase-substrate interactions and their physiological impact, as well as further expansion of these findings into investigations of cell type- and receptor-specific differences in signaling dynamics. Our *in vivo* results implicate atypical signaling in infectious disease inflammatory responses, which should be further explored in other pulmonary diseases such as bacterial infection, pneumonia, and chronic obstructive pulmonary disease. Additionally, the role of atypical signaling in inflammation can be expanded to diseases in other organs, such as retinopathies, cardiac disease, or systemic infection. Lastly, these studies provide important evidence for the necessity of further research and development of small molecule inhibitors capable of targeted disruption of the TAB1-p38 interaction.

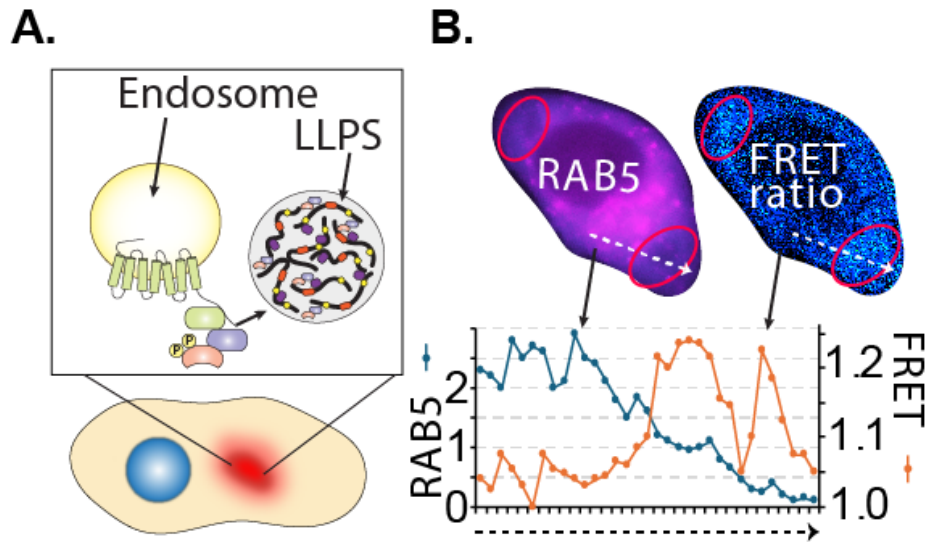


**Figure 4.1: Model of cytosolic p38 activity distribution.** Fluorescence Resonance Energy Transfer (FRET) MAPK p38 activity reporter can be used to identify pockets of increased cytosolic p38 activity using high resolution fluorescence microscopy. A.) Proposed mechanism that GPCR-mediated p38 activity trafficked by the endosome forms concentration gradients of active kinase complex via LLPS. B. HeLa cell transfected with Cyto-p38 activity reporter, PAR1, and RFP-tagged RAB5. FRET ratio is heat map indicating p38 activity after thrombin stimulation. Circles indicate areas of FRET ratio where p38 activity is higher than surroundings. Indicated arrow represents a line scan of fluorescence intensity of RFP-tagged RAB5, quantified by blue line, overlaid by FRET ratio of the same line in red.

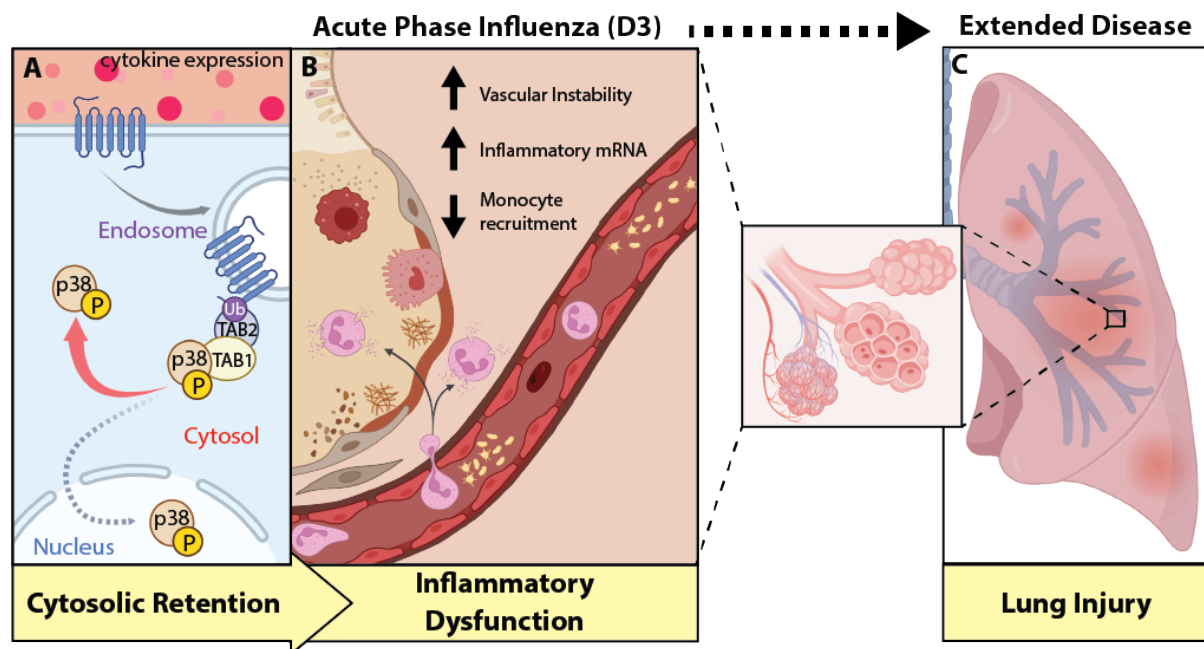


**Figure 4.2: Model of spatial restriction of p38 as a driver of acute lung injury.** Model of how spatial signaling may contribute to influenza-induced ALI pathology when the results of the present study are combined. A) Cytokine expression following infection/injury produces secretion of GPCR agonists such as thrombin and prostaglandin E2 among others, facilitating cytosolic retention of active p38 through interaction with TAB1/TAB2/polyubiquitinated GPCRs. B) During acute phase influenza, TAB1-p38 interaction drives inflammatory dysfunction through increased vascular instability and inflammatory mRNA expression and decreased monocyte recruitment to the lung. This results in lung injury and increased disease recovery time. Therefore, therapeutic targeting of the TAB1-p38 interaction may abrogate disease progression of ALI, as observed in the TAB1<sup>KI</sup> mouse model, encouraging future studies.

## REFERENCES

1. Han J, Lee JD, Bibbs L, Ulevitch RJ. A MAP kinase targeted by endotoxin and hyperosmolarity in mammalian cells. *Science*. 1994;265(5173):808-11. Epub 1994/08/05. doi: 10.1126/science.7914033. PubMed PMID: 7914033.
2. Kyriakis JM, Avruch J. Mammalian mitogen-activated protein kinase signal transduction pathways activated by stress and inflammation. *Physiol Rev*. 2001;81(2):807-69. Epub 2001/03/29. doi: 10.1152/physrev.2001.81.2.807. PubMed PMID: 11274345.
3. King TE, Jr., Bradford WZ, Castro-Bernardini S, Fagan EA, Glaspole I, Glassberg MK, Gorina E, Hopkins PM, Kardatzke D, Lancaster L, Lederer DJ, Nathan SD, Pereira CA, Sahn SA, Sussman R, Swigris JJ, Noble PW, Group AS. A phase 3 trial of pirfenidone in patients with idiopathic pulmonary fibrosis. *N Engl J Med*. 2014;370(22):2083-92. Epub 2014/05/20. doi: 10.1056/NEJMoa1402582. PubMed PMID: 24836312.
4. Valeyre D, Albera C, Bradford WZ, Costabel U, King TE, Jr., Leff JA, Noble PW, Sahn SA, du Bois RM. Comprehensive assessment of the long-term safety of pirfenidone in patients with idiopathic pulmonary fibrosis. *Respirology*. 2014;19(5):740-7. Epub 2014/05/20. doi: 10.1111/resp.12297. PubMed PMID: 24836849; PMCID: PMC4230393.
5. Min X, Akella R, He H, Humphreys JM, Tsutakawa SE, Lee SJ, Tainer JA, Cobb MH, Goldsmith EJ. The structure of the MAP2K MEK6 reveals an autoinhibitory dimer. *Structure*. 2009;17(1):96-104. Epub 2009/01/15. doi: 10.1016/j.str.2008.11.007. PubMed PMID: 19141286; PMCID: PMC3689539.
6. Cuadrado A, Nebreda AR. Mechanisms and functions of p38 MAPK signalling. *Biochem J*. 2010;429(3):403-17. Epub 2010/07/16. doi: 10.1042/BJ20100323. PubMed PMID: 20626350.
7. Raingeaud J, Whitmarsh AJ, Barrett T, Derijard B, Davis RJ. MKK3- and MKK6-regulated gene expression is mediated by the p38 mitogen-activated protein kinase signal transduction pathway. *Mol Cell Biol*. 1996;16(3):1247-55. Epub 1996/03/01. doi: 10.1128/mcb.16.3.1247. PubMed PMID: 8622669; PMCID: PMC231107.
8. Derijard B, Raingeaud J, Barrett T, Wu IH, Han J, Ulevitch RJ, Davis RJ. Independent human MAP-kinase signal transduction pathways defined by MEK and MKK isoforms. *Science*. 1995;267(5198):682-5. Epub 1995/02/03. doi: 10.1126/science.7839144. PubMed PMID: 7839144.
9. Moriguchi T, Kuroyanagi N, Yamaguchi K, Gotoh Y, Irie K, Kano T, Shirakabe K, Muro Y, Shibuya H, Matsumoto K, Nishida E, Hagiwara M. A novel kinase cascade mediated by mitogen-activated protein kinase kinase 6 and MKK3. *J Biol Chem*. 1996;271(23):13675-9. Epub 1996/06/07. doi: 10.1074/jbc.271.23.13675. PubMed PMID: 8663074.
10. Tanaka N, Kamanaka M, Enslen H, Dong C, Wysk M, Davis RJ, Flavell RA. Differential involvement of p38 mitogen-activated protein kinase kinases MKK3 and MKK6 in T-cell apoptosis. *EMBO Rep*. 2002;3(8):785-91. Epub 2002/08/02. doi: 10.1093/embo-reports/kvf153. PubMed PMID: 12151339; PMCID: PMC1084207.
11. Lu HT, Yang DD, Wysk M, Gatti E, Mellman I, Davis RJ, Flavell RA. Defective IL-12 production in mitogen-activated protein (MAP) kinase kinase 3 (Mkk3)-deficient mice. *Embo j*. 1999;18(7):1845-57. Epub 1999/04/15. doi: 10.1093/emboj/18.7.1845. PubMed PMID: 10202148; PMCID: PMC1171270.

12. Lin A, Minden A, Martinetto H, Claret FX, Lange-Carter C, Mercurio F, Johnson GL, Karin M. Identification of a dual specificity kinase that activates the Jun kinases and p38-Mpk2. *Science*. 1995;268(5208):286-90. Epub 1995/04/14. doi: 10.1126/science.7716521. PubMed PMID: 7716521.
13. Zhang YY, Mei ZQ, Wu JW, Wang ZX. Enzymatic activity and substrate specificity of mitogen-activated protein kinase p38alpha in different phosphorylation states. *J Biol Chem*. 2008;283(39):26591-601. Epub 2008/08/02. doi: 10.1074/jbc.M801703200. PubMed PMID: 18669639; PMCID: PMC3258911.
14. Brancho D, Tanaka N, Jaeschke A, Ventura JJ, Kelkar N, Tanaka Y, Kyuuma M, Takeshita T, Flavell RA, Davis RJ. Mechanism of p38 MAP kinase activation in vivo. *Genes Dev*. 2003;17(16):1969-78. Epub 2003/08/02. doi: 10.1101/gad.1107303. PubMed PMID: 12893778; PMCID: PMC196252.
15. Remy G, Risco AM, Inesta-Vaquera FA, Gonzalez-Teran B, Sabio G, Davis RJ, Cuenda A. Differential activation of p38MAPK isoforms by MKK6 and MKK3. *Cell Signal*. 2010;22(4):660-7. Epub 2009/12/17. doi: 10.1016/j.cellsig.2009.11.020. PubMed PMID: 20004242.
16. Marshall CJ. Specificity of receptor tyrosine kinase signaling: transient versus sustained extracellular signal-regulated kinase activation. *Cell*. 1995;80(2):179-85. Epub 1995/01/27. doi: 10.1016/0092-8674(95)90401-8. PubMed PMID: 7834738.
17. Irie T, Muta T, Takeshige K. TAK1 mediates an activation signal from toll-like receptor(s) to nuclear factor-kappaB in lipopolysaccharide-stimulated macrophages. *FEBS Lett*. 2000;467(2-3):160-4. Epub 2000/02/17. doi: 10.1016/s0014-5793(00)01146-7. PubMed PMID: 10675530.
18. Takaesu G, Surabhi RM, Park KJ, Ninomiya-Tsuji J, Matsumoto K, Gaynor RB. TAK1 is critical for IkappaB kinase-mediated activation of the NF-kappaB pathway. *J Mol Biol*. 2003;326(1):105-15. Epub 2003/01/28. doi: 10.1016/s0022-2836(02)01404-3. PubMed PMID: 12547194.
19. Brown K, Vial SC, Dedi N, Long JM, Dunster NJ, Cheetham GM. Structural basis for the interaction of TAK1 kinase with its activating protein TAB1. *J Mol Biol*. 2005;354(5):1013-20. Epub 2005/11/18. doi: 10.1016/j.jmb.2005.09.098. PubMed PMID: 16289117.
20. Shim JH, Xiao C, Paschal AE, Bailey ST, Rao P, Hayden MS, Lee KY, Bussey C, Steckel M, Tanaka N, Yamada G, Akira S, Matsumoto K, Ghosh S. TAK1, but not TAB1 or TAB2, plays an essential role in multiple signaling pathways in vivo. *Genes Dev*. 2005;19(22):2668-81. Epub 2005/11/02. doi: 10.1101/gad.1360605. PubMed PMID: 16260493; PMCID: PMC1283960.
21. Jiang Y, Chen C, Li Z, Guo W, Gegner JA, Lin S, Han J. Characterization of the structure and function of a new mitogen-activated protein kinase (p38beta). *J Biol Chem*. 1996;271(30):17920-6. Epub 1996/07/26. doi: 10.1074/jbc.271.30.17920. PubMed PMID: 8663524.
22. Jiang Y, Gram H, Zhao M, New L, Gu J, Feng L, Di Padova F, Ulevitch RJ, Han J. Characterization of the structure and function of the fourth member of p38 group mitogen-activated protein kinases, p38delta. *J Biol Chem*. 1997;272(48):30122-8. Epub 1997/12/31. doi: 10.1074/jbc.272.48.30122. PubMed PMID: 9374491.

23. Li Z, Jiang Y, Ulevitch RJ, Han J. The primary structure of p38 gamma: a new member of p38 group of MAP kinases. *Biochem Biophys Res Commun.* 1996;228(2):334-40. Epub 1996/11/12. doi: 10.1006/bbrc.1996.1662. PubMed PMID: 8920915.
24. O'Callaghan C, Fanning LJ, Barry OP. p38 $\delta$  MAPK: Emerging Roles of a Neglected Isoform. *Int J Cell Biol.* 2014;2014:272689. Epub 2014/10/15. doi: 10.1155/2014/272689. PubMed PMID: 25313309; PMCID: PMC4182853.
25. Adams RH, Porras A, Alonso G, Jones M, Vintersten K, Panelli S, Valladares A, Perez L, Klein R, Nebreda AR. Essential role of p38alpha MAP kinase in placental but not embryonic cardiovascular development. *Mol Cell.* 2000;6(1):109-16. Epub 2000/08/19. PubMed PMID: 10949032.
26. Mudgett JS, Ding J, Guh-Siesel L, Chartrain NA, Yang L, Gopal S, Shen MM. Essential role for p38alpha mitogen-activated protein kinase in placental angiogenesis. *Proc Natl Acad Sci U S A.* 2000;97(19):10454-9. doi: 10.1073/pnas.180316397. PubMed PMID: 10973481; PMCID: PMC27045.
27. Beardmore VA, Hinton HJ, Eftychi C, Apostolaki M, Armaka M, Darragh J, McIlrath J, Carr JM, Armit LJ, Clacher C, Malone L, Kollias G, Arthur JS. Generation and characterization of p38beta (MAPK11) gene-targeted mice. *Mol Cell Biol.* 2005;25(23):10454-64. Epub 2005/11/17. doi: 10.1128/MCB.25.23.10454-10464.2005. PubMed PMID: 16287858; PMCID: PMC1291241.
28. Greenblatt MB, Shim JH, Zou W, Sitara D, Schweitzer M, Hu D, Lotinun S, Sano Y, Baron R, Park JM, Arthur S, Xie M, Schneider MD, Zhai B, Gygi S, Davis R, Glimcher LH. The p38 MAPK pathway is essential for skeletogenesis and bone homeostasis in mice. *J Clin Invest.* 2010;120(7):2457-73. Epub 2010/06/17. doi: 10.1172/JCI42285. PubMed PMID: 20551513; PMCID: PMC2898605.
29. Nakamura K, Johnson GL. PB1 domains of MEKK2 and MEKK3 interact with the MEK5 PB1 domain for activation of the ERK5 pathway. *J Biol Chem.* 2003;278(39):36989-92. Epub 2003/08/13. doi: 10.1074/jbc.C300313200. PubMed PMID: 12912994.
30. Meister M, Tomasovic A, Banning A, Tikkanen R. Mitogen-Activated Protein (MAP) Kinase Scaffolding Proteins: A Recount. *Int J Mol Sci.* 2013;14(3):4854-84. Epub 2013/03/05. doi: 10.3390/ijms14034854. PubMed PMID: 23455463; PMCID: PMC3634400.
31. Grimsey NJ, Aguilar B, Smith TH, Le P, Soohoo AL, Puthenveedu MA, Nizet V, Trejo J. Ubiquitin plays an atypical role in GPCR-induced p38 MAP kinase activation on endosomes. *J Cell Biol.* 2015;210(7):1117-31. Epub 2015/09/24. doi: 10.1083/jcb.201504007. PubMed PMID: 26391660; PMCID: PMC4586747.
32. Grimsey NJ, Narala R, Rada CC, Mehta S, Stephens BS, Kufareva I, Lapek J, Gonzalez DJ, Handel TM, Zhang J, Trejo J. A Tyrosine Switch on NEDD4-2 E3 Ligase Transmits GPCR Inflammatory Signaling. *Cell Rep.* 2018;24(12):3312-23 e5. Epub 2018/09/21. doi: 10.1016/j.celrep.2018.08.061. PubMed PMID: 30232011; PMCID: PMC6226018.
33. Uhlik MT, Abell AN, Johnson NL, Sun W, Cuevas BD, Lobel-Rice KE, Horne EA, Dell'Acqua ML, Johnson GL. Rac-MEKK3-MKK3 scaffolding for p38 MAPK activation during hyperosmotic shock. *Nat Cell Biol.* 2003;5(12):1104-10. Epub 2003/11/25. doi: 10.1038/ncb1071. PubMed PMID: 14634666.
34. Galperin E, Sorkin A. Endosomal targeting of MEK2 requires RAF, MEK kinase activity and clathrin-dependent endocytosis. *Traffic.* 2008;9(10):1776-90. Epub 2008/07/29. doi: 10.1111/j.1600-0854.2008.00788.x. PubMed PMID: 18657070; PMCID: PMC2750913.

35. Canovas B, Nebreda AR. Diversity and versatility of p38 kinase signalling in health and disease. *Nat Rev Mol Cell Biol.* 2021;1-21. Epub 2021/01/29. doi: 10.1038/s41580-020-00322-w. PubMed PMID: 33504982; PMCID: PMC7838852 p38 $\alpha$  autophosphorylation (WO2020120576). A.R.N. is a named inventor on this application. B.C. declares no competing interests.
36. Han J, Wu J, Silke J. An overview of mammalian p38 mitogen-activated protein kinases, central regulators of cell stress and receptor signaling. *F1000Res.* 2020;9. Epub 2020/07/03. doi: 10.12688/f1000research.22092.1. PubMed PMID: 32612808; PMCID: PMC7324945.
37. Cuenda A, Sanz-Ezquerro JJ. p38 $\gamma$  and p38 $\delta$ : From Spectators to Key Physiological Players. *Trends Biochem Sci.* 2017;42(6):431-42. Epub 2017/05/06. doi: 10.1016/j.tibs.2017.02.008. PubMed PMID: 28473179.
38. Zu YL, Wu F, Gilchrist A, Ai Y, Labadia ME, Huang CK. The primary structure of a human MAP kinase activated protein kinase 2. *Biochem Biophys Res Commun.* 1994;200(2):1118-24. Epub 1994/04/29. doi: 10.1006/bbrc.1994.1566. PubMed PMID: 8179591.
39. Soni S, Anand P, Padwad YS. MAPKAPK2: the master regulator of RNA-binding proteins modulates transcript stability and tumor progression. *Journal of Experimental & Clinical Cancer Research.* 2019;38(1):121. doi: 10.1186/s13046-019-1115-1.
40. Tan Y, Rouse J, Zhang A, Cariati S, Cohen P, Comb MJ. FGF and stress regulate CREB and ATF-1 via a pathway involving p38 MAP kinase and MAPKAP kinase-2. *Embo j.* 1996;15(17):4629-42. Epub 1996/09/02. PubMed PMID: 8887554; PMCID: PMC452194.
41. Guay J, Lambert H, Gingras-Breton G, Lavoie JN, Huot J, Landry J. Regulation of actin filament dynamics by p38 map kinase-mediated phosphorylation of heat shock protein 27. *J Cell Sci.* 1997;110 ( Pt 3):357-68. Epub 1997/02/01. PubMed PMID: 9057088.
42. Soni S, Saroch MK, Chander B, Tirpude NV, Padwad YS. MAPKAPK2 plays a crucial role in the progression of head and neck squamous cell carcinoma by regulating transcript stability. *J Exp Clin Cancer Res.* 2019;38(1):175. Epub 2019/04/27. doi: 10.1186/s13046-019-1167-2. PubMed PMID: 31023373; PMCID: PMC6482562.
43. Reyskens KMSE, Arthur JSC. Emerging Roles of the Mitogen and Stress Activated Kinases MSK1 and MSK2. *Frontiers in Cell and Developmental Biology.* 2016;4:56.
44. Trempelec N, Dave-Coll N, Nebreda AR. SnapShot: p38 MAPK substrates. *Cell.* 2013;152(4):924- e1. Epub 2013/02/19. doi: 10.1016/j.cell.2013.01.047. PubMed PMID: 23415236.
45. Nunes-Xavier C, Romá-Mateo C, Ríos P, Tárrega C, Cejudo-Marín R, Tabernero L, Pulido R. Dual-specificity MAP kinase phosphatases as targets of cancer treatment. *Anticancer Agents Med Chem.* 2011;11(1):109-32. Epub 2011/02/04. doi: 10.2174/187152011794941190. PubMed PMID: 21288197.
46. Sun H, Charles CH, Lau LF, Tonks NK. MKP-1 (3CH134), an immediate early gene product, is a dual specificity phosphatase that dephosphorylates MAP kinase in vivo. *Cell.* 1993;75(3):487-93. Epub 1993/11/05. doi: 10.1016/0092-8674(93)90383-2. PubMed PMID: 8221888.
47. Chen HF, Chuang HC, Tan TH. Regulation of Dual-Specificity Phosphatase (DUSP) Ubiquitination and Protein Stability. *Int J Mol Sci.* 2019;20(11). Epub 2019/06/04. doi: 10.3390/ijms20112668. PubMed PMID: 31151270; PMCID: PMC6600639.

48. Tomida T, Takekawa M, Saito H. Oscillation of p38 activity controls efficient pro-inflammatory gene expression. *Nat Commun.* 2015;6:8350. Epub 2015/09/25. doi: 10.1038/ncomms9350. PubMed PMID: 26399197; PMCID: PMC4598561.
49. Takekawa M, Maeda T, Saito H. Protein phosphatase 2 $\alpha$  inhibits the human stress-responsive p38 and JNK MAPK pathways. *Embo j.* 1998;17(16):4744-52. Epub 1998/08/26. doi: 10.1093/emboj/17.16.4744. PubMed PMID: 9707433; PMCID: PMC1170803.
50. Liu G, Hu X, Sun B, Yang T, Shi J, Zhang L, Zhao Y. Phosphatase Wip1 negatively regulates neutrophil development through p38 MAPK-STAT1. *Blood.* 2013;121(3):519-29. Epub 2012/12/06. doi: 10.1182/blood-2012-05-432674. PubMed PMID: 23212517.
51. Topolska-Woś AM, Rosińska S, Filipek A. MAP kinase p38 is a novel target of CacyBP/SIP phosphatase. *Amino Acids.* 2017;49(6):1069-76. Epub 2017/03/12. doi: 10.1007/s00726-017-2404-7. PubMed PMID: 28283909; PMCID: PMC5437258.
52. Kumar S, Boehm J, Lee JC. p38 MAP kinases: key signalling molecules as therapeutic targets for inflammatory diseases. *Nature Reviews Drug Discovery.* 2003;2(9):717-26. doi: 10.1038/nrd1177.
53. Adams JL, Badger AM, Kumar S, Lee JC. 1 p38 MAP Kinase: Molecular Target for the Inhibition of Pro-inflammatory Cytokines. In: King FD, Oxford AW, editors. *Progress in Medicinal Chemistry*; Elsevier; 2001. p. 1-60.
54. Xing L, Shieh HS, Selness SR, Devraj RV, Walker JK, Devadas B, Hope HR, Compton RP, Schindler JF, Hirsch JL, Benson AG, Kurumbail RG, Stegeman RA, Williams JM, Broadus RM, Walden Z, Monahan JB. Structural bioinformatics-based prediction of exceptional selectivity of p38 MAP kinase inhibitor PH-797804. *Biochemistry.* 2009;48(27):6402-11. Epub 2009/06/06. doi: 10.1021/bi900655f. PubMed PMID: 19496616.
55. Wroblewski ST, Lin S, Dhar TG, Dyckman AJ, Li T, Pitt S, Zhang R, Fan Y, Doweyko AM, Tokarski JS, Kish KF, Kiefer SE, Sack JS, Newitt JA, Witmer MR, McKinnon M, Barrish JC, Dodd JH, Schieven GL, Leftheris K. The identification of novel p38 $\alpha$  isoform selective kinase inhibitors having an unprecedented p38 $\alpha$  binding mode. *Bioorg Med Chem Lett.* 2013;23(14):4120-6. Epub 2013/06/12. doi: 10.1016/j.bmcl.2013.05.047. PubMed PMID: 23746475.
56. Das J, Moquin RV, Pitt S, Zhang R, Shen DR, McIntyre KW, Gillooly K, Doweyko AM, Sack JS, Zhang H, Kiefer SE, Kish K, McKinnon M, Barrish JC, Dodd JH, Schieven GL, Leftheris K. Pyrazolo-pyrimidines: a novel heterocyclic scaffold for potent and selective p38 alpha inhibitors. *Bioorg Med Chem Lett.* 2008;18(8):2652-7. Epub 2008/03/25. doi: 10.1016/j.bmcl.2008.03.019. PubMed PMID: 18359226.
57. Xing L. Clinical candidates of small molecule p38 MAPK inhibitors for inflammatory diseases. *MAP Kinase* 2015. 2015;4(5508):7.
58. Devadas B, Selness SR, Xing L, Madsen HM, Marrufo LD, Shieh H, Messing DM, Yang JZ, Morgan HM, Anderson GD, Webb EG, Zhang J, Devraj RV, Monahan JB. Substituted N-aryl-6-pyrimidinones: a new class of potent, selective, and orally active p38 MAP kinase inhibitors. *Bioorg Med Chem Lett.* 2011;21(13):3856-60. Epub 2011/05/31. doi: 10.1016/j.bmcl.2011.05.006. PubMed PMID: 21620699.
59. Selness SR, Devraj RV, Devadas B, Walker JK, Boehm TL, Durley RC, Shieh H, Xing L, Rucker PV, Jerome KD, Benson AG, Marrufo LD, Madsen HM, Hitchcock J, Owen TJ, Christie L, Promo MA, Hickory BS, Alvira E, Naing W, Blevis-Bal R, Messing D, Yang J, Mao MK, Yalamanchili G, Vonder Embse R, Hirsch J, Saabye M, Bonar S, Webb E, Anderson G,

- Monahan JB. Discovery of PH-797804, a highly selective and potent inhibitor of p38 MAP kinase. *Bioorganic & Medicinal Chemistry Letters*. 2011;21(13):4066-71. doi: <https://doi.org/10.1016/j.bmcl.2011.04.121>.
60. Canovas B, Nebreda AR. Diversity and versatility of p38 kinase signalling in health and disease. *Nature Reviews Molecular Cell Biology*. 2021. doi: 10.1038/s41580-020-00322-w.
61. Grimes JM, Grimes KV. p38 MAPK inhibition: A promising therapeutic approach for COVID-19. *J Mol Cell Cardiol*. 2020;144:63-5. Epub 2020/05/19. doi: 10.1016/j.yjmcc.2020.05.007. PubMed PMID: 32422320; PMCID: PMC7228886.
62. Cheriyan J, Webb AJ, Sarov-Blat L, Elkhawad M, Wallace SM, Mäki-Petäjä KM, Collier DJ, Morgan J, Fang Z, Willette RN, Lepore JJ, Cockcroft JR, Sprecher DL, Wilkinson IB. Inhibition of p38 mitogen-activated protein kinase improves nitric oxide-mediated vasodilatation and reduces inflammation in hypercholesterolemia. *Circulation*. 2011;123(5):515-23. Epub 2011/01/26. doi: 10.1161/circulationaha.110.971986. PubMed PMID: 21262998.
63. Barbour AM, Sarov-Blat L, Cai G, Fossler MJ, Sprecher DL, Graggaber J, McGeoch AT, Maison J, Cheriyan J. Safety, tolerability, pharmacokinetics and pharmacodynamics of losmapimod following a single intravenous or oral dose in healthy volunteers. *Br J Clin Pharmacol*. 2013;76(1):99-106. Epub 2012/12/12. doi: 10.1111/bcp.12063. PubMed PMID: 23215699; PMCID: PMC3703232.
64. Christie JD, Vaslef S, Chang PK, May AK, Gunn SR, Yang S, Harges K, Kahl L, Powley WM, Lipson DA, Bayliffe AI, Lazaar AL. A Randomized Dose-Escalation Study of the Safety and Anti-Inflammatory Activity of the p38 Mitogen-Activated Protein Kinase Inhibitor Dilmapiomod in Severe Trauma Subjects at Risk for Acute Respiratory Distress Syndrome. *Critical care medicine*. 2015;43(9):1859-69. Epub 2015/06/24. doi: 10.1097/ccm.0000000000001132. PubMed PMID: 26102252.
65. Strâmbu IR, Kobalava ZD, Magnusson BP, MacKinnon A, Parkin JM. Phase II Study of Single/Repeated Doses of Acumapimod (BCT197) to Treat Acute Exacerbations of COPD. *Copd*. 2019;16(5-6):344-53. Epub 2019/11/05. doi: 10.1080/15412555.2019.1682535. PubMed PMID: 31682162.
66. Hölscher C, Gräb J, Hölscher A, Müller AL, Schäfer SC, Rybniker J. Chemical p38 MAP kinase inhibition constrains tissue inflammation and improves antibiotic activity in *Mycobacterium tuberculosis*-infected mice. *Scientific Reports*. 2020;10(1):13629. doi: 10.1038/s41598-020-70184-x.
67. Nichols C, Ng J, Keshu A, Kelly G, Conte MR, Marber MS, Fraternali F, De Nicola GF. Mining the PDB for Tractable Cases Where X-ray Crystallography Combined with Fragment Screens Can Be Used to Systematically Design Protein-Protein Inhibitors: Two Test Cases Illustrated by IL1 $\beta$ -IL1R and p38 $\alpha$ -TAB1 Complexes. *J Med Chem*. 2020;63(14):7559-68. Epub 2020/06/17. doi: 10.1021/acs.jmedchem.0c00403. PubMed PMID: 32543856.
68. Shah NG, Tulapurkar ME, Ramarathnam A, Brophy A, Martinez R, 3rd, Hom K, Hodges T, Samadani R, Singh IS, MacKerell AD, Jr., Shapiro P, Hasday JD. Novel Noncatalytic Substrate-Selective p38 $\alpha$ -Specific MAPK Inhibitors with Endothelial-Stabilizing and Anti-Inflammatory Activity. *J Immunol*. 2017;198(8):3296-306. Epub 2017/03/17. doi: 10.4049/jimmunol.1602059. PubMed PMID: 28298524; PMCID: PMC5649369.
69. Yang L, Sun X, Ye Y, Lu Y, Zuo J, Liu W, Elcock A, Zhu S. p38 $\alpha$  Mitogen-Activated Protein Kinase Is a Druggable Target in Pancreatic Adenocarcinoma. *Front Oncol*. 2019;9:1294.

Epub 2019/12/13. doi: 10.3389/fonc.2019.01294. PubMed PMID: 31828036; PMCID: PMC6890821.

70. Wang C, Hockerman S, Jacobsen EJ, Alippe Y, Selness SR, Hope HR, Hirsch JL, Mnich SJ, Saabye MJ, Hood WF, Bonar SL, Abu-Amer Y, Haimovich A, Hoffman HM, Monahan JB, Mbalaviele G. Selective inhibition of the p38 $\alpha$  MAPK-MK2 axis inhibits inflammatory cues including inflammasome priming signals. *J Exp Med*. 2018;215(5):1315-25. Epub 2018/03/20. doi: 10.1084/jem.20172063. PubMed PMID: 29549113; PMCID: PMC5940269.

71. De Nicola GF, Bassi R, Nichols C, Fernandez-Caggiano M, Golforoush PA, Thapa D, Anderson R, Martin ED, Verma S, Kleinjung J, Laing A, Hutchinson JP, Eaton P, Clark J, Marber MS. The TAB1-p38 $\alpha$  complex aggravates myocardial injury and can be targeted by small molecules. *JCI Insight*. 2018;3(16). Epub 2018/08/24. doi: 10.1172/jci.insight.121144. PubMed PMID: 30135318; PMCID: PMC6141180.

72. Astolfi A, Manfroni G, Cecchetti V, Barreca ML. A Comprehensive Structural Overview of p38 $\alpha$  Mitogen-Activated Protein Kinase in Complex with ATP-Site and Non-ATP-Site Binders. *ChemMedChem*. 2018;13(1):7-14. Epub 2017/12/07. doi: 10.1002/cmdc.201700636. PubMed PMID: 29210532.

73. Nichols C, Ng J, Keshu A, Kelly G, Conte MR, Marber MS, Fraternali F, De Nicola GF. Mining the PDB for Tractable Cases Where X-ray Crystallography Combined with Fragment Screens Can Be Used to Systematically Design Protein-Protein Inhibitors: Two Test Cases Illustrated by IL1 $\beta$ -IL1R and p38 $\alpha$ -TAB1 Complexes. *Journal of Medicinal Chemistry*. 2020;63(14):7559-68. doi: 10.1021/acs.jmedchem.0c00403.

74. De Nicola GF, Martin ED, Chaikuad A, Bassi R, Clark J, Martino L, Verma S, Sicard P, Tata R, Atkinson RA, Knapp S, Conte MR, Marber MS. Mechanism and consequence of the autoactivation of p38 $\alpha$  mitogen-activated protein kinase promoted by TAB1. *Nature Structural & Molecular Biology*. 2013;20(10):1182-90. doi: 10.1038/nsmb.2668.

75. Ge B, Gram H, Di Padova F, Huang B, New L, Ulevitch RJ, Luo Y, Han J. MAPKK-independent activation of p38 $\alpha$  mediated by TAB1-dependent autophosphorylation of p38 $\alpha$ . *Science*. 2002;295(5558):1291-4. Epub 2002/02/16. doi: 10.1126/science.1067289. PubMed PMID: 11847341.

76. Inagaki M, Omori E, Kim JY, Komatsu Y, Scott G, Ray MK, Yamada G, Matsumoto K, Mishina Y, Ninomiya-Tsuji J. TAK1-binding protein 1, TAB1, mediates osmotic stress-induced TAK1 activation but is dispensable for TAK1-mediated cytokine signaling. *J Biol Chem*. 2008;283(48):33080-6. Epub 2008/10/03. doi: 10.1074/jbc.M807574200. PubMed PMID: 18829460; PMCID: PMC2586273.

77. Scholz R, Sidler CL, Thali RF, Winssinger N, Cheung PC, Neumann D. Autoactivation of transforming growth factor beta-activated kinase 1 is a sequential bimolecular process. *J Biol Chem*. 2010;285(33):25753-66. Epub 2010/06/12. doi: 10.1074/jbc.M109.093468. PubMed PMID: 20538596; PMCID: PMC2919138.

78. Kishimoto K, Matsumoto K, Ninomiya-Tsuji J. TAK1 mitogen-activated protein kinase kinase is activated by autophosphorylation within its activation loop. *J Biol Chem*. 2000;275(10):7359-64. Epub 2000/03/04. doi: 10.1074/jbc.275.10.7359. PubMed PMID: 10702308.

79. Cheung PC, Campbell DG, Nebreda AR, Cohen P. Feedback control of the protein kinase TAK1 by SAPK2a/p38 $\alpha$ . *EMBO J*. 2003;22(21):5793-805. Epub 2003/11/01. doi: 10.1093/emboj/cdg552. PubMed PMID: 14592977.

80. Wolf A, Beuerlein K, Eckart C, Weiser H, Dickkopf B, Müller H, Sakurai H, Kracht M. Identification and functional characterization of novel phosphorylation sites in TAK1-binding protein (TAB) 1. *PLoS One*. 2011;6(12):e29256. Epub 2012/01/05. doi: 10.1371/journal.pone.0029256. PubMed PMID: 22216226; PMCID: PMC3245275.
81. De Nicola GF, Martin ED, Chaikuad A, Bassi R, Clark J, Martino L, Verma S, Sicard P, Tata R, Atkinson RA, Knapp S, Conte MR, Marber MS. Mechanism and consequence of the autoactivation of p38alpha mitogen-activated protein kinase promoted by TAB1. *Nat Struct Mol Biol*. 2013;20(10):1182-90. doi: 10.1038/nsmb.2668. PubMed PMID: 24037507; PMCID: 3822283.
82. Richardson L, Dixon CL, Aguilera-Aguirre L, Menon R. Oxidative stress-induced TGF-beta/TAB1-mediated p38MAPK activation in human amnion epithelial cells. *Biol Reprod*. 2018;99(5):1100-12. Epub 2018/06/13. doi: 10.1093/biolre/ioy135. PubMed PMID: 29893818; PMCID: PMC7190655.
83. Li J, Miller EJ, Ninomiya-Tsuji J, Russell RR, 3rd, Young LH. AMP-activated protein kinase activates p38 mitogen-activated protein kinase by increasing recruitment of p38 MAPK to TAB1 in the ischemic heart. *Circ Res*. 2005;97(9):872-9. Epub 2005/09/24. doi: 10.1161/01.Res.0000187458.77026.10. PubMed PMID: 16179588.
84. Ota A, Zhang J, Ping P, Han J, Wang Y. Specific regulation of noncanonical p38alpha activation by Hsp90-Cdc37 chaperone complex in cardiomyocyte. *Circ Res*. 2010;106(8):1404-12. doi: 10.1161/circresaha.109.213769. PubMed PMID: 20299663; PMCID: 2891038.
85. Theivanthiran B, Kathania M, Zeng M, Anguiano E, Basrur V, Vandergriff T, Pascual V, Wei WZ, Massoumi R, Venuprasad K. The E3 ubiquitin ligase Itch inhibits p38alpha signaling and skin inflammation through the ubiquitylation of Tab1. *Sci Signal*. 2015;8(365):ra22. doi: 10.1126/scisignal.2005903. PubMed PMID: 25714464.
86. Wang Q, Feng J, Wang J, Zhang X, Zhang D, Zhu T, Wang W, Wang X, Jin J, Cao J, Li X, Peng H, Li Y, Shen B, Zhang J. Disruption of TAB1/p38alpha interaction using a cell-permeable peptide limits myocardial ischemia/reperfusion injury. *Mol Ther*. 2013;21(9):1668-77. doi: 10.1038/mt.2013.90. PubMed PMID: 23877036; PMCID: 3776642.
87. Pei YJ, Wang QY, Zhang JY, Guo YH, Feng JN. Characterization and Evaluation of Key Sites in the Peptide Inhibitor of TAB1/p38 alpha Interaction. *International Journal of Peptide Research and Therapeutics*. 2018;24(2):225-33. doi: 10.1007/s10989-017-9607-3. PubMed PMID: WOS:000430984300001.
88. Zhou H, Zheng M, Chen J, Xie C, Kolatkar AR, Zarubin T, Ye Z, Akella R, Lin S, Goldsmith EJ, Han J. Determinants that control the specific interactions between TAB1 and p38alpha. *Mol Cell Biol*. 2006;26(10):3824-34. Epub 2006/05/02. doi: 10.1128/mcb.26.10.3824-3834.2006. PubMed PMID: 16648477; PMCID: PMC1489000.
89. Komatsu Y, Shibuya H, Takeda N, Ninomiya-Tsuji J, Yasui T, Miyado K, Sekimoto T, Ueno N, Matsumoto K, Yamada G. Targeted disruption of the Tab1 gene causes embryonic lethality and defects in cardiovascular and lung morphogenesis. *Mech Dev*. 2002;119(2):239-49. PubMed PMID: 12464436.
90. Grimsey NJ, Lin Y, Narala R, Rada CC, Mejia-Pena H, Trejo J. G protein-coupled receptors activate p38 MAPK via a non-canonical TAB1-TAB2 and TAB1-TAB3 dependent pathway in endothelial cells. *J Biol Chem*. 2019. Epub 2019/02/15. doi: 10.1074/jbc.RA119.007495. PubMed PMID: 30760523.

91. Salvador JM, Mittelstadt PR, Guszczynski T, Copeland TD, Yamaguchi H, Appella E, Fornace AJ, Jr., Ashwell JD. Alternative p38 activation pathway mediated by T cell receptor-proximal tyrosine kinases. *Nat Immunol.* 2005;6(4):390-5. Epub 2005/03/01. doi: ni1177 [pii] 10.1038/ni1177. PubMed PMID: 15735648.
92. Diskin R, Lebendiker M, Engelberg D, Livnah O. Structures of p38alpha active mutants reveal conformational changes in L16 loop that induce autophosphorylation and activation. *J Mol Biol.* 2007;365(1):66-76. Epub 2006/10/25. doi: 10.1016/j.jmb.2006.08.043. PubMed PMID: 17059827.
93. Flower DR. Modelling G-protein-coupled receptors for drug design. *Biochim Biophys Acta.* 1999;1422(3):207-34. Epub 1999/11/05. doi: 10.1016/s0304-4157(99)00006-4. PubMed PMID: 10548717.
94. Azzi M, Charest PG, Angers S, Rousseau G, Kohout T, Bouvier M, Piñeyro G.  $\beta$ -Arrestin-mediated activation of MAPK by inverse agonists reveals distinct active conformations for G protein-coupled receptors. *Proceedings of the National Academy of Sciences.* 2003;100(20):11406. doi: 10.1073/pnas.1936664100.
95. Gutkind JS. Regulation of Mitogen-Activated Protein Kinase Signaling Networks by G Protein-Coupled Receptors. *Science's STKE.* 2000;2000(40):re1. doi: 10.1126/stke.2000.40.re1.
96. McDonald PH, Chow C-W, Miller WE, Laporte SA, Field ME, Lin F-T, Davis RJ, Lefkowitz RJ.  $\beta$ -Arrestin 2: A Receptor-Regulated MAPK Scaffold for the Activation of JNK3. *Science.* 2000;290(5496):1574. doi: 10.1126/science.290.5496.1574.
97. Shenoy SK, Lefkowitz RJ. Seven-transmembrane receptor signaling through beta-arrestin. *Sci STKE.* 2005;2005(308):cm10. Epub 2005/11/04. doi: 10.1126/stke.2005/308/cm10. PubMed PMID: 16267056.
98. Burton JC, Grimsey NJ. Ubiquitination as a Key Regulator of Endosomal Signaling by GPCRs. *Front Cell Dev Biol.* 2019;7:43. Epub 2019/04/16. doi: 10.3389/fcell.2019.00043. PubMed PMID: 30984758; PMCID: PMC6449645.
99. Grimsey NJ, Trejo J. Integration of endothelial protease-activated receptor-1 inflammatory signaling by ubiquitin. *Curr Opin Hematol.* 2016;23(3):274-9. doi: 10.1097/MOH.0000000000000232. PubMed PMID: 26845544.
100. Dores MR, Chen B, Lin H, Soh UJ, Paing MM, Montagne WA, Meerloo T, Trejo J. ALIX binds a YPX(3)L motif of the GPCR PAR1 and mediates ubiquitin-independent ESCRT-III/MVB sorting. *J Cell Biol.* 2012;197(3):407-19. Epub 2012/05/02. doi: jcb.201110031 [pii] 10.1083/jcb.201110031. PubMed PMID: 22547407.
101. Dores MR, Grimsey NJ, Mendez F, Trejo J. ALIX Regulates the Ubiquitin-Independent Lysosomal Sorting of the P2Y1 Purinergic Receptor via a YPX3L Motif. *PLoS One.* 2016;11(6):e0157587. doi: 10.1371/journal.pone.0157587. PubMed PMID: 27301021; PMCID: PMC4907476.
102. Dores MR, Lin H, N JG, Mendez F, Trejo J. The alpha-arrestin ARRD3 mediates ALIX ubiquitination and G protein-coupled receptor lysosomal sorting. *Mol Biol Cell.* 2015;26(25):4660-73. Epub 2015/10/23. doi: 10.1091/mbc.E15-05-0284. PubMed PMID: 26490116; PMCID: PMC4678022.
103. Kulathu Y, Akutsu M, Bremm A, Hofmann K, Komander D. Two-sided ubiquitin binding explains specificity of the TAB2 NZF domain. *Nat Struct Mol Biol.* 2009;16(12):1328-30. Epub 2009/11/26. doi: nsmb.1731 [pii] 10.1038/nsmb.1731. PubMed PMID: 19935683.

104. Cuenda A, Rousseau S. p38 MAP-kinases pathway regulation, function and role in human diseases. *Biochim Biophys Acta*. 2007;1773(8):1358-75. doi: 10.1016/j.bbamcr.2007.03.010. PubMed PMID: 17481747.
105. Romero-Becerra R, Santamans AM, Folgueira C, Sabio G. p38 MAPK Pathway in the Heart: New Insights in Health and Disease. *Int J Mol Sci*. 2020;21(19). Epub 2020/10/15. doi: 10.3390/ijms21197412. PubMed PMID: 33049962; PMCID: PMC7582802.
106. Arabacilar P, Marber M. The case for inhibiting p38 mitogen-activated protein kinase in heart failure. *Front Pharmacol*. 2015;6:102. Epub 2015/06/02. doi: 10.3389/fphar.2015.00102. PubMed PMID: 26029107; PMCID: PMC4428223.
107. Song N, Ma J, Meng XW, Liu H, Wang H, Song SY, Chen QC, Liu HY, Zhang J, Peng K, Ji FH. Heat Shock Protein 70 Protects the Heart from Ischemia/Reperfusion Injury through Inhibition of p38 MAPK Signaling. *Oxid Med Cell Longev*. 2020;2020:3908641. Epub 2020/04/21. doi: 10.1155/2020/3908641. PubMed PMID: 32308802; PMCID: PMC7142395 of this paper.
108. Fiedler B, Feil R, Hofmann F, Willenbockel C, Drexler H, Smolenski A, Lohmann SM, Wollert KC. cGMP-dependent protein kinase type I inhibits TAB1-p38 mitogen-activated protein kinase apoptosis signaling in cardiac myocytes. *J Biol Chem*. 2006;281(43):32831-40. Epub 2006/09/01. doi: 10.1074/jbc.M603416200. PubMed PMID: 16943189.
109. Pei Y, Wang Q, Zhang J, Guo Y, Feng J. Characterization and Evaluation of Key Sites in the Peptide Inhibitor of TAB1/p38 $\alpha$  Interaction.
110. Tanno M, Bassi R, Gorog DA, Saurin AT, Jiang J, Heads RJ, Martin JL, Davis RJ, Flavell RA, Marber MS. Diverse mechanisms of myocardial p38 mitogen-activated protein kinase activation: evidence for MKK-independent activation by a TAB1-associated mechanism contributing to injury during myocardial ischemia. *Circ Res*. 2003;93(3):254-61. Epub 2003/06/28. doi: 10.1161/01.Res.0000083490.43943.85. PubMed PMID: 12829618.
111. Wang Q, Feng J, Wang J, Zhang X, Zhang D, Zhu T, Wang W, Wang X, Jin J, Cao J, Li X, Peng H, Li Y, Shen B, Zhang J. Disruption of TAB1/p38 $\alpha$  interaction using a cell-permeable peptide limits myocardial ischemia/reperfusion injury. *Mol Ther*. 2013;21(9):1668-77. Epub 2013/07/24. doi: 10.1038/mt.2013.90. PubMed PMID: 23877036; PMCID: PMC3776642.
112. Zheng DY, Zhou M, Jin J, He M, Wang Y, Du J, Xiao XY, Li PY, Ye AZ, Liu J, Wang TH. Inhibition of P38 MAPK Downregulates the Expression of IL-1beta to Protect Lung from Acute Injury in Intestinal Ischemia Reperfusion Rats. *Mediators Inflamm*. 2016;2016:9348037. Epub 2016/03/17. doi: 10.1155/2016/9348037. PubMed PMID: 26980948; PMCID: PMC4766341.
113. Du CS, Yang RF, Song SW, Wang YP, Kang JH, Zhang R, Su DF, Xie X. Magnesium Lithospermate B Protects Cardiomyocytes from Ischemic Injury Via Inhibition of TAB1-p38 Apoptosis Signaling. *Front Pharmacol*. 2010;1:111. Epub 2010/01/01. doi: 10.3389/fphar.2010.00111. PubMed PMID: 21607062; PMCID: PMC3095368.
114. Thapa D, Nichols C, Bassi R, Martin ED, Verma S, Conte MR, De Santis V, De Nicola GF, Marber MS. TAB1-Induced Autoactivation of p38 $\alpha$  Mitogen-Activated Protein Kinase Is Crucially Dependent on Threonine 185. *Mol Cell Biol*. 2018;38(5). Epub 2017/12/13. doi: 10.1128/mcb.00409-17. PubMed PMID: 29229647; PMCID: PMC5809688.
115. Wang S, Ding L, Ji H, Xu Z, Liu Q, Zheng Y. The Role of p38 MAPK in the Development of Diabetic Cardiomyopathy. *Int J Mol Sci*. 2016;17(7). Epub 2016/07/05. doi: 10.3390/ijms17071037. PubMed PMID: 27376265; PMCID: PMC4964413.

116. Al-Shabrawey M, Hussein K, Wang F, Wan M, Elmasry K, Elsherbiny N, Saleh H, Yu PB, Tawfik A, Ibrahim AS. Bone Morphogenetic Protein-2 Induces Non-Canonical Inflammatory and Oxidative Pathways in Human Retinal Endothelial Cells. *Front Immunol.* 2020;11:568795. Epub 2021/02/16. doi: 10.3389/fimmu.2020.568795. PubMed PMID: 33584642; PMCID: PMC7878387.
117. Zhang Y, Wang Y, Zhou D, Zhang LS, Deng FX, Shu S, Wang LJ, Wu Y, Guo N, Zhou J, Yuan ZY. Angiotensin II deteriorates advanced atherosclerosis by promoting MerTK cleavage and impairing efferocytosis through the AT(1)R/ROS/p38 MAPK/ADAM17 pathway. *Am J Physiol Cell Physiol.* 2019;317(4):C776-c87. Epub 2019/08/08. doi: 10.1152/ajpcell.00145.2019. PubMed PMID: 31390228.
118. Corre I, Paris F, Huot J. The p38 pathway, a major pleiotropic cascade that transduces stress and metastatic signals in endothelial cells. *Oncotarget.* 2017;8(33):55684-714. Epub 2017/09/15. doi: 10.18632/oncotarget.18264. PubMed PMID: 28903453; PMCID: PMC5589692.
119. Fisk M, Gajendragadkar PR, Maki-Petaja KM, Wilkinson IB, Cheriyan J. Therapeutic potential of p38 MAP kinase inhibition in the management of cardiovascular disease. *Am J Cardiovasc Drugs.* 2014;14(3):155-65. Epub 2014/02/08. doi: 10.1007/s40256-014-0063-6. PubMed PMID: 24504769.
120. Reustle A, Torzewski M. Role of p38 MAPK in Atherosclerosis and Aortic Valve Sclerosis. *Int J Mol Sci.* 2018;19(12). Epub 2018/11/30. doi: 10.3390/ijms19123761. PubMed PMID: 30486366; PMCID: PMC6321637.
121. Seitz I, Hess S, Schulz H, Eckl R, Busch G, Montens HP, Brandl R, Seidl S, Schomig A, Ott I. Membrane-type serine protease-1/matriptase induces interleukin-6 and -8 in endothelial cells by activation of protease-activated receptor-2: potential implications in atherosclerosis. *Arterioscler Thromb Vasc Biol.* 2007;27(4):769-75. Epub 2007/01/27. doi: 10.1161/01.ATV.0000258862.61067.14 [pii] 10.1161/01.ATV.0000258862.61067.14. PubMed PMID: 17255532.
122. Renda T, Baraldo S, Pelaia G, Bazzan E, Turato G, Papi A, Maestrelli P, Maselli R, Vatrella A, Fabbri LM, Zuin R, Marsico SA, Saetta M. Increased activation of p38 MAPK in COPD. *Eur Respir J.* 2008;31(1):62-9. Epub 2007/10/26. doi: 10.1183/09031936.00036707. PubMed PMID: 17959643.
123. Pelaia C, Vatrella A, Sciacqua A, Terracciano R, Pelaia G. Role of p38-mitogen-activated protein kinase in COPD: pathobiological implications and therapeutic perspectives. *Expert Rev Respir Med.* 2020;14(5):485-91. Epub 2020/02/23. doi: 10.1080/17476348.2020.1732821. PubMed PMID: 32077346.
124. Gaffey K, Reynolds S, Plumb J, Kaur M, Singh D. Increased phosphorylated p38 mitogen-activated protein kinase in COPD lungs. *Eur Respir J.* 2013;42(1):28-41. Epub 2012/10/13. doi: 10.1183/09031936.00170711. PubMed PMID: 23060629.
125. Armstrong J, Harbron C, Lea S, Booth G, Cadden P, Wreggett KA, Singh D. Synergistic effects of p38 mitogen-activated protein kinase inhibition with a corticosteroid in alveolar macrophages from patients with chronic obstructive pulmonary disease. *J Pharmacol Exp Ther.* 2011;338(3):732-40. Epub 2011/05/26. doi: 10.1124/jpet.111.180737. PubMed PMID: 21610141.

126. Huang C, Xie M, He X, Gao H. Activity of sputum p38 MAPK is correlated with airway inflammation and reduced FEV1 in COPD patients. *Med Sci Monit.* 2013;19:1229-35. Epub 2014/01/03. doi: 10.12659/msm.889880. PubMed PMID: 24382347; PMCID: PMC3890402.
127. Amano H, Murata K, Matsunaga H, Tanaka K, Yoshioka K, Kobayashi T, Ishida J, Fukamizu A, Sugiyama F, Sudo T, Kimura S, Tatsumi K, Kasuya Y. p38 Mitogen-activated protein kinase accelerates emphysema in mouse model of chronic obstructive pulmonary disease. *J Recept Signal Transduct Res.* 2014;34(4):299-306. Epub 2014/03/07. doi: 10.3109/10799893.2014.896380. PubMed PMID: 24593255.
128. Feng Y, Fang Z, Liu B, Zheng X. p38MAPK plays a pivotal role in the development of acute respiratory distress syndrome. *Clinics (Sao Paulo).* 2019;74:e509. Epub 2019/08/15. doi: 10.6061/clinics/2019/e509. PubMed PMID: 31411275; PMCID: PMC6683303.
129. Fang W, Cai SX, Wang CL, Sun XX, Li K, Yan XW, Sun YB, Sun XZ, Gu CK, Dai MY, Wang HM, Zhou Z. Modulation of mitogen-activated protein kinase attenuates sepsis-induced acute lung injury in acute respiratory distress syndrome rats. *Mol Med Rep.* 2017;16(6):9652-8. Epub 2017/10/19. doi: 10.3892/mmr.2017.7811. PubMed PMID: 29039541.
130. Christie JD, Vaslef S, Chang PK, May AK, Gunn SR, Yang S, Harges K, Kahl L, Powley WM, Lipson DA, Bayliffe AI, Lazaar AL. A Randomized Dose-Escalation Study of the Safety and Anti-Inflammatory Activity of the p38 Mitogen-Activated Protein Kinase Inhibitor Dilmapiomod in Severe Trauma Subjects at Risk for Acute Respiratory Distress Syndrome. *Critical Care Medicine.* 2015;43(9):1859-69. doi: 10.1097/ccm.0000000000001132. PubMed PMID: 00003246-201509000-00011.
131. Fang W, Cai SX, Wang CL, Sun XX, Li K, Yan XW, Sun YB, Sun XZ, Gu CK, Dai MY, Wang HM, Zhou Z. Modulation of mitogen-activated protein kinase attenuates sepsis-induced acute lung injury in acute respiratory distress syndrome rats. *Mol Med Rep.* 2017;16(6):9652-8. Epub 2017/10/19. doi: 10.3892/mmr.2017.7811. PubMed PMID: 29039541.
132. Bai X, Fan L, He T, Jia W, Yang L, Zhang J, Liu Y, Shi J, Su L, Hu D. SIRT1 protects rat lung tissue against severe burn-induced remote ALI by attenuating the apoptosis of PMVECs via p38 MAPK signaling. *Scientific Reports.* 2015;5(1):10277. doi: 10.1038/srep10277.
133. Xiong LL, Tan Y, Ma HY, Dai P, Qin YX, Yang RA, Xu YY, Deng Z, Zhao W, Xia QJ, Wang TH, Zhang YH. Administration of SB239063, a potent p38 MAPK inhibitor, alleviates acute lung injury induced by intestinal ischemia reperfusion in rats associated with AQP4 downregulation. *Int Immunopharmacol.* 2016;38:54-60. Epub 2016/05/30. doi: 10.1016/j.intimp.2016.03.036. PubMed PMID: 27236300.
134. Li D, Ren W, Jiang Z, Zhu L. Regulation of the NLRP3 inflammasome and macrophage pyroptosis by the p38 MAPK signaling pathway in a mouse model of acute lung injury. *Mol Med Rep.* 2018;18(5):4399-409. Epub 2018/08/29. doi: 10.3892/mmr.2018.9427. PubMed PMID: 30152849; PMCID: PMC6172370.
135. Cheng Y, Sun F, Wang L, Gao M, Xie Y, Sun Y, Liu H, Yuan Y, Yi W, Huang Z, Yan H, Peng K, Wu Y, Cao Z. Virus-induced p38 MAPK activation facilitates viral infection. *Theranostics.* 2020;10(26):12223-40. Epub 2020/11/19. doi: 10.7150/thno.50992. PubMed PMID: 33204339; PMCID: PMC7667676.
136. Mikkelsen SS, Jensen SB, Chiliveru S, Melchjorsen J, Julkunen I, Gaestel M, Arthur JS, Flavell RA, Ghosh S, Paludan SR. RIG-I-mediated activation of p38 MAPK is essential for viral induction of interferon and activation of dendritic cells: dependence on TRAF2 and TAK1. *J*

- Biol Chem. 2009;284(16):10774-82. Epub 2009/02/20. doi: 10.1074/jbc.M807272200. PubMed PMID: 19224920; PMCID: PMC2667765.
137. Börgeling Y, Schmolke M, Viemann D, Nordhoff C, Roth J, Ludwig S. Inhibition of p38 mitogen-activated protein kinase impairs influenza virus-induced primary and secondary host gene responses and protects mice from lethal H5N1 infection. *The Journal of biological chemistry*. 2014;289(1):13-27. Epub 2013/11/04. doi: 10.1074/jbc.M113.469239. PubMed PMID: 24189062.
138. Pan J, Yang Q, Shao J, Zhang L, Ma J, Wang Y, Jiang BH, Leng J, Bai X. Cyclooxygenase-2 induced  $\beta$ 1-integrin expression in NSCLC and promoted cell invasion via the EP1/MAPK/E2F-1/FoxC2 signal pathway. *Sci Rep*. 2016;6:33823. Epub 2016/09/23. doi: 10.1038/srep33823. PubMed PMID: 27654511; PMCID: PMC5031967.
139. Patel S, Vetale S, Teli P, Mistry R, Chiplunkar S. IL-10 production in non-small cell lung carcinoma patients is regulated by ERK, P38 and COX-2. *J Cell Mol Med*. 2012;16(3):531-44. Epub 2011/04/22. doi: 10.1111/j.1582-4934.2011.01329.x. PubMed PMID: 21507199; PMCID: PMC3822929.
140. Singh RK, Najmi AK. Novel Therapeutic Potential of Mitogen-Activated Protein Kinase Activated Protein Kinase 2 (MK2) in Chronic Airway Inflammatory Disorders. *Curr Drug Targets*. 2019;20(4):367-79. Epub 2018/08/17. doi: 10.2174/1389450119666180816121323. PubMed PMID: 30112991.
141. Wada M, Canals D, Adada M, Coant N, Salama MF, Helke KL, Arthur JS, Shroyer KR, Kitatani K, Obeid LM, Hannun YA. P38 delta MAPK promotes breast cancer progression and lung metastasis by enhancing cell proliferation and cell detachment. *Oncogene*. 2017;36(47):6649-57. doi: 10.1038/onc.2017.274.
142. Zhu N, Zhang XJ, Zou H, Zhang YY, Xia JW, Zhang P, Zhang YZ, Li J, Dong L, Wumaier G, Li SQ. PTPL1 suppresses lung cancer cell migration via inhibiting TGF- $\beta$ 1-induced activation of p38 MAPK and Smad 2/3 pathways and EMT. *Acta Pharmacol Sin*. 2021. Epub 2021/02/05. doi: 10.1038/s41401-020-00596-y. PubMed PMID: 33536603.
143. Koul HK, Pal M, Koul S. Role of p38 MAP Kinase Signal Transduction in Solid Tumors. *Genes Cancer*. 2013;4(9-10):342-59. Epub 2013/12/19. doi: 10.1177/1947601913507951. PubMed PMID: 24349632; PMCID: PMC3863344.
144. Igea A, Nebreda AR. The Stress Kinase p38alpha as a Target for Cancer Therapy. *Cancer Res*. 2015;75(19):3997-4002. doi: 10.1158/0008-5472.CAN-15-0173. PubMed PMID: 26377941.
145. Leelahavanichkul K, Amornphimoltham P, Molinolo AA, Basile JR, Koontongkaew S, Gutkind JS. A role for p38 MAPK in head and neck cancer cell growth and tumor-induced angiogenesis and lymphangiogenesis. *Mol Oncol*. 2014;8(1):105-18. doi: 10.1016/j.molonc.2013.10.003. PubMed PMID: 24216180; PMCID: PMC3946852.
146. Roy S, Roy S, Anuja K, Thakur S, Akhter Y, Padhi S, Banerjee B. p38 Mitogen-activated protein kinase modulates cisplatin resistance in Head and Neck Squamous Cell Carcinoma cells. *Arch Oral Biol*. 2021;122:104981. Epub 2020/12/11. doi: 10.1016/j.archoralbio.2020.104981. PubMed PMID: 33302041.
147. Liu C, Sadat SH, Ebisumoto K, Sakai A, Panuganti BA, Ren S, Goto Y, Haft S, Fukusumi T, Ando M, Saito Y, Guo T, Tamayo P, Yeerna H, Kim W, Hubbard J, Sharabi AB, Gutkind JS, Califano JA. Cannabinoids Promote Progression of HPV-Positive Head and Neck Squamous Cell Carcinoma via p38 MAPK Activation. *Clin Cancer Res*. 2020;26(11):2693-703.

- Epub 2020/01/15. doi: 10.1158/1078-0432.Ccr-18-3301. PubMed PMID: 31932491; PMCID: PMC7538010.
148. Avendano MS, Garcia-Redondo AB, Zalba G, Gonzalez-Amor M, Aguado A, Martinez-Revelles S, Beltran LM, Camacho M, Cachofeiro V, Alonso MJ, Salaices M, Briones AM. mPGES-1 (Microsomal Prostaglandin E Synthase-1) Mediates Vascular Dysfunction in Hypertension Through Oxidative Stress. *Hypertension*. 2018;72(2):492-502. Epub 2018/06/13. doi: 10.1161/HYPERTENSIONAHA.118.10833. PubMed PMID: 29891646.
149. Cánovas B, Igea A, Sartori AA, Gomis RR, Paull TT, Isoda M, Pérez-Montoyo H, Serra V, González-Suárez E, Stracker TH, Nebreda AR. Targeting p38 $\alpha$  Increases DNA Damage, Chromosome Instability, and the Anti-tumoral Response to Taxanes in Breast Cancer Cells. *Cancer Cell*. 2018;33(6):1094-110.e8. Epub 2018/05/29. doi: 10.1016/j.ccell.2018.04.010. PubMed PMID: 29805078.
150. Martínez-Limón A, Joaquin M, Caballero M, Posas F, de Nadal E. The p38 Pathway: From Biology to Cancer Therapy. *Int J Mol Sci*. 2020;21(6). Epub 2020/03/15. doi: 10.3390/ijms21061913. PubMed PMID: 32168915; PMCID: PMC7139330.
151. Kumar B, Koul S, Petersen J, Khandrika L, Hwa JS, Meacham RB, Wilson S, Koul HK. p38 Mitogen-Activated Protein Kinase–Driven MAPKAPK2 Regulates Invasion of Bladder Cancer by Modulation of MMP-2 and MMP-9 Activity. *Cancer Research*. 2010;70(2):832. doi: 10.1158/0008-5472.CAN-09-2918.
152. Lee JK, Kim NJ. Recent Advances in the Inhibition of p38 MAPK as a Potential Strategy for the Treatment of Alzheimer's Disease. *Molecules*. 2017;22(8). Epub 2017/08/03. doi: 10.3390/molecules22081287. PubMed PMID: 28767069; PMCID: PMC6152076.
153. Corrêa SA, Eales KL. The Role of p38 MAPK and Its Substrates in Neuronal Plasticity and Neurodegenerative Disease. *J Signal Transduct*. 2012;2012:649079. Epub 2012/07/14. doi: 10.1155/2012/649079. PubMed PMID: 22792454; PMCID: PMC3389708.
154. Germann UA, Alam JJ. P38 $\alpha$  MAPK Signaling-A Robust Therapeutic Target for Rab5-Mediated Neurodegenerative Disease. *Int J Mol Sci*. 2020;21(15). Epub 2020/08/06. doi: 10.3390/ijms21155485. PubMed PMID: 32751991; PMCID: PMC7432772.
155. Ittner A, Asih PR, Tan ARP, Prikas E, Bertz J, Stefanoska K, Lin Y, Volkerling AM, Ke YD, Delerue F, Ittner LM. Reduction of advanced tau-mediated memory deficits by the MAP kinase p38 $\gamma$ . *Acta Neuropathol*. 2020;140(3):279-94. Epub 2020/07/30. doi: 10.1007/s00401-020-02191-1. PubMed PMID: 32725265.
156. He J, Zhong W, Zhang M, Zhang R, Hu W. P38 Mitogen-activated Protein Kinase and Parkinson's Disease. *Transl Neurosci*. 2018;9:147-53. Epub 2018/11/27. doi: 10.1515/tnsci-2018-0022. PubMed PMID: 30473884; PMCID: PMC6234472.
157. Wang X, Sun X, Niu M, Zhang X, Wang J, Zhou C, Xie A. RAGE Silencing Ameliorates Neuroinflammation by Inhibition of p38-NF- $\kappa$ B Signaling Pathway in Mouse Model of Parkinson's Disease. *Front Neurosci*. 2020;14:353. Epub 2020/05/16. doi: 10.3389/fnins.2020.00353. PubMed PMID: 32410941; PMCID: PMC7201072.
158. Wang Q, Zheng H, Zhang ZF, Zhang YX. [Ginsenoside Rg1 modulates COX-2 expression in the substantia nigra of mice with MPTP-induced Parkinson disease through the P38 signaling pathway]. *Nan Fang Yi Ke Da Xue Xue Bao*. 2008;28(9):1594-8. Epub 2008/09/30. PubMed PMID: 18819875.

159. De Vos KJ, Hafezparast M. Neurobiology of axonal transport defects in motor neuron diseases: Opportunities for translational research? *Neurobiol Dis.* 2017;105:283-99. Epub 2017/02/27. doi: 10.1016/j.nbd.2017.02.004. PubMed PMID: 28235672; PMCID: PMC5536153.
160. Gibbs KL, Greensmith L, Schiavo G. Regulation of Axonal Transport by Protein Kinases. *Trends Biochem Sci.* 2015;40(10):597-610. Epub 2015/09/28. doi: 10.1016/j.tibs.2015.08.003. PubMed PMID: 26410600.
161. Gibbs KL, Kalmar B, Rhymes ER, Fellows AD, Ahmed M, Whiting P, Davies CH, Greensmith L, Schiavo G. Inhibiting p38 MAPK alpha rescues axonal retrograde transport defects in a mouse model of ALS. *Cell Death Dis.* 2018;9(6):596. Epub 2018/05/24. doi: 10.1038/s41419-018-0624-8. PubMed PMID: 29789529; PMCID: PMC5964181.
162. Simon CM, Van Alstyne M, Lotti F, Bianchetti E, Tisdale S, Watterson DM, Mentis GZ, Pellizzoni L. Stasimon Contributes to the Loss of Sensory Synapses and Motor Neuron Death in a Mouse Model of Spinal Muscular Atrophy. *Cell Reports.* 2019;29(12):3885-901.e5. doi: <https://doi.org/10.1016/j.celrep.2019.11.058>.
163. Kyosseva SV. Targeting MAPK Signaling in Age-Related Macular Degeneration. *Ophthalmol Eye Dis.* 2016;8:23-30. Epub 2016/07/08. doi: 10.4137/oed.S32200. PubMed PMID: 27385915; PMCID: PMC4920203.
164. Pons M, Cousins SW, Alcazar O, Striker GE, Marin-Castaño ME. Angiotensin II-Induced MMP-2 Activity and MMP-14 and Basigin Protein Expression Are Mediated via the Angiotensin II Receptor Type 1-Mitogen-Activated Protein Kinase 1 Pathway in Retinal Pigment Epithelium: Implications for Age-Related Macular Degeneration. *The American Journal of Pathology.* 2011;178(6):2665-81. doi: <https://doi.org/10.1016/j.ajpath.2011.02.006>.
165. Zou W, Luo S, Zhang Z, Cheng L, Huang X, Ding N, Pan Y, Wu Z. ASK1/p38-mediated NLRP3 inflammasome signaling pathway contributes to aberrant retinal angiogenesis in diabetic retinopathy. *Int J Mol Med.* 2021;47(2):732-40. Epub 2021/01/09. doi: 10.3892/ijmm.2020.4833. PubMed PMID: 33416127; PMCID: PMC7797434.
166. Tang L, Zhang C, Yang Q, Xie H, Liu D, Tian H, Lu L, Xu JY, Li W, Xu G, Qiu Q, Liu K, Luo D, Xu GT, Zhang J. Melatonin maintains inner blood-retinal barrier via inhibition of p38/TXNIP/NF- $\kappa$ B pathway in diabetic retinopathy. *J Cell Physiol.* 2021. Epub 2021/01/13. doi: 10.1002/jcp.30269. PubMed PMID: 33432588.
167. Lee BJ, Byeon HE, Cho CS, Kim YH, Kim JH, Che JH, Seok SH, Kwon JW, Kim JH, Lee K. Histamine causes an imbalance between pro-angiogenic and anti-angiogenic factors in the retinal pigment epithelium of diabetic retina via H4 receptor/p38 MAPK axis. *BMJ Open Diabetes Res Care.* 2020;8(2). Epub 2020/12/18. doi: 10.1136/bmjdr-2020-001710. PubMed PMID: 33328159; PMCID: PMC7745681.
168. Zou W, Zhang Z, Luo S, Cheng L, Huang X, Ding N, Yu J, Pan Y, Wu Z. p38 promoted retinal micro-angiogenesis through up-regulated RUNX1 expression in diabetic retinopathy. *Biosci Rep.* 2020;40(5). Epub 2020/04/23. doi: 10.1042/bsr20193256. PubMed PMID: 32319515; PMCID: PMC7201564.
169. Du Y, Tang J, Li G, Berti-Mattera L, Lee CA, Bartkowski D, Gale D, Monahan J, Niesman MR, Alton G, Kern TS. Effects of p38 MAPK inhibition on early stages of diabetic retinopathy and sensory nerve function. *Invest Ophthalmol Vis Sci.* 2010;51(4):2158-64. Epub 2010/01/15. doi: 10.1167/iovs.09-3674. PubMed PMID: 20071676; PMCID: PMC2868413.

170. Dapper JD, Crish SD, Pang IH, Calkins DJ. Proximal inhibition of p38 MAPK stress signaling prevents distal axonopathy. *Neurobiol Dis.* 2013;59:26-37. Epub 2013/07/19. doi: 10.1016/j.nbd.2013.07.001. PubMed PMID: 23859799; PMCID: PMC3775981.
171. Seki M, Lipton SA. Targeting excitotoxic/free radical signaling pathways for therapeutic intervention in glaucoma. *Prog Brain Res.* 2008;173:495-510. Epub 2008/10/22. doi: 10.1016/s0079-6123(08)01134-5. PubMed PMID: 18929130.
172. Schieven GL. The p38alpha kinase plays a central role in inflammation. *Curr Top Med Chem.* 2009;9(11):1038-48. Epub 2009/09/15. doi: 10.2174/156802609789630974. PubMed PMID: 19747121.
173. Choy EH, Panayi GS. Cytokine pathways and joint inflammation in rheumatoid arthritis. *N Engl J Med.* 2001;344(12):907-16. Epub 2001/03/22. doi: 10.1056/nejm200103223441207. PubMed PMID: 11259725.
174. Stokes DG, Kremer JM. Potential of tumor necrosis factor neutralization strategies in rheumatologic disorders other than rheumatoid arthritis. *Semin Arthritis Rheum.* 2003;33(1):1-18. Epub 2003/08/16. doi: 10.1053/sarh.2003.50022. PubMed PMID: 12920692.
175. Han J, Jiang Y, Li Z, Kravchenko VV, Ulevitch RJ. Activation of the transcription factor MEF2C by the MAP kinase p38 in inflammation. *Nature.* 1997;386(6622):296-9. Epub 1997/03/20. doi: 10.1038/386296a0. PubMed PMID: 9069290.
176. Guan Z, Buckman SY, Pentland AP, Templeton DJ, Morrison AR. Induction of cyclooxygenase-2 by the activated MEKK1 --> SEK1/MKK4 --> p38 mitogen-activated protein kinase pathway. *J Biol Chem.* 1998;273(21):12901-8. PubMed PMID: 9582321.
177. Badger AM, Roshak AK, Cook MN, Newman-Tarr TM, Swift BA, Carlson K, Connor JR, Lee JC, Gowen M, Lark MW, Kumar S. Differential effects of SB 242235, a selective p38 mitogen-activated protein kinase inhibitor, on IL-1 treated bovine and human cartilage/chondrocyte cultures. *Osteoarthritis Cartilage.* 2000;8(6):434-43. doi: 10.1053/joca.1999.0319. PubMed PMID: 11069728.
178. Wiehler S, Cuvelier SL, Chakrabarti S, Patel KD. p38 MAP kinase regulates rapid matrix metalloproteinase-9 release from eosinophils. *Biochem Biophys Res Commun.* 2004;315(2):463-70. Epub 2004/02/10. doi: 10.1016/j.bbrc.2004.01.078. PubMed PMID: 14766231.
179. Da Silva J, Pierrat B, Mary JL, Lesslauer W. Blockade of p38 mitogen-activated protein kinase pathway inhibits inducible nitric-oxide synthase expression in mouse astrocytes. *J Biol Chem.* 1997;272(45):28373-80. Epub 1997/11/14. doi: 10.1074/jbc.272.45.28373. PubMed PMID: 9353295.
180. Koprak S, Staruch MJ, Dumont FJ. A specific inhibitor of the p38 mitogen activated protein kinase affects differentially the production of various cytokines by activated human T cells: dependence on CD28 signaling and preferential inhibition of IL-10 production. *Cell Immunol.* 1999;192(2):87-95. Epub 1999/03/24. doi: 10.1006/cimm.1998.1448. PubMed PMID: 10087176.
181. Ananieva O, Darragh J, Johansen C, Carr JM, McIlrath J, Park JM, Wingate A, Monk CE, Toth R, Santos SG, Iversen L, Arthur JS. The kinases MSK1 and MSK2 act as negative regulators of Toll-like receptor signaling. *Nat Immunol.* 2008;9(9):1028-36. Epub 2008/08/12. doi: 10.1038/ni.1644. PubMed PMID: 18690222.
182. Lang R, Raffi FAM. Dual-Specificity Phosphatases in Immunity and Infection: An Update. *Int J Mol Sci.* 2019;20(11). Epub 2019/06/05. doi: 10.3390/ijms20112710. PubMed PMID: 31159473; PMCID: PMC6600418.

183. de la Cruz-Morcillo MA, García-Cano J, Arias-González L, García-Gil E, Artacho-Cordón F, Ríos-Arrabal S, Valero ML, Cimas FJ, Serrano-Oviedo L, Villas MV, Romero-Fernández J, Núñez MI, Sánchez-Prieto R. Abrogation of the p38 MAPK  $\alpha$  signaling pathway does not promote radioresistance but its activity is required for 5-Fluorouracil-associated radiosensitivity. *Cancer Lett.* 2013;335(1):66-74. Epub 2013/02/14. doi: 10.1016/j.canlet.2013.01.050. PubMed PMID: 23403078.
184. Lepore Signorile M, Grossi V, Di Franco S, Forte G, Disciglio V, Fasano C, Sanese P, De Marco K, Susca FC, Mangiapane LR, Nicotra A, Di Carlo G, Dituri F, Giannelli G, Ingravallo G, Canettieri G, Stassi G, Simone C. Pharmacological targeting of the novel  $\beta$ -catenin chromatin-associated kinase p38 $\alpha$  in colorectal cancer stem cell tumorspheres and organoids. *Cell Death Dis.* 2021;12(4):316. Epub 2021/03/27. doi: 10.1038/s41419-021-03572-4. PubMed PMID: 33767160.
185. Pereira L, Igea A, Canovas B, Dolado I, Nebreda AR. Inhibition of p38 MAPK sensitizes tumour cells to cisplatin-induced apoptosis mediated by reactive oxygen species and JNK. *EMBO Mol Med.* 2013;5(11):1759-74. Epub 2013/10/12. doi: 10.1002/emmm.201302732. PubMed PMID: 24115572; PMCID: PMC3840490.
186. Roche O, Fernández-Aroca DM, Arconada-Luque E, García-Flores N, Mellor LF, Ruiz-Hidalgo MJ, Sánchez-Prieto R. p38 $\beta$  and Cancer: The Beginning of the Road. *Int J Mol Sci.* 2020;21(20). Epub 2020/10/16. doi: 10.3390/ijms21207524. PubMed PMID: 33053909; PMCID: PMC7589630.
187. Sahu V, Nigam L, Agnihotri V, Gupta A, Shekhar S, Subbarao N, Bhaskar S, Dey S. Diagnostic Significance of p38 Isoforms (p38 $\alpha$ , p38 $\beta$ , p38 $\gamma$ , p38 $\delta$ ) in Head and Neck Squamous Cell Carcinoma: Comparative Serum Level Evaluation and Design of Novel Peptide Inhibitor Targeting the Same. *Cancer Res Treat.* 2019;51(1):313-25. Epub 2018/05/12. doi: 10.4143/crt.2018.105. PubMed PMID: 29747487; PMCID: PMC6333999.
188. Kremontsov DN, Thornton TM, Teuscher C, Rincon M. The emerging role of p38 mitogen-activated protein kinase in multiple sclerosis and its models. *Mol Cell Biol.* 2013;33(19):3728-34. Epub 2013/07/31. doi: 10.1128/mcb.00688-13. PubMed PMID: 23897428; PMCID: PMC3811866.
189. Ruano D, Revilla E, Gavilán MP, Vizquete ML, Pintado C, Vitorica J, Castaño A. Role of p38 and inducible nitric oxide synthase in the in vivo dopaminergic cells' degeneration induced by inflammatory processes after lipopolysaccharide injection. *Neuroscience.* 2006;140(4):1157-68. Epub 2006/05/23. doi: 10.1016/j.neuroscience.2006.02.073. PubMed PMID: 16713109.
190. Thapa D, Nichols C, Bassi R, Martin ED, Verma S, Conte MR, De Santis V, De Nicola GF, Marber MS. TAB1-Induced Autoactivation of p38 $\alpha$  Mitogen-Activated Protein Kinase Is Crucially Dependent on Threonine 185. *Mol Cell Biol.* 2018;38(5). Epub 2017/12/13. doi: 10.1128/MCB.00409-17. PubMed PMID: 29229647; PMCID: PMC5809688.
191. Fiedler B, Feil R, Hofmann F, Willenbockel C, Drexler H, Smolenski A, Lohmann SM, Wollert KC. cGMP-dependent Protein Kinase Type I Inhibits TAB1-p38 Mitogen-activated Protein Kinase Apoptosis Signaling in Cardiac Myocytes\*. *Journal of Biological Chemistry.* 2006;281(43):32831-40. doi: <https://doi.org/10.1074/jbc.M603416200>.
192. Mishra S, Guan J, Plovie E, Seldin DC, Connors LH, Merlini G, Falk RH, MacRae CA, Liao R. Human amyloidogenic light chain proteins result in cardiac dysfunction, cell death, and early mortality in zebrafish. *Am J Physiol Heart Circ Physiol.* 2013;305(1):H95-103. Epub

2013/04/30. doi: 10.1152/ajpheart.00186.2013. PubMed PMID: 23624626; PMCID: PMC3727100.

193. Shi J, Guan J, Jiang B, Brenner DA, del Monte F, Ward JE, Connors LH, Sawyer DB, Semigran MJ, Macgillivray TE, Seldin DC, Falk R, Liao R. Amyloidogenic light chains induce cardiomyocyte contractile dysfunction and apoptosis via a non-canonical p38 $\alpha$  MAPK pathway. *Proceedings of the National Academy of Sciences*. 2010;107(9):4188-93. doi: 10.1073/pnas.0912263107.

194. Richardson LS, Taylor RN, Menon R. Reversible EMT and MET mediate amnion remodeling during pregnancy and labor. *Science signaling*. 2020;13(618):eaay1486. doi: 10.1126/scisignal.aay1486. PubMed PMID: 32047115.

195. ten Hove W, Houben LA, Raaijmakers JAM, Bracke M, Koenderman L. Differential regulation of TNF $\alpha$  and GM-CSF induced activation of P38 MAPK in neutrophils and eosinophils. *Molecular Immunology*. 2007;44(9):2492-6. doi: <https://doi.org/10.1016/j.molimm.2006.10.009>.

196. Ohkusu-Tsukada K, Tominaga N, Udono H, Yui K. Regulation of the maintenance of peripheral T-cell anergy by TAB1-mediated p38 alpha activation. *Molecular and cellular biology*. 2004;24(16):6957-66. doi: 10.1128/MCB.24.16.6957-6966.2004. PubMed PMID: 15282297.

197. Lanna A, Henson SM, Escors D, Akbar AN. The kinase p38 activated by the metabolic regulator AMPK and scaffold TAB1 drives the senescence of human T cells. *Nat Immunol*. 2014;15(10):965-72. Epub 2014/08/26. doi: 10.1038/ni.2981. PubMed PMID: 25151490; PMCID: PMC4190666.

198. Angé M, Castanares-Zapatero D, De Poortere J, Dufeys C, Courtoy GE, Bouzin C, Quarck R, Bertrand L, Beauloye C, Horman S.  $\alpha$ 1AMP-Activated Protein Kinase Protects against Lipopolysaccharide-Induced Endothelial Barrier Disruption via Junctional Reinforcement and Activation of the p38 MAPK/HSP27 Pathway. *Int J Mol Sci*. 2020;21(15). Epub 2020/08/08. doi: 10.3390/ijms21155581. PubMed PMID: 32759774; PMCID: PMC7432762.

199. Kim L, Del Rio L, Butcher BA, Mogensen TH, Paludan SR, Flavell RA, Denkers EY. p38 MAPK autophosphorylation drives macrophage IL-12 production during intracellular infection. *J Immunol*. 2005;174(7):4178-84. Epub 2005/03/22. doi: 10.4049/jimmunol.174.7.4178. PubMed PMID: 15778378.

200. Hallé M, Gomez MA, Stuiblé M, Shimizu H, McMaster WR, Olivier M, Tremblay ML. The Leishmania surface protease GP63 cleaves multiple intracellular proteins and actively participates in p38 mitogen-activated protein kinase inactivation. *J Biol Chem*. 2009;284(11):6893-908. Epub 2008/12/10. doi: 10.1074/jbc.M805861200. PubMed PMID: 19064994; PMCID: PMC2652307.

201. Gupta P, Das PK, Ukil A. Antileishmanial effect of 18 $\beta$ -glycyrrhetic acid is mediated by Toll-like receptor-dependent canonical and noncanonical p38 activation. *Antimicrob Agents Chemother*. 2015;59(5):2531-9. Epub 2015/02/17. doi: 10.1128/AAC.03997-14. PubMed PMID: 25691644.

202. Makeeva N, Roomans GM, Welsh N. Role of TAB1 in nitric oxide-induced p38 activation in insulin-producing cells. *International Journal of Biological Sciences*. 2007;3(2):71-6. doi: 10.7150/ijbs.3.71.

203. Makeeva N, Roomans GM, Myers JW, Welsh N. Transforming Growth Factor- $\beta$ -Activated Protein Kinase 1-Binding Protein (TAB)-1 $\alpha$ , But Not TAB1 $\beta$ , Mediates Cytokine-Induced p38 Mitogen-Activated Protein Kinase Phosphorylation and Cell Death in Insulin-Producing Cells. *Endocrinology*. 2008;149(1):302-9. doi: 10.1210/en.2007-0690.
204. Jun JE, Kulhanek KR, Chen H, Chakraborty A, Roose JP. Alternative ZAP70-p38 signals prime a classical p38 pathway through LAT and SOS to support regulatory T cell differentiation. *Science Signaling*. 2019;12(591):eaa0736. doi: 10.1126/scisignal.aao0736.
205. Lu G, Kang YJ, Han J, Herschman HR, Stefani E, Wang Y. TAB-1 modulates intracellular localization of p38 MAP kinase and downstream signaling. *J Biol Chem*. 2006;281(9):6087-95. Epub 2006/01/13. doi: 10.1074/jbc.M507610200. PubMed PMID: 16407200.
206. Shi J, Guan J, Jiang B, Brenner DA, Del Monte F, Ward JE, Connors LH, Sawyer DB, Semigran MJ, Macgillivray TE, Seldin DC, Falk R, Liao R. Amyloidogenic light chains induce cardiomyocyte contractile dysfunction and apoptosis via a non-canonical p38 $\alpha$  MAPK pathway. *Proc Natl Acad Sci U S A*. 2010;107(9):4188-93. Epub 2010/02/13. doi: 10.1073/pnas.0912263107. PubMed PMID: 20150510; PMCID: PMC2840082.
207. Ohkusu-Tsukada K, Toda M, Udono H, Kawakami Y, Takahashi K. Targeted inhibition of IL-10-secreting CD25<sup>+</sup> Treg via p38 MAPK suppression in cancer immunotherapy. *Eur J Immunol*. 2010;40(4):1011-21. Epub 2010/02/04. doi: 10.1002/eji.200939513. PubMed PMID: 20127675.
208. Singh R. Model Predicts That MKP1 and TAB1 Regulate p38 $\alpha$  Nuclear Pulse and Its Basal Activity through Positive and Negative Feedback Loops in Response to IL-1. *PLoS One*. 2016;11(6):e0157572. Epub 2016/06/18. doi: 10.1371/journal.pone.0157572. PubMed PMID: 27314954; PMCID: PMC4912083.
209. Gupta P, Das PK, Ukil A. Antileishmanial effect of 18 $\beta$ -glycyrrhetic acid is mediated by Toll-like receptor-dependent canonical and noncanonical p38 activation. *Antimicrob Agents Chemother*. 2015;59(5):2531-9. Epub 2015/02/19. doi: 10.1128/aac.03997-14. PubMed PMID: 25691644; PMCID: PMC4394830.
210. Wang S, Li M, Yin B, Li H, Xiao B, Lü K, Huang Z, Li S, He J, Li C. Shrimp TAB1 interacts with TAK1 and p38 and activates the host innate immune response to bacterial infection. *Molecular Immunology*. 2017;88:10-9. doi: <https://doi.org/10.1016/j.molimm.2017.05.016>.
211. Makeeva N, Roomans GM, Welsh N. Role of TAB1 in nitric oxide-induced p38 activation in insulin-producing cells. *Int J Biol Sci*. 2006;3(2):71-6. Epub 2007/01/06. doi: 10.7150/ijbs.3.71. PubMed PMID: 17205106; PMCID: PMC1752226 exists.
212. Makeeva N, Roomans GM, Myers JW, Welsh N. Transforming growth factor-beta-activated protein kinase 1-binding protein (TAB)-1 $\alpha$ , but not TAB1 $\beta$ , mediates cytokine-induced p38 mitogen-activated protein kinase phosphorylation and cell death in insulin-producing cells. *Endocrinology*. 2008;149(1):302-9. Epub 2007/10/13. doi: 10.1210/en.2007-0690. PubMed PMID: 17932218.
213. Ohkusu-Tsukada K, Tominaga N, Udono H, Yui K. Regulation of the maintenance of peripheral T-cell anergy by TAB1-mediated p38  $\alpha$  activation. *Mol Cell Biol*. 2004;24(16):6957-66. Epub 2004/07/30. doi: 10.1128/mcb.24.16.6957-6966.2004. PubMed PMID: 15282297; PMCID: PMC479713.

214. Lanna A, Gomes DC, Muller-Durovic B, McDonnell T, Escors D, Gilroy DW, Lee JH, Karin M, Akbar AN. A sestrin-dependent Erk-Jnk-p38 MAPK activation complex inhibits immunity during aging. *Nat Immunol.* 2017;18(3):354-63. Epub 2017/01/24. doi: 10.1038/ni.3665. PubMed PMID: 28114291; PMCID: PMC5321575.
215. Richardson LS, Taylor RN, Menon R. Reversible EMT and MET mediate amnion remodeling during pregnancy and labor. *Sci Signal.* 2020;13(618). Epub 2020/02/13. doi: 10.1126/scisignal.aay1486. PubMed PMID: 32047115; PMCID: PMC7092701.
216. Kang YJ, Seit-Nebi A, Davis RJ, Han J. Multiple activation mechanisms of p38alpha mitogen-activated protein kinase. *J Biol Chem.* 2006;281(36):26225-34. Epub 2006/07/20. doi: 10.1074/jbc.M606800200. PubMed PMID: 16849316.
217. Kim SI, Kwak JH, Zachariah M, He Y, Wang L, Choi ME. TGF- $\beta$ -activated kinase 1 and TAK1-binding protein 1 cooperate to mediate TGF- $\beta$ 1-induced MKK3-p38 MAPK activation and stimulation of type I collagen. *American Journal of Physiology-Renal Physiology.* 2007;292(5):F1471-F8. doi: 10.1152/ajprenal.00485.2006.
218. Ge B, Xiong X, Jing Q, Mosley JL, Filose A, Bian D, Huang S, Han J. TAB1 $\beta$  (Transforming Growth Factor- $\beta$ -activated Protein Kinase 1-binding Protein 1 $\beta$ ), a Novel Splicing Variant of TAB1 That Interacts with p38 $\alpha$  but Not TAK1\*. *Journal of Biological Chemistry.* 2003;278(4):2286-93. doi: <https://doi.org/10.1074/jbc.M210918200>.
219. Xin F, Wu J. Crystal structure of the p38 $\alpha$  MAP kinase in complex with a docking peptide from TAB1. *Sci China Life Sci.* 2013;56(7):653-60. Epub 2013/06/01. doi: 10.1007/s11427-013-4494-0. PubMed PMID: 23722236.
220. Salvador JM, Mittelstadt PR, Belova GI, Fornace AJ, Ashwell JD. The autoimmune suppressor Gadd45 $\alpha$  inhibits the T cell alternative p38 activation pathway. *Nature Immunology.* 2005;6(4):396-402. doi: 10.1038/ni1176.
221. Dorn T, Kuhn U, Bungartz G, Stiller S, Bauer M, Ellwart J, Peters T, Scharffetter-Kochanek K, Semmrich M, Laschinger M, Holzmann B, Klinkert WEF, Straten PT, Køllgaard T, Sixt M, Brakebusch C. RhoH is important for positive thymocyte selection and T-cell receptor signaling. *Blood.* 2007;109(6):2346-55. doi: <https://doi.org/10.1182/blood-2006-04-019034>.
222. Round JL, Humphries LA, Tomassian T, Mittelstadt P, Zhang M, Miceli MC. Scaffold protein Dlg1 coordinates alternative p38 kinase activation, directing T cell receptor signals toward NFAT but not NF-kappaB transcription factors. *Nat Immunol.* 2007;8(2):154-61. Epub 2006/12/26. doi: 10.1038/ni1422. PubMed PMID: 17187070.
223. Liang Y, Yi P, Wang X, Zhang B, Jie Z, Soong L, Sun J. Retinoic Acid Modulates Hyperactive T Cell Responses and Protects Vitamin A-Deficient Mice against Persistent Lymphocytic Choriomeningitis Virus Infection. *The Journal of Immunology.* 2020;204(11):2984-94. doi: 10.4049/jimmunol.1901091.
224. Hirata S, Fukamachi T, Sakano H, Tarora A, Saito H, Kobayashi H. Extracellular acidic environments induce phosphorylation of ZAP-70 in Jurkat T cells. *Immunology Letters.* 2008;115(2):105-9. doi: <https://doi.org/10.1016/j.imlet.2007.10.006>.
225. Giardino Torchia ML, Dutta D, Mittelstadt PR, Guha J, Gaida MM, Fish K, Barr VA, Akpan IO, Samelson LE, Tagad HD, Debnath S, Miller Jenkins LM, Appella E, Ashwell JD. Intensity and duration of TCR signaling is limited by p38 phosphorylation of ZAP-70(T293) and destabilization of the signalosome. *Proc Natl Acad Sci U S A.* 2018;115(9):2174-9. Epub 2018/02/15. doi: 10.1073/pnas.1713301115. PubMed PMID: 29440413; PMCID: PMC5834678.

226. Jun JE, Kulhanek KR, Chen H, Chakraborty A, Roose JP. Alternative ZAP70-p38 signals prime a classical p38 pathway through LAT and SOS to support regulatory T cell differentiation. *Sci Signal*. 2019;12(591). Epub 2019/07/25. doi: 10.1126/scisignal.aao0736. PubMed PMID: 31337738; PMCID: PMC7340343.
227. Liu J, Guo K, Hu L, Luo T, Ma Y, Zhang Y, Lai W, Guo Z. ZAP70 deficiency promotes reverse cholesterol transport through MAPK/ERK pathway in Jurkat cell. *Molecular Immunology*. 2019;107:21-8. doi: <https://doi.org/10.1016/j.molimm.2019.01.001>.
228. Joffre C, Barrow R, Ménard L, Calleja V, Hart IR, Kermorgant S. A direct role for Met endocytosis in tumorigenesis. *Nature Cell Biology*. 2011;13(7):827-37. doi: 10.1038/ncb2257.
229. Gormal RS, Martinez-Marmol R, Brooks AJ, Meunier FA. Location, location, location: Protein kinase nanoclustering for optimised signalling output. *eLife*. 2024;13:e93902. doi: 10.7554/eLife.93902.
230. Lohse MJ, Bock A, Zaccolo M. G Protein-Coupled Receptor Signaling: New Insights Define Cellular Nanodomains. *Annu Rev Pharmacol Toxicol*. 2024;64:387-415. Epub 20230908. doi: 10.1146/annurev-pharmtox-040623-115054. PubMed PMID: 37683278.
231. Manning G, Whyte DB, Martinez R, Hunter T, Sudarsanam S. The protein kinase complement of the human genome. *Science*. 2002;298(5600):1912-34. doi: 10.1126/science.1075762. PubMed PMID: 12471243.
232. Chen X, Niu W, Fan X, Yang H, Zhao C, Fan J, Yao X, Fang Z. Oct4A palmitoylation modulates tumorigenicity and stemness in human glioblastoma cells. *Neuro Oncol*. 2023;25(1):82-96. doi: 10.1093/neuonc/noac157. PubMed PMID: 35727735; PMCID: PMC9825352.
233. Ko PJ, Dixon SJ. Protein palmitoylation and cancer. *EMBO Rep*. 2018;19(10). Epub 20180919. doi: 10.15252/embr.201846666. PubMed PMID: 30232163; PMCID: PMC6172454.
234. Qu M, Zhou X, Wang X, Li H. Lipid-induced S-palmitoylation as a Vital Regulator of Cell Signaling and Disease Development. *Int J Biol Sci*. 2021;17(15):4223-37. Epub 20211011. doi: 10.7150/ijbs.64046. PubMed PMID: 34803494; PMCID: PMC8579454.
235. Sun Y, Zhang H, Meng J, Guo F, Ren D, Wu H, Jin X. S-palmitoylation of PCSK9 induces sorafenib resistance in liver cancer by activating the PI3K/AKT pathway. *Cell Rep*. 2022;40(7):111194. doi: 10.1016/j.celrep.2022.111194. PubMed PMID: 35977495.
236. Zhou B, Hao Q, Liang Y, Kong E. Protein palmitoylation in cancer: molecular functions and therapeutic potential. *Mol Oncol*. 2023;17(1):3-26. Epub 20220910. doi: 10.1002/1878-0261.13308. PubMed PMID: 36018061; PMCID: PMC9812842.
237. Hu Q, Zhang H, Gutiérrez Cortés N, Wu D, Wang P, Zhang J, Mattison JA, Smith E, Bettcher LF, Wang M, Lakatta EG, Sheu SS, Wang W. Increased Drp1 Acetylation by Lipid Overload Induces Cardiomyocyte Death and Heart Dysfunction. *Circ Res*. 2020;126(4):456-70. Epub 20200103. doi: 10.1161/circresaha.119.315252. PubMed PMID: 31896304; PMCID: PMC7035202.
238. Li D, Yang Y, Wang S, He X, Liu M, Bai B, Tian C, Sun R, Yu T, Chu X. Role of acetylation in doxorubicin-induced cardiotoxicity. *Redox Biol*. 2021;46:102089. Epub 20210731. doi: 10.1016/j.redox.2021.102089. PubMed PMID: 34364220; PMCID: PMC8350499.
239. Liu W, Yuan Q, Cao S, Wang G, Liu X, Xia Y, Bian Y, Xu F, Chen Y. Review: Acetylation mechanisms and targeted therapies in cardiac fibrosis. *Pharmacol Res*. 2023;193:106815. Epub 20230606. doi: 10.1016/j.phrs.2023.106815. PubMed PMID: 37290541.

240. Su H, Cantrell AC, Chen JX, Gu W, Zeng H. SIRT3 Deficiency Enhances Ferroptosis and Promotes Cardiac Fibrosis via p53 Acetylation. *Cells*. 2023;12(10). Epub 20230519. doi: 10.3390/cells12101428. PubMed PMID: 37408261; PMCID: PMC10217433.
241. Tomczyk MM, Cheung KG, Xiang B, Tamanna N, Fonseca Teixeira AL, Agarwal P, Kereliuk SM, Spicer V, Lin L, Treberg J, Tong Q, Dolinsky VW. Mitochondrial Sirtuin-3 (SIRT3) Prevents Doxorubicin-Induced Dilated Cardiomyopathy by Modulating Protein Acetylation and Oxidative Stress. *Circ Heart Fail*. 2022;15(5):e008547. Epub 20220414. doi: 10.1161/circheartfailure.121.008547. PubMed PMID: 35418250; PMCID: PMC9117478.
242. Cai Y, Yang E, Yao X, Zhang X, Wang Q, Wang Y, Liu J, Fan W, Yi K, Kang C, Wu J. FUNDC1-dependent mitophagy induced by tPA protects neurons against cerebral ischemia-reperfusion injury. *Redox Biol*. 2021;38:101792. Epub 20201107. doi: 10.1016/j.redox.2020.101792. PubMed PMID: 33212415; PMCID: PMC7679257.
243. Cunnane SC, Trushina E, Morland C, Prigione A, Casadesus G, Andrews ZB, Beal MF, Bergersen LH, Brinton RD, de la Monte S, Eckert A, Harvey J, Jeggo R, Jhamandas JH, Kann O, la Cour CM, Martin WF, Mithieux G, Moreira PI, Murphy MP, Nave KA, Nuriel T, Oliet SHR, Saudou F, Mattson MP, Swerdlow RH, Millan MJ. Brain energy rescue: an emerging therapeutic concept for neurodegenerative disorders of ageing. *Nat Rev Drug Discov*. 2020;19(9):609-33. Epub 20200724. doi: 10.1038/s41573-020-0072-x. PubMed PMID: 32709961; PMCID: PMC7948516.
244. Głombik K, Detka J, Budziszewska B. Hormonal Regulation of Oxidative Phosphorylation in the Brain in Health and Disease. *Cells*. 2021;10(11). Epub 20211028. doi: 10.3390/cells10112937. PubMed PMID: 34831160; PMCID: PMC8616269.
245. Jennings D, Huntwork-Rodriguez S, Henry AG, Sasaki JC, Meisner R, Diaz D, Solanoy H, Wang X, Negrou E, Bondar VV, Ghosh R, Maloney MT, Propson NE, Zhu Y, Maciucia RD, Harris L, Kay A, LeWitt P, King TA, Kern D, Ellenbogen A, Goodman I, Siderowf A, Aldred J, Omidvar O, Masoud ST, Davis SS, Arguello A, Estrada AA, de Vicente J, Sweeney ZK, Astarita G, Borin MT, Wong BK, Wong H, Nguyen H, Scarce-Levie K, Ho C, Troyer MD. Preclinical and clinical evaluation of the LRRK2 inhibitor DNL201 for Parkinson's disease. *Sci Transl Med*. 2022;14(648):eabj2658. Epub 20220608. doi: 10.1126/scitranslmed.abj2658. PubMed PMID: 35675433.
246. Thijssen EH, La Joie R, Strom A, Fonseca C, Iaccarino L, Wolf A, Spina S, Allen IE, Cobigo Y, Heuer H, VandeVrede L, Proctor NK, Lago AL, Baker S, Sivasankaran R, Kieloch A, Kinhikar A, Yu L, Valentin MA, Jeromin A, Zetterberg H, Hansson O, Mattsson-Carlgrén N, Graham D, Blennow K, Kramer JH, Grinberg LT, Seeley WW, Rosen H, Boeve BF, Miller BL, Teunissen CE, Rabinovici GD, Rojas JC, Dage JL, Boxer AL. Plasma phosphorylated tau 217 and phosphorylated tau 181 as biomarkers in Alzheimer's disease and frontotemporal lobar degeneration: a retrospective diagnostic performance study. *Lancet Neurol*. 2021;20(9):739-52. doi: 10.1016/s1474-4422(21)00214-3. PubMed PMID: 34418401; PMCID: PMC8711249.
247. Chen X, He Z, Fu M, Wang Y, Wu H, Li X, Cao H, Zheng SJ. The E3 Ubiquitin Ligase Siah-1 Suppresses Avian Reovirus Infection by Targeting p10 for Degradation. *J Virol*. 2018;92(6). Epub 20180226. doi: 10.1128/jvi.02101-17. PubMed PMID: 29321312; PMCID: PMC5827385.
248. Deschamps T, Waisner H, Dogrammatzis C, Roy A, Chacko S, Perera C, Prisinzano TE, Kalamvoki M. Discovery of Small-Molecule Inhibitors Targeting the E3 Ubiquitin Ligase Activity of the Herpes Simplex Virus 1 ICP0 Protein Using an In Vitro High-Throughput

- Screening Assay. *J Virol.* 2019;93(13). Epub 20190614. doi: 10.1128/jvi.00619-19. PubMed PMID: 30996104; PMCID: PMC6580980.
249. Fiil BK, Gyrð-Hansen M. The Met1-linked ubiquitin machinery in inflammation and infection. *Cell Death Differ.* 2021;28(2):557-69. Epub 20210120. doi: 10.1038/s41418-020-00702-x. PubMed PMID: 33473179; PMCID: PMC7816137.
250. Hou J, Han L, Zhao Z, Liu H, Zhang L, Ma C, Yi F, Liu B, Zheng Y, Gao C. USP18 positively regulates innate antiviral immunity by promoting K63-linked polyubiquitination of MAVS. *Nat Commun.* 2021;12(1):2970. Epub 20210520. doi: 10.1038/s41467-021-23219-4. PubMed PMID: 34016972; PMCID: PMC8137702.
251. Smits VAJ, Cabrera E, Freire R, Gillespie DA. Claspin - checkpoint adaptor and DNA replication factor. *Febs j.* 2019;286(3):441-55. Epub 20180629. doi: 10.1111/febs.14594. PubMed PMID: 29931808.
252. Cohen P. The origins of protein phosphorylation. *Nat Cell Biol.* 2002;4(5):E127-30. doi: 10.1038/ncb0502-e127. PubMed PMID: 11988757.
253. Manning G, Plowman GD, Hunter T, Sudarsanam S. Evolution of protein kinase signaling from yeast to man. *Trends Biochem Sci.* 2002;27(10):514-20. doi: 10.1016/s0968-0004(02)02179-5. PubMed PMID: 12368087.
254. Fuhs SR, Hunter T. pHisphorylation: the emergence of histidine phosphorylation as a reversible regulatory modification. *Curr Opin Cell Biol.* 2017;45:8-16. Epub 20170125. doi: 10.1016/j.ceb.2016.12.010. PubMed PMID: 28129587; PMCID: PMC5482761.
255. Burton JC, Antoniadou W, Okalova J, Roos MM, Grimsey NJ. Atypical p38 Signaling, Activation, and Implications for Disease. *Int J Mol Sci.* 2021;22(8). Epub 2021/05/01. doi: 10.3390/ijms22084183. PubMed PMID: 33920735; PMCID: PMC8073329.
256. Zhang J, Yang PL, Gray NS. Targeting cancer with small molecule kinase inhibitors. *Nat Rev Cancer.* 2009;9(1):28-39. doi: 10.1038/nrc2559. PubMed PMID: 19104514.
257. Klaeger S, Heinzlmeir S, Wilhelm M, Polzer H, Vick B, Koenig PA, Reinecke M, Ruprecht B, Petzoldt S, Meng C, Zecha J, Reiter K, Qiao H, Helm D, Koch H, Schoof M, Canevari G, Casale E, Depaolini SR, Feuchtinger A, Wu Z, Schmidt T, Rueckert L, Becker W, Huenges J, Garz AK, Gohlke BO, Zolg DP, Kayser G, Vooder T, Preissner R, Hahne H, Tönisson N, Kramer K, Götze K, Bassermann F, Schlegl J, Ehrlich HC, Aiche S, Walch A, Greif PA, Schneider S, Felder ER, Ruland J, Médard G, Jeremias I, Spiekermann K, Kuster B. The target landscape of clinical kinase drugs. *Science.* 2017;358(6367). doi: 10.1126/science.aan4368. PubMed PMID: 29191878; PMCID: PMC6542668.
258. Reinhardt R, Leonard TA. A critical evaluation of protein kinase regulation by activation loop autophosphorylation. *Elife.* 2023;12. Epub 20230720. doi: 10.7554/eLife.88210. PubMed PMID: 37470698; PMCID: PMC10359097.
259. Noble ME, Endicott JA, Johnson LN. Protein kinase inhibitors: insights into drug design from structure. *Science.* 2004;303(5665):1800-5. doi: 10.1126/science.1095920. PubMed PMID: 15031492.
260. Bellon S, Fitzgibbon MJ, Fox T, Hsiao HM, Wilson KP. The structure of phosphorylated p38gamma is monomeric and reveals a conserved activation-loop conformation. *Structure.* 1999;7(9):1057-65. doi: 10.1016/s0969-2126(99)80173-7. PubMed PMID: 10508788.
261. Zhang YY, Wu JW, Wang ZX. Mitogen-activated protein kinase (MAPK) phosphatase 3-mediated cross-talk between MAPKs ERK2 and p38alpha. *J Biol Chem.* 2011;286(18):16150-

62. Epub 20110316. doi: 10.1074/jbc.M110.203786. PubMed PMID: 21454500; PMCID: PMC3091224.
262. Kumar GS, Clarkson MW, Kunze MBA, Granata D, Wand AJ, Lindorff-Larsen K, Page R, Peti W. Dynamic activation and regulation of the mitogen-activated protein kinase p38. *Proceedings of the National Academy of Sciences*. 2018;115(18):4655-60. doi: doi:10.1073/pnas.1721441115.
263. Shi G, Song C, Torres Robles J, Salichos L, Lou HJ, Lam TT, Gerstein M, Turk BE. Proteome-wide screening for mitogen-activated protein kinase docking motifs and interactors. *Science Signaling*. 2023;16(767):eabm5518. doi: doi:10.1126/scisignal.abm5518.
264. Torres Robles J, Lou HJ, Shi G, Pan PL, Turk BE. Linear motif specificity in signaling through p38 $\alpha$  and ERK2 mitogen-activated protein kinases. *Proc Natl Acad Sci U S A*. 2023;120(48):e2316599120. Epub 20231121. doi: 10.1073/pnas.2316599120. PubMed PMID: 37988460; PMCID: PMC10691213.
265. Levina A, Fleming KD, Burke JE, Leonard TA. Activation of the essential kinase PDK1 by phosphoinositide-driven trans-autophosphorylation. *Nat Commun*. 2022;13(1):1874. Epub 20220406. doi: 10.1038/s41467-022-29368-4. PubMed PMID: 35387990; PMCID: PMC8986801.
266. Bayliss R, Sardon T, Vernos I, Conti E. Structural basis of Aurora-A activation by TPX2 at the mitotic spindle. *Mol Cell*. 2003;12(4):851-62. doi: 10.1016/s1097-2765(03)00392-7. PubMed PMID: 14580337.
267. Eyers PA, Erikson E, Chen LG, Maller JL. A novel mechanism for activation of the protein kinase Aurora A. *Curr Biol*. 2003;13(8):691-7. doi: 10.1016/s0960-9822(03)00166-0. PubMed PMID: 12699628.
268. Cheng H, Addona T, Keshishian H, Dahlstrand E, Lu C, Dorsch M, Li Z, Wang A, Ocain TD, Li P, Parsons TF, Jaffee B, Xu Y. Regulation of IRAK-4 kinase activity via autophosphorylation within its activation loop. *Biochemical and Biophysical Research Communications*. 2007;352(3):609-16. doi: <https://doi.org/10.1016/j.bbrc.2006.11.068>.
269. Ferrao R, Zhou H, Shan Y, Liu Q, Li Q, Shaw DE, Li X, Wu H. IRAK4 dimerization and trans-autophosphorylation are induced by Myddosome assembly. *Mol Cell*. 2014;55(6):891-903. Epub 20140904. doi: 10.1016/j.molcel.2014.08.006. PubMed PMID: 25201411; PMCID: PMC4169746.
270. Cobbaut M, Derua R, Parker PJ, Waelkens E, Janssens V, Van Lint J. Protein kinase D displays intrinsic Tyr autophosphorylation activity: insights into mechanism and regulation. *FEBS Lett*. 2018;592(14):2432-43. Epub 20180723. doi: 10.1002/1873-3468.13171. PubMed PMID: 29933512; PMCID: PMC6099456.
271. Reinhardt R, Hirzel K, Link G, Eisler SA, Hägele T, Parson MAH, Burke JE, Hausser A, Leonard TA. PKD autoinhibition in *trans* regulates activation loop autophosphorylation in *cis*. *Proceedings of the National Academy of Sciences*. 2023;120(7):e2212909120. doi: doi:10.1073/pnas.2212909120.
272. Gong X, Ming X, Deng P, Jiang Y. Mechanisms regulating the nuclear translocation of p38 MAP kinase. *Journal of Cellular Biochemistry*. 2010;110(6):1420-9. doi: <https://doi.org/10.1002/jcb.22675>.
273. Sacco F, Perfetto L, Castagnoli L, Cesareni G. The human phosphatase interactome: An intricate family portrait. *FEBS Lett*. 2012;586(17):2732-9. Epub 20120521. doi: 10.1016/j.febslet.2012.05.008. PubMed PMID: 22626554; PMCID: PMC3437441.

274. Staples CJ, Owens DM, Maier JV, Cato AC, Keyse SM. Cross-talk between the p38alpha and JNK MAPK pathways mediated by MAP kinase phosphatase-1 determines cellular sensitivity to UV radiation. *J Biol Chem*. 2010;285(34):25928-40. Epub 20100611. doi: 10.1074/jbc.M110.117911. PubMed PMID: 20547488; PMCID: PMC2923983.
275. Miura H, Kondo Y, Matsuda M, Aoki K. Cell-to-Cell Heterogeneity in p38-Mediated Cross-Inhibition of JNK Causes Stochastic Cell Death. *Cell Rep*. 2018;24(10):2658-68. doi: 10.1016/j.celrep.2018.08.020. PubMed PMID: 30184500.
276. Ambrosino C, Mace G, Galban S, Fritsch C, Vintersten K, Black E, Gorospe M, Nebreda AR. Negative feedback regulation of MKK6 mRNA stability by p38alpha mitogen-activated protein kinase. *Mol Cell Biol*. 2003;23(1):370-81. doi: 10.1128/mcb.23.1.370-381.2003. PubMed PMID: 12482988; PMCID: PMC140674.
277. Miller CJ, Turk BE. Homing in: Mechanisms of Substrate Targeting by Protein Kinases. *Trends in Biochemical Sciences*. 2018;43(5):380-94. doi: <https://doi.org/10.1016/j.tibs.2018.02.009>.
278. Mugabo Y, Lim GE. Scaffold Proteins: From Coordinating Signaling Pathways to Metabolic Regulation. *Endocrinology*. 2018;159(11):3615-30. doi: 10.1210/en.2018-00705. PubMed PMID: 30204866; PMCID: PMC6180900.
279. Pearce LR, Komander D, Alessi DR. The nuts and bolts of AGC protein kinases. *Nature Reviews Molecular Cell Biology*. 2010;11(1):9-22. doi: 10.1038/nrm2822.
280. Taylor SS, Yang J, Wu J, Haste NM, Radzio-Andzelm E, Anand G. PKA: a portrait of protein kinase dynamics. *Biochimica et Biophysica Acta (BBA) - Proteins and Proteomics*. 2004;1697(1):259-69. doi: <https://doi.org/10.1016/j.bbapap.2003.11.029>.
281. Brunton LL, Hayes JS, Mayer SE. Functional compartmentation of cyclic AMP and protein kinase in heart. *Adv Cyclic Nucleotide Res*. 1981;14:391-7. PubMed PMID: 6269390.
282. Buxton IL, Brunton LL. Compartments of cyclic AMP and protein kinase in mammalian cardiomyocytes. *J Biol Chem*. 1983;258(17):10233-9. PubMed PMID: 6309796.
283. Steinberg SF, Brunton LL. Compartmentation of G protein-coupled signaling pathways in cardiac myocytes. *Annu Rev Pharmacol Toxicol*. 2001;41:751-73. doi: 10.1146/annurev.pharmtox.41.1.751. PubMed PMID: 11264475.
284. Lim CJ, Kain KH, Tkachenko E, Goldfinger LE, Gutierrez E, Allen MD, Groisman A, Zhang J, Ginsberg MH. Integrin-mediated protein kinase A activation at the leading edge of migrating cells. *Mol Biol Cell*. 2008;19(11):4930-41. Epub 20080910. doi: 10.1091/mbc.e08-06-0564. PubMed PMID: 18784251; PMCID: PMC2575143.
285. Bacsikai BJ, Hochner B, Mahaut-Smith M, Adams SR, Kaang BK, Kandel ER, Tsien RY. Spatially resolved dynamics of cAMP and protein kinase A subunits in *Aplysia* sensory neurons. *Science*. 1993;260(5105):222-6. doi: 10.1126/science.7682336. PubMed PMID: 7682336.
286. Gorshkov K, Mehta S, Ramamurthy S, Ronnett GV, Zhou FQ, Zhang J. AKAP-mediated feedback control of cAMP gradients in developing hippocampal neurons. *Nat Chem Biol*. 2017;13(4):425-31. Epub 20170213. doi: 10.1038/nchembio.2298. PubMed PMID: 28192412; PMCID: PMC5362298.
287. Nikolaev VO, Bünemann M, Schmitteckert E, Lohse MJ, Engelhardt S. Cyclic AMP imaging in adult cardiac myocytes reveals far-reaching beta1-adrenergic but locally confined beta2-adrenergic receptor-mediated signaling. *Circ Res*. 2006;99(10):1084-91. Epub 20061012. doi: 10.1161/01.RES.0000250046.69918.d5. PubMed PMID: 17038640.

288. Willoughby D, Cooper DM. Organization and Ca<sup>2+</sup> regulation of adenylyl cyclases in cAMP microdomains. *Physiol Rev.* 2007;87(3):965-1010. doi: 10.1152/physrev.00049.2006. PubMed PMID: 17615394.
289. Terrin A, Monterisi S, Stangherlin A, Zoccarato A, Koschinski A, Surdo NC, Mongillo M, Sawa A, Jordanides NE, Mountford JC, Zaccolo M. PKA and PDE4D3 anchoring to AKAP9 provides distinct regulation of cAMP signals at the centrosome. *J Cell Biol.* 2012;198(4):607-21. doi: 10.1083/jcb.201201059. PubMed PMID: 22908311; PMCID: PMC3514031.
290. Zaccolo M, Pozzan T. Discrete microdomains with high concentration of cAMP in stimulated rat neonatal cardiac myocytes. *Science.* 2002;295(5560):1711-5. doi: 10.1126/science.1069982. PubMed PMID: 11872839.
291. Tsvetanova NG, Trester-Zedlitz M, Newton BW, Peng GE, Johnson JR, Jimenez-Morales D, Kurland AP, Krogan NJ, von Zastrow M. Endosomal cAMP production broadly impacts the cellular phosphoproteome. *J Biol Chem.* 2021;297(1):100907. Epub 20210622. doi: 10.1016/j.jbc.2021.100907. PubMed PMID: 34166681; PMCID: PMC8294583.
292. Liu Y, Chen J, Fontes SK, Bautista EN, Cheng Z. Physiological and pathological roles of protein kinase A in the heart. *Cardiovasc Res.* 2022;118(2):386-98. doi: 10.1093/cvr/cvab008. PubMed PMID: 33483740; PMCID: PMC8803072.
293. Zaccolo M. Phosphodiesterases and compartmentalized cAMP signalling in the heart. *Eur J Cell Biol.* 2006;85(7):693-7. Epub 20060207. doi: 10.1016/j.ejcb.2006.01.002. PubMed PMID: 16466668.
294. Omar MH, Scott JD. AKAP Signaling Islands: Venues for Precision Pharmacology. *Trends Pharmacol Sci.* 2020;41(12):933-46. Epub 20201017. doi: 10.1016/j.tips.2020.09.007. PubMed PMID: 33082006; PMCID: PMC7890593.
295. Wong W, Scott JD. AKAP signalling complexes: focal points in space and time. *Nature Reviews Molecular Cell Biology.* 2004;5(12):959-70. doi: 10.1038/nrm1527.
296. Ma Y, Taylor SS. A molecular switch for targeting between endoplasmic reticulum (ER) and mitochondria: conversion of a mitochondria-targeting element into an ER-targeting signal in DAKAP1. *J Biol Chem.* 2008;283(17):11743-51. Epub 20080219. doi: 10.1074/jbc.M710494200. PubMed PMID: 18287098; PMCID: PMC2431083.
297. He Z, Xie L, Liu J, Wei X, Zhang W, Mei Z. Novel insight into the role of A-kinase anchoring proteins (AKAPs) in ischemic stroke and therapeutic potentials. *Biomedicine & Pharmacotherapy.* 2024;175:116715. doi: <https://doi.org/10.1016/j.biopha.2024.116715>.
298. Kritzer MD, Li J, Dodge-Kafka K, Kapiloff MS. AKAPs: the architectural underpinnings of local cAMP signaling. *J Mol Cell Cardiol.* 2012;52(2):351-8. Epub 20110511. doi: 10.1016/j.yjmcc.2011.05.002. PubMed PMID: 21600214; PMCID: PMC3168680.
299. Sorriento D, Fusco A, Ciccarelli M, Rungi A, Anastasio A, Carillo A, Dorn GW, Trimarco B, Iaccarino G. Mitochondrial G protein coupled receptor kinase 2 regulates proinflammatory responses in macrophages. *FEBS Letters.* 2013;587(21):3487-94. doi: <https://doi.org/10.1016/j.febslet.2013.09.002>.
300. Newlon MG, Roy M, Morikis D, Hausken ZE, Coghlan V, Scott JD, Jennings PA. The molecular basis for protein kinase A anchoring revealed by solution NMR. *Nat Struct Biol.* 1999;6(3):222-7. doi: 10.1038/6663. PubMed PMID: 10074940.
301. Gold MG, Lygren B, Dokurno P, Hoshi N, McConnachie G, Taskén K, Carlson CR, Scott JD, Barford D. Molecular basis of AKAP specificity for PKA regulatory subunits. *Mol Cell.* 2006;24(3):383-95. doi: 10.1016/j.molcel.2006.09.006. PubMed PMID: 17081989.

302. Götz F, Roske Y, Schulz Maike S, Autenrieth K, Bertinetti D, Faelber K, Zühlke K, Kreuchwig A, Kennedy EJ, Krause G, Daumke O, Herberg Friedrich W, Heinemann U, Klussmann E. AKAP18:PKA-RII $\alpha$  structure reveals crucial anchor points for recognition of regulatory subunits of PKA. *Biochemical Journal*. 2016;473(13):1881-94. doi: 10.1042/bcj20160242.
303. Alto NM, Soderling SH, Hoshi N, Langeberg LK, Fayos R, Jennings PA, Scott JD. Bioinformatic design of A-kinase anchoring protein-in silico: a potent and selective peptide antagonist of type II protein kinase A anchoring. *Proc Natl Acad Sci U S A*. 2003;100(8):4445-50. Epub 20030402. doi: 10.1073/pnas.0330734100. PubMed PMID: 12672969; PMCID: PMC153575.
304. Chen X, Crosby KC, Feng A, Purkey AM, Aronova MA, Winters CA, Crocker VT, Leapman RD, Reese TS, Dell'Acqua ML. Palmitoylation of A-kinase anchoring protein 79/150 modulates its nanoscale organization, trafficking, and mobility in postsynaptic spines. *Front Synaptic Neurosci*. 2022;14:1004154. Epub 20220915. doi: 10.3389/fnsyn.2022.1004154. PubMed PMID: 36186623; PMCID: PMC9521714.
305. Purkey AM, Woolfrey KM, Crosby KC, Stich DG, Chick WS, Aoto J, Dell'Acqua ML. AKAP150 Palmitoylation Regulates Synaptic Incorporation of Ca(2+)-Permeable AMPA Receptors to Control LTP. *Cell Rep*. 2018;25(4):974-87.e4. doi: 10.1016/j.celrep.2018.09.085. PubMed PMID: 30355502; PMCID: PMC6263960.
306. Lin X, Tomblor E, Nelson PJ, Ross M, Gelman IH. A novel src-and ras-suppressed protein kinase C substrate associated with cytoskeletal architecture. *Journal of Biological Chemistry*. 1996;271(45):28430-8.
307. Fraser ID, Tavalin SJ, Lester LB, Langeberg LK, Westphal AM, Dean RA, Marrion NV, Scott JD. A novel lipid-anchored A-kinase Anchoring Protein facilitates cAMP-responsive membrane events. *The EMBO Journal*. 1998.
308. Gillingham AK, Munro S. The PACT domain, a conserved centrosomal targeting motif in the coiled-coil proteins AKAP450 and pericentrin. *EMBO reports*. 2000;1(6):524-9-9. doi: <https://doi.org/10.1093/embo-reports/kvd105>.
309. Tonucci FM, Hidalgo F, Ferretti A, Almada E, Favre C, Goldenring JR, Kaverina I, Kierbel A, Larocca MC. Centrosomal AKAP350 and CIP4 act in concert to define the polarized localization of the centrosome and Golgi in migratory cells. *J Cell Sci*. 2015;128(17):3277-89. Epub 20150724. doi: 10.1242/jcs.170878. PubMed PMID: 26208639; PMCID: PMC4582191.
310. Hubbard SR, Miller WT. Receptor tyrosine kinases: mechanisms of activation and signaling. *Curr Opin Cell Biol*. 2007;19(2):117-23. Epub 20070216. doi: 10.1016/j.ceb.2007.02.010. PubMed PMID: 17306972; PMCID: PMC2536775.
311. Amsler K, Kuwada SK. Membrane receptor location defines receptor interaction with signaling proteins in a polarized epithelium. *American Journal of Physiology-Cell Physiology*. 1999;276(1):C91-C101. doi: 10.1152/ajpcell.1999.276.1.C91. PubMed PMID: 9886924.
312. Koetemann A, Wollscheid B. Apicobasal Surfaceome Architecture Encodes for Polarized Epithelial Functionality and Depends on Tumor Suppressor PTEN. *Int J Mol Sci*. 2022;23(24). Epub 20221219. doi: 10.3390/ijms232416193. PubMed PMID: 36555834; PMCID: PMC9788433.
313. Thapa N, Chen M, Horn HT, Choi S, Wen T, Anderson RA. Phosphatidylinositol 3-kinase signalling is spatially organized at endosomal compartments by microtubule-associated protein 4. *Nature Cell Biology*. 2020;22(11):1357-70. doi: 10.1038/s41556-020-00596-4.

314. Zhang M, Jang H, Nussinov R. PI3K Driver Mutations: A Biophysical Membrane-Centric Perspective. *Cancer Res.* 2021;81(2):237-47. Epub 20201012. doi: 10.1158/0008-5472.Can-20-0911. PubMed PMID: 33046444; PMCID: PMC7855922.
315. Bilanges B, Posor Y, Vanhaesebroeck B. PI3K isoforms in cell signalling and vesicle trafficking. *Nature Reviews Molecular Cell Biology.* 2019;20(9):515-34. doi: 10.1038/s41580-019-0129-z.
316. Kotzampasi DM, Premeti K, Papafotika A, Syropoulou V, Christoforidis S, Cournia Z, Leondaritis G. The orchestrated signaling by PI3K $\alpha$  and PTEN at the membrane interface. *Computational and Structural Biotechnology Journal.* 2022;20:5607-21. doi: <https://doi.org/10.1016/j.csbj.2022.10.007>.
317. Wills RC, Hammond GRV. PI(4,5)P<sub>2</sub>: signaling the plasma membrane. *Biochem J.* 2022;479(21):2311-25. doi: 10.1042/bcj20220445. PubMed PMID: 36367756; PMCID: PMC9704524.
318. Posor Y, Jang W, Haucke V. Phosphoinositides as membrane organizers. *Nature Reviews Molecular Cell Biology.* 2022;23(12):797-816. doi: 10.1038/s41580-022-00490-x.
319. Cockcroft S. The expanding roles of PI4P and PI(4,5)P<sub>2</sub> at the plasma membrane: Role of phosphatidylinositol transfer proteins. *Biochimica et Biophysica Acta (BBA) - Molecular and Cell Biology of Lipids.* 2024;1869(2):159394. doi: <https://doi.org/10.1016/j.bbalip.2023.159394>.
320. Rodgers SJ, Jones EI, Arumugam S, Hamila SA, Danne J, Gurung R, Eramo MJ, Nanayakkara R, Ramm G, McGrath MJ, Mitchell CA. Endosome maturation links PI3K signaling to lysosome repopulation during basal autophagy. *The EMBO Journal.* 2022;41(19):e110398. doi: <https://doi.org/10.15252/embj.2021110398>.
321. Oh B-C. Phosphoinositides and intracellular calcium signaling: novel insights into phosphoinositides and calcium coupling as negative regulators of cellular signaling. *Experimental & Molecular Medicine.* 2023;55(8):1702-12. doi: 10.1038/s12276-023-01067-0.
322. Mineo C, Ying YS, Chapline C, Jaken S, Anderson RG. Targeting of protein kinase Calpha to caveolae. *J Cell Biol.* 1998;141(3):601-10. doi: 10.1083/jcb.141.3.601. PubMed PMID: 9566962; PMCID: PMC2132740.
323. Newton AC. Protein kinase C: perfectly balanced. *Crit Rev Biochem Mol Biol.* 2018;53(2):208-30. doi: 10.1080/10409238.2018.1442408. PubMed PMID: 29513138; PMCID: PMC5901981.
324. Li C, Quintana Perez Y, Lamaze C, Blouin CM. Lipid nanodomains and receptor signaling: From actin-based organization to membrane mechanics. *Curr Opin Cell Biol.* 2024;86:102308. Epub 20240101. doi: 10.1016/j.ceb.2023.102308. PubMed PMID: 38168583.
325. Ouweneel AB, Thomas MJ, Sorci-Thomas MG. The ins and outs of lipid rafts: functions in intracellular cholesterol homeostasis, microparticles, and cell membranes: Thematic Review Series: Biology of Lipid Rafts. *J Lipid Res.* 2020;61(5):676-86. Epub 20201107. doi: 10.1194/jlr.TR119000383. PubMed PMID: 33715815; PMCID: PMC7193959.
326. Norris A, Grant BD. Endosomal microdomains: Formation and function. *Curr Opin Cell Biol.* 2020;65:86-95. Epub 20200401. doi: 10.1016/j.ceb.2020.02.018. PubMed PMID: 32247230; PMCID: PMC7529669.
327. Jang SW, Liu X, Fu H, Rees H, Yepes M, Levey A, Ye K. Interaction of Akt-phosphorylated SRPK2 with 14-3-3 mediates cell cycle and cell death in neurons. *J Biol Chem.* 2009;284(36):24512-25. Epub 20090710. doi: 10.1074/jbc.M109.026237. PubMed PMID: 19592491; PMCID: PMC2782043.

328. Zhou Z, Qiu J, Liu W, Zhou Y, Plocinik RM, Li H, Hu Q, Ghosh G, Adams JA, Rosenfeld MG, Fu XD. The Akt-SRPK-SR axis constitutes a major pathway in transducing EGF signaling to regulate alternative splicing in the nucleus. *Mol Cell*. 2012;47(3):422-33. Epub 20120621. doi: 10.1016/j.molcel.2012.05.014. PubMed PMID: 22727668; PMCID: PMC3418396.
329. Zhong XY, Ding JH, Adams JA, Ghosh G, Fu XD. Regulation of SR protein phosphorylation and alternative splicing by modulating kinetic interactions of SRPK1 with molecular chaperones. *Genes Dev*. 2009;23(4):482-95. doi: 10.1101/gad.1752109. PubMed PMID: 19240134; PMCID: PMC2648651.
330. Lu Y, Xu W, Ji J, Feng D, Sourbier C, Yang Y, Qu J, Zeng Z, Wang C, Chang X, Chen Y, Mishra A, Xu M, Lee MJ, Lee S, Trepel J, Linehan WM, Wang X, Yang Y, Neckers L. Alternative splicing of the cell fate determinant Numb in hepatocellular carcinoma. *Hepatology*. 2015;62(4):1122-31. Epub 20150703. doi: 10.1002/hep.27923. PubMed PMID: 26058814; PMCID: PMC4589429.
331. Yasuda J, Whitmarsh AJ, Cavanagh J, Sharma M, Davis RJ. The JIP group of mitogen-activated protein kinase scaffold proteins. *Mol Cell Biol*. 1999;19(10):7245-54. doi: 10.1128/mcb.19.10.7245. PubMed PMID: 10490659; PMCID: PMC84717.
332. Miyamoto T, Rho E, Sample V, Akano H, Magari M, Ueno T, Gorshkov K, Chen M, Tokumitsu H, Zhang J, Inoue T. Compartmentalized AMPK signaling illuminated by genetically encoded molecular sensors and actuators. *Cell Rep*. 2015;11(4):657-70. Epub 20150416. doi: 10.1016/j.celrep.2015.03.057. PubMed PMID: 25892241; PMCID: PMC4417068.
333. Schmitt DL, Curtis SD, Lyons AC, Zhang JF, Chen M, He CY, Mehta S, Shaw RJ, Zhang J. Spatial regulation of AMPK signaling revealed by a sensitive kinase activity reporter. *Nat Commun*. 2022;13(1):3856. Epub 20220705. doi: 10.1038/s41467-022-31190-x. PubMed PMID: 35790710; PMCID: PMC9256702.
334. Drake JC, Wilson RJ, Laker RC, Guan Y, Spaulding HR, Nichenko AS, Shen W, Shang H, Dorn MV, Huang K, Zhang M, Bandara AB, Brisendine MH, Kashatus JA, Sharma PR, Young A, Gautam J, Cao R, Wallrabe H, Chang PA, Wong M, Desjardins EM, Hawley SA, Christ GJ, Kashatus DF, Miller CL, Wolf MJ, Periasamy A, Steinberg GR, Hardie DG, Yan Z. Mitochondria-localized AMPK responds to local energetics and contributes to exercise and energetic stress-induced mitophagy. *Proceedings of the National Academy of Sciences*. 2021;118(37):e2025932118. doi: doi:10.1073/pnas.2025932118.
335. Zhang YL, Guo H, Zhang CS, Lin SY, Yin Z, Peng Y, Luo H, Shi Y, Lian G, Zhang C, Li M, Ye Z, Ye J, Han J, Li P, Wu JW, Lin SC. AMP as a low-energy charge signal autonomously initiates assembly of AXIN-AMPK-LKB1 complex for AMPK activation. *Cell Metab*. 2013;18(4):546-55. doi: 10.1016/j.cmet.2013.09.005. PubMed PMID: 24093678.
336. Zhang CS, Jiang B, Li M, Zhu M, Peng Y, Zhang YL, Wu YQ, Li TY, Liang Y, Lu Z, Lian G, Liu Q, Guo H, Yin Z, Ye Z, Han J, Wu JW, Yin H, Lin SY, Lin SC. The lysosomal v-ATPase-Ragulator complex is a common activator for AMPK and mTORC1, acting as a switch between catabolism and anabolism. *Cell Metab*. 2014;20(3):526-40. Epub 20140704. doi: 10.1016/j.cmet.2014.06.014. PubMed PMID: 25002183.
337. Kazgan N, Williams T, Forsberg LJ, Brenman JE. Identification of a nuclear export signal in the catalytic subunit of AMP-activated protein kinase. *Mol Biol Cell*. 2010;21(19):3433-42. Epub 20100804. doi: 10.1091/mbc.E10-04-0347. PubMed PMID: 20685962; PMCID: PMC2947478.

338. Bradley KJ, Bowl MR, Williams SE, Ahmad BN, Partridge CJ, Patmanidi AL, Kennedy AM, Loh NY, Thakker RV. Parafibromin is a nuclear protein with a functional monopartite nuclear localization signal. *Oncogene*. 2007;26(8):1213-21. Epub 20060911. doi: 10.1038/sj.onc.1209893. PubMed PMID: 16964291.
339. Suzuki A, Okamoto S, Lee S, Saito K, Shiuchi T, Minokoshi Y. Leptin stimulates fatty acid oxidation and peroxisome proliferator-activated receptor alpha gene expression in mouse C2C12 myoblasts by changing the subcellular localization of the alpha2 form of AMP-activated protein kinase. *Mol Cell Biol*. 2007;27(12):4317-27. Epub 20070409. doi: 10.1128/mcb.02222-06. PubMed PMID: 17420279; PMCID: PMC1900064.
340. Lu J, Wu T, Zhang B, Liu S, Song W, Qiao J, Ruan H. Types of nuclear localization signals and mechanisms of protein import into the nucleus. *Cell Commun Signal*. 2021;19(1):60. Epub 20210522. doi: 10.1186/s12964-021-00741-y. PubMed PMID: 34022911; PMCID: PMC8140498.
341. Afinanisa Q, Cho MK, Seong HA. AMPK Localization: A Key to Differential Energy Regulation. *Int J Mol Sci*. 2021;22(20). Epub 20211010. doi: 10.3390/ijms222010921. PubMed PMID: 34681581; PMCID: PMC8535671.
342. Vara-Ciruelos D, Dandapani M, Gray A, Egbani EO, Evans AM, Hardie DG. Genotoxic Damage Activates the AMPK- $\alpha$ 1 Isoform in the Nucleus via Ca(2+)/CaMKK2 Signaling to Enhance Tumor Cell Survival. *Mol Cancer Res*. 2018;16(2):345-57. Epub 20171113. doi: 10.1158/1541-7786.Mcr-17-0323. PubMed PMID: 29133590.
343. Zong Y, Zhang CS, Li M, Wang W, Wang Z, Hawley SA, Ma T, Feng JW, Tian X, Qi Q, Wu YQ, Zhang C, Ye Z, Lin SY, Piao HL, Hardie DG, Lin SC. Hierarchical activation of compartmentalized pools of AMPK depends on severity of nutrient or energy stress. *Cell Res*. 2019;29(6):460-73. Epub 20190404. doi: 10.1038/s41422-019-0163-6. PubMed PMID: 30948787; PMCID: PMC6796943.
344. Martín-Vega A, Ruiz-Peinado L, García-Gómez R, Herrero A, de la Fuente-Vivas D, Parvathaneni S, Caloto R, Morante M, von Kriegsheim A, Bustelo XR, Sacks DB, Casar B, Crespo P. Scaffold coupling: ERK activation by trans-phosphorylation across different scaffold protein species. *Science Advances*. 2023;9(7):eadd7969. doi: doi:10.1126/sciadv.add7969.
345. Maik-Rachline G, Zehorai E, Hanoch T, Blenis J, Seger R. The nuclear translocation of the kinases p38 and JNK promotes inflammation-induced cancer. *Sci Signal*. 2018;11(525). Epub 20180410. doi: 10.1126/scisignal.aao3428. PubMed PMID: 29636389.
346. Zehorai E, Seger R. Beta-like importins mediate the nuclear translocation of mitogen-activated protein kinases. *Molecular and cellular biology*. 2014;34(2):259-70. Epub 2013/11/11. doi: 10.1128/MCB.00799-13. PubMed PMID: 24216760.
347. Burton JC, Okalova J, Grimsey NJ. Fluorescence resonance energy transfer (FRET) spatiotemporal mapping of atypical P38 reveals an endosomal and cytosolic spatial bias. *Sci Rep*. 2023;13(1):7477. Epub 20230508. doi: 10.1038/s41598-023-33953-y. PubMed PMID: 37156828.
348. Pinder A, Loo D, Harrington B, Oakes V, Hill MM, Gabrielli B. JIP4 is a PLK1 binding protein that regulates p38MAPK activity in G2 phase. *Cell Signal*. 2015;27(11):2296-303. Epub 20150817. doi: 10.1016/j.cellsig.2015.08.009. PubMed PMID: 26291670.
349. Klauer MJ, Willette BKA, Tsvetanova NG. Functional diversification of cell signaling by GPCR localization. *Journal of Biological Chemistry*. 2024;300(3). doi: 10.1016/j.jbc.2024.105668.

350. Kahsai AW, Shah KS, Shim PJ, Lee MA, Shreiber BN, Schwalb AM, Zhang X, Kwon HY, Huang L-Y, Soderblom EJ, Ahn S, Lefkowitz RJ. Signal transduction at GPCRs: Allosteric activation of the ERK MAPK by  $\beta$ -arrestin. *Proceedings of the National Academy of Sciences*. 2023;120(43):e2303794120. doi: 10.1073/pnas.2303794120.
351. Tohgo A, Choy EW, Gesty-Palmer D, Pierce KL, Laporte S, Oakley RH, Caron MG, Lefkowitz RJ, Luttrell LM. The stability of the G protein-coupled receptor-beta-arrestin interaction determines the mechanism and functional consequence of ERK activation. *J Biol Chem*. 2003;278(8):6258-67. Epub 20021206. doi: 10.1074/jbc.M212231200. PubMed PMID: 12473660.
352. Luttrell LM, Roudabush FL, Choy EW, Miller WE, Field ME, Pierce KL, Lefkowitz RJ. Activation and targeting of extracellular signal-regulated kinases by beta-arrestin scaffolds. *Proc Natl Acad Sci U S A*. 2001;98(5):2449-54. Epub 20010220. doi: 10.1073/pnas.041604898. PubMed PMID: 11226259; PMCID: PMC30158.
353. Grundmann M, Merten N, Malfacini D, Inoue A, Preis P, Simon K, Rüttiger N, Ziegler N, Benkel T, Schmitt NK, Ishida S, Müller I, Reher R, Kawakami K, Inoue A, Rick U, Köhl T, Imhof D, Aoki J, König GM, Hoffmann C, Gomeza J, Wess J, Kostenis E. Lack of beta-arrestin signaling in the absence of active G proteins. *Nat Commun*. 2018;9(1):341. Epub 20180123. doi: 10.1038/s41467-017-02661-3. PubMed PMID: 29362459; PMCID: PMC5780443.
354. O'Hayre M, Eichel K, Avino S, Zhao X, Steffen DJ, Feng X, Kawakami K, Aoki J, Messer K, Sunahara R, Inoue A, von Zastrow M, Gutkind JS. Genetic evidence that  $\beta$ -arrestins are dispensable for the initiation of  $\beta(2)$ -adrenergic receptor signaling to ERK. *Sci Signal*. 2017;10(484). Epub 20170620. doi: 10.1126/scisignal.aal3395. PubMed PMID: 28634209; PMCID: PMC5751434.
355. Crilly SE, Puthenveedu MA. Compartmentalized GPCR Signaling from Intracellular Membranes. *J Membr Biol*. 2021;254(3):259-71. Epub 20201124. doi: 10.1007/s00232-020-00158-7. PubMed PMID: 33231722; PMCID: PMC8141539.
356. Tsvetanova NG, Irannejad R, von Zastrow M. G protein-coupled receptor (GPCR) signaling via heterotrimeric G proteins from endosomes. *J Biol Chem*. 2015;290(11):6689-96. Epub 2015/01/22. doi: 10.1074/jbc.R114.617951. PubMed PMID: 25605726; PMCID: PMC4358092.
357. Lavoie H, Gagnon J, Therrien M. ERK signalling: a master regulator of cell behaviour, life and fate. *Nature Reviews Molecular Cell Biology*. 2020;21(10):607-32. doi: 10.1038/s41580-020-0255-7.
358. Kwon Y, Mehta S, Clark M, Walters G, Zhong Y, Lee HN, Sunahara RK, Zhang J. Non-canonical  $\beta$ -adrenergic activation of ERK at endosomes. *Nature*. 2022;611(7934):173-9. doi: 10.1038/s41586-022-05343-3.
359. Willette BKA, Zhang J-F, Zhang J, Tsvetanova NG. Endosome positioning coordinates spatially selective GPCR signaling. *Nature Chemical Biology*. 2024;20(2):151-61. doi: 10.1038/s41589-023-01390-7.
360. Kanayama A, Seth RB, Sun L, Ea C-K, Hong M, Shaito A, Chiu Y-H, Deng L, Chen ZJ. TAB2 and TAB3 Activate the NF- $\kappa$ B Pathway through Binding to Polyubiquitin Chains. *Molecular Cell*. 2004;15(4):535-48. doi: 10.1016/j.molcel.2004.08.008.
361. Grimsey NJ, Coronel LJ, Cordova IC, Trejo J. Recycling and Endosomal Sorting of Protease-activated Receptor-1 Is Distinctly Regulated by Rab11A and Rab11B Proteins. *J Biol*

- Chem. 2016;291(5):2223-36. doi: 10.1074/jbc.M115.702993. PubMed PMID: 26635365; PMCID: PMC4732206.
362. Burton JC, Okalova J, Grimsey NJ. Fluorescence resonance energy transfer (FRET) spatiotemporal mapping of atypical P38 reveals an endosomal and cytosolic spatial bias. *Scientific Reports*. 2023;13(1):7477. doi: 10.1038/s41598-023-33953-y.
363. Maik-Rachline G, Lifshits L, Seger R. Nuclear P38: Roles in Physiological and Pathological Processes and Regulation of Nuclear Translocation. *Int J Mol Sci*. 2020;21(17). Epub 20200824. doi: 10.3390/ijms21176102. PubMed PMID: 32847129; PMCID: PMC7504396.
364. Dumelie JG, Chen Q, Miller D, Attarwala N, Gross SS, Jaffrey SR. Biomolecular condensates create phospholipid-enriched microenvironments. *Nature Chemical Biology*. 2024;20(3):302-13. doi: 10.1038/s41589-023-01474-4.
365. Nilsson D, Irbäck A. Finite-size scaling analysis of protein droplet formation. *Phys Rev E*. 2020;101(2-1):022413. doi: 10.1103/PhysRevE.101.022413. PubMed PMID: 32168715.
366. López-Palacios TP, Andersen JL. Kinase regulation by liquid–liquid phase separation. *Trends in Cell Biology*. 2023;33(8):649-66. doi: <https://doi.org/10.1016/j.tcb.2022.11.009>.
367. Tarantino N, Tinevez J-Y, Crowell EF, Boisson B, Henriques R, Mhlanga M, Agou F, Israël A, Laplantine E. TNF and IL-1 exhibit distinct ubiquitin requirements for inducing NEMO–IKK supramolecular structures. *Journal of Cell Biology*. 2014;204(2):231-45. doi: 10.1083/jcb.201307172.
368. Du M, Ea C-K, Fang Y, Chen ZJ. Liquid phase separation of NEMO induced by polyubiquitin chains activates NF- $\kappa$ B. *Molecular Cell*. 2022;82(13):2415-26.e5. doi: <https://doi.org/10.1016/j.molcel.2022.03.037>.
369. Osman S. Binding NEMO: Liquid–liquid phase separation captures immune regulator. *Nature Structural & Molecular Biology*. 2022;29(6):503-. doi: 10.1038/s41594-022-00795-7.
370. Zhang JZ, Lu T-W, Stolerman LM, Tenner B, Yang JR, Zhang J-F, Falcke M, Rangamani P, Taylor SS, Mehta S, Zhang J. Phase Separation of a PKA Regulatory Subunit Controls cAMP Compartmentation and Oncogenic Signaling. *Cell*. 2020;182(6):1531-44.e15. doi: 10.1016/j.cell.2020.07.043.
371. Hardy JC, Pool EH, Bruystens JGH, Zhou X, Li Q, Zhou DR, Palay M, Tan G, Chen L, Choi JLC, Lee HN, Strack S, Wang D, Taylor SS, Mehta S, Zhang J. Molecular determinants and signaling effects of PKA RI $\alpha$  phase separation. *Mol Cell*. 2024;84(8):1570-84.e7. Epub 20240326. doi: 10.1016/j.molcel.2024.03.002. PubMed PMID: 38537638; PMCID: PMC11031308.
372. Sagan SM, Weber SC. Let's phase it: viruses are master architects of biomolecular condensates. *Trends Biochem Sci*. 2023;48(3):229-43. Epub 20221019. doi: 10.1016/j.tibs.2022.09.008. PubMed PMID: 36272892.
373. Kleer M, Mulloy RP, Robinson CA, Evseev D, Bui-Marinis MP, Castle EL, Banerjee A, Mubareka S, Mossman K, Corcoran JA. Human coronaviruses disassemble processing bodies. *PLoS Pathog*. 2022;18(8):e1010724. Epub 20220823. doi: 10.1371/journal.ppat.1010724. PubMed PMID: 35998203; PMCID: PMC9439236.
374. Zhang X, Zheng R, Li Z, Ma J. Liquid-liquid Phase Separation in Viral Function. *J Mol Biol*. 2023;435(16):167955. Epub 20230113. doi: 10.1016/j.jmb.2023.167955. PubMed PMID: 36642156.

375. Jobe F, Kelly JT, Simpson J, Wells J, Armstrong SD, Spick M, Lacey E, Logan L, Geifman N, Hawes P, Bailey D. Viral PIC-pocketing: RSV sequestration of translational preinitiation complexes into bi-phasic biomolecular condensates. *J Virol*. 2024;98(3):e0015324. Epub 20240229. doi: 10.1128/jvi.00153-24. PubMed PMID: 38421168; PMCID: PMC10949503.
376. Kuroshima T, Matsuda AY, Hossain E, Yasuda M, Kitamura T, Kitagawa Y, Higashino F. Adenovirus infection controls processing bodies to stabilize AU-rich element-containing mRNA. *Virology*. 2022;573:124-30. Epub 20220616. doi: 10.1016/j.virol.2022.06.009. PubMed PMID: 35779334.
377. Castle EL, Robinson CA, Douglas P, Rinker KD, Corcoran JA. Viral Manipulation of a Mechanoresponsive Signaling Axis Disassembles Processing Bodies. *Mol Cell Biol*. 2021;41(11):e0039921. Epub 20210913. doi: 10.1128/MCB.00399-21. PubMed PMID: 34516278; PMCID: PMC8547432.
378. Kanakamani S, Suresh PS, Venkatesh T. Regulation of processing bodies: From viruses to cancer epigenetic machinery. *Cell Biol Int*. 2021;45(4):708-19. Epub 20201228. doi: 10.1002/cbin.11527. PubMed PMID: 33325125.
379. Mok BW, Song W, Wang P, Tai H, Chen Y, Zheng M, Wen X, Lau SY, Wu WL, Matsumoto K, Yuen KY, Chen H. The NS1 protein of influenza A virus interacts with cellular processing bodies and stress granules through RNA-associated protein 55 (RAP55) during virus infection. *J Virol*. 2012;86(23):12695-707. Epub 20120912. doi: 10.1128/JVI.00647-12. PubMed PMID: 22973032; PMCID: PMC3497642.
380. Li M, Hou Y, Zhou Y, Yang Z, Zhao H, Jian T, Yu Q, Zeng F, Liu X, Zhang Z, Zhao YG. LLPS of FXR proteins drives replication organelle clustering for beta-coronaviral proliferation. *J Cell Biol*. 2024;223(6). Epub 20240408. doi: 10.1083/jcb.202309140. PubMed PMID: 38587486; PMCID: PMC11001562.
381. Sathyavageswaran A, Bonesso Sabadini J, Perry SL. Self-Assembling Polypeptides in Complex Coacervation. *Acc Chem Res*. 2024;57(3):386-98. Epub 20240122. doi: 10.1021/acs.accounts.3c00689. PubMed PMID: 38252962.
382. Diot C, Richard CA, Risso-Ballester J, Martin D, Fix J, Eleouet JF, Sizun C, Rameix-Welti MA, Galloux M. Hardening of Respiratory Syncytial Virus Inclusion Bodies by Cyclopamine Proceeds through Perturbation of the Interactions of the M2-1 Protein with RNA and the P Protein. *Int J Mol Sci*. 2023;24(18). Epub 20230908. doi: 10.3390/ijms241813862. PubMed PMID: 37762166; PMCID: PMC10531356.
383. Liu Y, Yao Z, Lian G, Yang P. Biomolecular phase separation in stress granule assembly and virus infection. *Acta Biochim Biophys Sin (Shanghai)*. 2023;55(7):1099-118. doi: 10.3724/abbs.2023117. PubMed PMID: 37401177; PMCID: PMC10415189.
384. Brownsword MJ, Doyle N, Brocard M, Locker N, Maier HJ. Infectious Bronchitis Virus Regulates Cellular Stress Granule Signaling. *Viruses*. 2020;12(5). Epub 20200514. doi: 10.3390/v12050536. PubMed PMID: 32422883; PMCID: PMC7291021.
385. Gao B, Gong X, Fang S, Weng W, Wang H, Chu H, Sun Y, Meng C, Tan L, Song C, Qiu X, Liu W, Forlenza M, Ding C, Liao Y. Inhibition of anti-viral stress granule formation by coronavirus endoribonuclease nsp15 ensures efficient virus replication. *PLoS Pathog*. 2021;17(2):e1008690. Epub 20210226. doi: 10.1371/journal.ppat.1008690. PubMed PMID: 33635931; PMCID: PMC7946191.

386. Procter DJ, Banerjee A, Nukui M, Kruse K, Gaponenko V, Murphy EA, Komarova Y, Walsh D. The HCMV Assembly Compartment Is a Dynamic Golgi-Derived MTOC that Controls Nuclear Rotation and Virus Spread. *Dev Cell*. 2018;45(1):83-100 e7. doi: 10.1016/j.devcel.2018.03.010. PubMed PMID: 29634939; PMCID: PMC5896778.
387. White S, Kawano H, Harata NC, Roller RJ. Herpes Simplex Virus Organizes Cytoplasmic Membranes To Form a Viral Assembly Center in Neuronal Cells. *J Virol*. 2020;94(19). Epub 20200915. doi: 10.1128/JVI.00900-20. PubMed PMID: 32699089; PMCID: PMC7495378.
388. Zhou S, Fu Z, Zhang Z, Jia X, Xu G, Sun L, Sun F, Gao P, Xu P, Deng H. Liquid-liquid phase separation mediates the formation of herpesvirus assembly compartments. *J Cell Biol*. 2023;222(1). Epub 20221017. doi: 10.1083/jcb.202201088. PubMed PMID: 36250941; PMCID: PMC9579985.
389. Pulkkinen LIA, Barrass SV, Lindgren M, Pace H, Overby AK, Anastasina M, Bally M, Lundmark R, Butcher SJ. Simultaneous membrane and RNA binding by tick-borne encephalitis virus capsid protein. *PLoS Pathog*. 2023;19(2):e1011125. Epub 20230214. doi: 10.1371/journal.ppat.1011125. PubMed PMID: 36787339; PMCID: PMC9970071.
390. Boson B, Mialon C, Schichl K, Denolly S, Cosset FL. Nup98 Is Subverted from Annulate Lamellae by Hepatitis C Virus Core Protein to Foster Viral Assembly. *mBio*. 2022;13(2):e0292321. Epub 20220308. doi: 10.1128/mbio.02923-21. PubMed PMID: 35258330; PMCID: PMC9040885.
391. Li H, Ernst C, Kolonko-Adamska M, Greb-Markiewicz B, Man J, Parissi V, Ng BW-L. Phase separation in viral infections. *Trends in Microbiology*. 2022;30(12):1217-31. doi: 10.1016/j.tim.2022.06.005.
392. Jayabalan AK, Griffin DE, Leung AKL. Pro-Viral and Anti-Viral Roles of the RNA-Binding Protein G3BP1. *Viruses*. 2023;15(2). Epub 20230206. doi: 10.3390/v15020449. PubMed PMID: 36851663; PMCID: PMC9959972.
393. Kobiler O, Brodersen P, Taylor MP, Ludmir EB, Enquist LW. Herpesvirus replication compartments originate with single incoming viral genomes. *mBio*. 2011;2(6). Epub 20111220. doi: 10.1128/mBio.00278-11. PubMed PMID: 22186611; PMCID: PMC3269065.
394. Seyffert M, Georgi F, Tobler K, Bourqui L, Anfossi M, Michaelsen K, Vogt B, Greber UF, Fraefel C. The HSV-1 Transcription Factor ICP4 Confers Liquid-Like Properties to Viral Replication Compartments. *Int J Mol Sci*. 2021;22(9). Epub 20210424. doi: 10.3390/ijms22094447. PubMed PMID: 33923223; PMCID: PMC8123221.
395. Jobe F, Simpson J, Hawes P, Guzman E, Bailey D. Respiratory Syncytial Virus Sequesters NF-kappaB Subunit p65 to Cytoplasmic Inclusion Bodies To Inhibit Innate Immune Signaling. *J Virol*. 2020;94(22). Epub 20201027. doi: 10.1128/JVI.01380-20. PubMed PMID: 32878896; PMCID: PMC7592213.
396. Cifuentes-Munoz N, Brantje J, Slaughter KB, Dutch RE. Human Metapneumovirus Induces Formation of Inclusion Bodies for Efficient Genome Replication and Transcription. *J Virol*. 2017;91(24). Epub 20171130. doi: 10.1128/JVI.01282-17. PubMed PMID: 28978704; PMCID: PMC5709606.
397. Rao S, Cinti A, Temzi A, Amorim R, You JC, Mouland AJ. HIV-1 NC-induced stress granule assembly and translation arrest are inhibited by the dsRNA binding protein Staufen1. *RNA*. 2018;24(2):219-36. Epub 20171110. doi: 10.1261/rna.064618.117. PubMed PMID: 29127210; PMCID: PMC5769749.

398. Yu H, Lin L, Zhang Z, Zhang H, Hu H. Targeting NF-kappaB pathway for the therapy of diseases: mechanism and clinical study. *Signal Transduct Target Ther.* 2020;5(1):209. Epub 20200921. doi: 10.1038/s41392-020-00312-6. PubMed PMID: 32958760; PMCID: PMC7506548.
399. Fricke J, Koo LY, Brown CR, Collins PL. p38 and OGT Sequestration into Viral Inclusion Bodies in Cells Infected with Human Respiratory Syncytial Virus Suppresses MK2 Activities and Stress Granule Assembly. *Journal of Virology.* 2013;87(3):1333-47. doi: doi:10.1128/jvi.02263-12.
400. Greenwald EC, Mehta S, Zhang J. Genetically Encoded Fluorescent Biosensors Illuminate the Spatiotemporal Regulation of Signaling Networks. *Chemical Reviews.* 2018;118(24):11707-94. doi: 10.1021/acs.chemrev.8b00333.
401. Mehta S, Zhang Y, Roth RH, Zhang J-f, Mo A, Tenner B, Haganir RL, Zhang J. Single-fluorophore biosensors for sensitive and multiplexed detection of signalling activities. *Nature Cell Biology.* 2018;20(10):1215-25. doi: 10.1038/s41556-018-0200-6.
402. Kudo T, Jeknić S, Macklin DN, Akhter S, Hughey JJ, Regot S, Covert MW. Live-cell measurements of kinase activity in single cells using translocation reporters. *Nature Protocols.* 2018;13(1):155-69. doi: 10.1038/nprot.2017.128.
403. Miyawaki A, Llopis J, Heim R, McCaffery JM, Adams JA, Ikura M, Tsien RY. Fluorescent indicators for Ca<sup>2+</sup> based on green fluorescent proteins and calmodulin. *Nature.* 1997;388(6645):882-7.
404. Miyawaki A, Griesbeck O, Heim R, Tsien RY. Dynamic and quantitative Ca<sup>2+</sup> measurements using improved cameleons. *Proceedings of the National Academy of Sciences.* 1999;96(5):2135-40.
405. Zhang J, Hupfeld CJ, Taylor SS, Olefsky JM, Tsien RY. Insulin disrupts  $\beta$ -adrenergic signalling to protein kinase A in adipocytes. *Nature.* 2005;437(7058):569-73.
406. Ma L, Jongbloets BC, Xiong W-H, Melander JB, Qin M, Lameyer TJ, Harrison MF, Zemelman BV, Mao T, Zhong H. A highly sensitive A-kinase activity reporter for imaging neuromodulatory events in awake mice. *Neuron.* 2018;99(4):665-79. e5.
407. Violin JD, Zhang J, Tsien RY, Newton AC. A genetically encoded fluorescent reporter reveals oscillatory phosphorylation by protein kinase C. *The Journal of cell biology.* 2003;161(5):899-909.
408. Ross BL, Tenner B, Markwardt ML, Zviman A, Shi G, Kerr JP, Snell NE, McFarland JJ, Mauban JR, Ward CW. Single-color, ratiometric biosensors for detecting signaling activities in live cells. *Elife.* 2018;7:e35458.
409. Harvey CD, Ehrhardt AG, Cellurale C, Zhong H, Yasuda R, Davis RJ, Svoboda K. A genetically encoded fluorescent sensor of ERK activity. *Proceedings of the National Academy of Sciences.* 2008;105(49):19264-9.
410. Zhou X, Clister TL, Lowry PR, Seldin MM, Wong GW, Zhang J. Dynamic Visualization of mTORC1 Activity in Living Cells. *Cell Rep.* 2015;10(10):1767-77. Epub 20150312. doi: 10.1016/j.celrep.2015.02.031. PubMed PMID: 25772363; PMCID: PMC4567530.
411. Zhou X, Clister Terri L, Lowry Pamela R, Seldin Marcus M, Wong GW, Zhang J. Dynamic Visualization of mTORC1 Activity in Living Cells. *Cell Reports.* 2015;10(10):1767-77. doi: 10.1016/j.celrep.2015.02.031.
412. Keyes J, Ganesan A, Molinar-Inglis O, Hamidzadeh A, Zhang J, Ling M, Trejo J, Levchenko A, Zhang J. Signaling diversity enabled by Rap1-regulated plasma membrane ERK

- with distinct temporal dynamics. *Elife*. 2020;9. Epub 20200526. doi: 10.7554/eLife.57410. PubMed PMID: 32452765; PMCID: PMC7289600.
413. Zhou X, Zhong Y, Molinar-Inglis O, Kunkel MT, Chen M, Sun T, Zhang J, Shyy JYJ, Trejo J, Newton AC, Zhang J. Location-specific inhibition of Akt reveals regulation of mTORC1 activity in the nucleus. *Nature Communications*. 2020;11(1):6088. doi: 10.1038/s41467-020-19937-w.
414. Gao X, Zhang J. Spatiotemporal Analysis of Differential Akt Regulation in Plasma Membrane Microdomains. *Molecular Biology of the Cell*. 2008;19(10):4366-73. doi: 10.1091/mbc.e08-05-0449. PubMed PMID: 18701703.
415. Nikolaev VO, Bünemann M, Hein L, Hannawacker A, Lohse MJ. Novel single chain cAMP sensors for receptor-induced signal propagation. *J Biol Chem*. 2004;279(36):37215-8. Epub 20040701. doi: 10.1074/jbc.C400302200. PubMed PMID: 15231839.
416. Zhang JZ, Lu TW, Stolerman LM, Tenner B, Yang JR, Zhang JF, Falcke M, Rangamani P, Taylor SS, Mehta S, Zhang J. Phase Separation of a PKA Regulatory Subunit Controls cAMP Compartmentation and Oncogenic Signaling. *Cell*. 2020;182(6):1531-44.e15. Epub 20200825. doi: 10.1016/j.cell.2020.07.043. PubMed PMID: 32846158; PMCID: PMC7502557.
417. Bock A, Annibale P, Konrad C, Hannawacker A, Anton SE, Maiellaro I, Zabel U, Sivaramakrishnan S, Falcke M, Lohse MJ. Optical Mapping of cAMP Signaling at the Nanometer Scale. *Cell*. 2020;182(6):1519-30.e17. doi: 10.1016/j.cell.2020.07.035.
418. Suryavanshi SV, Jadhav SM, McConnell BK. Polymorphisms/Mutations in A-Kinase Anchoring Proteins (AKAPs): Role in the Cardiovascular System. *J Cardiovasc Dev Dis*. 2018;5(1). Epub 20180125. doi: 10.3390/jcdd5010007. PubMed PMID: 29370121; PMCID: PMC5872355.
419. Reggi E, Diviani D. The role of A-kinase anchoring proteins in cancer development. *Cellular Signalling*. 2017;40:143-55. doi: <https://doi.org/10.1016/j.cellsig.2017.09.011>.
420. Mayers CM, Wadell J, McLean K, Venere M, Malik M, Shibata T, Driggers PH, Kino T, Guo XC, Koide H, Gorivodsky M, Grinberg A, Mukhopadhyay M, Abu-Asab M, Westphal H, Segars JH. The Rho guanine nucleotide exchange factor AKAP13 (BRX) is essential for cardiac development in mice. *J Biol Chem*. 2010;285(16):12344-54. Epub 20100205. doi: 10.1074/jbc.M110.106856. PubMed PMID: 20139090; PMCID: PMC2852973.
421. Carnegie GK, Soughayer J, Smith FD, Pedroja BS, Zhang F, Diviani D, Bristow MR, Kunkel MT, Newton AC, Langeberg LK, Scott JD. AKAP-Lbc mobilizes a cardiac hypertrophy signaling pathway. *Mol Cell*. 2008;32(2):169-79. doi: 10.1016/j.molcel.2008.08.030. PubMed PMID: 18951085; PMCID: PMC3169907.
422. Appert-Collin A, Cotecchia S, Nenniger-Tosato M, Pedrazzini T, Diviani D. The A-kinase anchoring protein (AKAP)-Lbc-signaling complex mediates alpha1 adrenergic receptor-induced cardiomyocyte hypertrophy. *Proc Natl Acad Sci U S A*. 2007;104(24):10140-5. Epub 20070530. doi: 10.1073/pnas.0701099104. PubMed PMID: 17537920; PMCID: PMC1891209.
423. Liu Y, Zhao S, Wang J, Zhu Z, Luo L, Xiang Q, Zhou M, Ma Y, Wang Z, Zhao Z. MiR-629-5p Promotes Prostate Cancer Development and Metastasis by Targeting AKAP13. *Front Oncol*. 2021;11:754353. Epub 20211015. doi: 10.3389/fonc.2021.754353. PubMed PMID: 34722307; PMCID: PMC8554144.
424. Omar MH, Byrne DP, Shrestha S, Lakey TM, Lee KS, Lauer SM, Collins KB, Daly LA, Evers CE, Baird GS, Ong SE, Kannan N, Evers PA, Scott JD. Discovery of a Cushing's syndrome protein kinase A mutant that biases signaling through type I AKAPs. *Sci Adv*.

- 2024;10(8):eadl1258. Epub 20240221. doi: 10.1126/sciadv.adl1258. PubMed PMID: 38381834; PMCID: PMC10881042.
425. Chauhan AS, Zhuang L, Gan B. Spatial control of AMPK signaling at subcellular compartments. *Crit Rev Biochem Mol Biol.* 2020;55(1):17-32. Epub 20200218. doi: 10.1080/10409238.2020.1727840. PubMed PMID: 32069425; PMCID: PMC8237692.
426. Gurevich VV, Gurevich EV. GPCR Signaling Regulation: The Role of GRKs and Arrestins. *Front Pharmacol.* 2019;10:125. Epub 20190219. doi: 10.3389/fphar.2019.00125. PubMed PMID: 30837883; PMCID: PMC6389790.
427. Lefkowitz RJ, Shenoy SK. Transduction of receptor signals by  $\beta$ -arrestins. *science.* 2005;308(5721):512-7.
428. Gold JI, Martini JS, Hullmann J, Gao E, Chuprun JK, Lee L, Tilley DG, Rabinowitz JE, Bossuyt J, Bers DM, Koch WJ. Nuclear translocation of cardiac G protein-Coupled Receptor kinase 5 downstream of select Gq-activating hypertrophic ligands is a calmodulin-dependent process. *PLoS One.* 2013;8(3):e57324. Epub 20130305. doi: 10.1371/journal.pone.0057324. PubMed PMID: 23472081; PMCID: PMC3589474.
429. Woodall MC, Ciccarelli M, Woodall BP, Koch WJ. G protein-coupled receptor kinase 2: a link between myocardial contractile function and cardiac metabolism. *Circ Res.* 2014;114(10):1661-70. doi: 10.1161/circresaha.114.300513. PubMed PMID: 24812353; PMCID: PMC4095756.
430. Chen M, Sato PY, Chuprun JK, Peroutka RJ, Otis NJ, Ibeti J, Pan S, Sheu S-S, Gao E, Koch WJ. Prodeath Signaling of G Protein-Coupled Receptor Kinase 2 in Cardiac Myocytes After Ischemic Stress Occurs Via Extracellular Signal-Regulated Kinase-Dependent Heat Shock Protein 90-Mediated Mitochondrial Targeting. *Circulation Research.* 2013;112(8):1121-34. doi: 10.1161/CIRCRESAHA.112.300754.
431. Sato PY, Chuprun JK, Grisanti LA, Woodall MC, Brown BR, Roy R, Traynham CJ, Ibeti J, Lucchese AM, Yuan A, Drosatos K, Tilley DG, Gao E, Koch WJ. Restricting mitochondrial GRK2 post-ischemia confers cardioprotection by reducing myocyte death and maintaining glucose oxidation. *Sci Signal.* 2018;11(560). Epub 20181211. doi: 10.1126/scisignal.aau0144. PubMed PMID: 30538174; PMCID: PMC6463290.
432. Sato PY, Chuprun JK, Ibeti J, Cannavo A, Drosatos K, Elrod JW, Koch WJ. GRK2 compromises cardiomyocyte mitochondrial function by diminishing fatty acid-mediated oxygen consumption and increasing superoxide levels. *J Mol Cell Cardiol.* 2015;89(Pt B):360-4. Epub 20151023. doi: 10.1016/j.yjmcc.2015.10.002. PubMed PMID: 26506135; PMCID: PMC4689631.
433. Miller CJ, Turk BE. Homing in: Mechanisms of Substrate Targeting by Protein Kinases. *Trends Biochem Sci.* 2018;43(5):380-94. Epub 20180312. doi: 10.1016/j.tibs.2018.02.009. PubMed PMID: 29544874; PMCID: PMC5923429.
434. Grimsey NJ, Lin Y, Narala R, Rada CC, Mejia-Pena H, Trejo J. G protein-coupled receptors activate p38 MAPK via a non-canonical TAB1-TAB2 and TAB1-TAB3 dependent pathway in endothelial cells 2019. doi: 10.1074/jbc.RA119.007495.
435. Ripin N, Parker R. Formation, function, and pathology of RNP granules. *Cell.* 2023;186(22):4737-56. doi: <https://doi.org/10.1016/j.cell.2023.09.006>.
436. Trivedi P, Palomba F, Niedzialkowska E, Digman MA, Gratton E, Stukenberg PT. The inner centromere is a biomolecular condensate scaffolded by the chromosomal passenger

- complex. *Nat Cell Biol.* 2019;21(9):1127-37. Epub 20190903. doi: 10.1038/s41556-019-0376-4. PubMed PMID: 31481798; PMCID: PMC7341897.
437. Liu X, Liu X, Wang H, Dou Z, Ruan K, Hill DL, Li L, Shi Y, Yao X. Phase separation drives decision making in cell division. *Journal of Biological Chemistry.* 2020;295(39):13419-31. doi: <https://doi.org/10.1074/jbc.REV120.011746>.
438. Eiermann N, Haneke K, Sun Z, Stoecklin G, Ruggieri A. Dance with the Devil: Stress Granules and Signaling in Antiviral Responses. *Viruses.* 2020;12(9):984. PubMed PMID: doi:10.3390/v12090984.
439. Yamamoto S, Kitagawa D. Self-organization of Plk4 regulates symmetry breaking in centriole duplication. *Nature Communications.* 2019;10(1):1810. doi: 10.1038/s41467-019-09847-x.
440. Wegmann S, Eftekhazadeh B, Tepper K, Zoltowska KM, Bennett RE, Dujardin S, Laskowski PR, MacKenzie D, Kamath T, Commins C, Vanderburg C, Roe AD, Fan Z, Molliex AM, Hernandez-Vega A, Muller D, Hyman AA, Mandelkow E, Taylor JP, Hyman BT. Tau protein liquid-liquid phase separation can initiate tau aggregation. *The EMBO Journal.* 2018;37(7):e98049. doi: <https://doi.org/10.15252/embj.201798049>.
441. Case LB, De Pasquale M, Henry L, Rosen MK. Synergistic phase separation of two pathways promotes integrin clustering and nascent adhesion formation. *eLife.* 2022;11:e72588. doi: 10.7554/eLife.72588.
442. Schlütermann D, Berleth N, Deitersen J, Wallot-Hieke N, Friesen O, Wu W, Stuhldreier F, Sun Y, Berning L, Friedrich A, Mendiburo MJ, Peter C, Wiek C, Hanenberg H, Stefanski A, Stühler K, Stork B. FIP200 controls the TBK1 activation threshold at SQSTM1/p62-positive condensates. *Scientific Reports.* 2021;11(1):13863. doi: 10.1038/s41598-021-92408-4.
443. Turco E, Witt M, Abert C, Bock-Bierbaum T, Su M-Y, Trapannone R, Sztacho M, Danieli A, Shi X, Zaffagnini G, Gamper A, Schuschnig M, Fracchiolla D, Bernklau D, Romanov J, Hartl M, Hurley JH, Daumke O, Martens S. FIP200 Claw Domain Binding to p62 Promotes Autophagosome Formation at Ubiquitin Condensates. *Molecular Cell.* 2019;74(2):330-46.e11. doi: <https://doi.org/10.1016/j.molcel.2019.01.035>.
444. Kannangara AR, Poole DM, McEwan CM, Youngs JC, Weerasekara VK, Thornock AM, Lazaro MT, Balasooriya ER, Oh LM, Soderblom EJ, Lee JJ, Simmons DL, Andersen JL. BioID reveals an ATG9A interaction with ATG13-ATG101 in the degradation of p62/SQSTM1-ubiquitin clusters. *EMBO reports.* 2021;22(10):e51136. doi: <https://doi.org/10.15252/embr.202051136>.
445. Vargas JNS, Wang C, Bunker E, Hao L, Maric D, Schiavo G, Randow F, Youle RJ. Spatiotemporal Control of ULK1 Activation by NDP52 and TBK1 during Selective Autophagy. *Molecular Cell.* 2019;74(2):347-62.e6. doi: <https://doi.org/10.1016/j.molcel.2019.02.010>.
446. Chan T-Y, Egbert CM, Maxson JE, Siddiqui A, Larsen LJ, Kohler K, Balasooriya ER, Pennington KL, Tsang T-M, Frey M, Soderblom EJ, Geng H, Müschen M, Forostyan TV, Free S, Mercenne G, Banks CJ, Valdoz J, Whatcott CJ, Foulks JM, Bearss DJ, O'Hare T, Huang DCS, Christensen KA, Moody J, Warner SL, Tyner JW, Andersen JL. TNK1 is a ubiquitin-binding and 14-3-3-regulated kinase that can be targeted to block tumor growth. *Nature Communications.* 2021;12(1):5337. doi: 10.1038/s41467-021-25622-3.
447. Lin C-C, Suen KM, Lidster J, Ladbury JE. The emerging role of receptor tyrosine kinase phase separation in cancer. *Trends in Cell Biology.* 2024;34(5):371-9. doi: <https://doi.org/10.1016/j.tcb.2023.09.002>.

448. Sfakianos AP, Mellor LE, Pang YF, Kritsiligkou P, Needs H, Abou-Hamdan H, Désaubry L, Poulin GB, Ashe MP, Whitmarsh AJ. The mTOR-S6 kinase pathway promotes stress granule assembly. *Cell Death & Differentiation*. 2018;25(10):1766-80. doi: 10.1038/s41418-018-0076-9.
449. Shah KH, Nostramo R, Zhang B, Varia SN, Klett BM, Herman PK. Protein Kinases Are Associated with Multiple, Distinct Cytoplasmic Granules in Quiescent Yeast Cells. *Genetics*. 2014;198(4):1495-512. doi: 10.1534/genetics.114.172031.
450. Kobayashi T, Winslow S, Sunesson L, Hellman U, Larsson C. PKC $\alpha$  Binds G3BP2 and Regulates Stress Granule Formation Following Cellular Stress. *PLOS ONE*. 2012;7(4):e35820. doi: 10.1371/journal.pone.0035820.
451. Reineke Lucas C, Lloyd Richard E. The Stress Granule Protein G3BP1 Recruits Protein Kinase R To Promote Multiple Innate Immune Antiviral Responses. *Journal of Virology*. 2015;89(5):2575-89. doi: 10.1128/jvi.02791-14.
452. Wippich F, Bodenmiller B, Trajkovska MG, Wanka S, Aebersold R, Pelkmans L. Dual specificity kinase DYRK3 couples stress granule condensation/dissolution to mTORC1 signaling. *Cell*. 2013;152(4):791-805.
453. Reineke LC, Tsai W-C, Jain A, Kaelber JT, Jung SY, Lloyd RE. Casein Kinase 2 Is Linked to Stress Granule Dynamics through Phosphorylation of the Stress Granule Nucleating Protein G3BP1. *Molecular and Cellular Biology*. 2017;37(4):e00596-16. doi: 10.1128/MCB.00596-16.
454. Shattuck JE, Paul KR, Cascarina SM, Ross ED. The prion-like protein kinase Sky1 is required for efficient stress granule disassembly. *Nature Communications*. 2019;10(1):3614. doi: 10.1038/s41467-019-11550-w.
455. Krisenko MO, Higgins RL, Ghosh S, Zhou Q, Trybula JS, Wang W-H, Geahlen RL. Syk Is Recruited to Stress Granules and Promotes Their Clearance through Autophagy\*. *Journal of Biological Chemistry*. 2015;290(46):27803-15. doi: <https://doi.org/10.1074/jbc.M115.642900>.
456. Tauber D, Tauber G, Khong A, Van Treeck B, Pelletier J, Parker R. Modulation of RNA Condensation by the DEAD-Box Protein eIF4A. *Cell*. 2020;180(3):411-26.e16. doi: <https://doi.org/10.1016/j.cell.2019.12.031>.
457. Heberle AM, Razquin Navas P, Langelaar-Makkinje M, Kasack K, Sadik A, Faessler E, Hahn U, Marx-Stoelting P, Opitz CA, Sers C, Heiland I, Schäuble S, Thedieck K. The PI3K and MAPK/p38 pathways control stress granule assembly in a hierarchical manner. *Life Science Alliance*. 2019;2(2):e201800257. doi: 10.26508/lsa.201800257.
458. Su X, Ditlev JA, Hui E, Xing W, Banjade S, Okrut J, King DS, Taunton J, Rosen MK, Vale RD. Phase separation of signaling molecules promotes T cell receptor signal transduction. *Science*. 2016;352(6285):595-9. doi: doi:10.1126/science.aad9964.
459. Dabo S, Meurs EF. dsRNA-Dependent Protein Kinase PKR and its Role in Stress, Signaling and HCV Infection. *Viruses*. 2012;4(11):2598-635. PubMed PMID: doi:10.3390/v4112598.
460. Gao P, Liu Y, Wang H, Chai Y, Weng W, Zhang Y, Zhou L, Ge X, Guo X, Han J, Yang H. Viral evasion of PKR restriction by reprogramming cellular stress granules. *Proc Natl Acad Sci U S A*. 2022;119(29):e2201169119. Epub 20220711. doi: 10.1073/pnas.2201169119. PubMed PMID: 35858300; PMCID: PMC9303852.
461. Artham S, Gao F, Verma A, Alwhaibi A, Sabineni H, Hafez S, Ergul A, Somanath PR. Endothelial stromelysin1 regulation by the forkhead box-O transcription factors is crucial in the

- exudative phase of acute lung injury. *Pharmacological Research*. 2019;141:249-63. doi: <https://doi.org/10.1016/j.phrs.2019.01.006>.
462. Ramachandran V, Shah KH, Herman PK. The cAMP-dependent protein kinase signaling pathway is a key regulator of P body foci formation. *Mol Cell*. 2011;43(6):973-81. doi: 10.1016/j.molcel.2011.06.032. PubMed PMID: 21925385; PMCID: PMC3176436.
463. Mikuda N, Kolesnichenko M, Beaudette P, Popp O, Uyar B, Sun W, Tufan AB, Perder B, Akalin A, Chen W, Mertins P, Dittmar G, Hinz M, Scheidereit C. The I $\kappa$ B kinase complex is a regulator of mRNA stability. *The EMBO Journal*. 2018;37(24):e98658. doi: <https://doi.org/10.15252/embj.201798658>.
464. Hofweber M, Dormann D. Friend or foe-Post-translational modifications as regulators of phase separation and RNP granule dynamics. *J Biol Chem*. 2019;294(18):7137-50. Epub 20181226. doi: 10.1074/jbc.TM118.001189. PubMed PMID: 30587571; PMCID: PMC6509508.
465. Wang J, Choi J-M, Holehouse AS, Lee HO, Zhang X, Jahnel M, Maharana S, Lemaitre R, Pozniakovsky A, Drechsel D. A molecular grammar governing the driving forces for phase separation of prion-like RNA binding proteins. *Cell*. 2018;174(3):688-99. e16.
466. Deng Q, Holler CJ, Taylor G, Hudson KF, Watkins W, Gearing M, Ito D, Murray ME, Dickson DW, Seyfried NT. FUS is phosphorylated by DNA-PK and accumulates in the cytoplasm after DNA damage. *Journal of Neuroscience*. 2014;34(23):7802-13.
467. Monahan Z, Ryan VH, Janke AM, Burke KA, Rhoads SN, Zerze GH, O'Meally R, Dignon GL, Conicella AE, Zheng W. Phosphorylation of the FUS low-complexity domain disrupts phase separation, aggregation, and toxicity. *The EMBO journal*. 2017;36(20):2951-67.
468. Rhoads SN, Monahan ZT, Yee DS, Leung AY, Newcombe CG, O'Meally RN, Cole RN, Shewmaker FP. The prionlike domain of FUS is multiphosphorylated following DNA damage without altering nuclear localization. *Molecular biology of the cell*. 2018;29(15):1786-97.
469. Murray DT, Kato M, Lin Y, Thurber KR, Hung I, McKnight SL, Tycko R. Structure of FUS protein fibrils and its relevance to self-assembly and phase separation of low-complexity domains. *Cell*. 2017;171(3):615-27. e16.
470. Luo F, Gui X, Zhou H, Gu J, Li Y, Liu X, Zhao M, Li D, Li X, Liu C. Atomic structures of FUS LC domain segments reveal bases for reversible amyloid fibril formation. *Nature structural & molecular biology*. 2018;25(4):341-6.
471. Lin Y, Currie SL, Rosen MK. Intrinsically disordered sequences enable modulation of protein phase separation through distributed tyrosine motifs. *Journal of Biological Chemistry*. 2017;292(46):19110-20.
472. Han TW, Kato M, Xie S, Wu LC, Mirzaei H, Pei J, Chen M, Xie Y, Allen J, Xiao G. Cell-free formation of RNA granules: bound RNAs identify features and components of cellular assemblies. *Cell*. 2012;149(4):768-79.
473. Wang Y, Mandelkow E. Tau in physiology and pathology. *Nature reviews neuroscience*. 2016;17(1):22-35.
474. Kampers T, Friedhoff P, Biernat J, Mandelkow E-M, Mandelkow E. RNA stimulates aggregation of microtubule-associated protein tau into Alzheimer-like paired helical filaments. *FEBS letters*. 1996;399(3):344-9.
475. Wang XS, Wang DL, Zhao J, Qu MH, Zhou XH, He HJ, He RQ. The proline-rich domain and the microtubule binding domain of protein tau acting as RNA binding domains. *Protein and peptide letters*. 2006;13(7):679-85.

476. Ambadipudi S, Biernat J, Riedel D, Mandelkow E, Zweckstetter M. Liquid–liquid phase separation of the microtubule-binding repeats of the Alzheimer-related protein Tau. *Nature communications*. 2017;8(1):275.
477. Murakoshi H. Optogenetic Imaging of Protein Activity Using Two-Photon Fluorescence Lifetime Imaging Microscopy. *Adv Exp Med Biol*. 2021;1293:295-308. doi: 10.1007/978-981-15-8763-4\_18. PubMed PMID: 33398821.
478. Coelho S, Poland SP, Devauges V, Ameer-Beg SM. Adaptive optics for a time-resolved Förster resonance energy transfer (FRET) and fluorescence lifetime imaging microscopy (FLIM) in vivo. *Opt Lett*. 2020;45(10):2732-5. doi: 10.1364/ol.385950. PubMed PMID: 32412453; PMID: PMC7340371.
479. Ueda HH, Nagasawa Y, Murakoshi H. Imaging intracellular protein interactions/activity in neurons using 2-photon fluorescence lifetime imaging microscopy. *Neurosci Res*. 2022;179:31-8. Epub 20211016. doi: 10.1016/j.neures.2021.10.004. PubMed PMID: 34666101.
480. Shcherbakova DM, Cox Cammer N, Huisman TM, Verkhusha VV, Hodgson L. Direct multiplex imaging and optogenetics of Rho GTPases enabled by near-infrared FRET. *Nature chemical biology*. 2018;14(6):591-600.
481. Braicu C, Buse M, Busuioc C, Drula R, Gulei D, Raduly L, Rusu A, Irimie A, Atanasov AG, Slaby O, Ionescu C, Berindan-Neagoie I. A Comprehensive Review on MAPK: A Promising Therapeutic Target in Cancer. *Cancers (Basel)*. 2019;11(10). Epub 20191022. doi: 10.3390/cancers11101618. PubMed PMID: 31652660; PMID: PMC6827047.
482. Ganguly P, Macleod T, Wong C, Harland M, McGonagle D. Revisiting p38 Mitogen-Activated Protein Kinases (MAPK) in Inflammatory Arthritis: A Narrative of the Emergence of MAPK-Activated Protein Kinase Inhibitors (MK2i). *Pharmaceuticals (Basel)*. 2023;16(9). Epub 20230912. doi: 10.3390/ph16091286. PubMed PMID: 37765094; PMID: PMC10537904.
483. Wang L, Xia Z, Tang W, Sun Y, Wu Y, Kwok HF, Sun F, Cao Z. p38 activation and viral infection. *Expert Reviews in Molecular Medicine*. 2022;24:e4. Epub 2022/01/21. doi: 10.1017/erm.2021.29.
484. Machado TR, Machado TR, Pascutti PG. The p38 MAPK Inhibitors and Their Role in Inflammatory Diseases. *ChemistrySelect*. 2021;6(23):5729-42. doi: <https://doi.org/10.1002/slct.202100406>.
485. Gordon D, Hellriegel ET, Hope HR, Burt D, Monahan JB. Safety, Tolerability, Pharmacokinetics, and Pharmacodynamics of the MK2 Inhibitor ATI-450 in Healthy Subjects: A Placebo-Controlled, Randomized Phase 1 Study. *Clin Pharmacol*. 2021;13:123-34. Epub 20210610. doi: 10.2147/cpaa.S305308. PubMed PMID: 34140814; PMID: PMC8203602.
486. Bucko PJ, Lombard CK, Rathbun L, Garcia I, Bhat A, Wordeman L, Smith FD, Maly DJ, Hehnly H, Scott JD. Subcellular drug targeting illuminates local kinase action. *eLife*. 2019;8:e52220. doi: 10.7554/eLife.52220.
487. Wheeler RJ. Therapeutics—how to treat phase separation-associated diseases. *Emerging Topics in Life Sciences*. 2020;4(3):331-42. doi: 10.1042/etls20190176.
488. Matthay MA, Zemans RL, Zimmerman GA, Arabi YM, Beitler JR, Mercat A, Herridge M, Randolph AG, Calfee CS. Acute respiratory distress syndrome. *Nature Reviews Disease Primers*. 2019;5(1):18. doi: 10.1038/s41572-019-0069-0.
489. Mowery NT, Terzian WTH, Nelson AC. Acute lung injury. *Current Problems in Surgery*. 2020;57(5):100777. doi: <https://doi.org/10.1016/j.cpsurg.2020.100777>.

490. Revercomb L, Hanmandlu A, Wareing N, Akkanti B, Karmouty-Quintana H. Mechanisms of Pulmonary Hypertension in Acute Respiratory Distress Syndrome (ARDS). *Front Mol Biosci.* 2020;7:624093. Epub 20210118. doi: 10.3389/fmolb.2020.624093. PubMed PMID: 33537342; PMCID: PMC7848216.
491. Wynn TA. Common and unique mechanisms regulate fibrosis in various fibroproliferative diseases. *The Journal of clinical investigation.* 2007;117(3):524-9.
492. Bochaton-Piallat M-L, Gabbiani G, Hinz B. The myofibroblast in wound healing and fibrosis: answered and unanswered questions. *F1000Research.* 2016;5.
493. Upagupta C, Shimbori C, Alsilmi R, Kolb M. Matrix abnormalities in pulmonary fibrosis. *European Respiratory Review.* 2018;27(148).
494. Savin IA, Zenkova MA, Sen'kova AV. Pulmonary Fibrosis as a Result of Acute Lung Inflammation: Molecular Mechanisms, Relevant In Vivo Models, Prognostic and Therapeutic Approaches. *International Journal of Molecular Sciences.* 2022;23(23):14959. PubMed PMID: doi:10.3390/ijms232314959.
495. Li L-F, Yu L, Quinn DA. Ventilation-induced neutrophil infiltration depends on c-Jun N-terminal kinase. *American journal of respiratory and critical care medicine.* 2004;169(4):518-24.
496. Copland IB, Post M. Stretch-activated signaling pathways responsible for early response gene expression in fetal lung epithelial cells. *Journal of Cellular Physiology.* 2007;210(1):133-43. doi: <https://doi.org/10.1002/jcp.20840>.
497. Kotani M, Kotani T, Ishizaka A, Fujishima S, Koh H, Tasaka S, Sawafuji M, Ikeda E, Moriyama K, Kotake Y. Neutrophil depletion attenuates interleukin-8 production in mild-overstretch ventilated normal rabbit lung. *Critical care medicine.* 2004;32(2):514-9.
498. Zhang W, Dai H, Lin F, Zhao C, Wang X, Zhang S, Ge W, Pei S, Pan L. Ly-6Chigh inflammatory-monocyte recruitment is regulated by p38 MAPK/MCP-1 activation and promotes ventilator-induced lung injury. *International Immunopharmacology.* 2020;78:106015. doi: <https://doi.org/10.1016/j.intimp.2019.106015>.
499. Pleschka S. Overview of Influenza Viruses. In: Richt JA, Webby RJ, editors. *Swine Influenza.* Berlin, Heidelberg: Springer Berlin Heidelberg; 2013. p. 1-20.
500. Hale BG, Albrecht RA, García-Sastre A. Innate Immune Evasion Strategies of Influenza Viruses. *Future Microbiology.* 2010;5(1):23-41. doi: 10.2217/fmb.09.108.
501. De Vlugt C, Sikora D, Pelchat M. Insight into Influenza: A Virus Cap-Snatching. *Viruses.* 2018;10(11). Epub 20181116. doi: 10.3390/v10110641. PubMed PMID: 30453478; PMCID: PMC6266781.
502. Dou D, Revol R, Östbye H, Wang H, Daniels R. Influenza A Virus Cell Entry, Replication, Virion Assembly and Movement. *Front Immunol.* 2018;9:1581. Epub 20180720. doi: 10.3389/fimmu.2018.01581. PubMed PMID: 30079062; PMCID: PMC6062596.
503. Short KR, Kroeze E, Fouchier RAM, Kuiken T. Pathogenesis of influenza-induced acute respiratory distress syndrome. *Lancet Infect Dis.* 2014;14(1):57-69. Epub 20131113. doi: 10.1016/s1473-3099(13)70286-x. PubMed PMID: 24239327.
504. Bellingan GJ. The pulmonary physician in critical care \* 6: The pathogenesis of ALI/ARDS. *Thorax.* 2002;57(6):540-6. doi: 10.1136/thorax.57.6.540. PubMed PMID: 12037231; PMCID: PMC1746355.
505. Wang J, Nikrad MP, Travanty EA, Zhou B, Phang T, Gao B, Alford T, Ito Y, Nahreini P, Hartshorn K. Innate immune response of human alveolar macrophages during influenza A infection. *PloS one.* 2012;7(3):e29879.

506. Goritzka M, Makris S, Kausar F, Durant LR, Pereira C, Kumagai Y, Culley FJ, Mack M, Akira S, Johansson C. Alveolar macrophage-derived type I interferons orchestrate innate immunity to RSV through recruitment of antiviral monocytes. *Journal of Experimental Medicine*. 2015;212(5):699-714.
507. Theofilis P, Sagris M, Oikonomou E, Antonopoulos AS, Siasos G, Tsioufis C, Tousoulis D. Inflammatory Mechanisms Contributing to Endothelial Dysfunction. *Biomedicines*. 2021;9(7). Epub 20210706. doi: 10.3390/biomedicines9070781. PubMed PMID: 34356845; PMCID: PMC8301477.
508. Short KR, Kasper J, Aa Svd, Andeweg AC, Zaaraoui-Boutahar F, Goeijenbier M, Richard M, Herold S, Becker C, Scott DP, Limpens RWAL, Koster AJ, Bárcena M, Fouchier RAM, Kirkpatrick CJ, Kuiken T. Influenza virus damages the alveolar barrier by disrupting epithelial cell tight junctions. *European Respiratory Journal*. 2016;47(3):954-66. doi: 10.1183/13993003.01282-2015.
509. Rahman A, Fazal F. Blocking NF- $\kappa$ B: an inflammatory issue. *Proceedings of the American Thoracic Society*. 2011;8(6):497-503.
510. Dudek SM, Garcia JG. Cytoskeletal regulation of pulmonary vascular permeability. *Journal of applied physiology*. 2001;91(4):1487-500.
511. Turner JS, Lei T, Schmitz AJ, Day A, Choreño-Parra JA, Jiménez-Alvarez L, Cruz-Lagunas A, House SL, Zúñiga J, Ellebedy AH, Mudd PA. Impaired Cellular Immune Responses During the First Week of Severe Acute Influenza Infection. *The Journal of Infectious Diseases*. 2020;222(7):1235-44. doi: 10.1093/infdis/jiaa226.
512. Matsuoka Y, Lamirande EW, Subbarao K. The mouse model for influenza. *Curr Protoc Microbiol*. 2009;Chapter 15:Unit 15G.3. doi: 10.1002/9780471729259.mc15g03s13. PubMed PMID: 19412911.
513. Sarkar S, Heise MT. Mouse Models as Resources for Studying Infectious Diseases. *Clin Ther*. 2019;41(10):1912-22. Epub 20190918. doi: 10.1016/j.clinthera.2019.08.010. PubMed PMID: 31540729; PMCID: PMC7112552.
514. Gonzales JN, Lucas R, Verin AD. The Acute Respiratory Distress Syndrome: Mechanisms and Perspective Therapeutic Approaches. *Austin J Vasc Med*. 2015;2(1). PubMed PMID: 26973981; PMCID: PMC4786180.
515. Millar MW, Fazal F, Rahman A. Therapeutic Targeting of NF- $\kappa$ B in Acute Lung Injury: A Double-Edged Sword. *Cells*. 2022;11(20). Epub 20221021. doi: 10.3390/cells11203317. PubMed PMID: 36291185; PMCID: PMC9601210.
516. Fan J, Ye RD, Malik AB. Transcriptional mechanisms of acute lung injury. *American Journal of Physiology-Lung Cellular and Molecular Physiology*. 2001;281(5):L1037-L50.
517. Zhong M, Wang H, Ma L, Yan H, Wu S, Gu Z, Li Y. DMO-CAP inhibits influenza virus replication by activating heme oxygenase-1-mediated IFN response. *Virology journal*. 2019;16:1-9.
518. Bahadoran A, Lee SH, Wang SM, Manikam R, Rajarajeswaran J, Raju CS, Sekaran SD. Immune responses to influenza virus and its correlation to age and inherited factors. *Frontiers in microbiology*. 2016;7:1841.
519. He C, Sun S, Zhang Y, Xie F, Li S. The role of irreversible electroporation in promoting M1 macrophage polarization via regulating the HMGB1-RAGE-MAPK axis in pancreatic cancer. *OncoImmunology*. 2021;10(1):1897295. doi: 10.1080/2162402X.2021.1897295.

520. Baumann D, Drebant J, Hägele T, Burger L, Serger C, Lauenstein C, Dudys P, Erdmann G, Offringa R. p38 MAPK signaling in M1 macrophages results in selective elimination of M2 macrophages by MEK inhibition. *J Immunother Cancer*. 2021;9(7). doi: 10.1136/jitc-2020-002319. PubMed PMID: 34285105; PMCID: PMC8292803.
521. Li L, Hu J, He T, Zhang Q, Yang X, Lan X, Zhang D, Mei H, Chen B, Huang Y. P38/MAPK contributes to endothelial barrier dysfunction via MAP4 phosphorylation-dependent microtubule disassembly in inflammation-induced acute lung injury. *Sci Rep*. 2015;5:8895. doi: 10.1038/srep08895. PubMed PMID: 25746230; PMCID: PMC4352893.
522. Wu T, Shi J-X, Geng S, Zhou W, Shi Y, Su X. The MK2/HuR signaling pathway regulates TNF- $\alpha$ -induced ICAM-1 expression by promoting the stabilization of ICAM-1 mRNA. *BMC pulmonary medicine*. 2016;16:1-11.
523. She Q-B, Chen N, Dong Z. ERKs and p38 kinase phosphorylate p53 protein at serine 15 in response to UV radiation. *Journal of Biological Chemistry*. 2000;275(27):20444-9.
524. Gorgoulis VG, Zacharatos P, Kotsinas A, Kletsas D, Mariatos G, Zoumpourlis V, Ryan KM, Kittas C, Papavassiliou AG. p53 activates ICAM-1 (CD54) expression in an NF- $\kappa$ B-independent manner. *The EMBO journal*. 2003.
525. Pullmann Jr R, Rabb H. HuR and other turnover-and translation-regulatory RNA-binding proteins: implications for the kidney. *American Journal of Physiology-Renal Physiology*. 2014;306(6):F569-F76.
526. Zucal C, D'Agostino V, Loffredo R, Mantelli B, Thongon N, Lal P, Latorre E, Provenzani A. Targeting the multifaceted HuR protein, benefits and caveats. *Current drug targets*. 2015;16(5):499-515.
527. Dormoy-Raclet V, Cammas A, Celona B, Lian XJ, Van Der Giessen K, Zivojnovic M, Brunelli S, Riuzzi F, Sorci G, Wilhelm BT. HuR and miR-1192 regulate myogenesis by modulating the translation of HMGB1 mRNA. *Nature communications*. 2013;4(1):2388.
528. Valdés-Ferrer SI, Papoin J, Dancho ME, Olofsson PS, Li J, Lipton JM, Avancena P, Yang H, Zou Y-R, Chavan SS. HMGB1 mediates anemia of inflammation in murine sepsis survivors. *Molecular medicine*. 2015;21:951-8.
529. Moisy D, Avilov SV, Jacob Y, Laoide BM, Ge X, Baudin F, Naffakh N, Jestin JL. HMGB1 protein binds to influenza virus nucleoprotein and promotes viral replication. *J Virol*. 2012;86(17):9122-33. Epub 20120613. doi: 10.1128/jvi.00789-12. PubMed PMID: 22696656; PMCID: PMC3416134.
530. Marchant D, Singhera GK, Utokaparch S, Hackett TL, Boyd JH, Luo Z, Si X, Dorscheid DR, McManus BM, Hegele RG. Toll-like receptor 4-mediated activation of p38 mitogen-activated protein kinase is a determinant of respiratory virus entry and tropism. *J Virol*. 2010;84:11359.
531. Börgeling Y, Schmolke M, Viemann D, Nordhoff C, Roth J, Ludwig S. Inhibition of p38 mitogen-activated protein kinase impairs influenza virus-induced primary and secondary host gene responses and protects mice from lethal H5N1 infection. *J Biol Chem*. 2014;289:13.
532. Ananieva O, Darragh J, Johansen C, Carr JM, McIlrath J, Park JM, Wingate A, Monk CE, Toth R, Santos SG. The kinases MSK1 and MSK2 act as negative regulators of Toll-like receptor signaling. *Nature immunology*. 2008;9(9):1028-36.
533. Darragh J, Ananieva O, Courtney A, Elcombe S, Arthur JSC. MSK1 regulates the transcription of IL-1ra in response to TLR activation in macrophages. *Biochemical Journal*. 2010;425(3):595-602.

534. Zhou Y, Jin X, Lv Y, Wang P, Yang Y, Liang G, Wang B, Kang Y. Early application of airway pressure release ventilation may reduce the duration of mechanical ventilation in acute respiratory distress syndrome. *Intensive care medicine*. 2017;43:1648-59.
535. Bernard GR, Luce JM, Sprung CL, Rinaldo JE, Tate RM, Sibbald WJ, Kariman K, Higgins S, Bradley R, Metz CA. High-dose corticosteroids in patients with the adult respiratory distress syndrome. *New England Journal of Medicine*. 1987;317(25):1565-70.
536. Luce JM, Montgomery AB, Marks JD, Turner J, Metz CA, Murray JF. Ineffectiveness of high-dose methylprednisolone in preventing parenchymal lung injury and improving mortality in patients with septic shock. *Am Rev Respir Dis*. 1988;138(1):62-8.
537. Dellinger RP, Zimmerman JL, Taylor RW, Straube RC, Hauser DL, Criner GJ, Davis K, Hyers TM, Papadakos P. Effects of inhaled nitric oxide in patients with acute respiratory distress syndrome: results of a randomized phase II trial. *Critical care medicine*. 1998;26(1):15-23.
538. Morris PE, Papadakos P, Russell JA, Wunderink R, Schuster DP, Truitt JD, Vincent J-L, Bernard GR. A double-blind placebo-controlled study to evaluate the safety and efficacy of L-2-oxothiazolidine-4-carboxylic acid in the treatment of patients with acute respiratory distress syndrome\*. *Critical Care Medicine*. 2008;36(3):782-8. doi: 10.1097/ccm.0b013e318164e7e4. PubMed PMID: 00003246-200803000-00017.
539. Domenighetti G, Suter PM, Schaller M-D, Ritz R, Perret C. Treatment with N-acetylcysteine during acute respiratory distress syndrome: a randomized, double-blind, placebo-controlled clinical study. *Journal of critical care*. 1997;12(4):177-82.
540. Lee JW, Fang X, Gupta N, Serikov V, Matthay MA. Allogeneic human mesenchymal stem cells for treatment of E. coli endotoxin-induced acute lung injury in the ex vivo perfused human lung. *Proceedings of the national academy of Sciences*. 2009;106(38):16357-62.
541. Tzotzos S, Fischer B, Fischer H, Pietschmann H, Lucas R, Dupré G, Lemmens-Gruber R, Hazemi P, Prymaka V, Shabbir W. AP301, a synthetic peptide mimicking the lectin-like domain of TNF, enhances amiloride-sensitive Na<sup>+</sup> current in primary dog, pig and rat alveolar type II cells. *Pulmonary pharmacology & therapeutics*. 2013;26(3):356-63.
542. Krenn K, Lucas R, Croizé A, Boehme S, Klein KU, Hermann R, Markstaller K, Ullrich R. Inhaled AP301 for treatment of pulmonary edema in mechanically ventilated patients with acute respiratory distress syndrome: a phase IIa randomized placebo-controlled trial. *Critical Care*. 2017;21(1):194. doi: 10.1186/s13054-017-1795-x.
543. Bellingan G, Maksimow M, Howell DC, Stotz M, Beale R, Beatty M, Walsh T, Binning A, Davidson A, Kuper M. The effect of intravenous interferon-beta-1a (FP-1201) on lung CD73 expression and on acute respiratory distress syndrome mortality: an open-label study. *The Lancet Respiratory Medicine*. 2014;2(2):98-107.
544. Xie T, Liang J, Liu N, Wang Q, Li Y, Noble PW, Jiang D. MicroRNA-127 inhibits lung inflammation by targeting IgG Fcγ receptor I. *The Journal of Immunology*. 2012;188(5):2437-44.
545. Lan B, Dong X, Yang Q, Luo Y, Wen H, Chen Z, Chen H. Exosomal MicroRNAs: An Emerging Important Regulator in Acute Lung Injury. *ACS Omega*. 2023;8(39):35523-37. doi: 10.1021/acsomega.3c04955.
546. Puri NM, Romano GR, Lin TY, Mai QN, Irannejad R. The organic cation transporter 2 regulates dopamine D1 receptor signaling at the Golgi apparatus. *Elife*. 2022;11. Epub 2022/04/26. doi: 10.7554/eLife.75468. PubMed PMID: 35467530; PMCID: PMC9098220.

547. Irannejad R, Tomshine JC, Tomshine JR, Chevalier M, Mahoney JP, Steyaert J, Rasmussen SG, Sunahara RK, El-Samad H, Huang B, von Zastrow M. Conformational biosensors reveal GPCR signalling from endosomes. *Nature*. 2013;495(7442):534-8. Epub 2013/03/22. doi: 10.1038/nature12000. PubMed PMID: 23515162; PMCID: PMC3835555.
548. Tsvetanova NG, von Zastrow M. Spatial encoding of cyclic AMP signaling specificity by GPCR endocytosis. *Nat Chem Biol*. 2014;10(12):1061-5. doi: 10.1038/nchembio.1665. PubMed PMID: 25362359; PMCID: PMC4232470.
549. Lu S, Ouyang M, Seong J, Zhang J, Chien S, Wang Y. The spatiotemporal pattern of Src activation at lipid rafts revealed by diffusion-corrected FRET imaging. *PLoS Comput Biol*. 2008;4(7):e1000127. Epub 2008/08/20. doi: 10.1371/journal.pcbi.1000127. PubMed PMID: 18711637; PMCID: PMC2517613.
550. Gillooly DJ, Morrow IC, Lindsay M, Gould R, Bryant NJ, Gaullier JM, Parton RG, Stenmark H. Localization of phosphatidylinositol 3-phosphate in yeast and mammalian cells. *EMBO J*. 2000;19(17):4577-88. Epub 2000/09/06. doi: 10.1093/emboj/19.17.4577. PubMed PMID: 10970851; PMCID: PMC302054.
551. Hayakawa A, Hayes SJ, Lawe DC, Sudharshan E, Tuft R, Fogarty K, Lambright D, Corvera S. Structural Basis for Endosomal Targeting by FYVE Domains \*. *Journal of Biological Chemistry*. 2004;279(7):5958-66. doi: 10.1074/jbc.M310503200.
552. Depry C, Zhang J. Using FRET-based reporters to visualize subcellular dynamics of protein kinase A activity. *Methods Mol Biol*. 2011;756:285-94. Epub 2011/08/27. doi: 10.1007/978-1-61779-160-4\_16. PubMed PMID: 21870233; PMCID: PMC4386889.
553. Sakhrani NM, Padh H. Organelle targeting: third level of drug targeting. *Drug Des Devel Ther*. 2013;7:585-99. Epub 2013/07/31. doi: 10.2147/DDDT.S45614. PubMed PMID: 23898223; PMCID: PMC3718765.
554. Lawe D, Merithew E, Dumas J, Carrington W, Fogarty K, Lifshitz L, Tuft R, Lambright D, Corvera S. Sequential Roles for Phosphatidylinositol 3-Phosphate and Rab5 in Tethering and Fusion of Early Endosomes via Their Interaction with EEA1. *The Journal of biological chemistry*. 2002;277:8611-7. doi: 10.1074/jbc.M109239200.
555. Stenmark H, Parton RG, Steele-Mortimer O, Lutcke A, Gruenberg J, Zerial M. Inhibition of rab5 GTPase activity stimulates membrane fusion in endocytosis. *EMBO J*. 1994;13(6):1287-96. Epub 1994/03/15. PubMed PMID: 8137813.
556. Roberts RL, Barbieri MA, Pryse KM, Chua M, Morisaki JH, Stahl PD. Endosome fusion in living cells overexpressing GFP-rab5. *J Cell Sci*. 1999;112 ( Pt 21):3667-75. Epub 1999/10/19. PubMed PMID: 10523503.
557. Enslin H, Raingeaud J, Davis RJ. Selective activation of p38 mitogen-activated protein (MAP) kinase isoforms by the MAP kinase kinases MKK3 and MKK6. *J Biol Chem*. 1998;273(3):1741-8. Epub 1998/01/27. doi: 10.1074/jbc.273.3.1741. PubMed PMID: 9430721.
558. Chen B, Dores MR, Grimsey N, Canto I, Barker BL, Trejo J. Adaptor protein complex-2 (AP-2) and epsin-1 mediate protease-activated receptor-1 internalization via phosphorylation- and ubiquitination-dependent sorting signals. *J Biol Chem*. 2011;286(47):40760-70. Epub 2011/10/04. doi: [M111.299776 \[pii\]](https://doi.org/10.1074/jbc.M111.299776) 10.1074/jbc.M111.299776. PubMed PMID: 21965661.
559. Paing MM, Stutts AB, Kohout TA, Lefkowitz RJ, Trejo J. beta -Arrestins regulate protease-activated receptor-1 desensitization but not internalization or Down-regulation. *J Biol Chem*. 2002;277(2):1292-300. Epub 2001/11/06. doi: 10.1074/jbc.M109160200

M109160200 [pii]. PubMed PMID: 11694535.

560. Paing MM, Temple BR, Trejo J. A tyrosine-based sorting signal regulates intracellular trafficking of protease-activated receptor-1: multiple regulatory mechanisms for agonist-induced G protein-coupled receptor internalization. *J Biol Chem*. 2004;279(21):21938-47. Epub 2004/03/17. doi: 10.1074/jbc.M401672200

M401672200 [pii]. PubMed PMID: 15023990.

561. LaCroix R, Lin B, Kang T-Y, Levchenko A. Complex effects of kinase localization revealed by compartment-specific regulation of protein kinase A activity. *eLife*. 2022;11:e66869. doi: 10.7554/eLife.66869.

562. Schmitt DL, Curtis SD, Lyons AC, Zhang J-f, Chen M, He CY, Mehta S, Shaw RJ, Zhang J. Spatial regulation of AMPK signaling revealed by a sensitive kinase activity reporter. *Nature Communications*. 2022;13(1):3856. doi: 10.1038/s41467-022-31190-x.

563. Paing MM, Johnston CA, Siderovski DP, Trejo J. Clathrin adaptor AP2 regulates thrombin receptor constitutive internalization and endothelial cell resensitization. *Mol Cell Biol*. 2006;26(8):3231-42. Epub 2006/04/04. doi: 26/8/3231 [pii] 10.1128/MCB.26.8.3231-3242.2006. PubMed PMID: 16581796.

564. Shearer LJ, Petersen NO. Distribution and Co-localization of endosome markers in cells. *Heliyon*. 2019;5(9):e02375. doi: <https://doi.org/10.1016/j.heliyon.2019.e02375>.

565. Bucci C, Parton RG, Mather IH, Stunnenberg H, Simons K, Hoflack B, Zerial M. The small GTPase rab5 functions as a regulatory factor in the early endocytic pathway. *Cell*. 1992;70(5):715-28. doi: [https://doi.org/10.1016/0092-8674\(92\)90306-W](https://doi.org/10.1016/0092-8674(92)90306-W).

566. Kunselman JM, Zajac AS, Weinberg ZY, Puthenveedu MA. Homologous Regulation of Mu Opioid Receptor Recycling by G ( $\beta\gamma$ ), Protein Kinase C, and Receptor Phosphorylation. *Mol Pharmacol*. 2019;96(6):702-10. Epub 20191001. doi: 10.1124/mol.119.117267. PubMed PMID: 31575621; PMCID: PMC6820217.

567. Sposini S, De Pascali F, Richardson R, Sayers NS, Perrais D, Yu HN, Palmer S, Nataraja S, Reiter E, Hanyaloglu AC. Pharmacological Programming of Endosomal Signaling Activated by Small Molecule Ligands of the Follicle Stimulating Hormone Receptor. *Frontiers in Pharmacology*. 2020;11. doi: 10.3389/fphar.2020.593492.

568. Cargnello M, Roux PP. Activation and function of the MAPKs and their substrates, the MAPK-activated protein kinases. *Microbiol Mol Biol Rev*. 2011;75(1):50-83. doi: 10.1128/mmbr.00031-10. PubMed PMID: 21372320; PMCID: PMC3063353.

569. Faust D, Schmitt C, Oesch F, Oesch-Bartlomowicz B, Schreck I, Weiss C, Dietrich C. Differential p38-dependent signalling in response to cellular stress and mitogenic stimulation in fibroblasts. *Cell Commun Signal*. 2012;10:6. Epub 20120309. doi: 10.1186/1478-811x-10-6. PubMed PMID: 22404972; PMCID: PMC3352310.

570. Lin Y, Wozniak JM, Grimsey NJ, Girada S, Patwardhan A, Molinar-Inglis O, Smith TH, Lapek JD, Gonzalez DJ, Trejo J. Phosphoproteomic analysis of protease-activated receptor-1 biased signaling reveals unique modulators of endothelial barrier function. *Proc Natl Acad Sci U S A*. 2020;117(9):5039-48. Epub 2020/02/20. doi: 10.1073/pnas.1917295117. PubMed PMID: 32071217; PMCID: PMC7060683.

571. Rada CC, Mejia-Pena H, Grimsey NJ, Canto Cordova I, Olson J, Wozniak JM, Gonzalez DJ, Nizet V, Trejo J. Heat shock protein 27 activity is linked to endothelial barrier recovery after proinflammatory GPCR-induced disruption. *Sci Signal*. 2021;14(698):eabc1044. Epub 2021/09/14. doi: 10.1126/scisignal.abc1044. PubMed PMID: 34516752.

572. Kroeze WK, Sassano MF, Huang XP, Lansu K, McCorvy JD, Giguère PM, Sciaky N, Roth BL. PRESTO-Tango as an open-source resource for interrogation of the druggable human GPCRome. *Nat Struct Mol Biol.* 2015;22(5):362-9. Epub 20150420. doi: 10.1038/nsmb.3014. PubMed PMID: 25895059; PMCID: PMC4424118.
573. Dores MR, Paing MM, Lin H, Montagne WA, Marchese A, Trejo J. AP-3 regulates PAR1 ubiquitin-independent MVB/lysosomal sorting via an ALIX-mediated pathway. *Mol Biol Cell.* 2012. Epub 2012/07/27. doi: [mbc.E12-03-0251 \[pii\]](https://doi.org/10.1091/mbc.E12-03-0251) 10.1091/mbc.E12-03-0251. PubMed PMID: 22833563.
574. Marchese A, Raiborg C, Santini F, Keen JH, Stenmark H, Benovic JL. The E3 ubiquitin ligase AIP4 mediates ubiquitination and sorting of the G protein-coupled receptor CXCR4. *Dev Cell.* 2003;5(5):709-22. PubMed PMID: 14602072.
575. Sheu C-C, Gong MN, Zhai R, Bajwa EK, Chen F, Taylor Thompson B, Christiani DC. The influence of infection sites on development and mortality of ARDS. *Intensive care medicine.* 2010;36:963-70.
576. Klomp M, Ghosh S, Mohammed S, Nadeem Khan M. From virus to inflammation, how influenza promotes lung damage. *J Leukoc Biol.* 2021;110(1):115-22. Epub 20200908. doi: 10.1002/jlb.4ru0820-232r. PubMed PMID: 32895987; PMCID: PMC7937770.
577. Zhu W, Zhang Y, Wang Y. Immunotherapy strategies and prospects for acute lung injury: Focus on immune cells and cytokines. *Front Pharmacol.* 2022;13:1103309. Epub 20221222. doi: 10.3389/fphar.2022.1103309. PubMed PMID: 36618910; PMCID: PMC9815466.
578. Pillaiyar T, Laufer S. Kinases as Potential Therapeutic Targets for Anti-coronaviral Therapy. *Journal of Medicinal Chemistry.* 2022;65(2):955-82. doi: 10.1021/acs.jmedchem.1c00335.
579. Al Hamrashdi M, Brady G. Regulation of IRF3 activation in human antiviral signaling pathways. *Biochemical Pharmacology.* 2022;200:115026. doi: <https://doi.org/10.1016/j.bcp.2022.115026>.
580. Fajgenbaum DC, June CH. Cytokine storm. *New England Journal of Medicine.* 2020;383(23):2255-73.
581. Ramadass V, Vaiyapuri T, Tergaonkar V. Small molecule NF- $\kappa$ B pathway inhibitors in clinic. *International journal of molecular sciences.* 2020;21(14):5164.
582. Bai X-z, Fan L, He T, Jia W, Yang L, Zhang J, Liu Y, Shi J, Su L, Hu D. SIRT1 protects rat lung tissue against severe burn-induced remote ALI by attenuating the apoptosis of PMVECs via p38 MAPK signaling. *Scientific Reports.* 2015;5.
583. Li LB, Leung DY, Goleva E. Activated p38 MAPK in Peripheral Blood Monocytes of Steroid Resistant Asthmatics. *PLoS One.* 2015;10(10):e0141909. Epub 2015/10/31. doi: 10.1371/journal.pone.0141909. PubMed PMID: 26517722; PMCID: PMC4627650.
584. Abraham E. Neutrophils and acute lung injury. *Crit Care Med.* 2003;31(4 Suppl):S195-9. Epub 2003/04/12. doi: 10.1097/01.Ccm.0000057843.47705.E8. PubMed PMID: 12682440.
585. Kim SR, Lee KS, Park SJ, Jeon MS, Lee YC. Inhibition of p38 MAPK reduces expression of vascular endothelial growth factor in allergic airway disease. *J Clin Immunol.* 2012;32(3):574-86. Epub 2012/03/01. doi: 10.1007/s10875-012-9672-5. PubMed PMID: 22362129.

586. Nagy Z, Comer S, Smolenski A. Analysis of Protein Phosphorylation Using Phos-Tag Gels. *Curr Protoc Protein Sci.* 2018;93(1):e64. Epub 20180725. doi: 10.1002/cpps.64. PubMed PMID: 30044546.
587. Lee N, Wong CK, Chan PKS, Lun SWM, Lui G, Wong B, Hui DSC, Lam CWK, Cockram CS, Choi KW, Yeung ACM, Tang JW, Sung JJY. Hypercytokinemia and Hyperactivation of Phospho-p38 Mitogen-Activated Protein Kinase in Severe Human Influenza A Virus Infection. *Clinical Infectious Diseases.* 2007;45(6):723-31. doi: 10.1086/520981.
588. Kopecky-Bromberg SA, Martinez-Sobrido L, Palese P. 7a Protein of severe acute respiratory syndrome coronavirus inhibits cellular protein synthesis and activates p38 mitogen-activated protein kinase. *J Virol.* 2006;80:785.
589. Beyaert R, Cuenda A, Vanden Berghe W, Plaisance S, Lee JC, Haegeman G, Cohen P, Fiers W. The p38/RK mitogen-activated protein kinase pathway regulates interleukin-6 synthesis response to tumor necrosis factor. *The EMBO journal.* 1996;15(8):1914-23.
590. Singh RK, Najmi AK, Dastidar SG. Biological functions and role of mitogen-activated protein kinase activated protein kinase 2 (MK2) in inflammatory diseases. *Pharmacol Rep.* 2017;69(4):746-56. Epub 20170408. doi: 10.1016/j.pharep.2017.03.023. PubMed PMID: 28582691.
591. Burton JC, Royer F, Grimsey NJ. Spatiotemporal control of kinases and the biomolecular tools to trace activity. *Journal of Biological Chemistry.* doi: 10.1016/j.jbc.2024.107846.
592. Faist A, Schloer S, Mecate-Zambrano A, Janowski J, Schreiber A, Boergeling Y, Conrad BCG, Kumar S, Toebben L, Schughart K, Baumgardt M, Kessler M, Hoenzke K, Hocke A, Trautmann M, Hartmann W, Kato H, Rescher U, Christersson A, Kuehn J, Mellmann A, Wolff T, Kuempers P, Rovas A, Wiewrodt R, Wiebe K, Barth P, Ludwig S, Brunotte L. Inhibition of p38 signaling curtails the SARS-CoV-2 induced inflammatory response but retains the IFN-dependent antiviral defense of the lung epithelial barrier. *Antiviral Res.* 2023;209:105475. Epub 20221121. doi: 10.1016/j.antiviral.2022.105475. PubMed PMID: 36423831; PMCID: PMC9677559.
593. Yang S, Wang L, Pan X, Liang Y, Zhang Y, Li J, Zhou B. 5-Methoxyflavone-induced AMPK $\alpha$  activation inhibits NF- $\kappa$ B and P38 MAPK signaling to attenuate influenza A virus-mediated inflammation and lung injury in vitro and in vivo. *Cell Mol Biol Lett.* 2022;27(1):82. Epub 20220930. doi: 10.1186/s11658-022-00381-1. PubMed PMID: 36180831; PMCID: PMC9524045.
594. Hall DJ, Bates ME, Guar L, Cronan M, Korpi N, Bertics PJ. The role of p38 MAPK in rhinovirus-induced monocyte chemoattractant protein-1 production by monocytic-lineage cells. *J Immunol.* 2005;174(12):8056-63. doi: 10.4049/jimmunol.174.12.8056. PubMed PMID: 15944313.
595. Aegerter H, Kulikauskaite J, Crotta S, Patel H, Kelly G, Hessel EM, Mack M, Beinke S, Wack A. Influenza-induced monocyte-derived alveolar macrophages confer prolonged antibacterial protection. *Nat Immunol.* 2020;21(2):145-57. Epub 20200113. doi: 10.1038/s41590-019-0568-x. PubMed PMID: 31932810; PMCID: PMC6983324.
596. Ursin RL, Klein SL. Sex Differences in Respiratory Viral Pathogenesis and Treatments. *Annual Review of Virology.* 2021;8(Volume 8, 2021):393-414. doi: <https://doi.org/10.1146/annurev-virology-091919-092720>.
597. Lorenzo ME, Hodgson A, Robinson DP, Kaplan JB, Pekosz A, Klein SL. Antibody responses and cross protection against lethal influenza A viruses differ between the sexes in

- C57BL/6 mice. *Vaccine*. 2011;29(49):9246-55. doi: <https://doi.org/10.1016/j.vaccine.2011.09.110>.
598. Larcombe AN, Foong RE, Bozanich EM, Berry LJ, Garratt LW, Gualano RC, Jones JE, Dousha LF, Zosky GR, Sly PD. Sexual dimorphism in lung function responses to acute influenza A infection. *Influenza and Other Respiratory Viruses*. 2011;5(5):334-42. doi: <https://doi.org/10.1111/j.1750-2659.2011.00236.x>.
599. Latha K, Jamison KF, Watford WT. Tpl2 Ablation Leads to Hypercytokinemia and Excessive Cellular Infiltration to the Lungs During Late Stages of Influenza Infection. *Front Immunol*. 2021;12:738490. Epub 20211007. doi: 10.3389/fimmu.2021.738490. PubMed PMID: 34691044; PMCID: PMC8529111.
600. Schmitt DL, Mehta S, Zhang J. Study of spatiotemporal regulation of kinase signaling using genetically encodable molecular tools. *Current Opinion in Chemical Biology*. 2022;71:102224. doi: <https://doi.org/10.1016/j.cbpa.2022.102224>.
601. Hellweg L, Edenhofer A, Barck L, Huppertz M-C, Frei MS, Tarnawski M, Bergner A, Koch B, Johnsson K, Hiblot J. A general method for the development of multicolor biosensors with large dynamic ranges. *Nature Chemical Biology*. 2023;19(9):1147-57. doi: 10.1038/s41589-023-01350-1.
602. Li L, Gao G, Shankar J, Joshi B, Foster LJ, Nabi IR. p38 MAP kinase–dependent phosphorylation of the Gp78 E3 ubiquitin ligase controls ER–mitochondria association and mitochondria motility. *Molecular Biology of the Cell*. 2015;26(21):3828-40. doi: 10.1091/mbc.E15-02-0120. PubMed PMID: 26337390.
603. Cheng N, Trejo J. An siRNA library screen identifies CYLD and USP34 as deubiquitinases that regulate GPCR-p38 MAPK signaling and distinct inflammatory responses. *Journal of Biological Chemistry*. 2023;299(12):105370. doi: <https://doi.org/10.1016/j.jbc.2023.105370>.
604. Qiao J, Huang F, Lum H. PKA inhibits RhoA activation: a protection mechanism against endothelial barrier dysfunction. *American Journal of Physiology-Lung Cellular and Molecular Physiology*. 2003;284(6):L972-L80.
605. Aslam M, Härtel FV, Arshad M, Gündüz D, Abdallah Y, Sauer H, Piper HM, Noll T. cAMP/PKA antagonizes thrombin-induced inactivation of endothelial myosin light chain phosphatase: role of CPI-17. *Cardiovascular research*. 2010;87(2):375-84.
606. Xie L, Chiang ET, Wu X, Kelly GT, Kanteti P, Singleton PA, Camp SM, Zhou T, Dudek SM, Natarajan V. Regulation of thrombin-induced lung endothelial cell barrier disruption by protein kinase C delta. *PloS one*. 2016;11(7):e0158865.
607. Molinar-Inglis O, Wozniak JM, Grimsey NJ, Orduña-Castillo L, Cheng N, Lin Y, Gonzalez Ramirez ML, Birch CA, Lapek JD, Gonzalez DJ, Trejo J. Phosphoproteomic analysis of thrombin- and p38 MAPK-regulated signaling networks in endothelial cells. *Journal of Biological Chemistry*. doi: 10.1016/j.jbc.2022.101801.
608. Schulte D, Küppers V, Dartsch N, Broermann A, Li H, Zarbock A, Kamenyeva O, Kiefer F, Khandoga A, Massberg S, Vestweber D. Stabilizing the VE-cadherin–catenin complex blocks leukocyte extravasation and vascular permeability. *The EMBO Journal*. 2011;30(20):4157-70. doi: <https://doi.org/10.1038/emboj.2011.304>.
609. Klein SL. The effects of hormones on sex differences in infection: from genes to behavior. *Neuroscience & Biobehavioral Reviews*. 2000;24(6):627-38.

610. Grossman C. Possible underlying mechanisms of sexual dimorphism in the immune response, fact and hypothesis. *Journal of steroid biochemistry*. 1989;34(1-6):241-51.
611. Verthelyi D. Sex hormones as immunomodulators in health and disease. *International immunopharmacology*. 2001;1(6):983-93.
612. Jacobsen H, Klein SL. Sex Differences in Immunity to Viral Infections. *Frontiers in Immunology*. 2021;12. doi: 10.3389/fimmu.2021.720952.
613. Reizis B. Plasmacytoid Dendritic Cells: Development, Regulation, and Function. *Immunity*. 2019;50(1):37-50. doi: 10.1016/j.immuni.2018.12.027. PubMed PMID: 30650380; PMCID: PMC6342491.
614. Hagen SH, Henseling F, Hennesen J, Savel H, Delahaye S, Richert L, Ziegler SM, Altfeld M. Heterogeneous escape from X chromosome inactivation results in sex differences in type I IFN responses at the single human pDC level. *Cell reports*. 2020;33(10).
615. Liu D, Zhong Z, Karin M. NF- $\kappa$ B: A Double-Edged Sword Controlling Inflammation. *Biomedicines*. 2022;10(6):1250. PubMed PMID: doi:10.3390/biomedicines10061250.
616. Haller V, Nahidino P, Forster M, Laufer SA. An updated patent review of p38 MAP kinase inhibitors (2014-2019). *Expert Opin Ther Pat*. 2020;30(6):453-66. Epub 2020/04/02. doi: 10.1080/13543776.2020.1749263. PubMed PMID: 32228113.
617. González L, Díaz L, Pous J, Baginski B, Duran-Corbera A, Scarpa M, Brun-Heath I, Igea A, Martin-Malpartida P, Ruiz L, Pallara C, Esguerra M, Colizzi F, Mayor-Ruiz C, Biondi RM, Soliva R, Macias MJ, Orozco M, Nebreda AR. Characterization of p38 $\alpha$  autophosphorylation inhibitors that target the non-canonical activation pathway. *Nature Communications*. 2023;14(1):3318. doi: 10.1038/s41467-023-39051-x.
618. Liu X, Li M, Woo S. Subcellular Drug Distribution: Exploring Organelle-Specific Characteristics for Enhanced Therapeutic Efficacy. *Pharmaceutics*. 2024;16(9). Epub 20240904. doi: 10.3390/pharmaceutics16091167. PubMed PMID: 39339204; PMCID: PMC11434838.
619. Vohwinkel CU, Hoegl S, Eltzhig HK. Hypoxia signaling during acute lung injury. *Journal of Applied Physiology*. 2015;119(10):1157-63. doi: 10.1152/jappphysiol.00226.2015. PubMed PMID: 25977449.
620. Carty M, Guy C, Bowie AG. Detection of Viral Infections by Innate Immunity. *Biochemical Pharmacology*. 2021;183:114316. doi: <https://doi.org/10.1016/j.bcp.2020.114316>.
621. Cury J, Haudiquet M, Hernandez Trejo V, Mordret E, Hanouna A, Rotival M, Tesson F, Bonhomme D, Ofir G, Quintana-Murci L, Benaroch P, Poirier EZ, Bernheim A. Conservation of antiviral systems across domains of life reveals immune genes in humans. *Cell Host & Microbe*. 2024;32(9):1594-607.e5. doi: 10.1016/j.chom.2024.08.002.
622. Weber F. Antiviral innate immunity: introduction. *Encyclopedia of virology*. 2021:577.
623. Li J, Jie X, Liang X, Chen Z, Xie P, Pan X, Zhou B, Li J. Sinensetin suppresses influenza a virus-triggered inflammation through inhibition of NF- $\kappa$ B and MAPKs signalings. *BMC Complementary Medicine and Therapies*. 2020;20(1):135. doi: 10.1186/s12906-020-02918-3.
624. Ruan T, Sun Y, Zhang J, Sun J, Liu W, Prinz RA, Peng D, Liu X, Xu X. H5N1 infection impairs the alveolar epithelial barrier through intercellular junction proteins via Itch-mediated proteasomal degradation. *Communications Biology*. 2022;5(1):186. doi: 10.1038/s42003-022-03131-3.
625. van Riel D, den Bakker MA, Leijten LM, Chutinimitkul S, Munster VJ, de Wit E, Rimmelzwaan GF, Fouchier RA, Osterhaus AD, Kuiken T. Seasonal and pandemic human

- influenza viruses attach better to human upper respiratory tract epithelium than avian influenza viruses. *The American journal of pathology*. 2010;176(4):1614-8.
626. Nicholls J, Chan M, Chan W, Wong H, Cheung C, Kwong D, Wong M, Chui W, Poon L, Tsao S. Tropism of avian influenza A (H5N1) in the upper and lower respiratory tract. *Nature medicine*. 2007;13(2):147-9.
627. van Riel D, Munster VJ, de Wit E, Rimmelzwaan GF, Fouchier RA, Osterhaus AD, Kuiken T. H5N1 Virus Attachment to Lower Respiratory Tract. *Science*. 2006;312(5772):399. Epub 20060323. doi: 10.1126/science.1125548. PubMed PMID: 16556800.
628. Hui KP, Ho JC, Cheung M-c, Ng K-c, Ching RH, Lai K-l, Kam TT, Gu H, Sit K-Y, Hsin MK. SARS-CoV-2 Omicron variant replication in human bronchus and lung ex vivo. *Nature*. 2022;603(7902):715-20.
629. Busch CJ, Favret J, Geirsdóttir L, Molawi K, Sieweke MH. Isolation and Long-term Cultivation of Mouse Alveolar Macrophages. *Bio Protoc*. 2019;9(14). doi: 10.21769/BioProtoc.3302. PubMed PMID: 31909091; PMCID: PMC6944498.
630. Wang J, Niu N, Xu S, Jin ZG. A simple protocol for isolating mouse lung endothelial cells. *Scientific Reports*. 2019;9(1):1458. doi: 10.1038/s41598-018-37130-4.

## APPENDIX

### STANDARD LABORATORY METHODOLOGIES

1.1 Key Solutions Used in FRET Microscopy.....	209
1.2 General FRET Assay .....	211
1.3 Procedure for Neon Electroporation Transfection.....	214
1.4 cDNA Synthesis from mRNA and qPCR.....	216
1.5 General Immunoprecipitation Protocol.....	223
1.6 General Immunoblotting Protocol .....	228
2.1 Key Solutions Used in Mouse Experiments .....	233
2.2 Mouse Colony Maintenance .....	235
2.3 Genotyping TAB1-KI C57BL6 Mice.....	240
2.4 Intratracheal Injection of LPS.....	246
2.5 Lung Extraction for OCT Embedding and Cryostat Sectioning.....	250
2.6 Collection of Lung Homogenate Samples .....	253
2.7 Collection of Bronchoalveolar Lavage.....	255
2.8 Cytokine Panel.....	258

## 1.1 Key Solutions Used In FRET Microscopy:

FRET HBSS Imaging Buffer (50 mL aliquot):

Make fresh each time (does not keep well, even at 4°C)

- 40 mL MilliQ H<sub>2</sub>O
- 5 mL (10x) HBSS (Gibco, 14065-056)
- 1 mL 1M HEPES (20 mM final)
- 100 mg alpha-D-glucose (2 g/L final)
- 115  $\mu$ L 100mM Sodium Pyruvate (0.23 mM final) (Corning 25-000-CI)
  - Optional: 50  $\mu$ L 1M CaCl<sub>2</sub> (1 mM final)
- pH to 7.4 with NaOH 0.5M (appx. 28 drops from Pasteur pipet)
- Top to 50 mL with MilliQ H<sub>2</sub>O

Cells should be stable on FRET buffer for hours. Allow cells to acclimate for ~1H prior to imaging. Allow cells to acclimate to scope conditions for ~10 minutes prior to experimental image capture.

For NaCl used in FRET experiments:

87.6 mg NaCl dissolved into 5 mL FRET buffer for a 2x stock (450 mM NaCl, will be final of 300 mM when diluted 1:1). Keep an aliquot of NaCl 2x solution in the incubation chamber until time of use. Remove  $\frac{1}{2}$  media (750  $\mu$ L) from plate, replace with 750  $\mu$ L NaCl 2x.

For GPCR agonists (Thrombin) used in FRET experiments:

Stock diluted to 1 $\mu$ M (100x). 15  $\mu$ L of 100x stock kept on ice until time of stim. 100x stock diluted in 750  $\mu$ L warm imaging buffer from plate and entire volume added back to the cells.

For SB (or DMSO control) used in FRET experiments:

Dilute 10 mM stock SB in DMSO to 1 mM (for DMSO control, just add 5  $\mu$ l DMSO to 45  $\mu$ l FRET buffer.) Add 7.5  $\mu$ l of this working dilution to a separate tube. At time of use, pull off media from plate, dilute into tube, and add back all volume to plate.

For Starvation buffer (used for 48h transfection FRET experiments):

50  $\mu$ l 1M CaCl (1mM final), 500  $\mu$ l HEPES (10 mM final), 50 mg BSA (1 mg/mL) fill to 50 mL with phenol-red free DMEM. Filter with 0.2  $\mu$ M.

## 1.2 General FRET Assay

Experiments designed for 48H expression of plasmids, but can be adjusted for 24 of expression.

Simply perform PEI transfection and seed cells into plates containing Starvation buffer rather than full media.

Materials:

10% FBS in DMEM

Trypsin EDTA (0.25%)

OptiMem

BSA starvation buffer

Fibronectin 8.33ug/mL stock

Ibitreat u-dish 35mM (Ibidi)

PEI (freshly thawed)

Plasmid DNA

### Day 1: Transfection

- 1) Coat Ibidi plates with fibronectin
  - a) Stock 8.33ug/mL, add 1.5-2 mL per plate
  - b) Save fibronectin for 2 uses
- 2) Prepare OptiMem/PEI aliquot in 1.5mL tube, according to table 1
  - a) Incubate for 10 minutes at RT
  - b) Add PEI directly to OptiMem, not side of tube
  - c) Mix well

- 3) While OptiMem/PEI incubating, Ready DNA dilution aliquot in OptiMem according to instructions below
  - a) 270 ng/plate of GPCR is standard.
  - b) 972/plate ng of activity reporter is standard “1X”. NES-p38 uses “1X”, typically use other reporters at “1.5X” but can be adjusted to preference.
  - c) Typically reserve 20% of total OptiMem volume needed for DNA, with PEI/OptiMem incubating using 80% of total OptiMem volume
  - d) Mix well
- 4) While OptiMem/PEI incubating, trypsinize cells and spin down
  - a) 1000 rpm, 4 minutes
- 5) Combine DNA dilution aliquot and PEI aliquot. Let incubate at least 20 minutes at RT.
- 6) Count cells according to specification
  - a) 321k/35mm dish (48H expression)
- 7) Add DNA+PEI aliquot to cells (in full media for 48h transfection)
  - a) Mix well
- 8) Seed 2200uL per plate (2000 for cells + 200uL of DNA/PEI in OptiMem)

Transfection information:

**Day 2: switch to starvation buffer**

**Day 3: Imaging**

1. Wash cells and swap to fresh pre-warmed FRET buffer

Incubate ~40 minutes in FRET buffer before taking down to scope

2. Turn on scope while cells incubate in FRET buffer
  - a. Make sure incubator chamber is on and working, and that CO<sub>2</sub> is turned on
  - b. Check CO<sub>2</sub> calibration every 6 months
3. Place plate on incubation chamber and set up experimental conditions
  - a. Cells should be acclimated to incubator chamber for ~10 minutes prior to experimental image acquisition
4. Draw no more than 5 ROIs around live cells when doing live-imaging. Draw most ROIs after image acquisition is complete.
5. Adjust FRET channel intensity on example cells at baseline prior to stimulation with agonist until FRET ratio is between 0.9 and 1.4.
6. When stimulating with agonist, pause experiment and use both hands to steady pipet, avoid touching the plate itself.
7. When un-pausing software to resume image acquisition, do not click un-pause more than once. Sometimes the system lags, but multiple clicks can crash Zen-blue.

### **1.3 Procedure for Neon Electroporation Transfection**

Utilizing Neon Transfection System (Invitrogen MPK5000) to transfect Human Pulmonary Microvascular Endothelial Cells (HPMEC) with activity reporter plasmids.

Protocol adapted from kit protocol.

#### **General notes:**

- Protocol developed using the 10  $\mu$ L pipette system and Ibidi multi-well chambers coated in 5 $\mu$ g/cm<sup>2</sup> collagen.
- Do not use media containing antibiotics. After electroporation, move the cells as little as possible to avoid unnecessary cell stress.
- HPMEC cells best electroporated between passages 1-4.

#### **Protocol:**

1. Wash cells with excess 1X PBS, 2 washes
2. Trypsinize cells with 0.05% T/E buffer diluted from 0.25% stock solution using PBS (2 mL stock, + 8 mL PBS)
  - a. Do not trypsinize for longer than 3 minutes total, check every minute for cells to lift off of plate
  - b. Neutralize with trypsin neutralization solution or full media, collect cells in 15 mL tube
3. While trypsinizing, add 5 mL complete media to 50mL conical tube, coating sides of tube
4. Check flask, if cells rounded up, collect excess media into 50 mL conical
5. Incubate empty flask/plate for 1 minute, rap flask gently to dislodge remaining cells

6. Wash flask/plate with 5 mL TNS, collect into 50mL conical with other collected media+cells
7. Wash plate 1 more time with 5 mL PBS (Final volume should be ~25 mL)
8. Split cells so that there are cells for seeding maintenance and cells for experiment, be mindful of seeding densities required for healthy HPMEC subculture
  - a. A T75 flask yields about 1.2 million HPMECs
9. Add maintenance fraction to pre-blocked 15 mL tube
10. Spin down both populations of cells at 200 RCF for 5 minutes
11. Aspirate media
12. Seed maintenance plate at desired density
13. Resuspend experimental cells in 2mL RT PBS, move to 2 mL microcentrifuge tube.
14. Count 10  $\mu$ l of cells using hemocytometer
15. Spin down again for 5 minutes at 100rcf on benchtop microcentrifuge
16. Carefully aspirate PBS with p1000, use p200 for small remaining volume, do not disturb pellet
17. Resuspend cell pellet in "R" buffer to achieve working concentration (typically go for 150k cells/10  $\mu$ l)
18. Place plasmid DNA at desired amount into clean sterile microcentrifuge tube
19. Add in cells diluted to concentration needed, and account for extra (10uL needed for each electroporation)
20. Electroporate cells (HPMECs at 20 ms, 1400V, 2 pulses) and apply directly to warmed final media in plate (500  $\mu$ l complete media without antibiotics) + Revitacell media supplement at product specifications, to help cell recovery

## **1.4 cDNA Synthesis from mRNA for SYBR-Green qPCR**

Protocol developed for quantification of M Protein expression in mouse lung homogenate infected with Influenza A Virus, but adaptable for other sample types and probes.

Protocol Overview:

1. Isolate mRNA from Samples
2. Convert control mRNA to cDNA
3. Prepare and run SYBR-green qPCR

### **Protocol:**

#### **Isolate mRNA from Samples:**

Following the E.Z.N.A. Total RNA Kit 1 Protocol with modifications

Note: Samples are lysed into TRK + BME buffer prior to mRNA isolation.

Note: Samples should be treated in RNase-free conditions

1. Thaw RNA lysate samples on ice
2. Centrifuge at maximum speed (> 12,000g) for 5 minutes
3. Transfer cleared supernatant to clean 1.5 mL microcentrifuge tube. Careful not to transfer any fatty upper layer.
4. Insert Hi-Bind RNA mini column into 2 mL collection tube
5. Transfer up to 700  $\mu$ l sample into Hi-Bind RNA Mini Column
6. Centrifuge 10,000g for 1 minute. Discard the filtrate and reuse collection tube.
7. Repeat step 5-6 until samples have been transferred (should not take more than 1 step for our volumes)

8. Add 500  $\mu$ l RNA wash buffer 1. Centrifuge 10,000g for 30 seconds. Discard filtrate, reuse collection tube
9. Add 500  $\mu$ l RNA Wash Buffer 2 diluted with 100% ethanol. Centrifuge at 10,000g for 1 minute. Discard filtrate and reuse collection tube.
10. Repeat step 9 for second RNA Wash Buffer 2 wash step.
11. Centrifuge empty Hi-Bind RNA Mini Column at maximum speed for 2 minutes to dry column. This step is critical for removal of trace ethanol that may interfere with downstream applications
12. Add 40-70  $\mu$ l Nuclease-free Water. Centrifuge at maximum speed for 2 minutes. Store on ice, quantify using nanodrop, and make dilutions as necessary. Store eluted mRNA at -80°C or proceed to cDNA conversion.

### **Convert mRNA to cDNA**

Using Bio-rad iScript™ cDNA Synthesis Kit:

1. Calculate total number of samples to be converted, account for extra
2. Multiply number of samples by table below to calculate master mix needed
3. Add components of master mix (iScript mix, reverse transcriptase, and water)
4. Add master mix to PCR tubes
5. Add mRNA to each tube
6. Incubate reaction in thermal cycler (see below)

Note: You can modify total reaction volume to save reagent if you need less than 1  $\mu$ g of cDNA.

Reaction works well when volumes and amounts are halved to 10  $\mu$ l total.

Note: For downstream PCR, prepare a 1:10 dilution (10ul of cDNA + 90 ul nuclease-free water **NOT** DEPC), use 4  $\mu$ l (20ng/ PCR reaction if 1ug of RNA was used) for RT-PCR or quantitative RT-PCR.

iScript 20  $\mu$ l reaction:

<b>5x iScript Reaction Mix</b>	4 $\mu$ l
<b>iScript reverse transcriptase</b>	1 $\mu$ l
<b>mRNA 1 <math>\mu</math>g</b>	Volume for up to 1 $\mu$ g of mRNA
<b>H2O</b>	To make total volume 20 $\mu$ l

Thermal cycler settings:

5 min	25°C
20 min	46°C
1 min	95°C

Hold at 12° C (optional)

### Prepare and run SYBR-green qPCR

Protocol developed for QuantaBio PerfeCTA SYBR green Fastmix.

1. Calculate number of wells needed (samples typically run in duplicate, plus positive and negative controls) per mRNA species of interest, with 3-4 extra wells
2. If starting with stock cDNA, dilute 1:10 with nuclease-free water (20 ng total cDNA per well)

- a. Spin-mix-spin each cDNA before use
3. Keeping all components of kit on ice, prepare master mix containing SYBR green, Nuclease-free DEPC Free water, and primer mix (see below).
4. Add 16  $\mu$ l master mix to each well of 96 well plate (use reverse pipetting)
5. Add sample-specific cDNA to each well of 96 well plate (use reverse pipetting)
  - a. Place droplet of cDNA onto wall of tube, plate will be spun-down later
  - b. Use these specific plates: VWR 89049-178, PCR plate, 96 well Half-skirted, straight-side.
6. Apply plastic seal to lid of plate
  - a. VWR 60941-078 Adhesive Film for PCR plates
7. Spin plate down in plate centrifuge by holding the quick-spin button down until speed reaches maximum, hold for 20 seconds then release
8. Check to make sure all liquid has pooled at bottom of wells
9. Take plate to qPCR machine
  - a. If there is a delay or a wait for machine, wrap the plate in aluminum foil to protect from light and store on ice. If plate must be run next-day, place in freezer overnight and then replace plastic seal before running assay

20 µl reaction/well for a 96-well plate:

Used PerfeCTA SYBR-green

2 x SYBR green	10 µl
5 µM Mix of F primer and R primer	2 µl (500 nM final)
Nuclease-free, DEPC free H <sub>2</sub> O	5 µl
cDNA	4 µl ( 20ng )

Primer Preparation:

Primers reconstituted in Nuclease-Free water (100uM stock) and aliquoted into 100uL aliquots.

5uM dilution made by 1:20 dilution in nuclease free water.

Primers used for assessment of M Protein, designed by Grimsey lab using IDT Primer Designer tools:

eEF1a1\_f 5' TCC CTG TGG AAA TTC GAG AC 3'

eEF1a1\_r 5' CCA GGG TGT AAG CCA GAA GA 3'

M\_Protein\_Set 5\_F GTGACAACAACCAATCCACTAATC

M\_Protein\_Set 5\_R CTCCAGCTCTATGCTGACAAA

Based off of M Protein sequence shown below:

Agcgaaagcaggtagatattgaaagatgagtttttaaccgaggtcgaaacgtactctctatcatcccgtcaggccccctcaaagccg  
agatcgcacagagactgaagatgtctttgcaggaagaacaccgatcttgaggttctcatggaatggctaaagacaagaccaatcctgtca  
cctctgactaaggggattttaggatttggttcacgctcaccgtgccagtgagcgaggactgcagcgtagacgctttgtccaaatgccctta  
atgggaacggggatccaataacatggacaaagcagttaaactgtataggaagctcaagagggagataacattccatggggccaaagaa

atctcactcagttattctgctggtgcacttgccagttgtatgggcctcatatacaacaggatgggggctgtgaccactgaagtggcattggcct  
 ggatgtgcaacctgtgaacagattgtgactcccagcatcggctcataggcaaatggtgacaacaaccaatccactaatcagacatgaga  
 acagaatggtttagccagcactacagctaaggctatggagcaaatggctggatcgagtgagcaagcagcagaggccatggaggtgcta  
 gtcaggctagacaaatggtgcaagcgatgataaccattgggactcatcctagctccagtgtggtctgaaaaatgatcttcttgaatattgca  
 ggctatcagaaacgaatgggggtgcagatgcaacgggtcaagtatcctctcactattgccgcaaatatcattgggatcttgcacttgacatt  
 gtggatgcttgatcgtctttttcaatgcattaccgtcgtttaatacggactgaaaggaggccttctacggaaggagtccaaagtctat  
 gaggaagaatatcgaaggaacagcagagtgtgtggatactgacgatggtcattttgtcagcatagagctggagtaaaaaactacctgt  
 ttctact

20 µl reaction/well for a 96-well plate:

Used PerfeCTA SYBR green

2 x SYBR green	10 µl
5 µM Mix of F primer and R primer	2 µl (500 nM final)
Nuclease-free, DEPC free H <sub>2</sub> O	5 µl
cDNA	4 µl ( 20ng )

PCR conditions: standard SYBR green conditions on qPCR machine:

Step 1: 50° C for 2 minutes

Step 2: Increasing 1.6°C/s to 95°C, held for 10 minutes

Step 1 PCR stage: Increasing 1.6°C/s to 95°C 00:15 seconds

Step 2 PCR stage: Decreasing 1.6°C/s to 60°C 1:00 minute (Data collect at this stage)

Repeat PCR stage 40X

Step 1 Melt Curve Stage: Increasing 1.6°C/s to 95°C 00.15 seconds

Step 2 Melt Curve Stage: Decreasing 1.6°C/s to 60°C 1:00 minute

Step 3 (Dissociation): Increasing 0.15°C/s 95°C 0:01 second

## 1.5 General Immunoprecipitation

### DAY 1: BCA, IP

Note: Keep samples on ice.

1. Sample Preparation:
2. Thaw samples on ice
  - a. Add 2x lysis buffer + inhibitors to samples as they thaw
    - i. I.e., 700 uL of homogenate + 700 uL 2x buffer.
  - b. While samples thaw, prepare aliquot of 1x lysis buffer + inhibitors
3. Pipet samples to mix well
4. Spin down samples at 500 rcf for 8 minutes
5. Move supernatant to new tubes
6. Dilute samples 1:10 in some lysis buffer
  - a. Prepare 1x lysis buffer from 2x stock
  - b. 25 uL stock into 225 uL lysis buffer
7. Perform bicinchoninic acid (BCA) assay

**BCA:**

**Standard Prep:**

1. Prepare standards according to table below:
  - a. Dilute standards in the same lysis buffer composition used for samples
  - b. Freeze leftover standards for next experiment (no more than 3 thaws)

Vial	Buffer volume	Volume BSA stock	Final BSA Conc
A	980 µl	20 µl	2000 µg/ml
B	125 µl	375 µl of A	1500 µg/ml
C	325 µl	325 µl of A	1000 µg/ml
D	175 µl	175 µl of B	750 µg/ml
E	325 µl	325 µl of C	500 µg/ml
F	325 µl	325 µl of E	250 µg/ml
G	325 µl	325 µl of F	125 µg/ml
H	400 µl	100 µl of G	25 µg/ml
I	400 µl	0	0 µg/ml

2. Determine the total volume of working reagent needed

$$(\#Standards \times 2) + (\# \text{ of Unknown} \times 3) \times (\text{volume of WR per sample}) = \text{total}$$

Example:

$$18+6 \text{ extra} \quad + \quad 4(x3) \quad \times \quad 0.2\text{ml} \quad = \quad 7.2 \text{ mL WR}$$

(account for extra): 7.5 mL

3. Add 25µl of each standard or unknown sample into each well in duplicate

4. Prepare working reaction mix: 50 parts reagent A with 1 part reagent B

From example:

7.35 mL A

150 uL B

5. Add 200  $\mu$ l of WR to each well (96 well plate) using reverse pipetting

As soon as you add WR to well, starts to turn purple, work quickly

6. Cover plate and incubate at 37 C for 30 minutes

7. Measure absorbance at 562 nm on a plate reader.

8. Analyze protein concentration using BCA standard curve

9. Prepare Dilutions for downstream applications:

1. Prepare dilution for IP, (account for sepharose controls. 2  $\mu$ g/ $\mu$ l)

2. Prepare dilution for WB (1  $\mu$ g/ $\mu$ l in LSB+DTT) and phospho-tag gels.

**IP:**

1. Add 270  $\mu$ l of resuspended sepharose beads to new tube (bead volume depends on how many samples you're using. 30  $\mu$ l of beads per sample.)

1. Mix beads thoroughly, as they settle quickly

2. Wash with 850  $\mu$ l of lysis buffer (same as used above, but diluted to 1x with PBS to not change concentrations of salts in frozen samples).

3. Spin down with short burst (hold short button to spin to max speed, then let go of short button)

1. Pull off old lysis buffer, leaving ~150  $\mu$ l on top of beads

2. Add another 850  $\mu$ l lysis buffer, invert tube to mix

4. Repeat steps 2-3 (2x) more times

5. Pull out 900ug of protein (calculated from BCA) per sample
  1. Dilute samples to 2ug/ $\mu$ l (450  $\mu$ l total volume)
  2. Pull out 50  $\mu$ l for “input” fraction
6. Incubate sample aliquots with antibodies for overnight (for p38, santa cruz sc-271120)
  1. 7.5  $\mu$ l per sample
  2. Block beads during this step as well
7. Block beads with 1 mg/mL BSA in lysis buffer for 1h
  1. Use a 1:100 dilution of 100mg/mL BSA stock in volume on beads
8. Wash beads (2x) following steps 2-3
9. Resuspend beads in proportional volume
  1. I.e. resuspend beads in 900  $\mu$ l, 100  $\mu$ l per sample with 1 sample extra. Or resuspend in 350  $\mu$ l, 70  $\mu$ l per sample, 1 extra.
10. Add beads to sample aliquots, rock O/N at 4°C.

## **DAY 2**

### **IP part 2:**

1. Spin down beads with Short Burst
2. Remove post I.P lysate carefully and keep the supernatant in a separate tube, dilute per BCA calculations.
3. Add 1 mL (or appropriate amount) of lysis buffer to wash beads, remove wash carefully, leaving behind ~100 uL
  - a. Repeat three times
4. On third wash, remove supernatant one tube at a time using a 27 GA needle and syringe

- a. Keep bevel of needle against side of tube, careful to not lose beads when aspirating supernatant
  - b. Immediately add elution buffer after taking off supernatant
5. Elute samples in 40  $\mu$ l of 2x sample buffer
  - a. Heat to 50°C for 5 mins then to 95°C for 5 mins. Spin down and freeze if not proceeding to western blot immediately.
  - b. If using immediately, or thawing, spin max speed for 2 mins to compact bead pellet.  
Store at -80 C
6. Western blot, probe using 1 or 1.5 mm, 8-10% gel.
  - a. Use 10-20 ug of pre-IP lysate
  - b. Use 50-100% of post-IP eluate.

Run Western blot for IP samples.

## 1.6 General Immunoblotting Protocol

General-use immunoblotting protocol.

### Day 1:

#### Sample prep and running gel:

1. Prepare immunoblot loading sheet.
2. Retrieve samples from -80°C
3. Place in warming block (95°C) until liquid (~1min), vortex samples for ~20 sec, centrifuge for ~5 sec, take out and flip whole tray upside down to mix, centrifuge again for ~5 sec
  - a. Do all this with samples and MWM, but DON'T VORTEX MWM.
4. Retrieve SDS-page polyacrylamide gels from fridge (prepared within 2 weeks of use).
  - a. Place in western blot apparatus and take out comb
5. Pour in 1x running buffer (if none, dilute 10x running buffer) up to 2 gel line (unless using 1 gel)
  - a. Add slightly below line and top off gel part when done loading
6. Load samples with control on the left and samples on right (10µL for .75mm gel. If you need to use more volume, you must use a 1.0 or 1.5 mm gel)
  - a. Empty wells should be filled with some lysis buffer to maintain salt concentrations across running line
  - b. Remember to load from left to right when looking at the gels from the outside (load “backwards” facing gel in reverse)
7. Set to 180V, set time if you prefer, but will take around 50 minutes to run to completion
  - a. Complete once blue line has just run off the gel into the running buffer

8. Store samples back in  $-80^{\circ}\text{C}$  freezer immediately after loading

**Transfer to PVDF membrane:**

9. Assemble transfer cassette with sponges on either side of gel, 3x filter paper soaked with transfer buffer on either side of gel (2x if using thick blot paper)
10. Place 1 pre-cut PVDF membrane in plastic dish with some 100% MeOH-
  - a. use tweezers, don't touch with hands
11. Place 1x transfer buffer (contains SDS, 200mg per 2 liters, but no MeOH -> store in deli fridge) in small glass casserole dish with the 4 filter papers (2 for each side)
12. Pour out running buffer and rinse everything with DI water
13. Place membrane from MeOH container onto 3x filter paper in glass dish
  - a. Make sure it stays wet and isn't allowed to dry out
14. Gently peel off gel with green wedge, cut off wells, and lay on membrane
  - a. Be aware of how the gel is orientated on the PVDF membrane. Careful not to flip the gel either reverse or upside-down. Keep a close eye on this to prevent mistakes
15. Gently roll surface of PVDF with roller to remove bubbles
16. Place 3x filter paper on top of gel, roll with roller to remove bubble
17. Place sandwich of filter paper, PVDF, gel, and filter paper onto sponge in transfer cassette. Ensure a sponge is on either side of transfer cassette.
18. Place cassette into red and black cassette holder so that the black plate faces the black half of the cassette holder. Current will flow from black to red, so ensure that the gel and

PVDF membrane are oriented in the cassette holder so that protein will be pushed out of the gel and onto the PVDF membrane and not the other way around.

19. Fill with 1x transfer buffer (from casserole dish then bottle) and put whole apparatus on stir plate

a. Add stir bar and ice pack and place apparatus into a casserole dish with ice in it.

Ensure the apparatus is completely flat.

20. For standard transfer conditions, 400 milliamps for 1H 45M for 1-2 gels. Use 800 milliamps if running 4 gels, and thus 2 apparatus. The machine will split the current between the apparatus.

21. Put transfer buffer back into bottle and store at 4°C.

**After transfer:**

22. Pour a bit of TBST into glass casserole dish

23. Disassemble cassettes, throw away filter papers and gel (biohazard waste, not hazardous waste), and put PVDF membrane in glass dish with TBST resting on a glass plate used to make gels (better for cutting).

24. Pour fresh 5% milk buffer in TBST (10g milk powder into 250 mL glass bottle and add 1xTBST to 200 mL) into compartments of plastic container (or however many compartments you need for individual antibodies)

25. Can also use tupperware or boxes on shelf for bigger membranes

26. Draw where ladder markers are on PVDF membrane with pen on front of membrane (on side with proteins)

a. Side with proteins is where membrane was touching gel

- b. Use blue ballpoint pens only. No gel pens, no black ink.
27. Label blots with name and what you're testing for on side of PVDF not bound to protein.
  28. Place each membrane piece in its own chamber with protein side facing up in the milk. If running 2 blot pieces with the same antibody, face one of the blots downward and one upward so that the non-protein-bound sides of the PVDF membranes are facing each other. Ensure that you use enough antibody so that the blots "float" some when rocking.
  29. Put blots on rocker for 15 min
  30. Pour off milk, then gently pour more milk into each well, careful not to pour directly onto protein-bound part of PVDF.
  31. Pour off milk and wash blots with 1X TBST for 10 min
    - a. Repeat 3X
  32. Pour off TBST and add primary antibody
    - a.  Antibodies should be diluted into 3% BSA in TBST with NaA3 to prevent microbial growth
    - b. Prepare 50 mL 3% BSA TBST by adding 1.5g BSA (kept cold at 4°C) + 50mL TBST + 100µL NaA3 (sodium azide is very toxic, be careful with it). Store unused 3% BSA TBST at 4°C.
  33. Incubate overnight on rocker at 4°C

**Day 2:**

1. Remove antibodies from blots using serological pipettes. Store antibodies for repeat use.
2. 2x quick washes with TBST
3. 3x 10min washes with TBST

4. Prepare secondary antibody dilutions in 5% milk buffer
5. Incubate at room temperature for 1H
6. 2x quick washes with TBST
7. 3x 10min washes with TBST

**Developing and imaging:**

8. Mix ~100 $\mu$ L of either ECL substrate (clear and brown bottles) per piece of blot in 1.5mL tube
  - a. Careful not to mix
9. Use tweezers to pick up blots, dab on kimwipe/paper towel, and place on plastic wrap surface protein side up
10. Pipette ECL mixture onto blots and use pipet to gently spread it; make sure the whole surface is covered!
11. Place the box over blots for 5 min so they develop; after 2 mins, quickly flip blots over so the proteins are face down in the liquid.
12. Use tweezers to pick up blots, dab the edge on kimwipe, place on sheet of plastic
  - a. Make sure plastic is clean beforehand.
13. Align correctly and then put another sheet of plastic on top to make sandwich
  - a. Place from middle out to try to avoid bubbles -> smooth them out with paper towel gently once sandwiched
14. Image using black plate on ChemiDoc
15. After imaging, return blots to plastic chambers and 2x quick rise with 1x TBST. Blots can be stored in 4°C in TBST.

## **2.1 Key Solutions Used in Mouse Experiments:**

### **2,2,2-Tribromoethanol (Avertin) in 2% Tert-amyl alcohol used for deep sedation:**

Prepare stock by mixing equal parts Avertin with tert-amyl alcohol (i.e. 5 g avertin in 5 mL tert-amyl alcohol), mix at RT overnight in a foil-wrapped tube on rocker. Protect from light. Keep stock at 4°C for up to 2-3 months before starting to lose efficacy. Prepare working stock by diluting 0.5 mL stock solution with 24.5 mL PBS. When adding stock to PBS, add in volume and quickly cap and mix the tube. Vortex heavily. The avertin stock can crash out of solution if not mixed quickly enough. It will eventually go back into solution but will require lots of vortexing (tends to form a condensate at bottom of tube). Filter with 0.2 micron filter and protect from light. Solution good for 2 weeks at 4° C.

### **Ketamine/Xylazine mix used for very deep sedation (mice will be completely sedated for 30-min to 1H):**

Prepare Ketamine Xylazine; 9% Ketamine, 5% xylazine, 86% PBS. Use 27g needle to pull drugs from stock bottles. Drugs must be stored in drug lock box. Place extracted ketamine/xylazine into sterile 1.5 mL tube and use a p200 to measure the exact volume removed from glass vials. Accurate volumes must be recorded in FDA log. Weigh the glass vials and record.

**Triton Lysis Buffer 2X used for lysis of lung homogenate for protein extraction:**

Reagents are calculated to be 1x when diluted to final endpoint (added to LSB+DTT).

Concentrations in parenthesis are working stock when diluted to 1X in PBS.

- 180 mL MilliQ water
- 30 mL Tris 7.4 1M (100mM)
- 12 mL NaCl 5M (200mM)
- 6 mL 0.5M EDTA pH 8.0
- 1,258 mg NaF (100 mM)
- 2.676 g NaPP (20mM)
- 6 mL Triton x-100 (1%)
- pH to 7.4, fill to 300 mL, sterile filter through 0.2uM
- Sodium glycerophosphate added at 2x concentration (20mM final) to working aliquot
- Na3V04 added at 2x concentration (200 uM final) to working aliquot
- Pepstatin A, Aprotinin, Benzimidazole, Leupeptin 1mg/mL stock all added at 2X stock to working aliquot (Apr, Leu, PepA, 1uM final, Benz 10uM final).

## 2.2 Mouse Colony Maintenance

Mouse weaning notes:

-Mice may be weaned at 21 days (3 weeks) after birth at earliest, but can be held for 4 weeks if mice are small in size.

-Count pups around D8-10, minimize interacting with dames with pups younger than D3. Too much interaction can stress out dames.

-If working with harem cages and one female has given birth to a large litter, consider placing the other female, if pregnant, into her own cage. Give her plenty of bedding. This will lower stress of having high populations in the cage.

-Leave males with dames in breeding cages, do not separate the male when you see a litter, the males help with the pups.

-use Jax labs poster at back of Room 33 to estimate age of pups. If unsure, ask for help from the lab or from the facility technicians.

-freshly-weaned pups may take a while to learn how the water bottle works. Position the red houses just under the water spicket for the water bottle and soak some food pellets in water to put at the bottom of the cage.

-When selecting mice to use for breeders, try to avoid pairing mice from the same litter. Check the undersides of mice (especially males) for evidence of dermatitis. Do not use dermatitis mice for breeding. Use younger females, males can be swapped between cages if needed.

- Note on breeder cage cards when a litter is produced. If no litter for 3 months, carefully check the females for pregnancy, and if not pregnant, end the breeder cage. If no litter within 3 weeks of setting up a new breeder, consider swapping out males, or swapping out for younger females.
- Maintain a supply of “backup mice” in case breeders stop being effective. Prioritize female mice as “backup mice”, as females will be the limiting factor in colony bottlenecks.
- You can combine females from different litters in the same weaned cage but punch the ears and record on the google sheet AND the cage cards which mice have punched ears, so you can keep track with which mice come from which breeders. You cannot combine male mice from different litters. Single housed male mice should be euthanized or used at time of weaning for downstream experiments.
- When mice are selected for experiment, remember to put in a Change AUP request that must be completed before the mice can be used for the experiment so that mice are accounted for in the experimental AUP rather than colony maintenance.

**Weaning procedure:**

1. Clean off hood workspace with Peroxiguard
2. Prepare 2 fresh cages with food, a water bottle, fresh bedding pellet (manually pulled apart), and shelter, inside hood space
  - a. Sprinkle a little food onto the floor of the cage, in case pups haven't figured out how to climb to get food
3. Label cages “male” and “female”, fill out all information on new Grimsey lab cage cards

- a. Key info is cage the mice came from (breeder cage #), strain of mice, number of animals per cage, Date of Birth, Start Date, and User
4. Take breeder cage out of rack and place in hood area
5. Begin removing pups from cage
  - a. Remove house and bedding from breeder cage when pulling out pups, makes it easier to grab them
  - b. Swift, confident movements work best. The mice will only bite if you hesitate with your hand low in the cage. They just want to get away from you. They are more afraid of you than you are of them.
  - c. Pick up mice by the tail only. Grasp at end of tail.
  - d. Place lid back on cages if you get distracted or need to step away from the hood space. Mice can jump, and the adults will try to climb out of the cage. If they do, do not panic. The mice can't get away easily. Calmly take the mouse by the tail and return to its cage. Never leave cages unattended.
6. Sex mice (see pictures) and place in either male or female cages.
7. Repeat until all pups are removed
8. If there are more than 6 pups of either gender, you must split pups into additional cages.  
I.e. if you have 8 female pups, prepare 2 cages of 4 pups.
  - a. If weaning 2 breeding cages at the same time where both cages are the SAME GENOTYPE, you can combine FEMALES ONLY. Do NOT combine male pups

from different breeder pairs. When they reach sexual maturity, they will fight.

Females generally won't.

9. Document number of pups, by sex, as well as which cage you weaned, and the date of birth of the pups, into the online Grimsey Lab mouse room log book.

10. Place lids onto all cages, make sure they click on securely.

11. Return cages to racks.

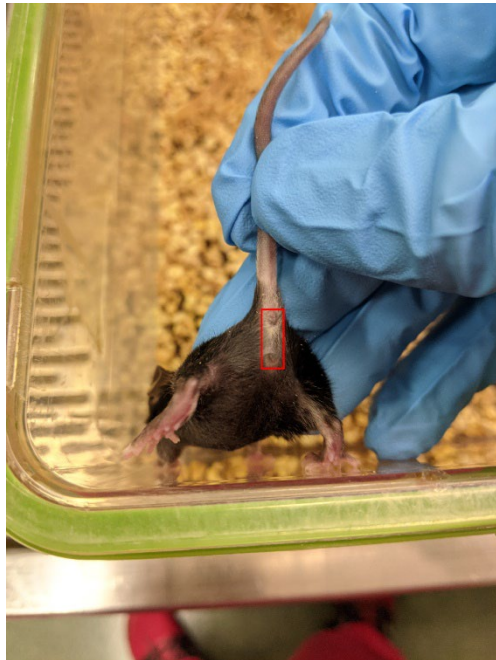
a. **CRITICAL:** Make sure pups have water bottles inserted into cages, and check that the bottles are not leaking (they will drip constantly if the nozzle is touching a shelter).

b. **CRITICAL:** Ensure that the cages are oriented so that the water port (small round metal hatch) at the back of the cage toward the rack. **CAGES LOADED IMPROPERLY ONTO RACK WILL CAUSE FLOODING AND DROWNING. CHECK EVERY CAGE YOU LOAD TO THE RACK FOR THE “CLICK” AND RED INDICATOR.**

12. Wipe down hood space with Peroxiguard when cleaning up

Mouse sex examples:  
Mice aged at 3 weeks.

Male



Female



Note “milk spots” on females. Males lack these.  
Note distance between anus and genitals. It is further on males, with a more pronounced prepuce.

## 2.3 Genotyping TAB1-KI C57BL6 mice

References: Thermo Fisher Phire Animal Direct PCR Kit online resources for genotyping transgenic mice

### Overview:

-DNA extraction (hair pull, tail clip, or ear punch)

-PCR

-Electrophoresis and Imaging Interpretation

### DNA extraction (hair pull):

Materials:

Tweezers (sterilized with Ethanol/Peroxiguard)

Microcentrifuge tubes

Method:

If working with a large tissue sample, use tweezers, scissors and razor blades to trim small pieces of tissue (about the size of the head of a pin is good). Ear punches work best, but can also use tail snips or pulls of hair as long as the follicles are in tact. Remember: when handling samples with tweezers, you **MUST** clean/sterilize tweezers between each sample. Avoid cross contamination by washing tweezers in ethanol and wiping down with clean paper towel. Due to the sensitivity of the Phire kit, it is essential that even a single hair does not get mixed between samples.

## **PCR:**

### Materials:

Thermo Fisher Phire Animal Direct PCR Kit (Cat #F-140WH)

PCR machine

PCR tube strips

10  $\mu$ M Working stock of Forward and Reverse genotyping primers (1:10 dilution from 100  $\mu$ M stock, in nuclease free water)

Nuclease free water

### Method:

Samples can be processed by one of 2 methods; Direct PCR protocol, or dilution and storage protocol. Dilution protocol is preferred for storing samples for later use or troubleshooting.

Direct method is for quick genotyping. If you're working with a limited amount of sample (i.e. you can't get more), recommend doing the dilution method as it is more forgiving of mistakes when running electrophoresis gels.

### Direct protocol:

1. Create master mix of PCR reagents according to table below
2. Add 50/25  $\mu$ l per reaction to PCR tubes
3. close all lids to PCR tubes
4. open 1 tube at a time to add tissue sample directly into PCR reagents.

- a. If using hair, use fine-tip tweezers to add sample
- b. Clean tweezers with 100% ethanol and wipe dry in between each sample

#### 5. Run PCR

Thermo Scientific DNA release Additive included in gel loading dye when analyzing products on agarose gel.

Note: We don't do the 50uL reactions normally, they are included as they come from the kit. For routine genotyping, use 25uL reactions.

Dilution protocol:

1. Place tissue into 20  $\mu$ l of Dilution Buffer containing 0.5  $\mu$ L of DNA Release Additive.
2. Incubate at RT for 2 minutes,
3. heat to 98°C for 2-5 minutes.
4. Spin samples down
5. Add 1  $\mu$ l of supernatant as a template, to 20  $\mu$ L PCR reaction tube (see below).
6. Supernatant can be transferred to a new tube and stored at -20° C for 1 year.

Prepare master mix of PCR reagents:

Don't forget to take into account positive and negative controls (positive control to test sample integrity uses the supplied Universal Control Primers found in the Phire kit. Ctrl universal primers are in a 25  $\mu$ M concentration, use 0.5  $\mu$ L of solution per 20  $\mu$ l reaction for a 0.5  $\mu$ M final concentration).

Negative ctrl: no template DNA (add 1  $\mu$ L H<sub>2</sub>O instead)

Calculation per sample:

(always account for 1 extra, 2 if using >15 samples)

Multiply numbers below for # of samples

Primers are diluted to 10  $\mu$ M in H<sub>2</sub>O prior to beginning (1:10).

Add all reagents in descending order as listed below;

Components	20 $\mu$ L reaction (dilute)	50 $\mu$ L reaction (direct)	25 $\mu$ L reaction (direct)	Final concentration
H <sub>2</sub> O	6.6	19	9.5	
2x Phire Animal Tissue PCR buffer	10 $\mu$ l	25 $\mu$ l	12.5	1x
Forward Primer (TAB1_KI_F)	1	2.5	1.25	0.5 $\mu$ M
Reverse Primer (TAB1_KI_R)	1	2.5	1.25	0.5 $\mu$ M
Phire Hot-Start II DNA polymerase	0.4 $\mu$ l	1 $\mu$ l	0.5	
Sample: Direct protocol		0.5 mm punch (pinch of hairs with follicles, at least 2-3)		
Dilution protocol	1 $\mu$ l			

Do not vortex PCR master mix, use pipette to mix up and down. Add enzyme to master mix last.

Add samples to tubes 1 at a time, be sure to close each prior tube before adding the next sample.

If you can't get clean results, try increasing the primer amount to 5  $\mu$ l per sample.

PCR instructions:

	2 step protocol		3-step protocol		Cycles
	Temp	time	Temp.	Time	
Cycle step	98°C	5 minutes	98°C	5 minutes	1
Denaturation	98°C	5 sec	98°C	5 sec	40
Annealing			59.8°C	5 sec	
Extension	72°C		72°C	20 sec	
Final Extension	72°C	1 minute	72°C	1 minute	1
	4°C	hold	4°C	hold	

Annealing temp based on lower T<sub>m</sub> of primers.

Use “TAB1-KI GENOTYPING” PCR protocol on PCR machine. Protocol takes ~1h to complete.

Recommended to use 3-step protocol with dilution protocol.

Preparation of 2% Agarose gel:

-Agarose (2g)

-1x TAE (100 mL)

-SybrSafe (APE BIO A8743 (10  $\mu$ l))

1. Add agarose to TAE and mix.
2. Microwave until boiling, swirl to mix agarose.
3. Once agarose is fully dissolved (apx. 2 minutes if swirled frequently, do not over boil as this changes concentration of gel) cool beaker over water until molten agarose is  $\sim 68^{\circ}\text{C}$ .
4. Add 10  $\mu\text{L}$  SyberSafe (solution will turn orange).
5. Pour into mold and place in dark space (SybrSafe is light sensitive).
6. Start making this when you begin the PCR and it will be ready by the time the PCR is finished. Alternatively, 2% agarose gels can be stored in bags and stored at  $4^{\circ}\text{C}$  in the dark.

### **Electrophoresis and Imaging Interpretation:**

Run electrophoresis for  $\sim 1\text{h}$  at 70 volts. Image on chemidoc (blue or black plate). Use 100bp ladder. Single band at 400 BP indicates Knock-In. Single band at roughly 250 BP indicates WT. Double band at both locations indicates heterozygous.

## 2.4 Intratracheal injection of LPS

Prior to beginning experiment:

-Sterilize 22g reusable feeding needles via 100% etOH soak. While in TC hood, attach needles to 5mL syringe and pipet pure etOH through needle, being sure to expel remaining etOH with air.

Use vacuum to dry the sterilized needles and place into sterile 15 mL tube.

-Prepare Ketamine Xylazine; 9% Ketamine, 5% xylazine, 86% PBS. Use 27g needle to pull drugs from stock bottle. Place extracted ketamine/xylazine into sterile 1.5 mL tube and use a p200 to measure the exact volume removed from glass vials. Accurate volumes must be recorded in FDA log. Weigh the glass vials and record.

1. Prepare isolation cage by placing a fresh mouse cage onto heated blanket turned up to medium heat. Leave half of mouse cage off of the heat.
2. Weigh mouse in grams. Dose at 0.01 mL/g IP. Delivers 90 mg/kg K, 10mg/kg X.  
Average mouse: 24g = .24 mL K+X.
3. Using the non-dominant hand, the mouse will be scruffed, securing the entire loose skin along the back in the palm of the hand. Secure the tail using the smallest finger. Turn palm upward so that mouse is lying on its back with its abdomen exposed.
4. Tip the animals' head downward to allow the internal organs to move forward to the chest cavity.
5. The needle will be inserted at a 15-20 degree angle into the animals' lower right quadrant by using the smallest needle that will easily pass the material, one no larger than

25g (use 27g). Once the needle has penetrated the abdominal cavity, keep it straight to prevent slicing abdominal organs with needle tip.

6. Retract syringe plunger to verify no blood, feces, or urine is present before making injection. If contaminates are drawn up into syringe, try again with new needle.
  - a. If mouse wriggles free of the needle before injecting but after puncture, switch to the lower left quadrant for injecting to avoid leakage
7. After injection, place mouse in isolation cage and observe until mouse loses consciousness. Mouse will be unconscious for ~30 minutes before beginning to move again
8. Ensure mouse is fully unconscious with toe pinch prior to moving forward
9. Use a small spatula to apply ophthalmic gel to mouse's eyes to prevent drying out

LPS/PBS injection:

Pre-dilute LPS to 5 mg/kg (using 5 mg/mL stock).

1. Pipet 35  $\mu$ l into sterile syringe.
2. Tap bubble of liquid toward bottom of syringe with affixed feeding needle, and re-insert plunger.
3. Carefully tap liquid bubble to seal bottom of syringe, then push plunger VERY CAREFULLY but smoothly until a bead of liquid appears at end of feeding tube.
4. Immediately stop pushing plunger, and retract the bubble of liquid back into tube. Liquid is now loaded into the needle itself, for most accurate administration.

Injection procedure:

1. Secure mouse with tape to 60° procedure board
2. Suspend sedated mouse by upper incisors from the thread attached to the positioning screws of the procedure platform. Make sure animal's dorsum lies flat on platform surface.
3. Place piece of tape loosely across lower (caudal) portion of thoracic cavity, just above diaphragm (prevent ventilation) Place tight enough to maintain proper alignment during procedure.
4. Use sterile blunt end forcep to locate tongue. Be careful to avoid lower incisors, grip and draw out of mouth.
5. Slide the pneumatic otoscope down throat carefully
  - a. Be very careful not to over-stretch mouse's jaw, can cause injury
  - b. Stabilize hand holding the otoscope (usually left hand)
6. Lower the 22G sterile feeding needle, with attached syringe containing bolus of PBS or LPS+PBS
7. Feed needle down throat until tip of needle passes through epiglottis
  - a. Epiglottis has a whitish look, will contract rapidly when the needle passes through it
8. Deposit 35 uL LPS with or without inhibitor or other condition

9. Recover mouse on heated blanket until mouse is mobile again. Carefully monitor mouse temperature (usually by hand) to make sure mouse does not get too cold or overheat.  
Move mouse to be half on, half off warmed portion of cage
10. Move and adjust mouse's position while it is unconscious to help blood flow to all limbs and prevent injury, will also help to rouse mouse awake

## 2.5 Lung Extraction for OCT Embedding and Cryostat Sectioning

1. Weigh mouse and record on log sheet (provided on google drive)
2. Euthanize mouse with injection of 2% Avertin working stock in PBS
3. Dilute 500  $\mu$ l of working solution (made by dissolving 25 g avertin in 25 mL tert-amyl alcohol overnight and filtered through 0.22  $\mu$ M filter) in 24.5 mL PBS. Solution good for 2 weeks at 4°C. Protect from light. Euthanize mouse by injecting 900-1000  $\mu$ l IP. Mouse should quickly lose consciousness and breathing should slow or stop. Cervical dislocate.
4. Pin mouse to dissection board by paws. Use scissors to cut through skin from abdomen to under neck. Pull skin apart, exposing rib cage and neck muscles.
5. Remove muscles, fat tissue from trachea, exposing it all around (careful not to puncture trachea)
6. Use scissors to cut arteries at either side of neck, and soak up blood with paper towel
7. Wait for blood flow to cease (or perform cardiac puncture and drain blood through right ventricle).
8. Prior to catheter insertion, pre-fill 1mL syringe with 300uL of 1:1 PBS/OCT mixture
9. Insert 20g catheter through trachea
10. Tie off the catheter and needle down the trachea close to the lungs after inserting it through the trachea (about 5-6mm down into trachea)
11. Slowly remove the needle from the catheter
12. Use scissors to cut tissue away around head and catheter. Sever head, being careful to cut trachea above where the catheter was inserted
13. Place head on ice for further processing
14. Use scissors to cut away ribcage, exposing heart and lungs. Be careful not to nick lungs.

15. Attach syringe filled with 300uL 1:1 PBS/OCT mixture to catheter
16. Inject PBS/OCT mixture into mouse lungs, lungs should inflate but should not leak OCT.
17. Remove catheter, tying off suture immediately to prevent leakage
18. Carefully dissect heart, careful not to cut trachea or lungs
19. Use scissors to cut tissue above trachea, and carefully lift trachea by suture strings with one hand, trimming away with small scissors any tissue that clings to the trachea
20. Continue this process, carefully lifting trachea and cutting tissue away from it, until lungs and trachea lift out of the ribcage
21. Carefully annotate OCT freezing vessel to orient lungs
22. Move lungs (by suture strings) to PBS bath
23. Prepare freezing chamber of isopentane and liquid nitrogen
24. Cold isopentane in metal canister, laid into styrofoam box filled with liquid nitrogen
25. Lift lungs by the trachea with tweezers, and carefully place into OCT-filled chamber, oriented to be able to identify left and right lung upon cryo-sectioning
26. With lungs placed, add additional OCT on top of lungs
27. Take either side of freezing container with tweezers, and carefully lower into isopentane bath
28. Either hold tissue in place or release and allow to float in isopentane until OCT is fully frozen
29. Remove OCT-embedded tissue from isopentane and store on dry ice or at -80°C
30. Move lungs to clean plate, and coat with OCT, careful not to get too many bubbles
31. Fill freezing vessel with about 5mm OCT, and place lungs in

32. Take a photograph of lungs oriented in freezing vessel for future reference
33. Trim sutures down to bare minimum of knot
34. When lungs freeze in OCT, ensure entirety of lungs are covered, add more OCT to ensure
35. Remove and store lungs in sealed bag, keep on dry ice/at  $-80^{\circ}\text{C}$ .

## 2.6 Collection of Lung Homogenate Samples

1. Euthanize mouse with 1 mL 2% Avertin and cervical dislocation.
2. Confirm deep sedation plane by no response to deep toe pinch.
3. Harvest blood via cardiac puncture.
4. Spray fur with ethanol.
5. Open the abdominal cavity and cut the renal artery.
6. Open the chest cavity by cutting the diaphragm and cutting up both sides of the rib cage, being careful not to touch the lungs.
7. Perfuse with 5-10 mL cold PBS + 1 mM EDTA through the right ventricle of the heart.
8. Remove the lungs using tweezers to pluck, making sure the heart is not taken with the lungs and place in bead mill tube (round bottom, locking) with 1 mL PBS and 1 ball bearing.
9. Centrifuge blood in brown cap serum tube for 5 min at 10,000 rpm at room temperature.
10. Harvest the serum into microcentrifuge tubes and store at -80°C.
11. Homogenize lungs in pre-chilled holders at 25 Hz for 2 min.
12. Centrifuge samples at 4°C for 5 min at 500xg.
13. Remove 150 µl into separate epi tube and centrifuge for 5 min at 5000xg at 4°C for cytokines.
14. While that is spinning, aliquot the low-speed supernatants for:

RNA: 2 tubes (100 µl sample + 350 µl TRK lysis buffer for RNA)

Protein: 300  $\mu$ l into 300  $\mu$ l of 2X Lysis buffer prepared with phosphorylation/protease inhibitors  
(2X Triton Lysis Buffer)

15. Harvest the clarified supernatant from the high-speed spin into a separate epi tube for cytokine analysis.

16. Freeze samples at  $-80^{\circ}\text{C}$ .

## 2.7 Collection of Bronchoalveolar Lavage

Protocol developed to extract bronchoalveolar lavage (BAL) from mouse lungs from influenza-infected mice to assess immune cell investment and protein secretion.

**Day 1:** Infect mice with  $10^4$  PFU X31 influenza.

-72h post infection for analysis of D3 IAV vs vehicle ctrl

**Day 4:**

Prepare:

Wash: cold PBS + 1mM EDTA

Antibody list:

Invitrogen 12-1702-82  
Anti-Mo CD170 (Siglec F)  
Clone: 1RNM44N

eBioscience 45-4801-82  
Anti-mouse F4/80  
PerCP-Cy5.5  
Clone: BM8

Invitrogen: eBioscience 17-9668-82  
Anti-MO Ly-6G  
APC  
Clone: 1A8-Lys6G

Tonbo Bioscience: 35-0112-U500  
Anti-human/mouse CD116  
FITC  
Clone: M1/70

CD11c (Efluor 450, Invitrogen/eBioScience)

### **Isolation of BAL:**

1. Euthanize mice by Avertin overdose (1 mL)
2. Cut open and away mouse ribcage, cut and expose mouse trachea
3. Insert 18-20 gauge catheter into trachea
4. Attach syringe containing 1 mL BAL wash
5. Slowly inject 1 mL BAL wash, watch lungs inflate
6. Pull back plunger on syringe, drawing up BAL.
7. Repeat step 4-5 (2) more times
  - a. BAL will be foamy from surfactant protein
8. Place BAL into 15 mL microcentrifuge tube on ice
9. Repeat step 4-7 (2) more times
10. Take mouse ear samples for genotype verification
11. Repeat steps 1-10 for all mice
12. Spin down BAL at 1250 RPM for 10 minutes
13. Carefully remove supernatant and save in separate tube.
14. Resuspend cell pellet fraction in flow-sort buffer
  - a. Count cells using hemacytometer/cell counter and adjust volume

- b. Prep comp samples (note for future: have extra mice used just for comps, OR use beads)
- 15. With samples on ice, transport to Coverdell for cell-counting by flow cytometry
- 16. Perform flow-cytometry quantification of immune cell types with
  - a. If sorted populations are low, pool cells together after count
- 17. Lyse sorted cells for mRNA quantification
  - a. Spin cells down at 5000g for 5 minutes
  - b. Remove supernatant
  - c. Lyse in Buffer RLT + BME (350 uL) for RNA quantification
- 18. Perform downstream RNA extraction, purification, for downstream qPCR analysis
  - a. If sufficient RNA extracted for PCR, save aliquots for downstream NG-RNAseq

## 2.8 Cytokine Panel

Protocol developed toward assessment of proinflammatory cytokines in mouse lungs after influenza infection in TAB1-KI vs WT mice. Protocol adapted from ProcartaPlex Mouse and Rat Mix & Match Panel (Invitrogen).

### Note on sample preparation:

Lung homogenate in PBS obtained from whole murine lungs, mechanical homogenization via bead agitator, spun down and supernatant extracted (~150 uL/sample). Samples have been stored in PBS at -80.

Markers Selected for Investigation:

GRO alpha (CXCL1) - chemoattractant produced by immune cells, neutrophils

IFN beta - antiviral function, enhances type 1 immune response (TH1)

IL-1 beta - master regulator of inflammatory response, MMP, COX2, IL-6 production

IL-10 - anti-inflammatory cytokine

IL-19 - anti-inflammatory cytokine, produced by macrophages, negative feedback regulator

IL-17A (CTLA-8) - T cell and neutrophil activation

IL-28 - antiviral cytokine

IL-4 - activates naive T cells into TH2

IL-6 - acute proinflammatory mediator, stimulates aB proliferation

MCP-1 (CCL2)

TNF alpha - proinflammatory cytokine produced by macrophages/monocytes during ALI

VEGF-A - upregulated by inflammatory cytokines, promotes angiogenesis

Experiment flow:

Experiment #1: Limited tester titration to determine if surfactant proteins in our cytokine samples may affect interaction (masking effects) of analytes with detection aBs, and to assess appropriate concentrations for samples

Experiment #2: Full panel of 2x 96 well plates, male and female samples, baseline, D3, and D5 post-infection.

### **Protocol:**

Notes prior to beginning experiment:

- use multichannel pipette and reagent reservoirs when possible
- Ensure MagPix instrument has been properly calibrated and set up prior to preparing and running assay
- Ensure that MagPix operator, all personnel, and the room space for the experiment as well as tissue handling and disposal is accounted for in project AUP.
- Begin experiment in morning to allow for all wait times

### **Preparation of Samples and Buffers**

Prepare “Thawing Buffer” or 2X lysis buffer that is added to samples immediately following thawing

Intended to minimize protease activity

For 4.5 mL of 4x triton lysis buffer (enough for two full plates of samples), add;  
18 uL each of Apr, Leu, PepA (1 mg/ml stock)  
180 uL Benz (1 mg/ml stock)  
18 uL of 10mM Na<sub>3</sub>V04 stock  
27.6 mg glycerophosphate  
Added to 4.5 mL PBS

(Prepare 2 aliquots of this, one that is further diluted in PBS to 1X for dilutions)

1. Thaw frozen samples on ice and mix well by vortexing and spinning down, keep cold
2. Centrifuge at 10,000 x g for 10 minutes at 4° C to pellet out particulates
3. Transport 120 µl protein to new tube. Volume must be exact for proper dilution.
4. Move 120 µl into a new tube. If sample has less than 120, adjust dilution accordingly.

Prepare wash buffer from 10x stock (supplied)

1. Bring 10x stock to RT.
2. Vortex 15 seconds
3. Mix 20 mL Wash Buffer Concentrate with 180 mL ddH<sub>2</sub>O. Mix gently to avoid foam.

### **Dilution of Samples**

Note: Before running full plate, perform small-scale dilution experiment (Experiment #1) to test dilutions and surfactant protein masking.

-take 2 samples, infected and uninfected WT samples

3 concentrations;

Neat, 1:4, 1:10 dilution. Dilute in buffer prepared above. Dilution buffer should be prepared with appropriate concentrations of protease inhibitors.

	Vol. Sample	Vol. Dilut.	Vol. Sample (2.2x)	Vol. Dilut. (2.2x)		
Neat	25	0	55	0		
1:4	6.25	18.75	13.75	30.25		
1:10	2.5	22.5	5.5	49.5		

Run and analyze tester samples following protocol below.

Identified Tester Samples:

WT D0, D5, male and female.

23JB179 (female D5)

23JBx03 (male D5)

22JB51 (male D0)

22JB54 (female D0)

Based on this experiment, we decided to do a 1:4 dilution for all samples.

**Sample prep and dilutions for main exp:**

1. Prepare samples as shown above in section 2.1
2. Prepare each sample with a dilution as shown below

Note: 1 extra well

	Vol. Sample	Vol. Dilut.	Vol. Sample (3x)	Vol. Dilut. (3x)		
1:4	6.25	18.75	18.75	56.25		

**Prepare antigen standard:**

Notes:

1. Change pipet tips between each dilution step and avoid air bubbles
2. Check each step as performed
3. Avoid loss of beads by securing plate (by hand) on both sides of handheld magnetic plate washer during procedure
  1. This protocol was developed using Hand-Held Magnetic Plate Washer EXP-55555-000.
4. Centrifuge each different standard mix stock vial at 2,000 / g for 10 seconds.
5. Add 62.5 uL of diluent (1x PBS buffer with protease inhibitors) to each stock vial (4 standards, IFN- $\beta$ , Standard Mix A, 1B, 1C).
6. Vortex the vials at high speed for 30 seconds and centrifuge at 2,000 x g for 10 seconds to collect contents at bottom of vial

3. Incubate on ice for 10 minutes to ensure complete reconstitution
7. Pool entire content of each stock into 1 of the vials (should be 250 uL final.)
8. Prepare 4-fold serial dilutions of standards:
9. Note: Use forward pipetting techniques, and swap pipette tips between dilutions
10. Label tubes in an 8-Tube Strip: Std1, Std 2, Std3, Std 4, Std 5, Std6 and Std7
11. Add 200 uL of reconstituted standard mix to Std1 tube
12. Add 150 uL of diluent (1X PBS buffer + inhibitors) into Std2-7 tubes
13. *Transfer 50 uL of mixed standards from Std1 to Std 2 tube.*
14. *Mix by pipetting 10 times*
15. *Transfer 50 uL of standard mixes from Std2 tube to Std3 tube using new pipette tip.*
16. *Mix by pipetting up and down 10 times.*
17. Repeat 4-7 for tubes Std4-Std7, changing pipette tips between dilution steps
18. Add 150 uL of diluent to last tube of 8-tube strip to serve as background
19. Keep tubes on ice until ready to use
20. Standards cannot be stored, use fresh and use immediately
21. **Assay protocol:**
22. Add capture bead mix to plate
23. Vortex the 1x Capture Bead Mix Vial for 30 seconds at high speed
24. Follow-up with sonication, then vortex again for 30 seconds
25. Transfer contents off Capture Bead mix Vial to a small-volume trough
26. Using a multichannel pipette, add 40 uL of Capture Bead Mix to each well of the plate
27. Wash beads using a Hand-Held Magnetic Plate Washer

28. Place plate on plate washer and wait 2 minutes to allow beads to settle on bottom of each well
29. Remove liquid by quickly inverting washer/plate assembly over sink or waste container
30. Maneuver plate exactly like this: hold straight-up, U-Turn, straight down. FIRMLY HOLD MAGNET TO PLATE DURING THIS PROCESS.
31. Gently blot the inverted washer/plate assembly onto several layers of paper towels or absorbent surface to remove any residual liquid
32. Use fresh paper towel space for every touch, and note that any contact with sample material should be bleached before disposal in biohazard waste
33. Remove magnet and add 150 uL of 1X wash buffer into each well and wait 30 seconds
34. Re-apply magnet, wait 2 minutes. Then, remove the liquid by quickly inverting the washer/plate assembly over a sink or waste container
35. Gently blot the inverted washer/plate assembly onto several layers of paper towels or absorbent surface to remove any residual liquid
36. Remove plate from magnet and proceed to step 3
37. Add samples and standards to the plate (see Table 1)
38. Add 25 uL of 1X PBS + inhibitors to each well followed by 25 uL of prepared standards or samples as defined by plate layout. Add additional 25 uL of 1X PBS + Inhibitors (or whatever the wash buffer is) to wells designated as backgrounds. (50 uL final volume per well).
39. Seal the plate using a provided Plate Seal and cover with provided Microplate Lid. Shake 96 well plate for 30 min at 600 rpm RT, then transfer to 4\* on level surface for **overnight incubation**

40. Remove and discard Plate Seal in biohazard waste. Wash the plate following steps below:
41. Add 100 uL wash buffer to each well
42. Place the plate on magnetic plate washer and wait 2 minutes to allow particles to settle on bottom of each well
43. Remove liquid by quickly inverting washer/plate assembly over a sink or waste container (or aspirate)
44. Gently blot the inverted washer/plate assembly onto several layers of paper towels or absorbent surface to remove any residual liquid (Disregard step if you aspirated instead)
45. Remove magnet and add 150 uL of 1X wash buffer into each well and wait 30 seconds
46. Remove liquid by quickly inverting the washer/plate assembly over a sink or waste container (Or aspirated)
47. Gently blot the inverted washer/plate assembly onto several layers of paper towels or absorbent surface to remove liquid (same as 4d)
48. Repeat 4d-f once for a total of 3 washes.
49. Remove plate from magnet and proceed to next step
50. Add Biotinylated detection antibody mix to plate
51. Using multichannel pipette, add 25uL of detection antibody solution to each well of the plate. Gently tap the plate to evenly distribute solution in the well
52. Note: Use a narrow trough to prevent volume loss
53. Hold pipette completely vertical to prevent cross-contamination
54. Seal the plate using a new plate seal and cover with the provided microplate lid. Shake at 600 rpm for 1H at room temperature.

55. Wash the plate following step 4.
56. Add streptavidin-PE (SA-PE) to the plate.
57. Add 50 uL of SA-PE solution to each well
58. Seal the plate using new Plate Seal and cover with the provided Microplate lid. SHake at  
600 rpm for 30 minutes at room temperature.
59. Wash the plate following step 4.
60. Prepare the plate for analysis on a xMAP instrument.
61. Add 120 uL of 1X wash buffer into each well
62. Seal the plate using new Plate Seal and cover with the provided Microplate Lid. Shake at  
600 rpm for 5 minutes at room temperature
63. Remove the Plate Seal and run on MagPix instrument for downstream analysis